Effects of Base Station Power Control and Soft Handoff on the Outage and Capacity in the Forward Link of CDMA Systems

by

Dongdong Li

Presented to the Faculty of the Graduate School of
The University of Texas at Arlington in Partial Fulfillment
of the Requirements
for the Degree of

DOCTOR OF PHILOSOPHY

THE UNIVERSITY OF TEXAS AT ARLINGTON
December 2005

ACKNOWLEDGEMENTS

I would like to thank my supervising professor Dr. Vasant Prabhu for his invaluable advice and inspirations during my research. I wish to thank my academic advisors Dr. Jonathan Bredow, Dr. Alan Davis, Dr. Chien-Pai Han, and Dr. Qilian Liang for their interest in my research and for taking time to serve in my dissertation committee.

I would like to extend my sincerely appreciation to all the friends and colleagues in University of Texas at Arlington, with whom I have a happy time. I am grateful to Dr. Jaber A. Khoja for his invaluable comments and discussions from the beginning of my research. I would also like to appreciate Dr. Will Egner and other colleagues in Cerion Inc. for their continuous supports.

Personally, I would like to express my deep gratitude to my parents and sister, who always encourage me on my graduate study. I am also grateful to my lovely wife, whom I am blessed to have.

Finally, I like the idea of trying my best to be excellent.

December 2, 2005

ABSTRACT

Effects of Base Station Power Control and Soft Handoff on the Outage and Capacity in the Forward Link of CDMA Systems

Publication No. _____

Dongdong Li, Ph.D.

The University of Texas at Arlington, 2005

Supervising Professor: Vasant K. Prabhu

This thesis focuses on the capacity analysis of the forward link of code division multiple access (CDMA) systems by characterizing the base station (BS) power distribution. With the rapid growth of data and multi-media traffic, the forward link becomes the system bottleneck. How to design an efficient call admission algorithm in the forward link to effectively use the limited base station power while guaranteeing certain quality of service is important to increase the forward link capacity. To effectively use the limited BS power, we need to understand the BS power distribution given a certain traffic pattern. However, the characterization of the BS power in the forward link has not been adequately addressed in the literature and the limit of the BS power on the capacity has not been fully studied. By taking into consideration of channel characteristics and system parameters, such as the network traffic pattern, call admission algorithm, power control strategies, and soft handoff approach, we characterize the BS power distribution and obtain a closed-form expression of the forward link capacity. Furthermore, previous

work studying the forward link performance assumes equal BS power throughout the system and obtains a static capacity without considering the correlation and interactional relation among BS powers, which is rarely true in the real CDMA systems. By further considering the interaction among BS powers, we introduce an iterative process to determine the dynamic forward link capacity. From the system engineering aspects, our research can provide an analytical framework to facilitate the design and benchmark of CDMA networks compared to pure computer simulations. The models established in our research also provide an accurate estimation of the network capacity. Since the air interface of future networks or networks being deployed recently, such as wide-band CDMA (WCDMA), CDMA 2000, and Universal Mobile Telecommunication Services (UMTS), is CDMA based, we are expecting that our research is useful to design call admission algorithms in wireless systems.

TABLE OF CONTENTS

LIST OF FIGURES

LIST OF TABLES

CHAPTER 1

Introduction

1.1 Overview

Following the first field test conducted by Bell labs in 1978, wireless communication experienced rapid growth in 1990's. In more than twenty years development, three generations of wireless systems emerged.

The first generation wireless system is an analog system using frequency modulation (FM). In US, the first generation wireless system is called Advanced Mobile Phone system (AMPS). The AMPS was deployed after the Federal Communications Commission (FCC) allocated 40 MHz of spectrum to support 666 duplex channels in 1983. Each of the channel uses one-way bandwidth of 30 kHz [2]. In Europe, the first generation wireless system is called the European Total Access Communication System (ETACS), which was developed in the mid 1980's and each channel uses 25 kHz bandwidth.

The second generation (2G) wireless system includes GSM in Europe, IS-95 in US, PDC in Japan, and U.S. Digital Cellular (USDC) systems in US. GSM is the abbreviation of Groupe Spécial Mobile (GSM), which is a study group formed by the Conference of European Posts and Telegraphs (CEPT) in 1982 to study and develop a pan-European public land mobile system. This is because in early 1980's, the Europeans realized that it was cost-saving and economies of scale to establish a unified standard to make the cellular systems in different European countries compatible with each other [3]. In 1989, GSM responsibility was transferred to the European Telecommunication Standards Institute (ETSI), and phase I of the GSM specifications was published in 1990. Commercial service was started in mid-1991. GSM uses time division multiple access (TDMA) tech-

nology to support 8 time slots in 200 kHz bandwidth. Traditional GSM works in the 900 MHz frequency band and was called GSM900. Later on, ETSI defined an alternative of GSM in 1989 operating in 1800 MHz frequency band. By the end of 1993, the commercial GSM system operating in 1800 MHz band was adopted in several non-European countries in South America, Asia, and Australia and was called the Digital Cellular System (DCS1800) (also known Personal Communication Network (PCN) in Europe). In 1997, DCS1800 was renamed GSM1800. In 1994, the US FCC auctioned spectrum in the 1900MHz band to provide the Personal Communications Service (PCS). The PCS licenses in US were neutral with respect to technology. The GSM standard was accepted in the United States in 1995. GSM-1900 cellular systems have been operating in the US since 1996, with the first network in the Washington, D.C. area. The GSM service in US operating in 1900 MHz was called PCS1900 and later was renamed GSM1900 in 1997. In November 1995, American Personal Communications (APC) launched the first commercial GSM service in the US. As of January 1999, GSM has more than 120 million subscribers, according to the GSM Memorandum of Understanding (MoU) Association [4]. With 324 GSM networks in 129 countries in operation, the acronym GSM now stands for Global System for Mobile communications. Since the channel experiences larger loss in higher frequency, the GSM900 can provide nationwide coverage economically due to its larger coverage area. However, GSM900 has a smaller spectrum bandwidth compared to GSM1800 (or GSM1900) and can not support dense populated area. Therefore, dual-band GSM is design to operate in both 900 MHz and 1800 MHz (or 1900MHz) band.

Personal Digital Cellular (PDC) is a second-generation digital cellular telephone communication system in Japan [5], operating in the 800MHz and 1500MHz bands. PDC is currently only used in Japan, with the first system introduced by NTT DoCoMo in 1991 as a replacement for the earlier analog networks. PDC is very similar to USDC.

USDC is the second-generation digital cellular communication system in US, which evolved from the AMPS system. After the FCC declared in 1987 that cellular licensees could employ alternative cellular technologies in the 900 MHz band, the cellular industry began to research new transmission technology as an alternative to AMPS [6]. In 1988, the Cellular Technology Industry Association (CTIA) was established to work with the cellular service operators and researchers to identify new technology requirements and set goals. The Telecommunications Industry Association (TIA) released a standard specification called the TDMA Interim Standard 54 or TDMA IS-54 in early 1991. Based on TDMA IS-54, IS-136 (also called Digital AMPS or D-AMPS) was released in 1994 operating in both the 900 MHz and 1900 MHz bands in North America. One difference between IS-54 and IS-136 is that IS-136 extended the use of TDMA to the control channel. USDC uses TDMA to support 3 time slots in 30 kHz AMPS band and theoretically triples the capacity of AMPS.

IS-95A is also the second-generation wireless system in US based on Code Division Multiple Access (CDMA) technology operating in both 900 MHz and 1900 MHz. CDMA type technology dates back to the 1940's, when spread spectrum technology was used in military communications systems because its resistant to interference from enemy signals [6]. The Qualcomm corporation began developing a CDMA wireless system in the late 1980's that was accepted as the IS-95A standard in 1993. IS-95A is the first CDMA cellular standard provides voice services, and can provide circuit-switched data connections at 14.4 Kbps [7].

The third generation (3G) wireless system is called International Mobile Telephony (IMT-2000) within the International Telecommunications Union (ITU). IMT-2000 radio interface specifications were approved in ITU meeting in Helsinki, Finland in November 1999. The early work of the 3G wireless systems dates back to the World Administrative

Radio Conference (WARC) in 1992. ITU Recommendation ITU-R M.1457 specifies five types of 3G radio interfaces [8]:

1. IMT-2000 CDMA Direct Spread, also known as the Universal Mobile Telecommunication System (UMTS) terrestrial radio access (UTRA) direct sequence frequency division duplex (FDD), is supported by the GSM network operators and vendors and includes wideband CDMA (WCDMA) in Japan's Association of Radio Industries and Businesses (ARIB)/DoCoMo recommendation. UMTS is developed by the Third Generation Partnership Project (3GPP). UMTS is often used interchangeable with WCDMA when referring to the 3G evolution of GSM network using WCDMA air interface. To avoid the confusion, the GSM Association now refers to UMTS/WCDMA systems as 3GSM [9]. In early 1998, the European Telecommunications Standardizations Institute (ETSI) selected the UMTS as the basis for a single global cellular system and as a successor to GSM and later was officially accepted by ITU as one of five radio interfaces for the IMT-2000 3G mobile communications standards [10]. NTT DoCoMo of Japan successfully launched the technology in 2001. Recently, pre-commercial UMTS networks were officially opened in Monaco. Western European countries will officially launch UMTS networks in 2003, the United States in 2004, and number of Eastern European and Rest of the World countries in 2005.
2. IMT-2000 CDMA Multi-carrier, also known as CDMA 2000 3x developed by 3GPP2. This mode is supported by the US cellular network operators and vendors. CDMA 2000 includes CDMA 2000 1x (1x means one carrier), which is to be commercially deployed in October 2000 and allows a data speed of 144 Kbps. The next step is CDMA 1xEVDO (evolution data optimized or evolution data only) and CDMA 1xEVDV (evolution data and voice). CDMA 2000 1xEVDO delivers peak data speeds of 2.4 Mbps in a bandwidth of 1.25 MHz and supports applications such as

MP3 transfers and video conferencing. CDMA 2000 1xEVDV provides integrated voice and simultaneous high-speed packet data multimedia services at speeds of up to 3.09 Mbps [7].

3. IMT-2000 CDMA time division duplex (TDD), also known as UTRA TDD and TD-SCDMA. TD-SCDMA is developed in China and supported by TD-SCDMA Forum.
4. IMT-2000 TDMA Single Carrier, also known as Enhanced Data Rates for GSM Evolution (EDGE) supported by Universal Wireless Communications Consortium (UWCC) [11]. EDGE is a new air-interface technology to support the global evolution of GSM and TDMA to 3G. EDGE uses 8 Phase Shift Key Modulation (8PSK), rather than normal GSM Gaussian modulation shift keying (GMSK). EDGE is designed to provide smooth evolution from existing GSM and TDMA networks to 3G system.
5. IMT-2000 Digital Enhanced Cordless Telecommunications (DECT) supported by DECT Forum using Frequency Division Multiple Access (FDMA). DECT is evolved from UK cordless telephone CT2 standard and the Swedish CT3. The initial standards focused upon developing the air interface between the cordless telephone and its base station, which plugged into the telephone socket, as well as the standards and protocols to support handovers between several base stations all connected to the same office switchboard (PABX) or public telecommunication switch. DECT wireless PABX products have found real success in a number of key sectors - notably warehouses, hospitals and factories. The first ETSI DECT standards were produced in 1992. In 1999 in the UK dual mode DECT/GSM service was launched. Other countries have also indicated an intention to launch such services. However, as of 2002, they do not appear to have taken off.

Aside from these 3G proposals, the 2.5G wireless system is implemented as a smooth transition to 3G system. 2.5G technologies include GPRS and IS-95B. The General Packet Radio Service (GPRS) is a new non-voice value added service that allows information to be sent and received across a mobile telephone network [12]. It supplements today's Circuit Switched Data and Short Message Service. GPRS involves overlaying a packet based air interface on existing circuit switched GSM network. This gives the user an option to use a packet-based data service. The most attractive feature of GPRS is to enable mobile users to connect to the Internet with a theoretical maximum speeds of up to 171.2 kbps. In reality, the downlink speed of the GPRS can be 64 kbps, just like using a dialup modem or standard ISDN device. IS-95B is a 2.5G standard that can offer 64 kbps packet-switched data in addition to voice services [7]. IS-95B was first deployed in September 1999 in Korea and has since been adopted by operators in Japan and Peru. IS-95 A&B are operated in the name of cdmaOne by Qualcomm corporation.

The IMT-2000 family of 3G systems include three types of Core Network technology and all the five radio interfaces must support IS-41 and GSM MAP [8]:

1. GSM based (using Mobile Application Part (MAP) protocols on top of SS7 protocols for signalling).
2. IS-41 based.
3. Internet Protocol based (in future, to be specified)

The evolution path from 2G to 3G is shown in Fig. 1.1 [13]. Some of the recent progress of 3G systems are listed below as [14]:

- October 31, 2002 Ericsson announced the milestone of 10,000 commercial UMTS/ WCDMA macro base stations shipped. Nokia is assumed to have shipped about the same amount.
- November 18, 2002 Nokia introduces the worlds first GSM/EDGE 3G mobile phone-Nokia 6200.

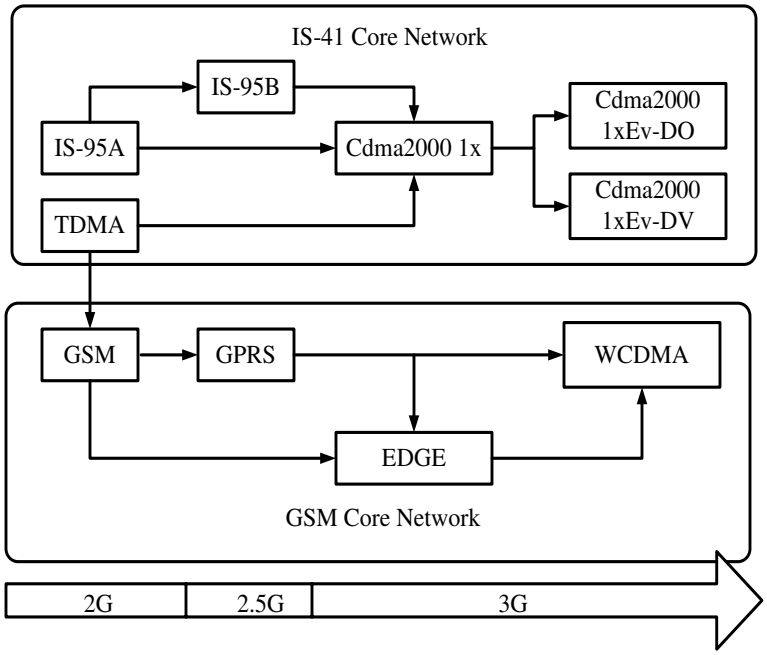

Figure 1.1 Evolution from 2G to 3G wireless system.

- November 29, 2002 Nokia and Vodafone Omnitel carry out 3G WCDMA call handover to commercial GSM network.
- January 31, 2003 Ericsson conducts the world's first IPv6 over 3G UMTS/WCDMA network demonstration.
- February 10, 2003 LG introduced the world's first dual band, dual mode phone for both CDMA and WCDMA.
- January 31, 2003 Ericsson conducts the world's first IPv6 over 3G UMTS/WCDMA network demonstration.
- February 2003, Korean mobile operator KTF announced plans to begin transmitting TV pictures direct to 3G mobile phones via the CDMA 2000 1xEVDO system.
- July 1, 2003, Cingular Wireless announced the world's first commercial deployment of wireless services using EDGE technology.

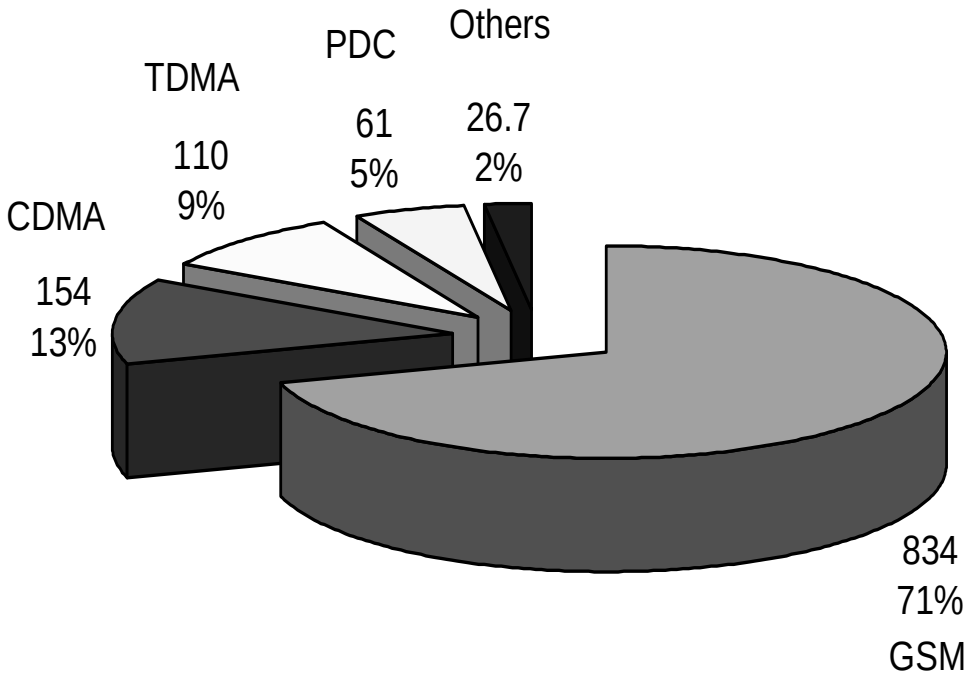

Figure 1.2 Number of wireless users (in Millions).

- August 27, 2003, Nokia announced that the world's first CDMA 2000 1xEVDV high-speed packet data phone call, achieving a peak data rate of 3.09 Mbps, was completed in San Diego.

According to the EMC world cellular database of June, 2003, there are over 1.1 billion wireless users in the world and the market share is shown in Fig. [15].

The 3G wireless systems are designed to support high data rate service. For example, the UMTS is designed to support 2.048 Mbps for pico-cell (and micro-cell) applications, 384 kbps for medium size cells (micro and small macro cells), 144 kbps and 64 kbps for large cell applications (Large macro cells), 14.4 kbps for continuous low speed data applications in very large cells, 12.2kbps for speech (4.75 kbps - 12.2 kbps), 9.6 kbps for satellite [8].

Since the air interface of 3G systems are going to use CDMA air interface, it is instructive to look at the system architecture as follows.

1.1.1 CDMA System Introduction

IS-95 is the second generation of CDMA systems in US utilizing 1.25 MHz bandwidth to provide data rate up to 64 kbps. CDMA 2000 increases the channel bandwidth to 5 MHz to provide 144 kHz data rate for mobile users and 2 MHz for stationary users [16]. Second generation system using TDMA can provide approximate three time capacity increases than AMPS [17]. CDMA is interference limited system and has more capacity than TDMA wireless system in a cell environment due to the following reasons:

- CDMA system can reuse the same spectrum in every cell and all sectors. If there are no cell planning needed such as in satellite communication system, TDMA is more efficient than CDMA [18]. However, in cellular wireless systems, where frequency reuse is needed and intercell interference exists, CDMA system has more capacity due to the use of spectrum spreading technology to reduce interference strength [17] [19].
- Multipath experienced in wireless propagation due to reflection and deflection is the headache of TDMA system, where equalizer and other digital processors are employed to reduce intersymbol interference. However, CDMA system can utilize Rake receiver to combine multipath signals to achieve macrodiversity gain.
- Since CDMA system is interference limited, voice activity can be used to improve the system capacity for voice service [17].
- MS in CDMA system is connecting to mulitple BS's to reduce the "ping-pong" effects when it switches calls at cell boundary, which is called soft handoff. In contract, many TDMA systems use break-before-make technology and the mobile user is usually connecting to one BS at a time, which results into more chances of dropping calls and unstable communications [16].

Table 1.1 Base Class 0 System Frequecies

System	Reverse Link (MHz)	Forward Link (MHz)
A	824-835 845-846.5	869-880 890-891.5
B	835-845 846.5-849	880-890 891.5-894

1.1.1.1 Spectrum Allocation

CDMA system can offer about 7 to 10 times the capacity of analog technologies and up to 6 times the capacity of digital technologies such as TDMA. The IS-95B CDMA system is used in North America. It provides data from 8 kbps up to 64 kbps at 1.25 MHz channel bandwidth and mainly supports voice service and low data rate service. The custom of IS-95 CDMA systems has reached about 3.0 million in 1999 [16]. CDMA 2000 systems based on IS-95 CDMA systems support wireline-quality voice service and high data rate service with data rate ranging from 144 kbps to 2 Mbps.

IS-95 CDMA system can operate on the same channel band as that of AMPS at 900 MHZ. The channel spectrum separation between forward link and reverse link is 45 MHz. The forward link (from BS to MS) occupies bandwidth from 869-894 MHz. The reverse link (from MS to BS) occupies bandwidth from 824-849 MHz. IS-95 can also operate on 1.9 GHz band to support PCS [20]. The reverse link occupies 1850-1910 MHz and the forward link occupies 1930-1990 MHz with a separation of 20 MHz [21]. A CDMA system is implemented using N different wideband RF carriers and each can support M channels, which is called CDMA/FDD system. The band of each RF carrier is 1.2288 MHz for IS-95 CDMA system. Each channel is defined by a different code sequence. The spectrum allocated at 900MHz (Band Class 0) is shown in Table 1.1 [16]. The spectrum allocated at 1.9 GHz (Band Class 1) is shown in Table 1.2.

Table 1.2 Base Class 1 System Frequecies

Band	Reverse Link (MHz)	Forward Link (MHz)
A	1850-1865	1930-1945
D	1865-1870	1945-1950
B	1870-1885	1950-1965
E	1885-1890	1965-1970
F	1890-1895	1970-1975
F	1895-1910	1975-1990

1.1.2 IS-95 CDMA System

Code-Excited Linear Prediction (CELP) is used to reduce voice rate rate to 9.6 kbps. Traditional pulse code modulation (PCM), adaptive differential code modulation (ADPCM) are used to code voice data in time domain. The data rates of these techniques are high: 64kbps for PCM and 16-32 kbps for ADPCM. When even high data rate is needed, CELP is used to provide voice coded data rate from 4.8 to 9.6 kbps. CELP generates channel parameters at a rate of 192 bits every 20 ms, which is called a speech frame.

1.1.2.1 Forward Link

64 Walsh codes are used to identify forward link channels. The forward link channel consists of a pilot channel (using Walsh code #0), a synchronization channel (using Walsh code #32), up to seven paging channels (using Walsh code #1-#7) and up to sixty-three data channels. The orthogonality properties of Walsh code is used to eliminate intracell interference from the users in the same cell with coherent detection is employed at MS. The speed of Walsh code symbol is 4.8 ksps (4.8 ksps $\times$ 64=307.2 kbps)[1]. Channel coding is 1/2 convolution coding (channel data rate is 19.2 kbps) and Viterbi decoding.

[1]sps: symbol per second

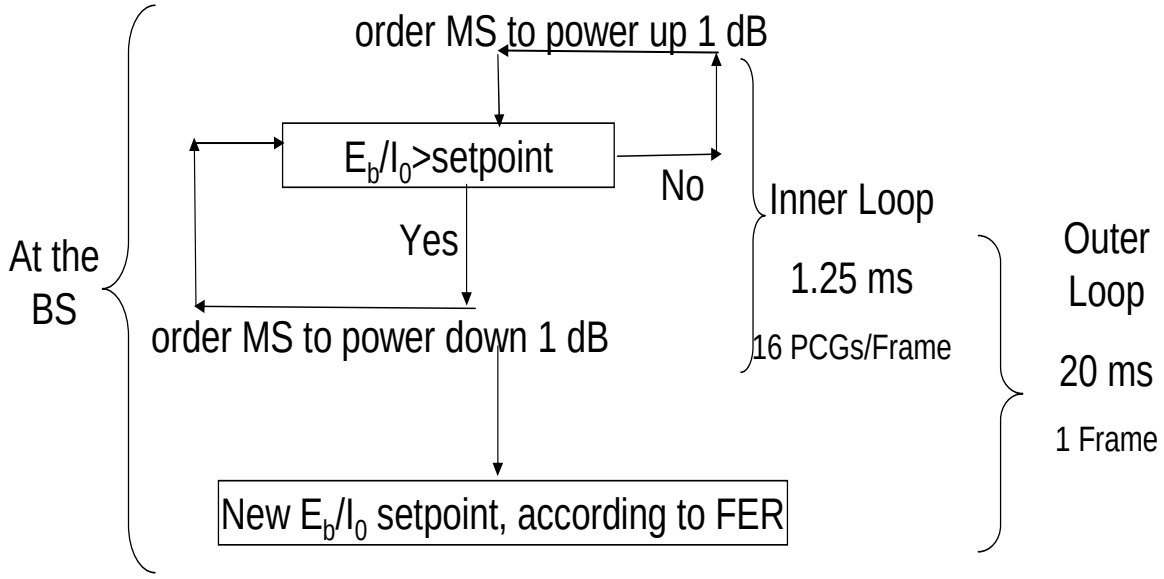

Figure 1.3 Reverse link power control in IS-95 system.

Interleaving is used to reduce burst errors with 20 ms span in a 24 bits array ($240.02 = 19.2\ kbps$). The spreading gain of coded data is typical 64. However, the spreading gain of user voice data is 128. Walsh code rate is 19.2 ksps, which equal to the channel data rate or each channel bit is spread using 64 Walsh code chips. Rake receiver is used to take advantage of multipath signals with delay greater than 1 μs (> 0.8143 μs of chip duration). PN codes generated for MS with maximum length of $2^{42} - 1$ is decimated to 1.2288 Mcps to scramble channel data. It is further decimated to 800 cps to scramble punctured channel data containing power control bits. All 64 channels are combined and multiplied with two PN codes generated for BS with maximum length of $2^{15} - 1$ to form I and Q channels of linearly QPSK signals. The PN codes generated for BS are the same for users in the same cell and are the time-shifted versions for users at different cells with chip rate of 1.2288Mcps [2]. All BS's are synchronized using global position system (GPS).

The pilot channel is used to retrieve accurate estimations of time delay, phase and magnitude of three strongest multipath channels. The pilot signal for all BS's is about 4 to 6 dB higher than traffic channel signal with a constant value, spread by the PN codes of BS and transmitted every 26.67 ms (37.5 sps or 2^{15}-1=32,768 cps) and the channel fading parameters can be assumed to be constant during that time (corresponding to a vehicle speed of 20 miles/hour). The PN sequences for all BS's are the same and have an unique chips offset from each other in an increment of 64 chips for identification (total of 32,76864=512 identifications).

Once the MS identifies the three strongest pilot offsets. It will check the synchronization channels to get the time of day and long-code synchronization with the particular BS. After synchronization, the MS is ready to receive information from the BS. Punctuation is used to transmit the reverse link power control bits in channel data, which is used to assure that the BS receives the same power from MS. The power control commands are generated by measuring the signal-to-interference E_b/I_0 at the BS. Power control bits are transmitted every 1.25 ms (800 bps or 16 times every 20 ms speech frame). For the channel data rate of 19.2 kbps, it means that one power control bit is sent every 24 channel data bits. A 20-ms frame is divided into 16 time slots and each of these time slots is called Power Control Groups (PCG's). There are two power control loops. The outer-loop power control measures the frame error rate (FER) at the BS and sends power control command to MS in order to maintain the target E_b/I_0 at frame basis. The inner-loop power control adjusts the E_b/I_0 to the target value within a frame and provides more accurate maintenance of the target E_b/I_0. The close-loop power control in the reverse link is shown in Fig. 1.3.

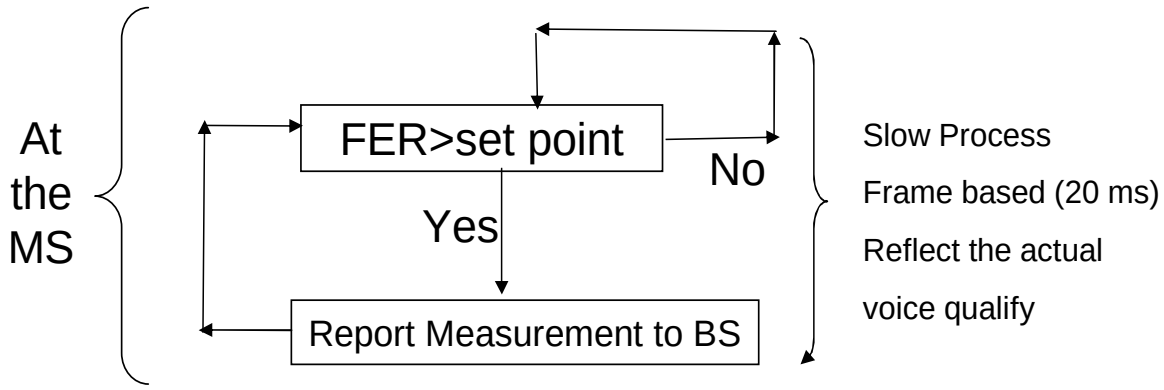

Figure 1.4 Forward link power control in IS-95 system.

1.1.2.2 Reverse Link

Channels of the reverse link are divided into access channels or traffic channels. There are up to 62 traffic channels and up to 32 access channels. The access channel is used to transmit teletraffic information, such as originating calls. On the reverse link, 9.6kbps user data is passed to 1/3 convolutional encoder and the output data rate is 28.8 kbps. After interleaving, each group of 6 bits is mapped into one of the 64 Walsh codes and the output data rate is 307.2 kcps, where the Walsh code symbol rate is 4.8ksps and equals to 64×4.8=307.2 kcps. PN code of MS is used to scramble the data into rate of 1.2288 Mcps. The usage of higher channel convolutional coding rate and Walsh codes modulation results in a greater tolerance of interference, since non-coherent detection is used at the reverse link. The power control command is transmitted every 20 ms at a frame-based interval from the MS to the BS to conduct the forward link power control. The power control is relatively slow in the forward link. The close-loop power control is shown in Fig. 1.4, which provides a frame-based control to maintain the target FER.

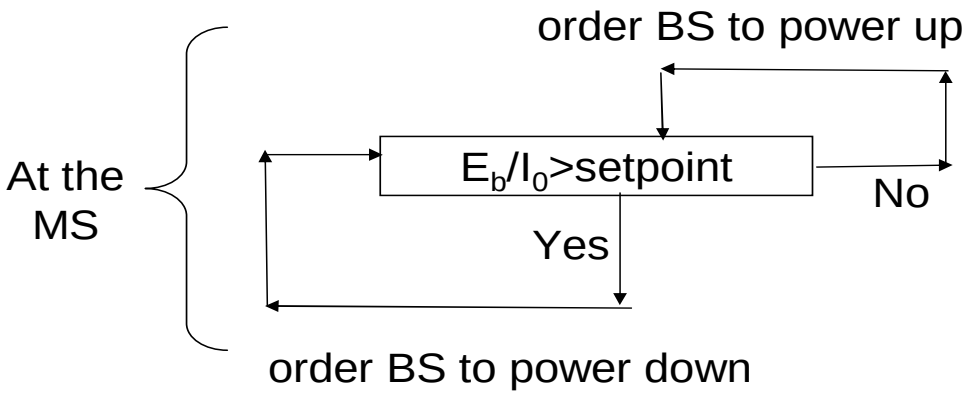

Figure 1.5 Forward link power control in CDMA 2000 system.

Table 1.3 The Gain of Fast Power Control at the MS in WCDMA

	Slow Power Control	Fast Power Control	Gain
ITU Pedestrian A (3 km/h)	11.3 dB	5.5 dB	5.8 dB
ITU Vehicle A (50 km/h)	8.5 dB	6.7 dB	1.8 dB

1.2 Forward link power control in 3G CDMA systems

According to [22], fast power control can reduce the required SIR at the MS in the WCDMA system and therefore, decrease the power requirement from the MS as shown in Table 1.3.

Fast power control is used in the 3G system. For example, a 1.5 kHz power control algorithm is implemented in WCDMA systems, while a 800 Hz power control is conducted in CDMA 2000. The fast power control scheme in the forward link of CDMA 2000 system is shown in Fig. 1.5, which is very similar to the fast power control in the reverse link of IS95 CDMA systems.

The fast power control is conducted at such a high speed in the 3G CDMA systems that the multipath fading components need to be taken into account in the continuously varying wireless channels, which is covered in the following section.

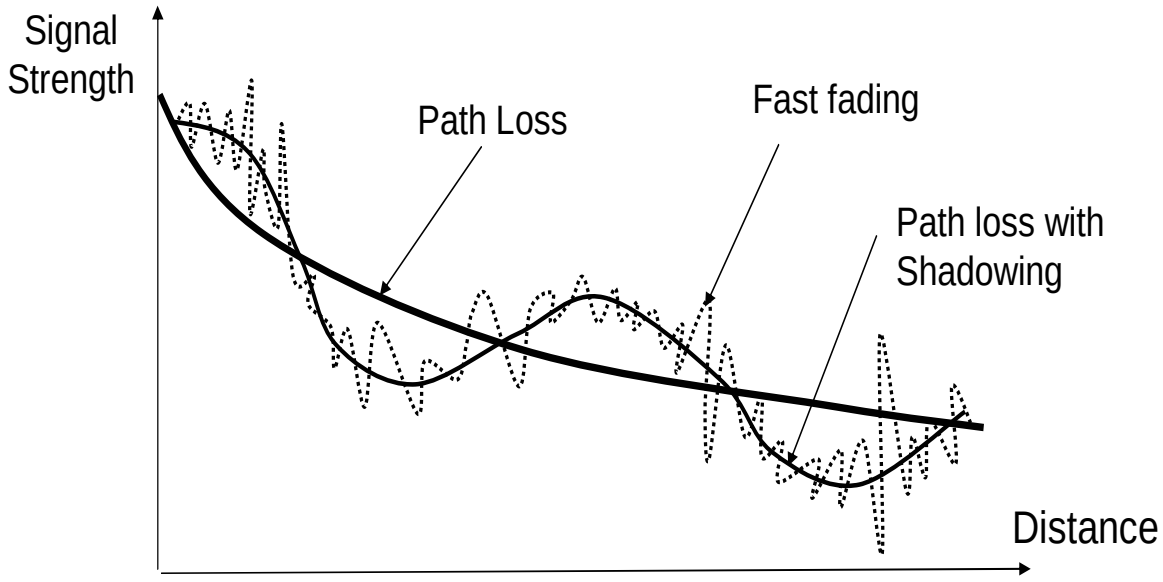

Figure 1.6 Received signal strength related with distance.

1.2.1 Wireless Propagation Channel

The transmitted signals from the the BS to the MS through wireless propagation channel experience both the large-scale shadowing (lognormal path loss with shadowing) and the small-scale fading (multipath fading).

As shown in Fig. 1.6, large-scale shadowing path loss is estimated by averaging the received signal strength at a large distance (over several hundreds meters). On the other hand, the small-scale fading describes the rapid fluctuation of the received signals over short travel distances (a few wavelengths) or short time durations (on the order of seconds).

Measurements have shown that the path loss at any given distance is random and distributed lognormally (normal in dB) around the mean distance dependent value as

$$l(d) = 10^{X_\sigma/10} d^n \tag{1.1}$$

Table 1.4 Path Loss Exponents for Different Environment

Environments	Path Loss Exponent (n)
In building line-of-sight	1.6-1.8
Free Space	2
Obstructed in Factories	2-3
Urban Area	2.7-3.5
Shadowed Urban Area	3-5
Obstructed in Building	4-6

where X_σ follows the normal distribution with zero mean and σ standard deviation. In most of the research, σ is chosen to be 8. n is the path loss exponent and given in table 1.4 [2, pg. 104].

The received signal experiences fast fading if the Doppler shift is significant compared to the RF spectrum of signal. On the other hand, for smaller Doppler shift, the received signal undergoes slow fading. In CDMA systems, slow fading is expected since a large RF bandwidth is used. During a certain time period, if the transmitted signal is $x(t)$, the received signal is expressed by a series of baseband signals and given by

$$h_b(\tau) = \sum_{i=1}^{\infty} \alpha_i x(t - \tau_i) \tag{1.2}$$

where α_i is the i^{th} multipath and usually modeled as the Rayleigh distribution when non-line-of-sight path exists between the BS and MS. When there is line-of-sight path existing between the BS and MS, the first multipath a_1 follows a Rice distribution. τ_i is the delay of the i_{th} multipath fading.

In order to model both the large-scale fading and small-scale fading, a composed distribution called the Suzuki distribution is used, where the average power of local multipath fading follows the lognormal distribution.

In addition to the above factors affecting the received signals strength, the SIR achieved at the MS is also decided by the interference.

1.2.2 Interference in CDMA System

The interferences are classified into the other-cell interference, the owner-cell interference, and multipath non-orthogonality interference.

Because of the ubiquitous frequency reuse in every cell, the power in other cells received at the MS in the owner cell posed as interference. The other-cell interference is shown in Fig. 1.7 in solid lines, where the gray cell is the owner cell. The owner cell, which contains the owner BS serving the MS, is a term traditionally used in the reverse link of CDMA systems. Each of the BS's communicating with the MS in soft handoff in the reverse link receives a replica of the signal from the MS. Then all these replica of signals are transmitted from the BS's to the central BS, where the strongest replica of the signal is retained and all the other replica are discarded. The MS monitors the pilot channels and when it receives the strongest average pilot signal strength from a BS, the MS decides that BS is the owner cell. Due to the symmetric of the channel, the MS intelligently knows that when it transmits signals back to the owner BS, the owner BS more likely receives the strongest average signal strength. Therefore, the signal received at the owner BS from the MS are more likely to be the selected as the central BS.

A similar definition of the owner BS is used in the forward link, where the MS more likely receives the strongest average signals from the owner BS. Since the path loss is reversely proportional to the distance, for the sake of simplification, a area within a certain distance from the owner BS is defined as the serving area of the owner BS. The owner cell is thereby defined as the cell containing the owner BS.

The dotted line in Fig. 1.7 indicates the owner-cell interference and multipath non-orthogonality interference. The power transmitting from the owner BS to other MS's in the owner cell is posed as the owner-cell interference to a specific MS. As mentioned earlier in section 1.2.1, the MS receives a series of delayed replica of signals from a BS. When the Rake receiver is deployed at the MS to capture these replica, the replica received at one

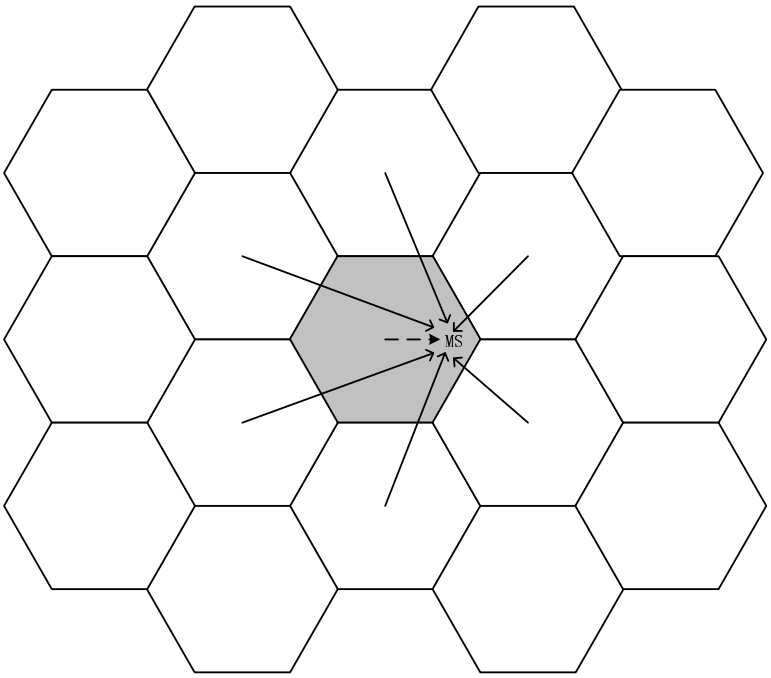

Figure 1.7 Interference model.

time slot is posed as interference to another replica of signals received at another time slot due to the non-orthogonality of the delayed PN sequence. This type of interference is called the multipath non-orthogonality interference.

When the MS is close to the owner BS, the other-cell interference becomes weak and the SIR is mainly affected by the owner-cell interference and multipath non-orthogonality interference. While the MS is far from the owner BS, e.g., at the cell edge, the other-cell interference is much stronger and dominates the achievable SIR.

In order to guarantee the call quality of the MS at the cell edge, soft handoff is the commonly used approach in the CDMA systems to reduce the call drop rate. When the received signal strength at the MS is strong enough and the MS only needs to combine multipath components from a single BS, it is said to be in the non-soft handoff mode (NSHM). When the signal strength received at the MS is weak and the MS connects to multiple BS's and combines multipath components from different BS's, it is said to be in

the soft handoff mode (SHM). It was reported that soft handoff can reduce the call drop rate compared to the TDMA systems. The soft handoff schemes is discussed as follows.

1.2.3 Soft handoff

For example, IS-95 use a "make before break" soft handoff method to transfer calls when the MS moves from one cell to another cell. In IS-95, constant $Tadd$, $Tdrop$ handoff thresholds and a $Drop$ timer are specified as shown in Fig. 1.8. MS monitors pilot signal strengths from BS's and compares them with handoff thresholds. BS's having pilot signal strengths exceeding the $Tadd$ threshold are put into the active set of MS. The active set is the set of BS's having stronger signal strengths so that the MS selects these qualified BS's to communicate with and requires power from. If pilot signal strengths of BS's in the active set drop below the $Tdrop$ threshold for a time period longer than $Tdrop$, the BS's are taken away from the active set. MS receives and combines signals from BS's in the active set to obtain diversity gain. When MS can not maintain a certain E_b/I_0, MS will suffer from unstable communications and probably result into drop of connections with BS's and the MS is said to be in outage. Average outage probability is an important criterion to evaluate system performance.

In CDMA systems, due to the loss of synchronization with the BS's in the active set or limited number of Rake fingers, the MS can only connect to part of the active set. The BS's that the MS is actually connected to and requires power from is called the soft handoff set. If all BS's in the active set are communicating with the MS, the active set is equivalent to the soft handoff set.

1.3 Outage, Blocking, and Capacity Considerations

By using the soft handoff, the MS in a fast power-controlled CDMA systems continuously measures the received SIR E_b/I_0. If the E_b/I_0 at the MS is below a certain

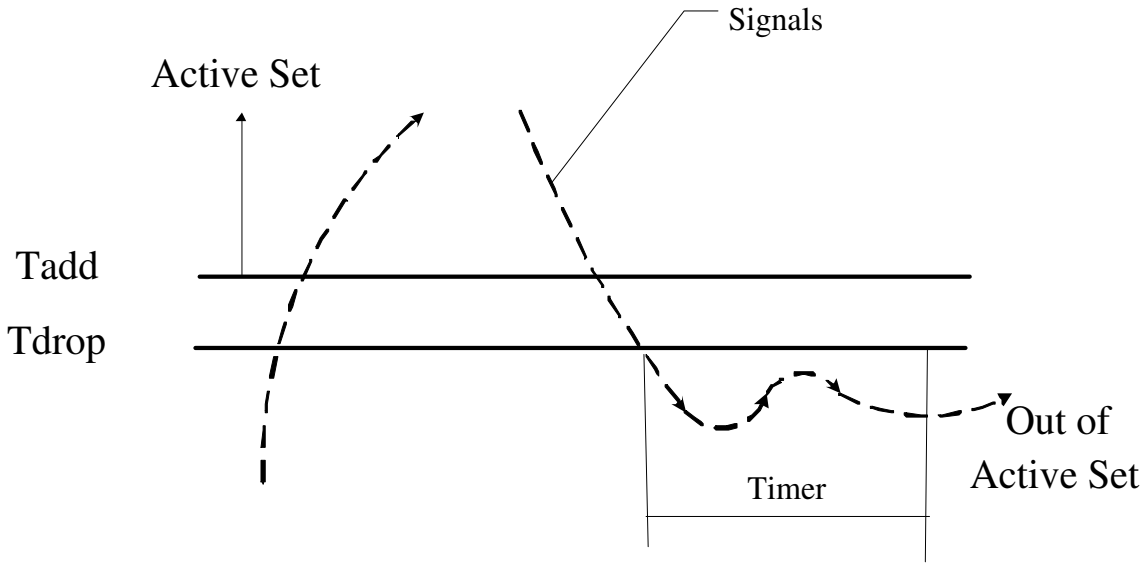

Figure 1.8 Soft handoff scheme with two thresholds.

threshold, the MS will ask the BS connected to it to allocate more fraction of power. If the target E_b/I_0 is less than a target threshold, the MS will ask the BS in the soft handoff set to decrease the fraction of power allocated to it. This fraction is different when the MS combines different number of multipath components from a single BS in the NSHM or multipath components from multiple BS's in the SHM.

Therefore, if we can model the SIR as a function of the fraction of BS power, we can manage to control the fraction of BS power to achieve the target SIR by using the fast power control. The amount of SIR achieved at the MS is affected by the wireless fading channels and interference from the owner-cell, the other cells, and orthogonality among the multipath components. For a given cells placement and a specific MS location, the interference suffered by the MS is a random variate and its statistical characterization can be determined from the channel parameters, such as the shadowing and fading severity. If the BS's in the soft handoff set transmits more power to the MS, a larger average SIR is achieved at MS and therefore, the outage, which is defined when the SIR achieved

at the MS is larger than a target value, will become smaller. In a power controlled CDMA systems, the SIR should maintain at a fixed value under perfect power control or a range of values with power control error (PCE) at the MS regardless of the variation of the fading channels and different soft handoff set configurations. Therefore, in a power-controlled CDMA system, outage happens when the fraction of power allocated from BS's in the soft handoff with the MS exceeds a maximum value.

The BS can allocate appropriate amount of fraction of power to the MS to maintain a reasonable outage for a certain soft handoff set. By considering all soft handoff combinations and taking the average, the average outage experienced by a MS can be related to the limit of the maximum amount of fraction of BS power allocated to the MS.

The individual outage probability experienced by a MS is different from the blocking probability from the viewpoint of the BS. A BS needs to support every MS communicating with it. If the total amount of power required by all MS's exceeds the maximum BS power, the BS can not admit more MS's into the system and the blocking happens. The blocking probability is an important criteria of quality of service (QOS) to determine how many MS's can be accommodated into the system for a given BS power.

The problem of the blocking is complex since the BS power in one cell is posed as interference to another cell and vice versa. From above discussions, we know that the BS power is decided by the number of MS's that it serves and the fraction of power required by each MS. Since the number of MS's in a cell is a random variate governed by the call arrival rate and call duration, it is more appropriate to treat the BS power as a random variate.

Since the owner-cell interference is decided in part by the total amount of transmitting power of the owner BS and other BS's, the amount of interference experienced by a MS is a function of surrounding BS powers. Therefore, the fraction of BS power required by an individual MS, which is affected by the amount of interference, is a function of

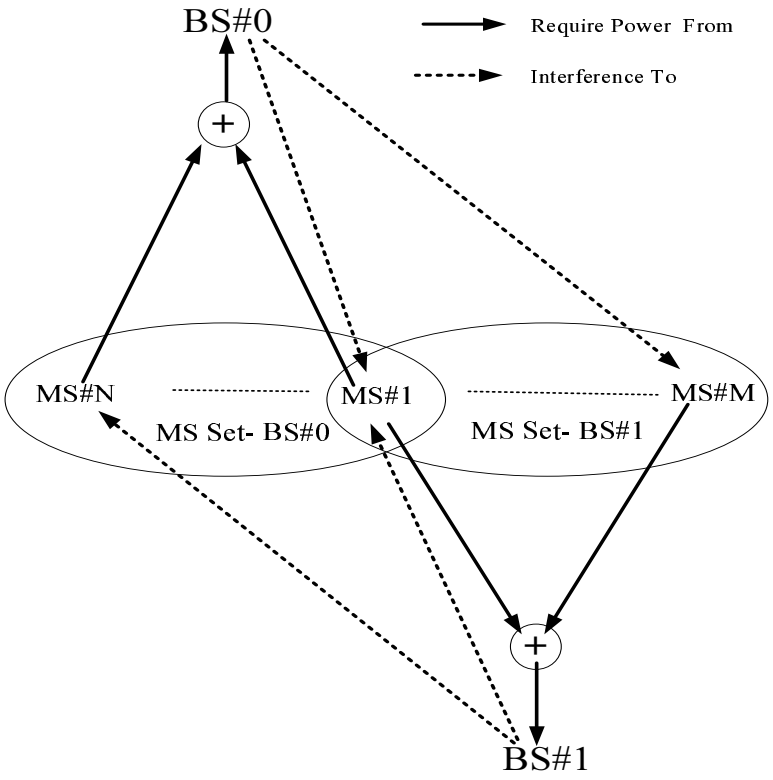

Figure 1.9 Iterative process of finding the number of MS's supported by a BS.

the powers of surrounding BS's. Subsequently, since the power distribution of one BS is decided by the fraction of power required by an individual MS, the power distribution of one BS is a function of its power and the powers of other BS's. Therefore, the decision of the power distribution of one BS is an iterative process. Since the power distribution of a BS is directly related to the number of MS's, the number of MS's supported by a BS is also an iterative process, which is shown clearly in Fig. 1.9.

These are two definitions of the capacity: the first definition treats the capacity as the maximum number of MS's that can be supported in a system without considering the call arrival rate or call duration. This kind of definition can be used to estimate the peak system load, which is useful in the call admission control. The other definition considering the call arrival rate and call duration, which provide a dynamic estimation

of the number of users in a system. If both the call arrival interval and call duration are exponentially distributed, the capacity is called Erlang capacity as in [19].

1.4 Objective

This thesis focus on establishing a unified analytical model to characterize the distribution of the fraction of BS power allocated to a MS communicating with any soft handoff set.

By using this distribution, we open an easy and effective analytical approach to reconcile the argument in the literature on whether capacity gain is possible for the soft handoff in the forward link [1] [23].

Furthermore, by using that distribution, the distribution of the BS power needed by a single MS is obtained by summing the BS powers required by every soft handoff set. Subsequently, the power needed by all MS's around a specific BS can be obtained. By setting a target outage probability at a maximum limit on the fraction of BS power available to a MS, the capacity is obtained in a closed form at a certain blocking probability. Consequently, a fine power control can be conducted on the level of soft handoff set at a MS and its effects on the system performance can be determined.

In addition, by considering the power correlation between different BS's, the call arrival rate, and call duration, our proposed model can be applied to real CDMA systems. Moreover, this model is used to study the influence of the power requests from MS's in other cells on the number of MS's supported at a specific BS. In addition, the effects of real system parameters, such as the available Rake fingers, the soft handoff threshold, the power control error, and the data rate, on the system performance is addressed from viewpoint of the limitation of the fraction of BS power allocated to a MS.

In summary, an analytical framework of characterizing the fraction of BS power and studying its effects on the CDMA system is established in this thesis.

1.5 Outline of Chapters

The thesis is organized as follows:

1. The first chapter gives an overview of the progress and architecture of wireless systems and the key technologies used in 3G CDMA systems. The problems and issues that need to be taken into consideration in the 3G CDMA systems are discussed. Based on these discussions, the importance of the challenge work done in this thesis is revealed.
2. Chapter 2 continues to discuss the previous work and problems existed in these work, based on which we propose our new work.
3. Chapter 3 gives a brief introduction to the wireless channels, which is useful to understand the model proposed in the later of the thesis.
4. Chapter 4 goes ahead to propose our new model to characterize the distribution of the fraction of BS power while considering the reference BS as the owner BS. How to use this fraction of the BS power to obtain a closed-form expression of capacity at a certain outage probability is presented. We further apply our model to reconcile the arguments of whether the soft handoff can provide capacity gain or not in the forward link of CDMA systems.
5. By extending the analysis in chapter 4, we propose an analytical approach to characterize the distribution of the BS power allocated to a single soft handoff set, a single MS, and all MS's in the cell in chapter 5. We show how to design the call admission control to accommodate a certain number of MS's at certain outage and blocking probabilities.
6. In chapter 6, we extend the analysis in chapter 5 by considering the unbalanced BS power in real CDMA systems and propose an iterative process to determine the dynamic capacity caused by the unbalanced BS power. By considering the call

arrival rate and call duration, we also show how to determine the capacity of real CDMA systems.

1.6 Summary of Contributions

The key contributions of this thesis to wireless communications are:

1. Propose a unified approach to characterize the distribution of the fraction of BS power allocated to a MS communicating with any soft handoff set in the forward link of CDMA systems.
2. Extend the concept of non-orthogonality factor to a general case considering soft handoff by introducing the concept of macro non-orthogonality factor.
3. Establish an analytical model to characterize the power distribution of a specific BS as a function of the number of MS's supported by a specific BS.
4. A closed-form expression of capacity is obtained at certain blocking and outage probabilities.
5. Introduce an analytical iterative process of determining the number of MS's supported by a specific BS as a function the number of MS's supported by other BS's.
6. Reveal that soft handoff gain is determined by the limitation of the fraction of BS power available to a MS and other system parameters.
7. Extensive numerical results of the system performance by considering real CDMA system parameters, such as the limitation of the fraction of BS power available to a MS, ON/OFF traffic model, the location of the MS, the available Rake fingers, the soft handoff threshold, the power control error, and so on.

CHAPTER 2

Previous Work and Proposed New Research

As discussed in previous chapters, with the emergency of the 3G CDMA systems including WCDMA and CDMA2000, the SIR-based power control is also incorporated in the forward link. The SIR-based fast power control that partially mitigates the effects of multipath fading was reported to reduce the required SIR and thereby, improve the system performance [22, pg. 215]. Therefore, it is of great interest to evaluate the system performance by considering the SIR-based power control in forward link. The multipath fading was usually neglected in previous studies of forward link CDMA system capacity for simplifying the analysis [1] [24]. However, the multipath fading is essential in a fast power-controlled CDMA systems and can not be omitted.

The Rake receiver is the most commonly used approach in the CDMA system to track these multipath components. Traditional Rake receiver only tracks the multipath components from one BS. As an extension, the generalized Rake receiver tracks multipath components from multiple BS's.

This chapter is organized as follows: first, we give an introduce to the generalized rake structure used in practical CDMA systems, which is used to combine multipath signals from different BS's to achieve the diversity gain. Second, we discuss the previous work. Then, we summarize the contribution of previous work and propose our new work.

2.1 Overview

2.1.1 Rake Receiver

If multipath signals are received at the MS, Rake receiver can be employed to combine these signals to achieve macrodiversity gain. Recently, generalized Rake receivers are discussed in literature [25] [26]. Generalized Rake receivers combine signals from multiple BS's to achieve macro BS diversity gain as shown in Fig. 2.1.

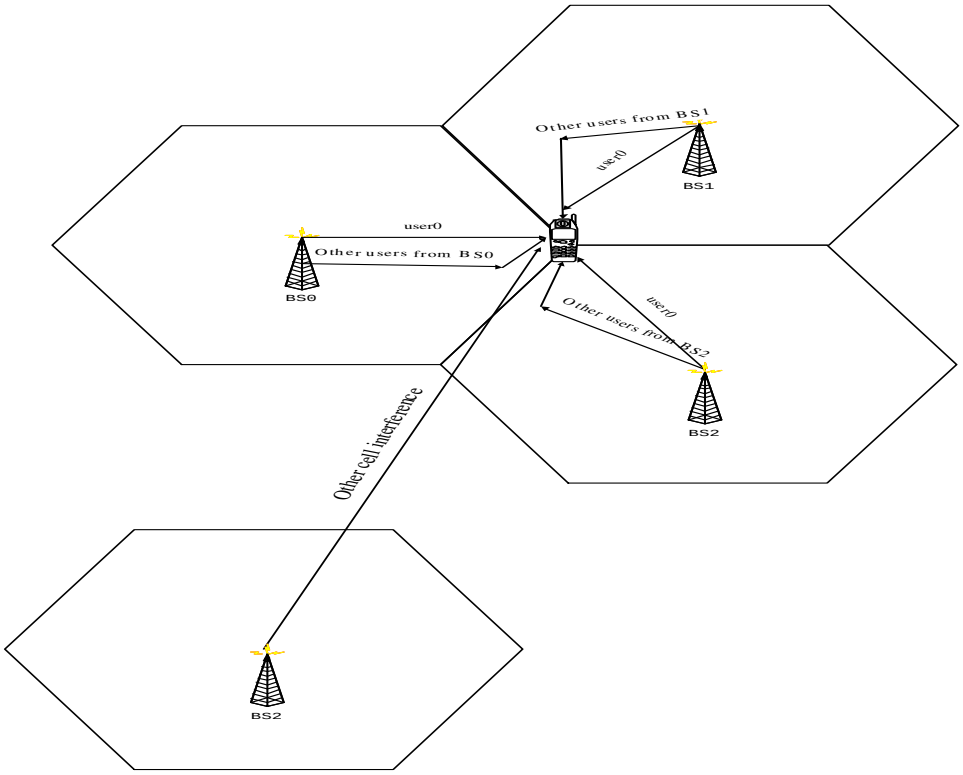

Figure 2.1 MS connected to multiple BS's.

The detailed structure of the generalized Rake receiver is shown in Fig. 2.2 and Fig. 2.3.

The principle of Rake receiver is the same for both the traditional Rake receivers and generalized Rake receivers. Each branch is tuned at different incoming signals. The

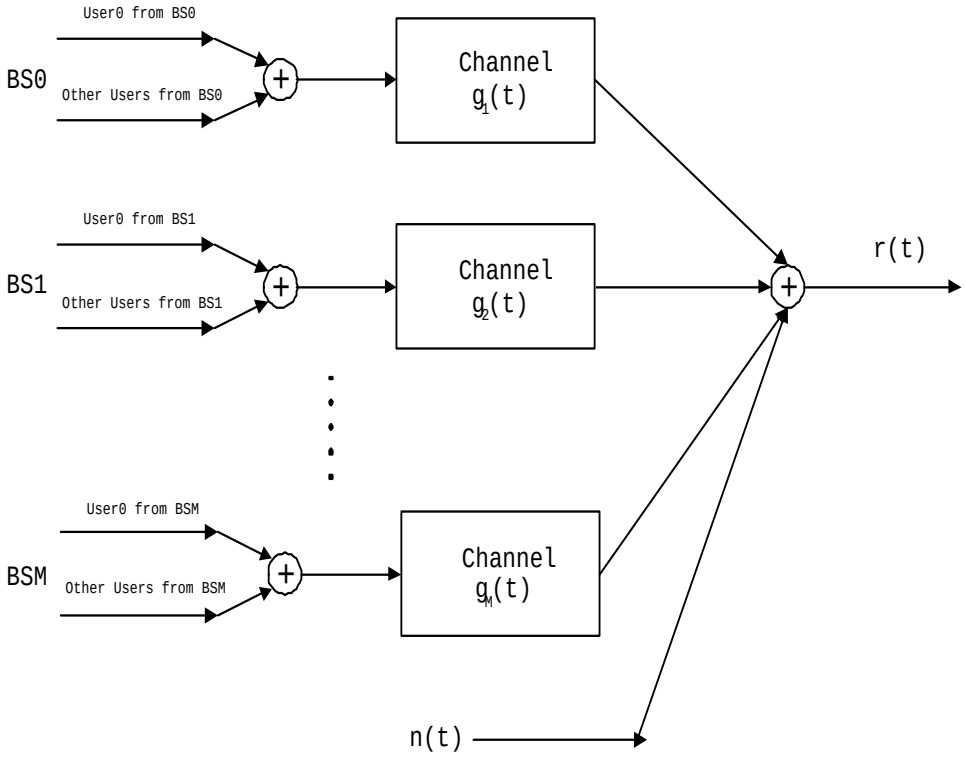

Figure 2.2 Signal at Receiver Input.

incoming signals are first multiplied with a specific weight and summed together. Suppose the signal and interference amplitude of the ith branch of the Rake receiver is a_i and b_i and the weight is w_i, then the output SIR at Rake receive is $\sum_{i=1}^{N} a_i w_i/(b_i w_i)$, where N is the total number of branches at Rake receiver. If w_i equals to the input SIR $(E_b/I_0)_i$ at branch i, the output SIR at Rake receiver reaches its maximum value and is given by $E_b/I_0 = \sum_{i=1}^{N}(E_b/I_0)_i$. The phase and amplitude of incoming signals are estimated using pilot channels in CDMA systems.

2.1.2 Generalized Rake Receiver

Wang and Bottomley [25] analyzed the generalized Rake receiver structure and discussed how to suppress both own-cell and other cell-interference in the forward link of

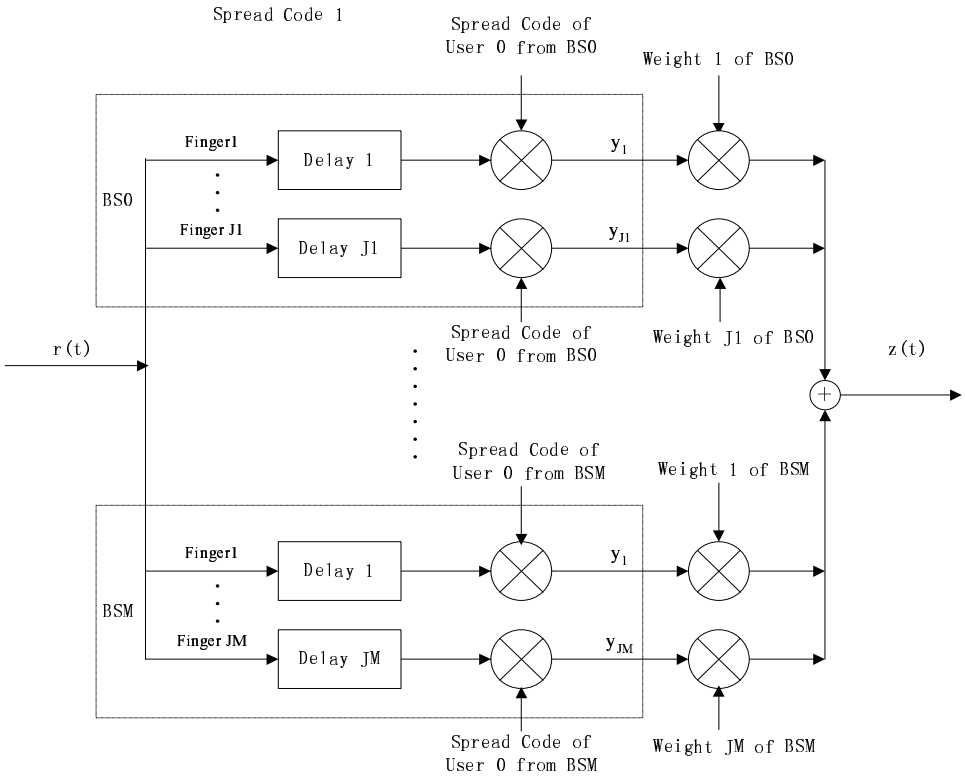

Figure 2.3 Generalized Rake Receiver Structure.

CDMA systems. Let us take BS_k as an example. Assume b_i is the i^{th} transmitted symbol and the corresponding shaping waveform is $b(t), 0 \leq t \leq T$, where T is the symbol chip duration of the symbol. Each symbol is spreaded by the PN sequence, which is expressed as $b(t) = \sum_{j=1}^{M} p_j p(t - jT_c), 0 \leq t \leq T$, where T_c is the chip rate, $p(t), 0 \leq t \leq T_c$, is the waveform of the PN sequence, p_j is the sign of the j^{th} chip, and each symbol contains M chips. Then the transmitted symbol $x(t)$ is

$$x(t) = \sum_{i=1}^{N} b_i b(t - iT) = \sum_{i=1}^{N} b_i \sum_{j=1}^{M} p_j p(t - iT - jT_c) \tag{2.1}$$

The multiple path channel can be characterized by a series of delays and is expressed as

$$h(t) = \sum_{f=1}^{F} a_f h(t - \tau_f) \tag{2.2}$$

where f is the f^{th} multipath, F is the total number of multipaths and a_f is the channel gain of the f^{th} multipath, which is called the fast fading or small-scale fading [2]. Usually, τ_f is chosen to be a multiple of chip duration, which means $\tau_f = fT_c$. Then, by assuming the path loss is l_k from BS_k, the received signal $r(t)$ at the MS is

$$r(t) = x(t)/l_i \otimes h(t) = \sum_{f=1}^{F} a_f x(t-\tau_f)/l_k = \sum_{f=1}^{F}\sum_{i=1}^{N} b_i a_f / l_k \sum_{j=1}^{M} p_j p(t-iT-jT_c-fT_c) \quad (2.3)$$

where $\otimes$ means the convolution operation.

At the receiver, the received signal $r(t)$ is first convolved with the corresponding PN sequence and then passes through a low-pass filter, which is essentially a matched-filter structure. The demodulated signal $y_q(t)$ of the u^{th} multipath of BS_k at time interval $[qT - \tau_u - T, qT - \tau_u]$, which equals to $[qT - uT_c - T, qT - uT_c]$ if $\tau_u = uT_c$, is expressed as

$$\begin{aligned}
r(t) &= \int_{qT-uT_c-T}^{qT-uT_c} \sum_{m=1}^{M} p_m p(t - qT - mT_c) y(t) dt \\
&= \int_{qT-uT_c-T}^{qT-uT_c} \sum_{f=1}^{F}\sum_{i=1}^{N} b_i \frac{a_f}{l_k} \sum_{m=1}^{M}\sum_{j=1}^{M} p_m p(t - qT - mT_c - uT_c) p_j p(t - iT - jT_c - fT_c) dt \\
&= \sum_{f=1}^{F} b_q a_f / l_k \int_{qT-uT_c-T}^{qT-uT_c} \sum_{m=1}^{M}\sum_{j=1}^{M} p_m p(t - qT - mT_c - uT_c) p_j p(t - qT - jT_c - fT_c) dt \\
&= \sum_{f=1}^{F} b_q a_f / l_k \int_{-T}^{0} \sum_{m=1}^{M}\sum_{j=1}^{M} p_m p(t - mT_c) p_j p(t - jT_c - (f-u)T_c) dt \\
&= \sum_{f=1}^{F} b_q a_f / l_k R_{f-u}
\end{aligned} \quad (2.4)$$

and

$$R_{f-u} = \int_{-T}^{0} \sum_{m=1}^{M}\sum_{j=1}^{M} p_m p(t - mT_c) p_j p(t - jT_c - (f-u)T_c) dt \quad (2.5)$$

where R_{f-u} is the correlation between the spreading sequence with fT_c delay and that with kT_c delay. If $f = k$, the demodulated data is completely demodulated and we get

the signal term as $b_q a_u / l_k$. If $f \neq k$, R_{f-u} can be viewed as a gaussian noise. The ratio of R_0/R_{f-u} is the spreading gain G.

2.2 Previous Work

2.2.1 Previously Work on the Expression of SIR

Wang and Bottomley [25] uses the following approach to obtain the SIR after passing the received signal through a decorrelator, which is essentially a multi-user detection scheme. Let $\vec{Y}$ be a vector consisting of outputs from all the fingers as $\vec{Y} = [\vec{y_1^T}, ..., \vec{y_{M'}^T}]$, where $\vec{y_i^T} = [y_1, ..., y_{Ji}]^T$ is a vector of outputs from fingers tuning at BS_i. Assuming $\vec{H}$ is the channel response and $\vec{U}$ is the interference term consisting of thermal noise, own-cell interference, and other-cell interference, the received signal $\vec{Y}$ is expressed as $\vec{Y} = \vec{H} * s0 + \vec{U}$, where $s0$ is the transmitted symbol. Further assume $\vec{U}$ is a vector of Gaussian noise with zero mean and covariance $\vec{R_u}$. The decision vector is $\vec{Z} = \vec{W}^T \vec{H}$. The maximum likelihood (ML) estimation of $\vec{W}$ is as follows

$$\vec{W} = \vec{R_u}^{-1} \vec{H}. \tag{2.6}$$

The SIR at the output of Rake receiver is shown to be

$$SIR = \frac{\vec{W}^T \vec{H} \vec{H}^T \vec{W}}{\vec{W}^T \vec{R}^u \vec{W}} \tag{2.7}$$

Substituting (2.6) into (2.7), the SIR is written as

$$SIR = \vec{H}^T \vec{R}_u^{-1} \vec{H} \tag{2.8}$$

and the bit error rate (BER) is given by

$$BER = 0.5 erfc(\sqrt{\alpha SIR}) \tag{2.9}$$

where $\alpha = 1$ for BPSK and $\alpha = 0.5$ for QPSK.

In the numerical results of their paper, two data sets are considered. The first data set is chosen to be IS-95 with a data rate of 19.2 kbps and spreading gain of 64. The second data set is 153.6 kbps for CDMA2000. Two kinds of Rayleigh fading channel are considered. The first consists of a single fading ray. The second consists of 3-ray with relative powers of 0, -1 and -2 dB and is generated using the classic Jake's model and a Doppler shift of 7 Hz. Different finger allocation schemes are discussed. The results show that the bit error rate of the generalized Rake receiver is less than that of the conventional Rake receiver. The improvement is based on the following observation: if strong interference from other BS's exist, the MS had better include this BS into the active set to achieve better SIR.

The deficiencies of their model are as follows

- No clear handoff model is used. The MS in SHM is defined as the MS connected to a single BS all the time without specifying the relative strength of received signals from different BS's. The results are obtained for the MS in NSHM and SHM separately.
- No path loss is specified (only Rayleigh fading is considered). Probably, it assumes that the path loss can be taken care of by using the perfect power-control that can ask BS to transmit exactly the inverse proportion to the path loss. However, in practical CDMA system, this is not the case, since the BS always sets a maximum power that can be allocated to the MS. If the BS allocates more power to the MS than the maximum power threshold, it means that the MS is in deep fading and it is better to drop the connection with the MS (or after a certain period) to guarantee the service of other MS's.
- If the path loss can not be neglected, then the above analysis will result into a large discrepancy from that observed in practical CDMA systems and the frame error rate will vary for MS's at different location in the cell.

- Owner-cell interference is neglected and the authors argue that coding is employed to combat the error caused by owner-cell interference. This is not the case in practical CDMA systems. One example is for MS near BS where owner-cell interference is a big factor.
- The other cell interference is modeled as a Gaussian noise. This is not true for CDMA systems and the only possible MS location is at the cell edge. Zhang and Aalo [27] showed analytically that the other cell interference follows Gamma distribution. It is also shown in [28] that the other-to-owncell interference ratio varies from 0.1 to 0.4.
- Rayleigh fading is modeled by a fixed decaying profile with 0, -1 and -2 dB losses. This can be improved by using more complex statistical model.
- Since the multi-user detection scheme is more appropriate to be used in the reverse link rather than in the forward link due to its computational complex, this multi-user technique is not practical in the forward link.

In summary, the statistical modeled used in the above paper [25] is more suitable for the reverse link rather than the forward link.

2.2.2 Previous Work on the Forward Link Capacity of Soft Handoff

Several studies have been conducted on the forward link capacity [1]. Let us look at one of the pioneer work done by Lee and Steele [1].

Assuming the fraction of BS power allocated to MS_k is ϕ_k and there are total M users in the cell, then $\sum_{k=0}^{M} \phi_k = 1$. The number of users M supported in the cell can be obtained by simulations [16]. However, analytical analysis is instructive to shed insight on this problem. In the paper [1], the fraction of BS power allocated to every MS is assumed to be constant and equals to $\phi = 1/M$, if the total used power of every BS

is assumed to be 1. Neglecting fast fading terms, the E_b/I_0 at the output of the Rake receiver tracking the multipath signals from BS_k is written as

$$\left(\frac{E_b}{I_0}\right)_k = \frac{G\phi/l_k}{((1-1/M)/l_k) + \sum_{n=1,n\neq k}^{N} 1/l_n}. \tag{2.10}$$

If multiple BS's are involved in the diversity and assume the active set is $N_{set} = \{BS_{N0}, BS_{N1}, \ldots, BS_{Nk}\}$, the E_b/I_0 at the output of the generalized Rake receiver is

$$\frac{E_b}{I_0} = \sum_{k=1}^{N}\left(\frac{E_b}{I_0}\right)_k = \sum_{k=1}^{N}\frac{G\phi/l_k}{((1-\phi)/l_k) + \sum_{n=1,n\neq k}^{N} 1/l_n}. \tag{2.11}$$

The average value of the E_b/I_0 is written as

$$\begin{aligned} E[\tfrac{E_b}{I_0}] &= \sum_{k=1}^{N} E[\left(\tfrac{E_b}{I_0}\right)_k] \\ &= E[\sum_{k=1}^{N} \tfrac{G\phi/l_k}{((1-\phi)/l_k)+\sum_{n=1,n\neq k}^{N} 1/l_n}] \ . \\ &\geq \sum_{k=1}^{N} \tfrac{G\phi}{1-\phi+E[\sum_{n=1,n\neq k}^{N} l_k/l_n]} \end{aligned} \tag{2.12}$$

The last inequality is obtained by using Jensen's inequality. By solving (2.12) for ϕ for a target E$[E_b/I_0]$ (7dB is chosen in that paper), the number of user supported at the a certain location in the cell is $M = 1/\phi$.

If MS is in diversity with two or more BS's, it occupies multiple channels and degrades system capacity. On the other hand, due to the macrodiversity combination gain, MS needs less BS power to maintain the target E_b/I_0, which increases system capacity. Two BS's in the active set are chosen to study the net system capacity in a certain location of the cell as shown in Fig. 2.4.

In Fig. 2.4, soft handoff is chosen to be a zone with distance 0.84 from BS_0. The results show that soft handoff capacity losses due to occupying multiple channels from BS's is 7.2%, but the capacity increase due to macodiversity gain is 7.0% for voice active factor (VAF) of 3/8 and 6.1% for VAF of 1/2. The net capacity losses are 0.2% and 1.1% respectively. Sectorization is also studied, the capacity losses due to utilizing multiple

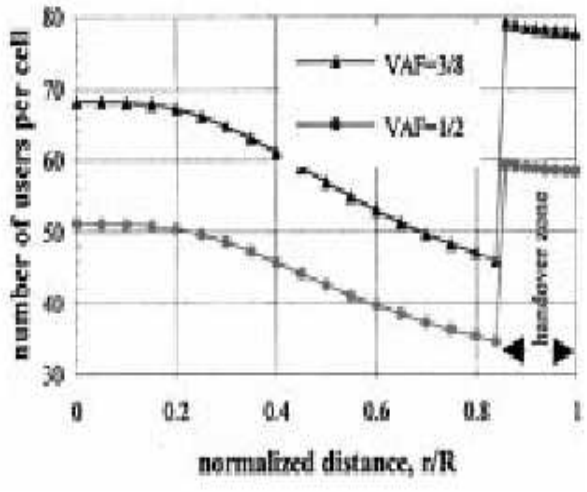

Figure 2.4 System capacity along the x-axis from BS_0 (Fig. 7 in [1]) .

channels is 9% but the capacity gain is 40%, which results into great improvement of forward link capacity of 31%.

The problems of the above calculations are as follows

- Power control is not considered, which is an essential part of the CDMA system. In a power-control CDMA system, MS tries to maintain a target E_b/I_0 (For example 7dB) even though the multipath fading exists. Therefore, the average in (2.12) is not appropriate in the 3G CDMA systems where SIR-based power control is deployed.
- Jensen's inequality is used in (2.12), the bound of which may be very loose.
- If the soft handoff can improve system capacity as shown in Fig. 2.4, then MS needs to be in soft handoff all the way to BS_0, which is not the case in real CDMA systems.
- The capacity gain is said to be limited when the MS is located at 0.84 from BS_0. The system capacity is said to be equal to the capacity of NSH at this intersection

point. According to Fig. 2.4, the MS in every point of the cell should be in soft handoff, which is not the case in practical CDMA system.

- Fast fading is neglected in the capacity evaluation. This results into a large discrepancy in the characterization of the SIR and thereby, affects the system capacity calculation, which is particular true for MS's at cell boundary as shown in Fig. 2.5 [29]. The fraction of power allocated to MS in Fig. 2.5 is $\phi = 0.1$.
- Outage is not addressed.

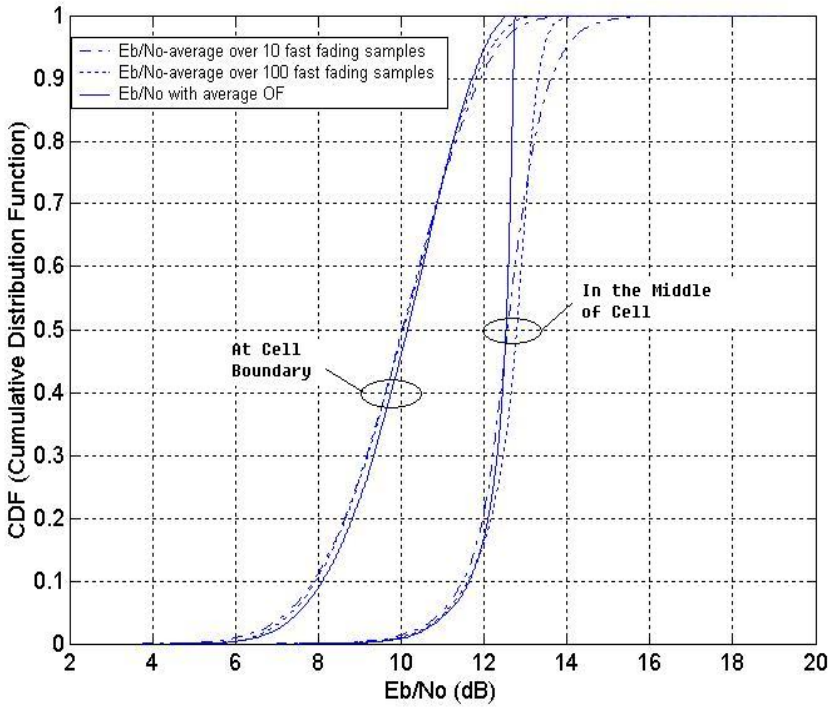

Figure 2.5 Difference between SIRs by using OF and averaging fast fading.

2.2.3 SIR Expression Considering Power Control Error

An excellent method in calculating E_b/I_0 considering fast fading is very instructive [27]. Neglecting path loss, the $(E_b/I_0)_k$ from BS_k can be written as

$$\left(\frac{E_b}{I_0}\right)_k = \frac{G\phi X_0}{X_0 P_{cek} + \sum_{n=1,n\neq k}^{N} P_{cen} X_n l_0/l_n} \tag{2.13}$$

where P_{cen} is the power control error of BS_n, which follows a lognormal distribution, X_k is the fast fading from BS_k following the Gamma distribution. In the paper, the interference terms are approximate using the average of Gaussian noise as

$$\left(\frac{E_b}{I_0}\right)_k = \frac{G\phi X_0}{M\exp(1/(2\sigma_e^2)) + Y} \tag{2.14}$$

where $Y = (\sum_{n=1,n\neq k}^{N} P_{cen} X_n l_0/l_n)/X_0$ follows the beta distribution of the second kind [27] (or the F-distribution [30]) and σ_e is the standard deviation of the Gaussian noise.

The bit error rate is obtained as

$$P_e = \int 0.5 erfc(\alpha \frac{E_b}{I_0}(y)) f_Y(y) dy \tag{2.15}$$

However, the following problems exist,

- Soft handoff is not considered and path loss with shadowing is neglected.
- Power-control is not considered, which can be seen from their approach to calculate the bit error rate.

2.3 Summary of Previous Work

In summary, even though the capacity and outage of forward link has been studied [1] [27], the current research on the CDMA forward link is far from enough due to the neglecting of the soft handoff threshold and multipath fading.

Furthermore, the 3G CDMA systems are designed to support both the high data rate and voice services after the successfully deployment of the 2G CDMA systems, such

as IS-95, to support mainly the voice service. The high data rate services embody the property of asymmetry, that is, the forward link is capacity-limited due to its high-volume traffic. The forward link performance of a CDMA system has been analyzed by treating the SIR E_b/I_0 as a random parameter taking all possible values in [1]. However, the SIR is considered to be a fixed value in a perfect power-controlled CDMA system or a random variable with a small variance in the presence of the power-control error [24]. Since the power allocated from the base station (BS) connected to the mobile station (MS) decides the amount of SIR achieved at the MS, it is more appropriate to evaluate the system performance from the viewpoint of the fraction of BS power allocated to a MS, which is the essence of the SIR-based fast power control in the forward link.

The SIR-based fast power control in the forward link is quite different from that in the reverse link. In the reverse link, the other cell interference can be well approximated by a Gaussian variable [19] [31]. However, in the forward link, the interference at the output of each branch of the Rake receiver was shown to be approximated by a Gamma variable by using the channel-gain-matched combining and assuming a perfect slow power control [27]. But the statistical property of the interference in a SIR-based fast power control is still unavailable for the the maximum ratio combining (MRC). The MRC is optimal in the sense of maximizing the total SIR at the output of the Rake receiver and the total SIR is the summation of the individual SIR's at the output of each branch of the Rake receiver. The analytical expression of the total SIR is complicated by using the MRC, since the signal term in one branch of the Rake receiver is treated as the interference in another branch. It was reported in the literature that when the MS is connected to only a single BS in the non-soft handoff mode (NSHM), the concept of the orthogonality factor (OF) can be used to simplify the total SIR expression into one term [32]. However, it is very complex to simplify the total SIR expression into one term for the MS communicating with multiple BS's in the soft handoff mode (SHM), since the soft

handoff threshold (SHT) truncates the strengths of both the signal and interference as discussed later. Therefore, due to this truncation, current models in the literature [33], are not applicable. The problem is further complicated by considering the unequal BS power, the power control error (PCE), the data rate, and the available Rake fingers in real CDMA systems. Computer simulation was the commonly used approach to obtain the BS power and estimate the blocking probability [34]. Recently, a Chernoff bound of the blocking probability was obtained in [35]. However, an exact closed-form expression of the blocking probability is still not available.

In addition, for simplicity, majority of the previous work studying the forward link performance assumes equal BS powers throughout the system [1] [35] [24] and a static capacity is obtained without considering the time-variant property of the interference caused by other-cells.

2.4 Proposed New Work

In order to obtain an exact forward link capacity, in this thesis, we introduce an analytical model to characterize the distributions of the base station power required by a single soft handoff set, a single mobile station, and all mobile stations in the cell in the forward link of a SIR-based power-controlled CDMA system, which leads to a closed-form expression of the capacity at specific outage and blocking probabilities. By considering real system parameters, such as the soft handoff threshold and the power control error, simulation results show that the statistics of the distributions of BS power experienced in the system are consistent with assuming that these probability densities can be used to characterize the BS power.

In the characterization of these distributions, multipath fading needs to be taken into account, which is often neglected in previous studied for the simplicity of analysis [1] [24]. Soft handoff is well-modeled in this thesis by considering the soft handoff

threshold (SHT). For a certain SHT, the MS connects to different soft handoff sets with different probabilities. In [36], we proposed an analytical model introducing the concept of macrodiversity non-orthogonality factor to simplify the SIR into one term for any MS connected to different soft handoff sets. Since the fraction of the BS power required by a MS is inversely proportional to the SIR, an analytical expression of the distribution of the BS power was derived. But the analysis in [36] is only limited to an identical multipath fading model and the reference BS must be the owner BS, which is the BS having the smallest path loss among BS's in the soft handoff set. By extending the model in [36] and considering the case when the reference BS is not the owner BS, we propose a unified approach to characterize the distribution of the fraction of BS power required by a MS communicating with any soft handoff set. The outage probability of a single MS, which is defined as the probability that the MS asks the BS to allocate more power than a maximum limit, can be obtained in a closed form. By multiplying the fraction of BS power required by every possible soft handoff combinations at the MS with the corresponding probability and summing them together, we manage to derive the average power required by a single MS. Further summing the fractions of BS power required from all the MS's in different locations around a specific BS, we derive the distribution of the BS power and therefore, a closed form of capacity is obtained at a certain blocking probability.

In addition, by considering the time-variant interferences, we propose an iterative process to determine the dynamic capacity in the CDMA systems. This iterative process is made simplified by using the closed-form expressions of the outage and capacity for certain outage and blocking probabilities.

By using these distributions, both the outage probability experienced by a single MS and the blocking probability experienced in the network can be expressed in closed-form expressions. By controlling the maximum fraction of BS power allocated to a single

soft handoff set at an individual MS to achieve a certain outage probability, the blocking probability can be related to the maximum number of MS's in the system. Therefore, our approach provides an efficient and analytical way to study the effects of the behavior of a single MS on other MS's and on the system performance. A fine control of the fraction of BS power allocated to a single MS in the level of soft handoff set is made possible, which provides a flexible and analytical approach to design an efficient call admission control algorithm. Our work is pioneer in the field of wireless communication systems to study the forward link power-controlled system performance from the viewpoint of BS power.

In summary, the new work proposed for this thesis includes the following:

1. Simplify the SIR expression into one term by proposing the concept of macro non-orthogonality factor for MS's in the soft handoff or non-soft handoff.
2. By using the simplified expression of SIR, we derive the distribution of the fraction of BS power for a single soft handoff set by a single BS.
3. By averaging all the soft handoff combinations available to a single MS, we derive the distribution of the BS power used by a single MS and thereby, a closed-form expression of outage probability experienced by a single MS.
4. By averaging all MS's supported by a specific BS, the distribution of the BS power consumed by all MS's is obtained and thereby, the closed-from expression of capacity is derived for certain outage and blocking probabilities.
5. A closed-form expression of capacity is obtained for certain outage and blocking probabilities.
6. An analytical iterative process to determine the dynamic capacity is proposed.

CHAPTER 3

The Mobile Radio Propagation Characteristics

Propagation models predicting the average received signal strength at a large distance (over several hundreds meters) from the transmitter are useful to estimate the coverage area of a transmitter and are called large-scale propagation models [2]. On the other hand, propagation models that characterize the rapid fluctuation of the received signals over short travel distances (a few wavelengths) or short time durations (on the order of seconds) are called small-scale fading models with amplitude fluctuation of 30 or 40 dB. The reason for the small-scale fading is the phase summation of different rays coming from the transmitter vary widely. The local mean of the local average received signal is computed by using the large-scale propagation model, which is taken average over received signals for 5λ or 40λ (corresponding to a distance of 1m to 10m in 1GHz or 2GHz band) [2]. For example, as the correlation between envelope samples follows the Bessel function of the first kind of zero order ($J_0^2(2\pi d/\lambda)$) and the uncorrelated sample distance is $d = 0.38\lambda$, at least 85 samples are needed to achieve a confidence interval of 90% for a standard deviation of 5.57dB of the lognormal distribution, which corresponds to 22λ [37].

3.1 Antenna Gain

The antenna gain is the ratio of the power radiated (or received) per unit solid angle by the the antenna in a given direction to the power radiated (or received) per unit solid angle by an isotropic antenna fed with the same power [18]. The maximum antenna

gain is in the direction of maximum radiation (the electromagnetic axis of the antenna, also called boresight) and equal to

$$G_{max} = 4\pi A_{eff}/\lambda^2 \tag{3.1}$$

where A_{eff} is the effective aperture area of the antenna. For an antenna with circular aperture or reflector of diameter D and geometric surface area $A = \pi D^2/4$, $A_{eff} = \eta$A. Therefore, (3.1) is rewritten as

$$G_{max} = \eta(\pi D/\lambda)^2. \tag{3.2}$$

The 3dB beamwidth is related to the ratio λ/D by $\theta_{3dB} = 70\lambda/D$ (in degree) for small angle. Then, (3.2) is rewritten as

$$G_{max} = \eta(\pi 70/\theta_{3dB})^2 \tag{3.3}$$

In direction θ with respect to the boresight, the gain is

$$G_\theta = G_{max}/10^{1.2(\theta/\theta_{3dB})^2} \tag{3.4}$$

For an isotropic antenna fed from a source of power P_t, the power radiated per unit solid angle is $P_t/4\pi$ for a ball with surface of 4π. For a direction with antenna gain G_t, the power radiated per unit solid angle is $G_t P_t/(4\pi)$. For a receiver antenna with effective area of A_{eff}, the received power is $P_r = A_{eff} G_t P_t/(4\pi R^2)$. As $A_{eff} = G_r/(4\pi/\lambda^2)$, the received power is

$$P_r = G_t P_t G_r(\lambda/4\pi R)^2 = \mid E \mid^2 G_r\lambda^2/(377 \times 4\pi) \tag{3.5}$$

where $\mid E \mid^2$ represents the magnitude of the radiating portion of the electric field in the far-field (in unit of Volt/meter).

The above model is called the Friis free space model to predict received power at the far-field of the transmitting antenna. The far-field (or Fraunhofer region) d_f of a transmitter antenna must satisfy the following three conditions

$$d_f = 2D^2/\lambda \tag{3.6}$$

$$d_f \gg D \tag{3.7}$$

$$d_f \ll \lambda \tag{3.8}$$

3.2 Basic propagation mechanism

Reflection, diffraction and scattering are the three basic propagation mechanisms [2]. Reflection occurs when a propagating electromagnetic wave impinges upon an object (surface of the earth, building or walls) with large dimensions when compared to the wavelength of the propagation wave. Diffraction occurs when the radio path between the transmitter and receiver is obstructed by a surface with sharp irregularities (edges). The second wave generated by diffraction can propagate into a shadowed region. Scattering occurs when objects with dimensions that are small compared to the wavelength and when the number of obstacles per unit volume is large.

For the 2-ray model (one LOS path and one path reflected from ground), the received power considering reflection can be expressed as

$$P_r = G_t P_t G_r (h_t h_r)^2 / d^4 \tag{3.9}$$

where h_t and h_r are the height of transmitter and receiver antenna, respectively. Note the loss decays with distance at the rate of 40dB, while the propagation model in free space decays at the rate of 20dB. This 2-ray model can be used to estimate the capacity of wireless systems.

The knife-edge obstruction blocking the LOS path is considered for the diffraction model. Scattering is measured by the surface roughness, which compares the incident

angle of arrival ray and the wavelength. The path loss models are classified into large-scale model and small-scale model.

3.3 Large-scale fading model

3.3.1 Path loss with distance

The average large-scale path loss at distance d from the transmitter is related to the distance as

$$P_l(d) \propto (d/d_0)^n \tag{3.10}$$

where $d_f \leq d_0 \leq d$ is the close-in reference distance and n is the path loss slope. d_0 is chosen to be 1m in indoor environments and 100m or 1km in outdoor environment. In most of the research, the path loss slope is chosen to be 4.

3.3.2 Lognormal shadowing

Measurements have shown that the path loss at any given distance is random and distributed lognormally (normal in dB) [19]. The path loss l_i from BS_i is expressed as $l_i = r_i^u 10^{x_i/10}$, where r_i is the normalized distance from BS_i to the MS (normalized to the cell radius), u is the path loss slope with a typical value of 4, and x_i is a Gaussian random variable with zero mean and σ standard deviation with a typical value of 8 dB. The path loss can be expressed in dB as

$$L_i = 10\log_{10} l_i = 10\log_{10}(r_i^u 10^{x_i/10}) = M_i + a\xi + b\xi_i \tag{3.11}$$

where $M_i = 10u\log_{10}(r_i)$ and x_i is expressed as the weighed summation of two independent Gaussian random variables ξ and ξ_i with identical zero mean and σ standard deviation to account for correlation effects. Signals from different BS's are assumed to have the same correlation coefficient of $E[x_i x_j]/\sigma^2 = a^2$, $i \neq j$ if we limit $a^2 + b^2 = 1$.

3.4 Small-scale fading model

Small-scale fading is classified into flat fading and frequency selective fading with the following characteristics:

- Flat fading: Multiple rays from a symbol arrive in one time slot, which results in a distortion of received signals. The spectrum of the channel is almost flat at the range of signal spectrum and the signal in time domain experiences insignificant spreading.
- Frequency selective fading: Multiple rays from a symbol arrive at different time slots. The spectrum of the channel causes significant distortion of signal spectrum and therefore, the time spreading of signals is obvious and results in ISI.

In both cases, received signals experience fading (or distortion) due to the Doppler shift. If the Doppler shift is significant compared to the RF spectrum of signal, the received signals experience fast fading. On the other hand, for a smaller Doppler shift compared to RF spectrum, the received signal experiences slow fading. For CDMA system, slow fading is expected at a large RF bandwidth.

When a single ray is received with amplitude a and phase θ (anti-clockwise from the direction of the travel of the car) at time t and amplitude a and phase $\theta + d\theta$ at time $t + dt$, the distance traveled by the car at this time interval is $dl = v \times dt \cos\theta$, where v is the speed of the car as shown in Fig. 3.1. The phase change of the received signal is therefore $d\phi = 2\pi dl/\lambda = 2\pi v \cos\theta dt/\lambda$, which is equal to a frequency shift of $df = \cos\theta d\phi/(2\pi dt) = \cos\theta f_c v/c$, where c is the speed of light equal to $3 \times 10^8 m/s$, v is the vehicle speed, and f_c is the carrier frequency. The maximum Doppler shift f_m is equal to $f_m = f_c v/c$. Fig. 3.2 shows the maximum Doppler frequency shift for different vehicle speeds and carrier frequencies. The higher the carrier frequency and vehicle speed, the larger the frequency shift is.

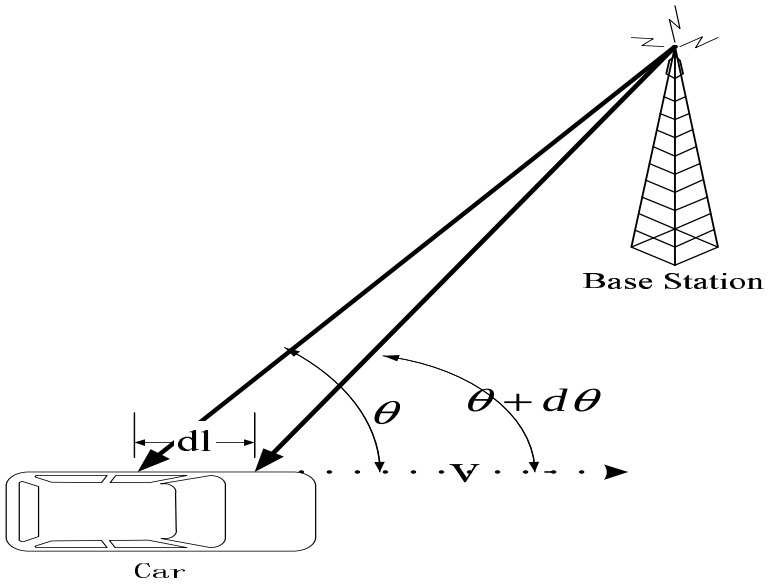

Figure 3.1 Concept of doppler shift.

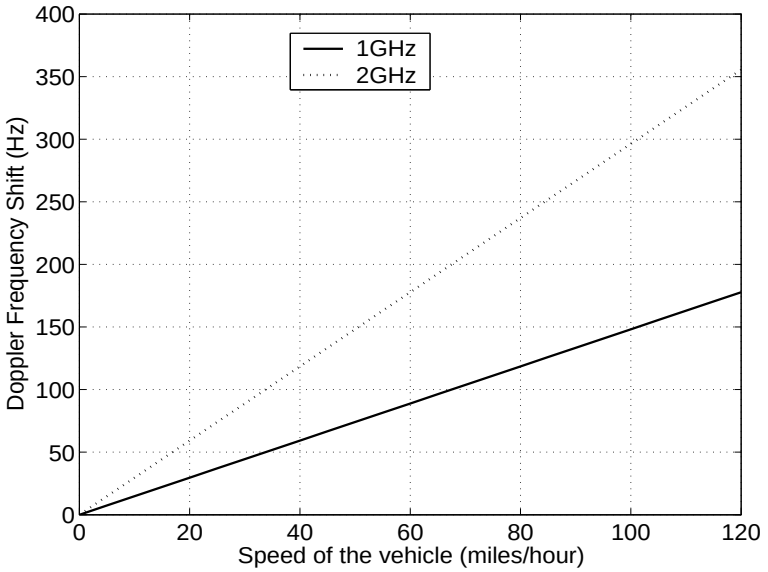

Figure 3.2 Simulation of doppler shift.

The correlation of received signals can be expressed as $R(dt) = J_0(2\pi d/\lambda) = J_0(2\pi v \cos\theta_m \frac{dt}{\lambda}) = J_0(2\pi df \times dt)$, where $J_0(z) = \frac{1}{\pi}\int_0^{\pi} \cos(z\sin\theta)d\theta = \frac{2}{\pi}\int_0^{\pi/2} \cos(z\sin\theta)d\theta$ is the Bessel function of the first kind of zero order [38, pg. 69]. Fig. 3.3 shows the correlation between symbols for different vehicle speeds and carrier frequencies at data rate of 10 ksps. The number of symbols with correlation greater than 0.5 is 80 for a walking speed of 10 miles/hour and is only 10 for a vehicle with a high speed of 90 miles/hour in a PCS system operating at 2GHz and data rate of 10 ksps. For data rate of 20 ksps, the number of symbols above the same correlation value is 2 times of that of 10 ksps. So there are 10 symbols available to estimate the channel characteristics for a vehicle traveling with a speed of 90 miles/hour at a central carrier frequency of 2GHz.

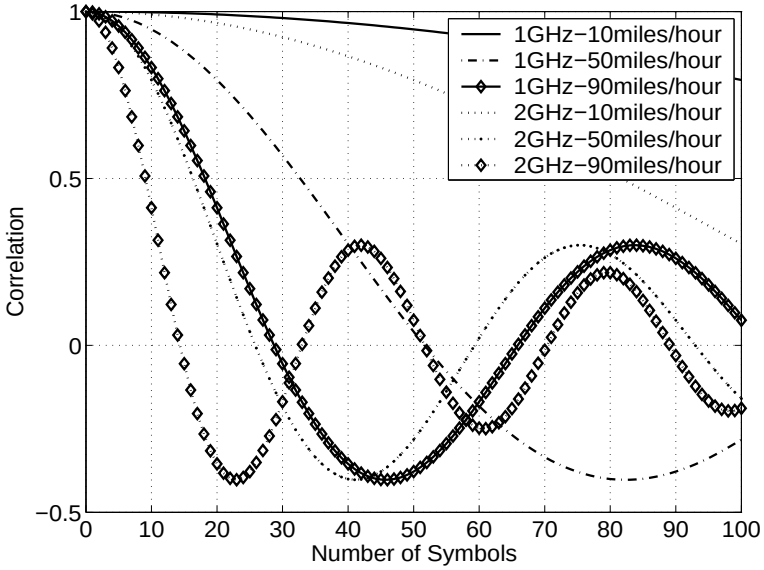

Figure 3.3 Symbol correlation for data rate=10ksps.

Assume that $x_b(t)$ is the baseband transmitted signal and $h_d(d,t)$ is the baseband channel impulse response at position d. The baseband received signal is expressed as

$$y_b(d,t) = x_b(t) \bigotimes h_b(d,t) = \int_{-\infty}^{t} x_b(\tau) h_b(d, t-\tau) d\tau \tag{3.12}$$

Let us denote τ_0 as the time delay of the first arriving multipath component and $\tau_i = i\Delta\tau$ as the i^{th} excessive delay, then the frequency resolution of the multipath is $1/2\Delta\tau$. h_b is expressed as

$$h_b(d,t) = x_b(t) \bigotimes h_b(d,t) = \int_{-\infty}^{t} x_b(\tau) h_b(vt, t-\tau) d\tau \tag{3.13}$$

where v is the speed of the vehicle. Since $h_b(vt, t-\tau)$ is a function of t and τ, $h_b(vt, t-\tau)$ can be written as

$$h_b(t,\tau) = \sum_{i=0}^{N} a_i(t, \tau_i(t)) exp[j(2\pi f_c \tau_i(t) + \phi_i(t, \tau_i(t)))] \delta(\tau - \tau_i(t)) \tag{3.14}$$

where $a_i(t,\tau)$ and $\tau_i(t)$ are the real amplitudes and excess delays at time t respectively. During a specific time, we drop the parameter t and absorb the uniformly distributed phase ϕ into a_i, the channel response at time t is written as

$$h_b(\tau) = \sum_{i=0}^{N} a_i exp[j(2\pi f_c \tau_i)] \delta(\tau - \tau_i) \tag{3.15}$$

where a_i follows the Rayleigh distribution.

3.4.1 Clarke's model for flat fading

As stated above, the frequency shift of incident ray arriving at the receiver with an angle of θ is $df(\theta) = \cos\theta d\phi/(2\pi dt) = \cos\theta f_c v/c$ and the corresponding gain is $G(\theta)$. Then, the received power is $P_r = \int_0^{2\pi} G(\theta) p(\theta) d\theta$. Assume the power spectrum of the received signal is $S(f)$, then we have $S(f) \mid df \mid = [p(\theta)G(\theta) + p(-\theta)G(-\theta)] \mid d\theta \mid$ and

$$S(f) = \frac{[p(\theta)G(\theta) + p(-\theta)G(-\theta)]}{f_m \sqrt{(1 - (\frac{f}{f_m})^2}}, |f| \leq f_m \tag{3.16}$$

The fourier transform of $\frac{1}{2\pi f_m \sqrt{(1-(\frac{f}{f_m})^2}}$ is $J_0(2\pi f_m \tau)$ [37]. Clark's model is a 2-dimension model, where received waves are assumed to be in the horizonal direction.

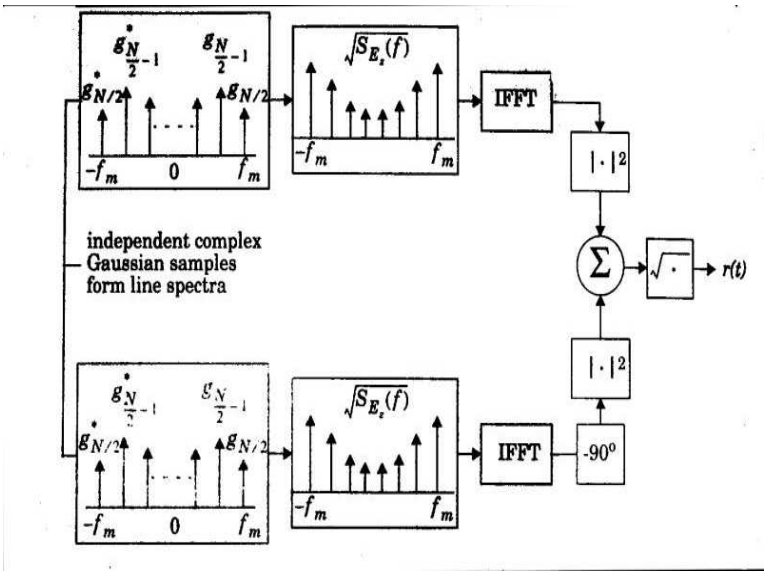

Figure 3.4 Simulation of Rayleigh fading.

Clark's model is commonly used to generate Rayleigh fading [2, page 181-185], the flow chart of which is shown in Fig. 3.4.

The problem of the above simulation approach is its time resolution. For example, for the doppler shift of $f_m = 100Hz$, the time resolution if only $1/(2 * fm) = 5ms$. However, the first zero cross point of $J_0(2\pi x) = 0$ is $x = 0.38$, which corresponding to $\tau = 0.38/100 = 3.8ms$ or a distance of $0.38\lambda = 5.7cm$ for frequency of 2GHz. Generally, as the time resolution of fading samples is greater than the first zero cross point of $(\tau = 1/2f_m > 0.38/f_m)$, this approach can not resolve the smaller time interval, which is shown in Fig. 3.5 and Fig. 3.6. If the time resolution is not good (larger than $0.38/f_m$), the output amplitude will vary rapidly as the correlation between samples is low.

An improvement of the above approach is to extend the frequency range over the maximum doppler shift f_m, which can resolve more accurately in the time domain. However, the disadvantage of this approach is its inability to simulate small time duration

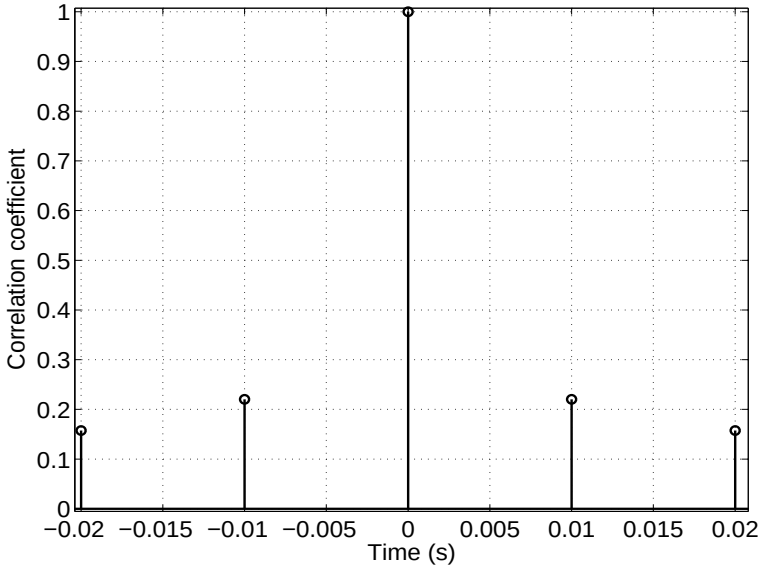

Figure 3.5 Correlation of gaussian samples (sample interval=10ms).

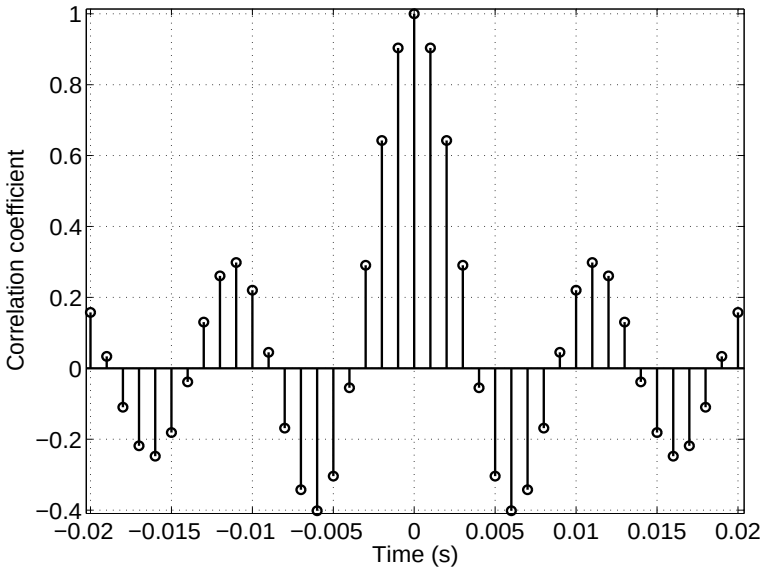

Figure 3.6 Correlation of gaussian samples (sample interval=1ms).

or low frequency resolution. As the period to simulate in the time domain is small, the frequency interval that the approach can resolve is large.

The second approach to simulate the Rayleigh fading is to filter the quadrature gaussian samples through a filter constructed from the fast fourier transform (FFT) of $J_0(2\pi f_m \tau)$. By using this method, one snapshot of Rayleigh samples of duration 200ms for doppler shift of 100Hz is shown in Fig. 3.7, where level cross rate is 24.6446 crossings per period and average fade duration is 0.4 ms for normalized level 0.1 (-20dB normalized to the local RMS amplitude of the fading envelop). The level crossing rate is defined as the number of positive-going direction crossing a specified level in a specified time. The average fade duration is defined as the average period of time for which the received signal is below a specified level [2]. The disadvantage of this approach is that it will result in jitter in the FFT transformation as the truncation of Bessel function in the time domain.

The third method is using Jake's approach, where a series of oscillators are used to produce the channel samples [38, page 67-76].

3.4.2 Suzuki distribution

Large-scale fading follows the lognormal distribution and small-scale fading is usually modeled as the Rayleigh fading. In order to transit from the local distribution (Rayleigh fading) to the global distribution of the path strength [39], Suzuki proposed a mixed distribution, which assumes the average of local fading follows the lognormal distribution. Denote the pdf of Rayleigh fading R.V. x as

$$f(x) = \frac{x}{\sigma^2} \exp(-\frac{x^2}{2\sigma^2}) \tag{3.17}$$

then mean of x is $E[x] = \sigma\sqrt{\pi/2}$ and $E[x^2] = 2\sigma^2$.

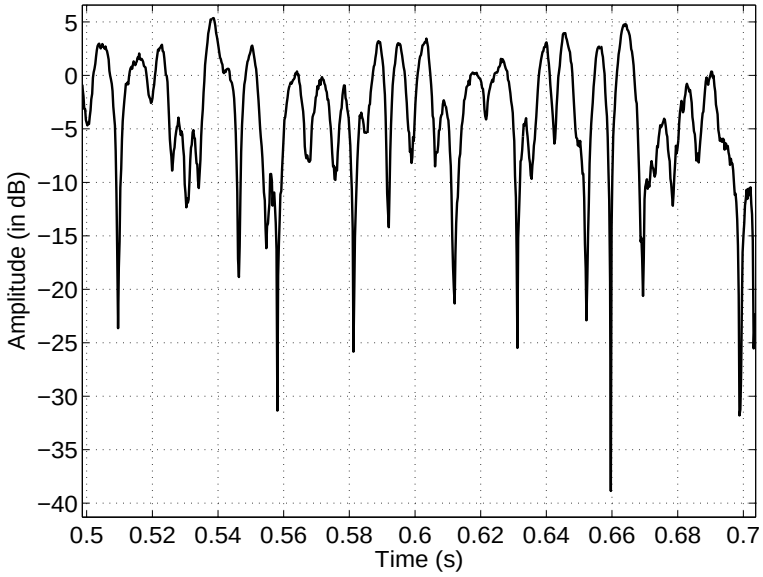

Figure 3.7 Rayleigh samples (doppler shift is 100Hz).

The pdf of lognormal R.V. y (assume y is the envelope, $20\log_{10} y$ follows a Gaussian distribution with zero mean and λ standard deviation) is expressed as

$$f(y) = \frac{20}{\ln(10)\sqrt{2\pi}\lambda y}\exp(-20\log_{10}(y)/2\lambda^2). \tag{3.18}$$

The Suzuki distribution $z = xy$ (x and y are independent) can be obtained as

$$f(z) = \int_0^{+\infty} f(z|y)f(y)dy = \int_0^{+\infty} \frac{z}{y^2\sigma^2}\exp(-\frac{z^2}{y^2\sigma^2})\frac{20}{\ln 10\sqrt{2\pi}\lambda y}\exp(-20\log_{10}(y)/2\lambda^2)dy \tag{3.19}$$

In the Suzuki distribution, the lognormal path loss is due to the multiple reflection and/or diffractions along the path from transmitter to receiver. After the signal arrives at the local cluster, the signal path breaks into local subpaths due to scattering from local objects. The subpaths all arrive at the receiver with roughly the same delay, but with different carrier phase, which results the small-scale fading (for example, the Rayleigh fading) [39]. In our research, the power of Rayleigh fading ($E[x^2]$) is chosen to be equal to 1, which corresponds to $\sigma = 0.707$. λ is chosen to be 8 (in dB).

The square of the envelop is the power of signal, which is $z^2 = x^2y^2$. Then x^2 follows a Gamma distribution and $10\log(y^2)$ follows a Gaussian distribution with zero mean and λ standard deviation.

3.4.3 Delay Spread Model

As discussed before, the channel received a series of replica of the original transmitted signal under multipath fading. The channel impulse response of received signal powers can be written as

$$h_b(\tau) = \sum_{i=0}^{N} \alpha_{ki}\delta(\tau - \tau_i) \tag{3.20}$$

where α_{ki} is the amplitude of the i^{th} multipath component from BS_k, which is usually modeled by the Rayleigh fading. $X_{ki} = |\alpha_i|$ is the power of the i^{th} multipath component from BS_k, and τ_i is the delay of the i^{th} multipath.

As shown in Fig. 3.8, without loss of generality, we order the received multipath components according to their power $|a_i|^2$. Every multipath component is independent of each other and the average power delay is exponentially distributed as shown in dot line in Fig. 3.8.

The root mean square (RMS) of the delay spread (DS) is the commonly used parameter to measure the dispersion of the received multipath components and is given by

$$\tau_{rms} = \left(\bar{\tau^2} - \bar{\tau}^2\right)^{1/2} = \left(\frac{\sum\limits_i |a_i|^2\tau_i^2}{\sum\limits_i |a_i|^2} - \left(\frac{\sum\limits_i |a_i|^2\tau_i}{\sum\limits_i |a_i|^2} \right)^2 \right)^{1/2} \tag{3.21}$$

Typical value of the RMS of the DS is given in Table 3.1 [2, page 162]:

The delay spread model affects the distribution of the E_b/I_0 and should be chosen carefully [40]. Recently, the Greensteins model [41] was proposed to characterize the

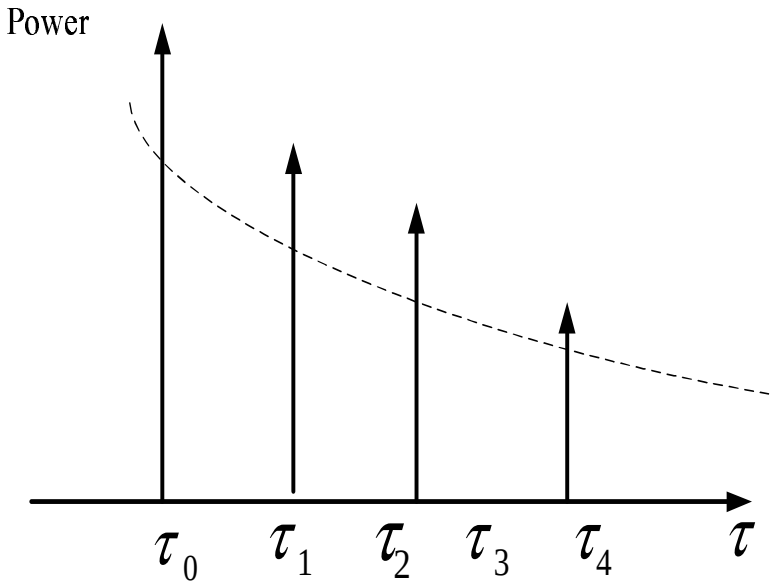

Figure 3.8 Delay Spread Model.

Table 3.1 Typical Values of RMS Delay Spread

Environment	Frequency (MHz)	RMS Delay Spread
Urban	910	1.3 μs
Suburban	910	200 ns avg. typical case 200 ns avg. extreme case
Indoor	1900	$70 - 94ns$ average $1470ns$ max.

delay spread (DS) and adopted in the COST259 radio channel model [40]. The root mean square (RMS) of the DS at distance d from the BS is expressed as

$$\tau_{rms} = T_1 d^{\epsilon} y \tag{3.22}$$

where T_1 is the median DS at distance 1km, ϵ is an exponent of the distance, and y is a random variable following a lognormal distribution. $10\log_{10}(y)$ follows the gaussian distribution with zero mean and σ_y standard deviation.

The average power delay profile (PDP) of the multipath components from a given BS is exponential distributed as [16, page 244] [42]

$$p(\tau) = \exp(-\tau/\tau_{rms})/\tau_{rms} \tag{3.23}$$

In [41] [43], the average value of the median of the DS over the whole cell area was studied and used to estimate the number of Rake receiver fingers to be assigned in order to track a given percentage of total multipath power. For the simplification of the simulation, in this chapter, we propose to use the average RMS value of the DS as

$$\tau_{avg} = E[\tau_{rms}] = T_1 d^{\epsilon} E[y] = \exp\left(\frac{(\sigma_y \ln 10/10)^2}{2}\right) T_1 d^{\epsilon} \tag{3.24}$$

For the urban area, T_1 can be chosen to be 0.5 μs, ϵ is chosen to be 0.5, and σ_y is set to be 4 dB [40] [41]. For the parameters chosen above, $\tau_{avg} = 1$ μs at a typical BS-to-BS distance $d = 1.5$ km [40], which is in the range of the values listed in [2, page 162]. Assume that $\tau_i = iT_c$, where τ_i is the delay of the i^{th} multipath and T_c is the chip duration of the spread code. By using (3.23) and assuming that the first multipath from BS_k has the average power of $E[X_{k1}]$, we know that the average power of the i^{th} multipath is $E[X_{ki}] = E[X_{k1}]\exp(-(i-1)T_c/\tau_{avg})$ [40] [44]. By summing the energies of all the multipath components and assuming the number of multipath is large, the total average power that the Rake receiver can track is $E[X_{k1}]/(1-\exp(-T_c/\tau_{avg}))$. Therefore, the i^{th} path can track $\exp(-(i-1)T_c/\tau_{avg})/(1-\exp(-T_c/\tau_{avg}))$ fraction of total average power. It was reported in [44] that the Rake receiver can deploy 4 fingers to track most of the power from a BS. Our simulation results show that the Rake receiver can deploy 4 fingers to track about 80 % of the total received average power for a chip rate of 3.84 $Mcps$[1] at the cell boundary and about 90 % in the middle of the cell. If two or more BS's are in the soft handoff set, we expand the total number of fingers in the Rake receiver to 6 in order to track most of the multipath energy from BS's in the soft handoff set.

[1] cps: chip per second

In this thesis, we assume that the power X_{ki} of the i^{th} multipath from BS_k has i.i.d gamma distribution with probability density function (PDF) $f(x) = c^b x^{b-1} e^{-cx}/\Gamma(b)$, $x \geq 0$ [45], which is denoted as $Gamma(b, c)$. $\Gamma(b) = \int_0^\infty x^{b-1} e^{-x} dx$ is the complete gamma function and equals to $(b-1)!$ for integer b. In order to normalize the total average power to be 1, we first generate a Gamma variable X'_{ki} with a distribution of $Gamma(\rho, \rho)$, then we multiply it with $[1 - \exp(-T_c/\tau_{avg})] \exp(-(i-1)T_c/\tau_{avg})$. Therefore, the total average power of all the multipath components $E[X_k]$ is normalized to 1. Particularly, in this chapter, by assuming that the non-line of sight (NLOS) exists between the BS and MS, α_k^i is Rayleigh distributed and $\rho = 1$.

CHAPTER 4

The Distribution of BS Power with an Owner BS

4.1 Overview

Most of the previous studies on the forward-link CDMA system performance neglect the fast power control, which is crucial to improve the system capacity in the third generation CDMA systems. In the forward link of an SIR-based fast power-controlled CDMA system, the fraction of BS power allocated to a MS acts as a key factor affecting the system performance. This fraction is different when the MS combines different number of multipath components from a single BS in the non-soft handoff mode (NSHM) or multipath components from multiple BS's in the soft handoff mode (SHM). This chapter establishes a unified analytical model to characterize the distribution of the fraction of BS power allocated to a MS in either the NSHM or SHM when the reference BS is the owner BS. By using that distribution and limiting the maximum fraction of BS power, the capacity can be obtained by a simple integral and the outage is calculated by the incomplete Beta function. Therefore, the model provides an easy and effective way to investigate the effects of system parameters, such as the number of resolvable multipath components, the available Rake fingers, the soft handoff threshold, any unbalance in BS power, the power control error, and the data rate, on the system outage and capacity from the viewpoint of the limitation of the fraction of BS power allocated to a MS.

Our analysis of outage probability of any MS and capacity of soft and non-soft handoff shows that the non-soft handoff is the primary cause of outage. We also show that soft handoff does not always improve capacity and the capacity gain may result depending on the choice of the maximum fraction of base station power, the available

Rake fingers, and the soft handoff threshold. The model is also used to compare the performance of the wideband CDMA and multicarrier CDMA systems and show how to adjust the fraction of BS power to obtain a certain outage.

4.2 Introduction

Since the the fraction of BS power allocated to any MS is inversely proportional to SIR achieved at the MS, we propose a novel approach to approximate the summation of the total SIR into one term for any MS and validate its accuracy by using the Kolmogorov-Smirnov (KS) test [46]. This approach of simplifying the total SIR into one term leads to a simplified analytical expression of the fraction of BS power allocated to any MS, which is further approximated by a function of the ratio of two Gamma variables. Thereby, the the capacity is calculated by a simple integral and the outage is obtained by the incomplete Beta function.

This model provides a theoretical base to study if a capacity gain is achievable in the case of the soft handoff (SH). It was shown that the sot handoff can provide less outage than the non-soft handoff (NSH) does in both the reverse link [19] and the forward link [24]. We show in this chapter that the inconsistency is resulted because of some of the important system parameters, such as the multipath fading, number of available Rake fingers and the soft handoff threshold, are neglected. By using our proposed model, we show that the possible capacity gain depends on the choice of the maximum fraction of base station power allocated to the MS, the available Rake fingers, and the soft handoff threshold.

By changing the delay spreading, we manage to model the CDMA systems in a general case, which is exemplified by comparing the system performance of the WCDMA and multicarrier CDMA (MC-CDMA) in the CDMA 2000. The flexibility and strength of our proposed model is further illustrated by taking into account the strong interference

caused by the temporary failure of resolving the signals from BS's in soft handoff with a MS or the limitation on the number of fingers in the Rake receiver in the real CDMA systems. In addition, the design approach to obtain a target outage probability by choosing the appropriate maximum fraction of BS power is also addressed.

This chapter is organized as follows: section 4.3 describes the soft handoff model and shows how to use the path loss considering shadowing and relative SHT to classify the MS's into the SHM or the NSHM. Section 4.4 shows how to simplify the summation of E_b/I_0 at the output of the Rake receiver into one term for the MS in either the SHM or NSHM. Since the fraction of BS power is inversely proportional to the E_b/I_0, section 4.5 derives the expression of the fraction of BS power and show how to obtain the capacity and outage by using the result in section 4.4. Section 4.6 gives the numerical results and shows how the system parameters, such as the PCE, the maximum limitation on the fraction of BS power allocated to a MS, the soft handoff threshold, the availability of the Rake fingers, the variable data rates, affect capacity and outage. Section 4.9 summarizes the chapter.

4.3 System model

A 13 hexagonal cell cluster in Fig. 4.1 is considered to study the system performance and minimize the edge effect, which is caused if the BS's are not distributed symmetric around the MS. The MS's inside the triangle are sufficient to model the performance of the cell due to symmetry [19].

4.3.1 Soft Handoff Model

Soft handoff is a key technology used in CDMA communication systems to achieve smoother transition when a mobile station (MS) moves from one base station to another. CDMA systems like IS-95 use a "make before break" soft handoff method to transfer

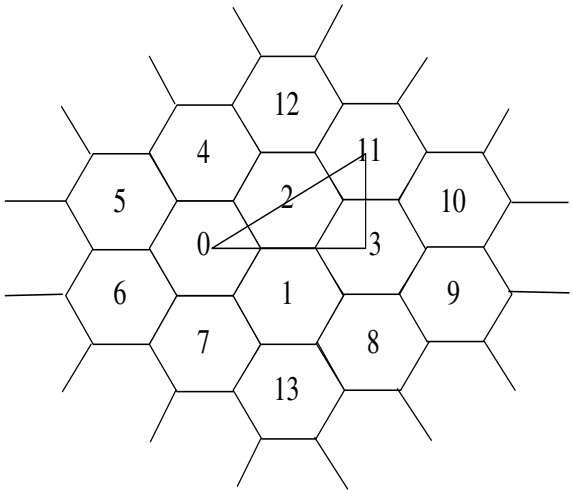

Figure 4.1 Hexagonal cell placement.

calls. Lee and Steele proposed a soft handoff model using a deterministic approach, which divided the cell into a soft handoff zone (SHZ) and a non-soft handoff zone (NSHZ) [1]. The NSHZ is the area around the owner BS within a radius less than a certain distance. The MS in the NSHZ is only connected to the owner BS. The SHZ is the rest of the cell area and the MS in the SHZ must connect to multiple BS's. This approach was adopted by a large number of studies due to its simplicity [24] [23] [47]. Uc-Rios and Lara-Rodriguez suggested that shadowing in the path loss should be considered to obtain a flexible location of the boundary of the NSHZ and more accurate capacity calculations [23]. In this chapter, we extend the approach proposed in [23] to establish a soft handoff model to select the BS's into the active set. The active set is the set of BS's that the MS is likely to communicate with and require power from. The proposed approach can model any number of BS's in the active set and the 2-BS soft handoff is just a special case. By using our proposed model, we can determine that the MS in the SHZ can connect to a single BS with a certain probability and vice versa.

Our proposed model is established as follows (referring to Fig. 4.2): first, if the fraction of BS power allocated to a MS from different BS's is assumed to be same in the

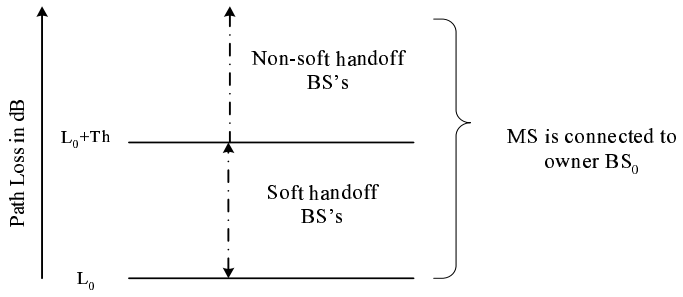

Figure 4.2 Soft handoff model (owner BS_0).

forward link of a power-controlled CDMA system, the normalized path loss can be used to define the owner BS_0 as the one having the smallest path loss [19]. Second, if the path loss of a BS exceeds that of the owner BS_0 by less than Th dB, that BS is put in the active set. Th is the SHT and can take values up to 6 dB [23]. If the path loss of a BS exceeds that of the owner BS_0 by more than Th dB, that BS is not in the active set. Third, if any other BS has path loss less than the current owner BS_0, the owner BS is changed to that BS. The MS is always connected to the BS's in the active set if there are enough Rake fingers, and the active set always includes the owner BS.

The definition of owner BS in the forward link is similar to that in the reverse link. Because the owner BS has the lowest path loss and due to the symmetry of propagation [16, page 199], the signal received at the owner BS from the MS is the strongest one. Therefore, the owner BS is more likely to be the power-control BS for the MS in the reverse link [48].

4.3.2 Soft handoff and Non-soft Handoff Probabilities

Assume the active set is $N_{set} = \{0, i_1, i_2, ..., i_M\}$, $i_k \in \{1, 2, \ldots, N\}$, where N is the total number of BS's taken into consideration (referring to Fig. 4.1, N is 13 in our cell cluster structure). By using the path loss model in the previous chapter and the

definition of the SH and NSH in section 4.3.1, the probability of SH with active set N_{set} is derived as

$$\begin{aligned} P\{SH\ with\ N_{set}\} =& P\{L_0 < L_i < L_0 + Th, L_j > L_0 + Th, i \in N_{set}, i \neq 0, j \notin N_{set}\} \\ =& E_z[\prod_{\substack{i \in N_{set} \\ i \neq 0}} \{Q(z + c_{1i}) - Q(z + c_{2i})\} \prod_{j \notin N_{set}} Q(z + c_j)] \end{aligned} \tag{4.1}$$

where $c_{1i} = (M_0 - M_i)/(b\sigma)$, $c_{2i} = (M_0 - M_i + Th)/(b\sigma)$, $c_j = (M_0 - M_j + Th)/(b\sigma)$, Th is the SHT, $Q(z) = \int_z^{+\infty} \frac{1}{\sqrt{2\pi}} \exp(-x^2/2)dx$, and $E_z\{.\}$ is the mean value evaluated by assuming that z is a Gaussian random variable with zero mean and a unit standard deviation.

By using (4.2) and setting $N_{set} = \{0\}$, the probability that the MS is in the NSHM and connected only to the owner BS_0 is

$$P\{NSH\} = P\{L_0 + Th < L_i, i = 1, 2, \cdots, N\} = E_z[\prod_{i=1}^{N} Q(z + c_i)] \tag{4.2}$$

where $c_i = (M_0 - M_i + Th)/(b\sigma)$.

4.4 A Unified Approach to Express the Signal-to-interference Ratio

In the above section, the soft handoff model was established to select the BS's into the active set of a MS. Knowing the active set, the Rake receiver at the MS combines the multipath signals from the BS's in the active set to achieve macrodiversity gain. The MRC was adopted in the literature [1] [42] to obtain an optimal combination of received signals. By using the MRC, the total E_b/I_0 at the output of the Rake receiver is a sum of the individual E_b/I_0's at the output of different branches of the Rake receiver.

In real CDMA systems, since the Rake receiver has limited number of fingers or the MS can temporarily lose synchronization with the BS in the active set, it is possible that only signals from a subset of BS's in the active set are combined at the MS, which

is denoted as the soft handoff set N_{sh}. We have $N_{sh} \subseteq N_{set}$ and denote the BS set in the active set but not in the soft handoff set as $N_{sh}^c = N_{set} - N_{sh}$.

By assuming that the first f_k multipath components from BS_k in the soft handoff set are tracked by the Rake receiver, the target E_b/I_0 at the output of the Rake receiver that the MS tries to maintain can be expressed as

$$\frac{E_b}{I_0} = \sum_{k \in N_{sh}} \sum_{i=1}^{f_k} \left(\frac{E_b}{I_0} \right)_{ki}^0 \tag{4.3}$$

where $(E_b/I_0)_{ki}^0$ is the nominal SIR at the output of the Rake receiver of the MS tracking the i^{th} multipath of BS_k, which is the SIR that the MS has measured and based on it to send power control command. Due to such factors as a fixed power control step, the latency of the feedback power control commands, the inaccurate estimation of the SIR, the change of surrounding BS's powers, etc., the nominal SIR can not be obtained and leads to the power control error (PCE). The PCE is usually modeled as a lognormal distribution, which means that the PCE in dB is Gaussianly distributed [27]. Therefore, we can express the PCE of BS_k as $l_{ku}^e = 10^{(\alpha\xi^e + \beta\xi_k^e)/10}$, where ξ^e and ξ_k^e's are independent normal variables with zero mean and σ_e standard deviation. α and β satisfy $\alpha^2 + \beta^2 = 1$ to account for the symmetric PCE correlation between BS's in the soft handoff set. Notice that the PCE is modeled in such a way that it depends only on the specific BS that the MS is connected to and is independent of the multipath components from a given BS that the Rake receiver at the MS is tuned to. This is because that the factors that causing the PCE, e.g. the actually allocated BS power to the MS, is always BS dependent. The amount of correlation of the PCE dependents on the actual implementation of the power control algorithms. When the BS's in the soft handoff set are required to increase their powers allocated to the MS at the same time and by the same amount, the correlation becomes larger. If, otherwise, the BS's in the soft handoff set are required to change the amount of power allocated to the MS individually, the correlation becomes smaller.

Following the analysis in [27], the actual $(E_b/I_0)_{ki}$ achieved at the output of the Rake receiver of the MS_u tracking the i^{th} multipath from BS_k can be expressed as

$$\begin{aligned}\left(\frac{E_b}{I_0}\right)_{ki} &= \left(\frac{E_b}{I_0}\right)_{ki}^{0} l_{ku}^{e} \\ &= \frac{G\frac{P_{ku}X_{ki}}{l_k}}{\frac{P_{ku}X_{ki}^{c}}{l_k} + \sum\limits_{\substack{m=1 \\ m\neq u}}^{M_k} \frac{P_{km}X_{ki}^{c}}{l_k} + \sum\limits_{\substack{n=1 \\ n\neq k}}^{N}\sum\limits_{m=1}^{M_n} \frac{P_{nm}X_n}{l_n} + \eta_{ki}} \\ &= \frac{G\frac{P_{ku}X_{ki}}{l_k}}{\frac{P_kX_{ki}^{c}}{l_k} + \sum\limits_{\substack{n=1 \\ n\neq k}}^{N} \frac{P_nX_n}{l_n} + \eta_{ki}}\end{aligned} \tag{4.4}$$

where

G spreading gain;

N total number of BS's in a cell cluster;

M_n total number of MS's in the n^{th} cell;

Furthermore, α_k^i is the i^{th} multipath from BS_k, $X_{ki} = |\alpha_k^i|^2$ is the power of the i^{th} multipath from the BS_k, $X_{ki}^c = \sum_{f=1,f\neq i}^{F_k} X_{kf}$ is the power summation of all the multipath components from the BS_k except the i^{th} multipath, $X_n = \sum_{f=1}^{F_n} X_{kf}$ is the power summation of all the multipath components from the BS_n, and F_n is the total number of multipath components of BS_n. l_n is the path loss from BS_n to MS_u follows the lognormal distribution. η_{ki} is the additive Gaussian noise that generated at the Rake receiver of the MS tuning to the i^{th} multipath of BS_k.

Moreover, P_{nm} is the transmitted power allocated from BS_n to MS_m dedicated to the data transmission and $P_n = \sum_{m=1}^{M_n} P_{nm}$ is the total transmitted power from BS_n in the data channel. The total power of each BS P_n used to transmit data was usually assumed to be equal [24, eqn. 38], which was based on the assumption that all BS's are equally loaded. This assumption is not validate in the real CDMA systems, since unequal total transmitted power from each BS in the data channel is expected over a period of time. Let us denote the maximum total power that available at a BS to transmit data

as P. By assuming that the noise-to-signal ratio is very small (e.g $-20\ dB$) and can be neglected, (4.4) is rewritten as

$$\left(\frac{E_b}{I_0}\right)^0_{ki} = \frac{G\phi_{ku}\frac{X_{ki}}{l_k l^e_{ku}}}{\frac{\varphi_k X^c_{ki}}{l_k} + \sum\limits_{\substack{n=1 \\ n\neq k}}^{N} \frac{\varphi_n X_n}{l_n}} \tag{4.5}$$

where $\phi_{ku} = P_{ku}/P$ is the fraction of BS power allocated by BS_k to MS_u in the data transmission. Notice that P is the amount total power available to the data transmission and the BS power used for the pilot and control channels are not included. P_{ku} also means the amount of power dedicated to the data transmission to a certain MS and does not include the BS power used in the pilot and control channels. $\varphi_n = P_k/P$ is used to account for the fraction of total power of BS_k that is actually utilized to transmit data, which is in the interval $[0, 1]$ and is usually considered to take the value of 1 [1] [24].

4.4.1 Simplification of the SIR for the MS in the NSHM

If we set $N_{sh} = \{k\}$ in (4.3), which means that the MS is only connected to a single BS_k, by using (4.5), the target $(E_b/I_0)_k$ at the output of the Rake receiver of the MS_u tracking the first f_k multipath of BS_k can be expressed as

$$\left(\frac{E_b}{I_0}\right)_k = \sum_{i=1}^{f_k}\left(\frac{E_b}{I_0}\right)^0_{ki} = \sum_{i=1}^{f_k}\frac{G\phi_{ku}\frac{X_{ki}}{l_k l^e_{ku}}}{\frac{\varphi_k X^c_{ki}}{l_k} + \sum\limits_{\substack{n=1 \\ n\neq k}}^{N} \frac{\varphi_n X_n}{l_n}}. \tag{4.6}$$

The expression in (4.6) is hard to simplify. However, the concept of non-orthogonal factor can be used to approximate (4.6) as

$$\left(\frac{E_b}{I_0}\right)_k \approx \frac{G\phi_{ku}\sum_{i=1}^{f_k} X_{ki}/(l_k l^e_{ku})}{h_k/l_k + \sum_{n=1,n\neq k}^{N}\varphi_n X_n/l_n} \tag{4.7}$$

where (1-h_k) is defined as orthogonal factor and h_k is called non-orthogonal factor [32] (or multipath loss factor [49]). The non-orthogonality factor determines the degradation

caused by non-orthogonality among different multipath components. Since the other cell interference term $\sum_{n=1,n\neq k} \varphi_n X_n / l_n$ is negligible when the MS is near the owner BS_k, we can set these terms to zero and equal (4.6) to (4.7) to derive h_k as

$$h_k = \sum_{i=1}^{f_k} X_{ki} [\sum_{i=1}^{f_k} \frac{X_{ki}}{\varphi_k X_{ki}^c}]^{-1}. \tag{4.8}$$

4.4.2 Simplification of the SIR for the MS in the SHM

The results derived in above section 4.4.1 can be extended to consider the MS in the SHM. By using (4.3) and (4.5), the target E_b/I_0 that the MS tries to maintain can be written as

$$\frac{E_b}{I_0} = \sum_{k\in N_{sh}} \sum_{i=1}^{f_k} \left(\frac{E_b}{I_0}\right)_{ki}^{0} = \sum_{k\in N_{sh}} \sum_{i=1}^{f_k} \frac{G\phi \frac{X_{ki}}{l_k l_{ku}^e}}{\frac{\varphi_k X_{ki}^c}{l_k} + \sum\limits_{\substack{n\in N_{set} \\ n\neq k}} \frac{\varphi_n X_n}{l_n} + \sum\limits_{n\notin N_{set}} \frac{\varphi_n X_n}{l_n}} \tag{4.9}$$

where the fraction of power allocated by BS's in the soft handoff set to the MS is assumed to be the same as in [1, eqn. 12], and is denoted as ϕ.

The interference term from BS's that are not in the active set N_{set} is $\sum_{n\notin N_{set}} \varphi_n X_n / l_n$, which is weaker compared to the interference term from BS's that are in the active set according to the soft handoff model in section 4.3.1. This is because the path losses of the BS's not in the active set are at least Th dB greater than those of the BS's in the active set. It is more likely that the interference term from BS's that are not in the active set is very weak. Furthermore, for the interference term coming from BS's that not included in the N_{sh} due to the limitation on the available fingers in the Rake receiver, they embody symmetric form in the summation. Therefore, we want to approximate (4.9) by using

$$\frac{E_b}{I_0} \approx \frac{G\phi \sum\limits_{k\in N_{sh}} \sum\limits_{i=1}^{f_k} \frac{X_{ki}}{l_k l_{ku}^e}}{\sum\limits_{k\in N_{sh}} \frac{h_k}{l_k} + \sum\limits_{n\in N_{sh}^c} \frac{\varphi_n X_n}{l_n} + \sum\limits_{n\notin N_{set}} \frac{\varphi_n X_n}{l_n}} \tag{4.10}$$

By setting the all interference terms from BS's that are not in the soft handoff set to zero and equal (4.9) to (4.10), h_k is derived as

$$h_k = h_c \sum_{i=1}^{f_k} X_{ki}/l_{ku}^e \tag{4.11}$$

$$h_c = [\sum_{k\in N_{sh}} \sum_{i=1}^{f_k} \frac{\frac{X_{ki}}{l_k l_{ku}^e}}{\frac{\varphi_k X_{ki}^c}{l_k} + \sum\limits_{\substack{n\in N_{sh}\\ n\neq k}} \frac{\varphi_n X_n}{l_n}}]^{-1}. \tag{4.12}$$

h_c is the same for every BS_k and is called the normalized macrodiversity non-orthogonality factor (MNOF) in this chapter. h_k is called the macrodiversity non-orthogonality factor of BS_k. Letting $N_{sh} = \{k\}$, (4.11) is reduced to (4.8) and (4.10) is reduced to (4.7).

The KS-test [46] is passed to validate the above approximations at the 5 % significance level. The results are shown in chapter 4.8.1. The unified approach to express E_b/I_0 for the MS in both the SHM and the NSHM is established so far.

4.5 Outage and Capacity Obtained from the BS Power Distribution

By deriving the simplified approximation to the E_b/I_0 considering the multipath fading, power control error, soft handoff threshold, and macrodiversity in the above section 4.4, the fraction of the BS power is easy to be derived by using (4.10) as

$$\phi = \frac{E_b/I_0}{G}[h_c + \frac{U}{V}] \tag{4.13a}$$

$$U = \sum_{n\notin N_{set}} \frac{\varphi_n X_n l_0}{l_n} + \sum_{n\in N_{sh}^c} \frac{\varphi_n X_n l_0}{l_n} = \sum_{\substack{n\notin N_{set}\\ or\ n\in N_{sh}^c}} \frac{\varphi_n l_0}{l_n} \sum_{i=1}^{F_n} X'_{ni}(1-q_n)q_n^{i-1}$$

$$V = \sum_{k\in N_{sh}} \sum_{i=1}^{f_k} X_{ki} \frac{l_0}{l_k l_{ku}^e} = \sum_{k\in N_{sh}} \frac{l_0}{l_k l_{ku}^e} \sum_{i=1}^{f_k} X'_{ki}(1-q_k)q_k^{i-1}$$

where the BS_0 is assumed to be the owner BS, $q_k = \exp(-T_c/\tau_{avg}(r_k))$, and $\tau_{avg}(r_k) = \exp(\frac{(\sigma_y \ln 10/10)^2}{2})T_1 r_k^{\epsilon}$ is the average DS of the signal received at the MS from BS_k. X'_{ki}'s are independent Gamma variables with distribution of $Gamma(\rho, \rho)$ and we have $E[X_k] = 1$ for a large F_k.

The non-orthogonality properties are extensively treated in the literature when the MS is combining multipath components from a single BS [50] [40] [51]. The effects of the non-orthogonality factor on the system performance for MS in the NSHM were studied by choosing different values [52] [32]. It should be noticed that in these studies, the average value of non-orthogonality factor is of special interest since it provides a simple evaluation of the system performance. In our chapter, the statistical characteristics of h_c defined in (4.12) and considering soft handoff is difficult to model. Therefore, we are interested in the average value of h_c. By using the average value of h_c and (4.13a), a simplified calculation of the fraction of power ϕ is given by

$$\phi \approx \frac{E_b/I_0}{G}[E[h_c] + \frac{U}{V}],\ \phi \geq \phi_{min} \tag{4.14}$$

where $\phi_{min} = E[h_c](E_b/I_0)/G$ is the minimum fraction of BS power allocated to the MS.

The accuracy of this approximation is discussed in chapter 4.8.1. At the vicinity of the owner BS, the effect of h_c is dominant and the ratio of the other cell interference from BS's not in the active set to signal strengths in the soft handoff set (i.e. U/V) is very small. By using the average value of h_c, a good approximation of the average capacity can be obtained by referring to (4.13a). When the MS moves to the cell boundary, the U/V becomes larger and dominates, then the inaccuracy caused by using of the average value of $E[h_c]$ is lessened.

In addition to facilitate the calculation of ϕ, the simplification by using the average value of h_c also helps to model a minimum fraction of BS power available to the MS. In the real CDMA systems, the BS at least allocates a minimum fraction of power to

the MS connected to it, which takes a reasonable value greater than zero. By taking the average value of the non-orthogonality caused by the multipath components as the minimum fraction, the U/V can make the fraction of BS power ϕ a random variable and thereby, the effects of the ratio of the interference to the signal level on the fraction of BS power can be well modeled. Notice that the average value of h_c is also a function of the distance and the multipath components. Therefore, the minimum fraction of BS power ϕ_{min} is different when the MS is at different locations in the cell and for different delay spread parameters. The value of $E[h_c]$ can be obtained through simulation.

4.5.1 The Correlation among BS Powers Allocated to Different MS's

It is interesting to look at the correlation among ϕ's in equation (4.14) for different users and see if the correlation is significant or not. Let take two users as an example. For user $\#a$, we define

$$\phi_a \approx \frac{(E_b/I_0)_a}{G_a}[E[h_c]_a + \frac{U_a}{V_a}],\ \phi_a \geq \phi_{min} \tag{4.15}$$

where

$$\begin{aligned} U_a &= \sum_{n \notin (N_{set})_a} \frac{\varphi_n (X_n)_a (l_0)_a}{(l_n)_a} + \sum_{n \in (N^c_{sh})_a} \frac{\varphi_n (X_n)_a (l_0)_a}{(l_n)_a} \qquad (4.16a) \\ &= \sum_{\substack{n \notin (N_{set})_a \\ or\ n \in (N^c_{sh})_a}} \frac{\varphi_n (l_0)_a}{(l_n)_a} \sum_{i=1}^{\infty} (X'_{ni})_a (1 - (q_n)_a)(q_n)_a^{i-1} \end{aligned}$$

$$V_a = \sum_{k \in (N_{sh})_a} \sum_{i=1}^{(f_k)_a} (X_{ki})_a \frac{(l_0)_a}{(l_k)_a (l^e_{ku})_a} = \sum_{k \in (N_{sh})_a} \frac{(l_0)_a}{(l_k)_a (l^e_{ku})_a} \sum_{i=1}^{(f_k)_a} (X'_{ki})_a (1 - (q_k)_a)(q_k)_a^{i-1} \tag{4.16b}$$

For user #2, we have

$$\phi_b \approx \frac{(E_b/I_0)_b}{G_b}[E[h_c]_b + \frac{U_b}{V_b}],\ \phi_b \geq \phi_{min} \tag{4.17}$$

where

$$U_b = \sum_{n \notin (N_{set})_b} \frac{\varphi_n (X_n)_b (l_0)_b}{(l_n)_b} + \sum_{n \in (N_{sh}^c)_b} \frac{\varphi_n (X_n)_b (l_0)_b}{(l_n)_b} \tag{4.18a}$$

$$= \sum_{\substack{n \notin (N_{set})_b \\ or \ n \in (N_{sh}^c)_b}} \frac{\varphi_n (l_0)_b}{(l_n)_b} \sum_{i=1}^{\infty} (X'_{ni})_b (1 - (q_n)_b)(q_n)_b^{i-1}$$

$$V_b = \sum_{k \in (N_{sh})_b} \sum_{i=1}^{(f_k)_b} (X_{ki})_b \frac{(l_0)_b}{(l_k)_b (l^e_{ku})_b} = \sum_{k \in (N_{sh})_b} \frac{(l_0)_b}{(l_k)_b (l^e_{ku})_b} \sum_{i=1}^{(f_k)_b} (X'_{ki})_b (1 - (q_k)_b)(q_k)_b^{i-1} \tag{4.18b}$$

In equations (4.16a), (4.16b), (4.18a), and (4.18b), $(X_n)_a$ is the multipath fading from BS_n received by user $\#a$, $(l_n)_a$ is the path loss with shadowing between user $\#a$ and BS_n, $(q_k)_a$ is the decay rate of the multipath components received at user $\#a$ from BS_n, $(f_n)_a$ is the number of multipath components captured by user $\#a$ from BS_n. The same denotations apply to user $\#b$.

Since the total used BS powers φ_n's appear in the calculations of both ϕ_a and ϕ_b, correlation exists between them. For a simple case of a two-user system, the total used BS power is $\phi_t = \phi_a + \phi_b$. The correlation among ϕ_a and ϕ_b does not affect the mean value of ϕ_t, that is, $E[\phi_t] = E[\phi_a] + E[\phi_b]$ regardless of the correlation among ϕ_a and ϕ_b. But the variance of ϕ_t is affected by the correlation among ϕ_a and ϕ_b. From the definition of ϕ_t, we have $VAR[\phi_t] = VAR[\phi_a] + VAR[\phi_b] + 2(E[\phi_a \phi_b] - E[\phi_a]E[\phi_b])$, where $VAR[.] = E[(.)^2] - E^2[.]$. Obviously, if ϕ_a and ϕ_b are independent, $VAR[\phi_t] = VAR[\phi_a] + VAR[\phi_b]$. Therefore, the variance of ϕ_t affected by the correlation among ϕ_a and ϕ_b is reflected in the term $2(E[\phi_a \phi_b] - E[\phi_a]E[\phi_b])$. This deviation term can be calculated as follows.

By using equations (4.15) and (4.17), the cross correlation between user $\#a$ and $\#b$ is

$$\begin{aligned} E[\phi_a\phi_b] =& E[\frac{(E_a/I_0)_a}{G_a}[E[h_c]_a + \frac{U_a}{V_a}]\frac{(E_b/I_0)_b}{G_b}[E[h_c]_b + \frac{U_b}{V_b}],\ \phi_a \geq \phi_{min},\ \phi_b \geq \phi_{min}] \\ =& \frac{(E_a/I_0)_a}{G_a}\frac{(E_b/I_0)_b}{G_b}(E[h_c]_a[E[h_c]_b + E[h_c]_b E[\frac{U_a}{V_a}] + E[h_c]_a E[\frac{U_b}{V_b}] + E[\frac{U_a}{V_a}]E[\frac{U_b}{V_b}]). \end{aligned} \tag{4.19}$$

So we have

$$E[\phi_a\phi_b] - E[\phi_a]E[\phi_b] = \frac{(E_a/I_0)_a}{G_a}\frac{(E_b/I_0)_b}{G_b}(E[\frac{U_a}{V_a}\frac{U_b}{V_b}] - E[\frac{U_a}{V_a}]E[\frac{U_b}{V_b}]). \tag{4.20}$$

Since V_a and V_b are uncorrelated and are not function of ϕ_n's, they are independent for different users. Therefore, we have

$$E[\phi_a\phi_b] - E[\phi_a]E[\phi_b] = \frac{(E_a/I_0)_a}{G_a}\frac{(E_b/I_0)_b}{G_b}(E[U_aU_b] - E[U_a]E[U_b])E[\frac{1}{V_a}]E[\frac{1}{V_b}]. \tag{4.21}$$

The ratio of the deviation of the variance of ϕ_t to the variance of ϕ_t can be used to measure the relative deviation of the variance caused by the correlation between ϕ_a and ϕ_b, which is given by

$$\rho = \frac{2(E[\phi_a\phi_b] - E[\phi_a]E[\phi_b])}{VAR[\phi_t]} \tag{4.22}$$

Actually, ρ is the correlation coefficient between ϕ_a and ϕ_b. As a simplified example, we can assume that user $\#a$ and $\#b$ are co-located. So we have $E[\phi_a] = E[\phi_b]$ and $VAR[\phi_a] = VAR[\phi_b]$. Then equation (4.22) is simplified to

$$\rho = \frac{E[\phi_a\phi_b] - E^2[\phi_a]}{VAR[\phi_a]} \tag{4.23}$$

First, let us calculate the cross correlation between U_a and U_b. By using (4.16a) and (4.18a), we have

$$\begin{aligned} E[U_a U_b] =& E[\sum_{\substack{n\notin(N_{set})_a \\ or\ n\in(N_{sh}^c)_a}} \frac{\varphi_n(l_0)_a}{(l_n)_a}(X_n)_a \sum_{\substack{k\notin(N_{set})_b \\ or\ k\in(N_{sh}^c)_b}} \frac{\varphi_k(l_0)_b}{(l_k)_b}(X_k)_b] \\ =& \sum_{\substack{n\notin(N_{set})_a \\ or\ n\in(N_{sh}^c)_a}} \sum_{\substack{k\notin(N_{set})_b \\ or\ k\in(N_{sh}^c)_b}} E[\frac{\varphi_n(l_0)_a}{(l_n)_a}(X_n)_a \frac{\varphi_k(l_0)_b}{(l_k)_b}(X_k)_b] \end{aligned} \tag{4.24}$$

We also know that

$$\begin{aligned} E[U_a]E[U_b] =& E[\sum_{\substack{n\notin(N_{set})_a \\ or\ n\in(N_{sh}^c)_a}} \frac{\varphi_n(l_0)_a}{(l_n)_a}(X_n)_a]E[\sum_{\substack{k\notin(N_{set})_b \\ or\ k\in(N_{sh}^c)_b}} \frac{\varphi_k(l_0)_b}{(l_k)_b}(X_k)_b] \\ =& \sum_{\substack{n\notin(N_{set})_a \\ or\ n\in(N_{sh}^c)_a}} \sum_{\substack{k\notin(N_{set})_b \\ or\ k\in(N_{sh}^c)_b}} E[\frac{\varphi_n(l_0)_a}{(l_n)_a}(X_n)_a]E[\frac{\varphi_k(l_0)_b}{(l_k)_b}(X_k)_b]. \end{aligned} \tag{4.25}$$

For a normalized multipath fading profile, we know that $E[(X_k)_a] = E[(X_k)_b] = 1$. Therefore, we have

$$\begin{aligned} & E[U_a U_b] - E[U_a]E[U_b] \\ =& \sum_{\substack{n\notin(N_{set})_a \\ or\ n\in(N_{sh}^c)_a}} \sum_{\substack{k\notin(N_{set})_b \\ or\ k\in(N_{sh}^c)_b}} \{E[\frac{\varphi_n(l_0)_a}{(l_n)_a}(X_n)_a \frac{\varphi_k(l_0)_b}{(l_k)_b}(X_k)_b] - E[\frac{\varphi_n(l_0)_a}{(l_n)_a}(X_n)_a]E[\frac{\varphi_k(l_0)_b}{(l_k)_b}(X_k)_b]\} \\ =& \sum_{n\notin(N_{set})_a\ or\ n\in(N_{sh}^c)_a} \sum_{\substack{k\notin(N_{set})_b \\ or\ k\in(N_{sh}^c)_b}} \{E[\frac{\varphi_n(l_0)_a}{(l_n)_a}\frac{\varphi_k(l_0)_b}{(l_k)_b}] - E[\frac{\varphi_n(l_0)_a}{(l_n)_a}]E[\frac{\varphi_k(l_0)_b}{(l_k)_b}]\} \\ =& \sum_{\substack{n\notin(N_{set})_a \\ or\ n\in(N_{sh}^c)_a}} \sum_{\substack{k\notin(N_{set})_b \\ or\ k\in(N_{sh}^c)_b}} \{E[\varphi_n\varphi_k]E[\frac{(l_0)_a}{(l_n)_a}]E[\frac{(l_0)_b}{(l_k)_b}] - E[\varphi_n]E[\varphi_k]E[\frac{(l_0)_a}{(l_n)_a}]E[\frac{(l_0)_b}{(l_k)_b}]\} \\ =& \sum_{\substack{n\notin(N_{set})_a \\ or\ n\in(N_{sh}^c)_a}} \sum_{\substack{k\notin(N_{set})_b \\ or\ k\in(N_{sh}^c)_b}} \{E[\varphi_n\varphi_k] - E[\varphi_n]E[\varphi_k]\}E[\frac{(l_0)_a}{(l_n)_a}]E[\frac{(l_0)_b}{(l_k)_b}]. \end{aligned} \tag{4.26}$$

Since the correlation between φ_n and φ_k is only 0.1, we can neglect the term $E[\varphi_n\varphi_k] - E[\varphi_n]E[\varphi_k]$, when $n \neq k$. So the above equation can be simplified to

$$\begin{aligned} & E[U_aU_b] - E[U_a]E[U_b] \\ \approx & \sum_{\substack{n\notin(N_{set})_a \\ or\ n\in(N^c_{sh})_a}} VAR[\varphi_n]E[\frac{(l_0)_a}{(l_n)_a}]E[\frac{(l_0)_b}{(l_k)_b}] \\ = & VAR[\varphi_n] \sum_{\substack{n\notin(N_{set})_a \\ or\ n\in(N^c_{sh})_a}} E^2[\frac{(l_0)_a}{(l_n)_a}]. \end{aligned} \tag{4.27}$$

where the second equation is obtained by assuming the powers of all BS's are identically distributed, that is, $E[\phi_n] = E[\phi_k]$ and $VAR[\phi_n] = VAR[\phi_k]$. We also assume user $\#a$ is co-located with user $\#b$. Therefore, $E[\phi_a\phi_b] - E[\phi_a]E[\phi_b]$ can be viewed as a scale of $E[\phi_a\phi_b|\varphi_n = \varphi_k = 1] - E[\phi_a|\varphi_n = \varphi_k = 1]E[\phi_b|\varphi_n = \varphi_k = 1]$. The scale factor is $VAR[\varphi_n]$.

It is also easy to see that $VAR[\phi_a]$ can also be viewed as a scale of $VAR[\phi_a|\varphi_n = 1]$ and the scale factor is also $VAR[\varphi_n]$. Therefore, the correlation coefficient ρ between ϕ_a and ϕ_b is not a function of surrounding BS powers φ_n's under the assumption of identical distributed BS powers φ_n's and co-located users, which makes the calculation of the correlation coefficient easier and also tells us that the choice of different BS power distributions does not significantly affect the correlation coefficient ρ between ϕ_a and ϕ_b.

It is easy to observe from (4.26) that when φ_n is a constant value, $E[U_aU_b] - E[U_a]E[U_b] = 0$ and therefore, $\rho = 0$, which means ϕ_a is independent of ϕ_b. In our research, we treat φ_n's as random variables.

The correlation between ϕ_a and ϕ_b can be obtained by the analytical approach outlined above or using simulation. For simplicity, we did a simulation of ϕ_a and ϕ_b at different locations in the cell and for different soft handoff sets. We choose φ_n's as lognormal distribution variables with $10\log(\varphi_n) \sim N(0.348269, 0.189449^2)$ as an example. As discussed above, since the choice of different BS power distributions does not significantly

affect the correlation coefficient ρ between ϕ_a and ϕ_b, choosing different parameters for φ_n does not significantly affect the simulation results of ρ's. We further assume the target SIR and spread gain are the same for these two users, so that ρ is not a function of the SIR and spreading gain. The correlation coefficient ρ obtained through the simulation is given in Table 4.1.

Table 4.1 Correlation Coefficient Between BS Powers Used by Two Different Users

User $\#a$		User $\#b$		Correlation
Location	Handoff Set	Location	Handoff Set	Coefficient ρ
cell edge	$\{BS_0, BS_1\}$	cell edge	$\{BS_0, BS_1\}$	0.0281
cell edge	$\{BS_0\}$	cell edge	$\{BS_0\}$	0.0508
cell edge	$\{BS_0, BS_1\}$	cell edge	$\{BS_0\}$	0.0425
middle of the cell	$\{BS_0, BS_1\}$	middle of the cell	$\{BS_0, BS_1\}$	0.0969
middle of the cell	$\{BS_0\}$	middle of the cell	$\{BS_0\}$	0.0069
middle of the cell	$\{BS_0, BS_1\}$	middle of the cell	$\{BS_0\}$	0.0386
cell edge	$\{BS_0, BS_1\}$	middle of the cell	$\{BS_0, BS_1\}$	0.0413
cell edge	$\{BS_0, BS_1\}$	middle of the cell	$\{BS_0\}$	0.0261
cell edge	$\{BS_0\}$	middle of the cell	$\{BS_0, BS_1\}$	0.0449

In Table 4.1, the user at the cell edge means that the user is located at a normalized distance 1 from BS_0 and the user in the middle of the cell means that the user is located at a normalized distance 0.5 from BS_0. The user at the cell edge will experience more interference and more likely to be in soft handoff with multiple BS's to achieve macro-diversity gain. We could see that when both users are at cell edge and in soft handoff with $\{BS_0, BS_1\}$, the correlation coefficient ρ is 0.0281 and can be safely neglected. When the user is in the middle of the cell, it is more likely to be in non-soft handoff mode and connect to only a single BS. We could see that when both users are in the middle of the cell and connect to BS_0 only , the correlation coefficient ρ is 0.0069 and can be neglected. There are cases when both users are in the middle of the cell and connect to $\{BS_0, BS_1\}$,

the correlation is 0.0969 but the probability that this happens is very small compared to the case when both users are in the middle of the cell and connect to BS_0 only. For all other cases listed in Table 4.1, the correlation coefficient is in the range $0.02 - 0.05$ and can be neglected.

In summary, the correlation among the BS powers used by different users is small and we can treat the BS powers used by different users as independent variables.

4.5.2 Capacity and Outage Probability

After obtaining the simplified expression of ϕ, we need to find the statistical properties of U and V to characterize the distribution of ϕ. At the first glance, U and V are a sum of Suzuki random variables [39]. The Suzuki distribution can be approximated by a lognormal distribution [37, page 160-162] and the sum of lognormal random variables can be approximated by another lognormal distributed variable by Schwartz and Yeh's method [33]. However, as the soft handoff threshold is taken into consideration in this chapter, the path loss of BS's in the active set are truncated (exceeding the path loss of the owner BS by less than Th dB, eqn. (4.1)) and the path loss of BS's not in the active set are also truncated (exceeding the path loss of the owner BS by more than Th dB, eqn. (4.1)). Therefore, we are compelled to use a new approach to approximate the distribution of U and V. The Gaussian approximation of the interference term is not a good approach. For example, in [27], the interference term was approximated by using a Gamma random variable and assuming the path loss could be compensated by the power control. It is well known that the sum of Gamma variables can be approximated by another Gamma variable or series [53] [54]. We observe that the ratio of the path loss of the owner BS_0 to the path loss of the BS_k in the active set is $10^{-Th/10} \leq l_0/l_k \leq 1$ and the ratio of the path loss of owner BS_0 to that of the BS_k not in the active set is $0 \leq l_0/l_k \leq 10^{-Th/10}$. If the path loss threshold Th is not very large (e.g. 6 dB), l_0/l_k

does not vary significantly. Therefore, we can approximate U in (4.13b) and V (4.13b) as gamma distributions. The accuracy of this approximation is discussed in chapter 4.8.2. Assume U follows a distribution of $Gamma(b_u, c_u)$ and V follows a distribution of $Gamma(b_v, c_v)$. The parameters b_u, c_u, b_v, and c_v are also derived in the chapter 4.8.2. Notice that parameters b_u, c_u, b_v, and c_v are functions of the soft handoff threshold, because the path loss should satisfy the relation given in (4.1).

By using the above obtained statistical properties of U and V, the distribution of the fraction of BS power ϕ can be obtained as follows. Neglecting the correlation between U and V as discussed in chapter 4.8.2, U/V follows an F-distribution [30, page 946]. Since c_uU/c_v follows a distribution of $Gamma(b_u, c_v)$, $V/(V+c_uU/c_v)$ follows a beta distribution $Beta(b_v, b_u)$, which has the PDF of $f(x) = x^{b_v-1}(1-x)^{b_u-1}/B(b_v, b_u), 0 \le x \le 1$. Beta function is denoted as $B(b_v, b_u) = \int_0^1 x^{b_v-1}(1-x)^{b_u-1}dx$ [30, page 258]. Therefore, the CDF of ϕ conditional on $E[h_c]$ is

$$F_\phi(x|E[h_c]) = 1 - B(b_v, b_u, [(\frac{Gx}{E_b/I_0} - E[h_c])\frac{C_u}{C_v} + 1]^{-1}), x \ge \phi_{min} \tag{4.28}$$

where $B(b_v, b_u, \alpha) = \frac{1}{B(b_v,b_u)} \int_0^\alpha z^{b_v-1}(1-z)^{b_u-1}dz$ is the incomplete beta function.

The capacity at a specific location in the cell is defined as the number of MS's that the system can support if the BS allocates all of its power to the MS, which was adopted in [1] to compare the capacity of the SH and NSH. Therefore, by using (4.14) and (4.28), the average number of MS's in SH with the soft handoff set N_{sh} is given by

$$\begin{aligned}
&E[N|SH\ with\ N_{sh}] = E[1/\phi|SH\ with\ N_{sh}|\phi_{\min} \le \phi \le \phi_{\max}] \\
=&\frac{E[1/\phi, \phi_{\min} \le \phi \le \phi_{\max}|SH\ with\ N_{sh}]}{P[\phi_{\min} \le \phi \le \phi_{\max}]} \\
=&\frac{G}{E_b/I_0}\frac{1}{B(b_v, b_u)}\frac{1}{1 - B(b_v, b_u, \gamma_{\max})}\int_{\gamma_{\max}}^1 [(\frac{1}{x} - 1)\frac{C_v}{C_u} + E[h_c]]^{-1}x^{b_v-1}(1-x)^{b_u-1}dx.
\end{aligned} \tag{4.29}$$

where $\phi_{min} = E[h_c](E_b/I_0)/G$ is the minimum fraction of BS power allocated to the MS and ϕ_{max} is the maximum fraction of BS power (MFBP), and $\gamma_{\max} = [(G\phi_{\max}/(E_b/I_0) - E[h_c])(C_u/C_v) + 1]^{-1}$.

The outage happens when the fraction of BS power exceeds the maximum value. By using (4.14), the outage is calculated as

$$P_{out}(SH\ with\ N_{sh}) = P(\phi > \phi_{max}) = B(b_v, b_u, \gamma_{\max}) \tag{4.30}$$

As pointed out in [1], the capacity loss was taken into account by assuming that the 2-BS soft handoff included in the soft handoff utilizes one more channel than the non-soft handoff does. Here each of BS in the soft handoff transmits the same amount of fraction of power to the MS [1]. From the viewpoint of the BS power, this means that more total fraction of BS powers is used. By assuming that the number of BS in the soft handoff set is N_t and the total fraction of power is limited by ϕ_{max}, we have $N_t\phi < \phi_{max}$. Therefore, $\gamma_{\max} = [(G\phi_{\max}/(E_b/I_0) - E[h_c])(C_u/C_v) + 1]^{-1}$ should be used in (4.29) and (4.30) to obtain the capacity and outage respectively.

Without considering the capacity loss due to the additional channels used in the soft handoff, we keep the MFBP the same regardless of the soft handoff condition of the MS, i.e. $\phi < \phi_{max}$ for each BS in the soft handoff set and (4.29) and (4.30) can be used directly to obtain the capacity and outage respectively. By using this approach, a comparison to the results in the literature [1] is possible. It is worth noticing that when the MS changes from the non-soft handoff mode to the soft handoff mode and there are extra powers in the BS's in the soft handoff set, the MFBP can be kept the same. Actually, soft handoff is triggered to consume extra (or unbalanced) BS power in the real CDMA systems [16, pg. 172].

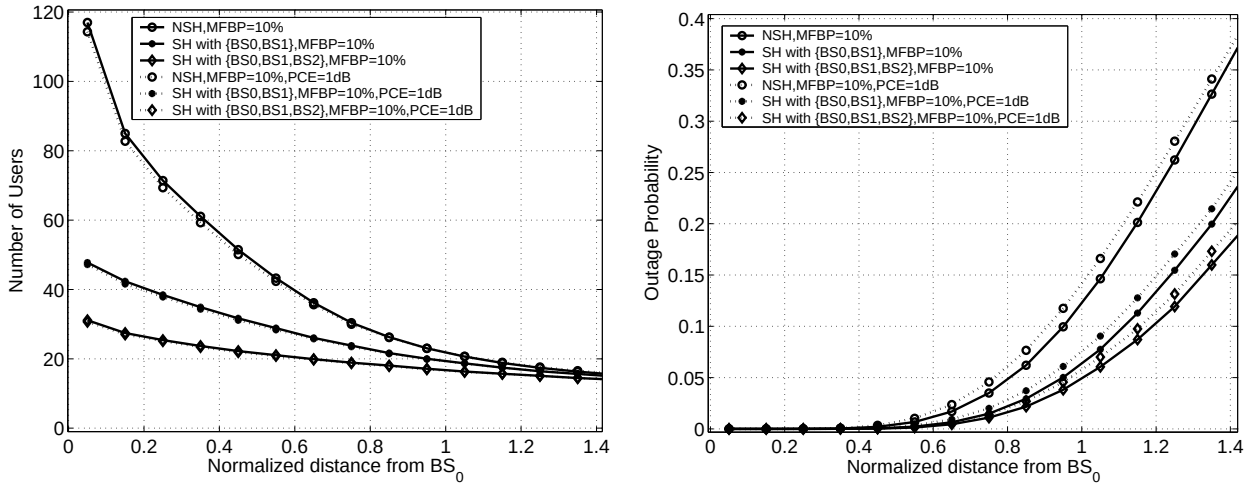

(a) (b)

Figure 4.3 Capacity (a) and outage (b) with a 10 % MFBP and a 3 dB SHT.

In order to compare the average capacity and outage of the SH and NSH, the capacity in (4.29) and the outage in (4.30) should be multiplied with their corresponding probability in (4.1). Therefore, the weighed (or average) capacity is

$$E[N] = E[N|SH\ with\ N_{sh}]P[SH\ with\ N_{sh}] \tag{4.31}$$

and the corresponding weighed (or average) outage probability is given by

$$P_{outavg} = P_{out}(SH\ with\ N_{sh})P(SH\ with\ N_{sh}) \tag{4.32}$$

4.6 Numerical results and analysis

This section is to utilize the above derived formula to study the effects of the limitation on the fraction of BS power, the PCE, the available Rake fingers, the unequal BS powers, and the data rate, on the capacity and outage.

In order to achieve uniformly distributed user density, the triangle shown in Fig. 1 is divided into 30 bins in x-axis and 18-bins in y-axis. The ratio of the number of bins is

equal to the ratio of the width and length of the triangle. The spreading gain G is 128 for a chip rate of 3.84 $Mcps$ and a data rate of 30 $kbps$. The path loss slope u is chosen to be 4. Standard deviation σ of shadowing is set to be 8 dB. Correlation coefficient of the shadowing a^2 is chosen to be 0.5. The correlation between the PCE's among different BS's in the soft handoff set is $\alpha^2 = 0.5$. Other default simulation parameters include that the actual power used to transmit data in each BS is equal and equals to the maximum total available power dedicated to the data transmission, that is, $\varphi_0 = \varphi_1 = \cdots = 1.0$, the soft handoff threshold is 3 dB, the PCE is chosen to be 0 dB, and the Rake receive captures 3 multipath components from each BS in the soft handoff set. The E_b/I_0 is chosen to be 5 dB. The Monte Carlo simulation is used to derive the mean and variance of U and V. Throughout the rest of the chapter, without stated explicitly, we means that when the MS is in the soft handoff mode, the soft handoff set is $\{BS_0, BS_1\}$.

The default finger allocation scheme is as follows: the Rake receiver deploys 6 fingers and equally assigns them to the BS's in the soft handoff set. If the ratio of the number of fingers to the number of BS's in the active set is not an integer, we first assign fingers to each BS in the soft handoff set, the number of which equals to the integer quotient of the ratio. Then we assign the remaining fingers to BS's in the soft handoff set according to their numbers in Fig. 4.1 in the ascending order. The owner BS_0 is always included in both assignments.

Two approaches to calculate the capacity and outage are discussed in section 4.5: the first one does not consider the capacity loss due to additional channels involved in the soft handoff and assumes that the fraction of BS power allocated to the MS from each BS in the soft handoff set is limited by a maximum value, that is $\phi < \phi_{max}$. The second approach assumes that the total fraction of BS power allocated from all the BS's in the soft handoff set is limited by a maximum value $N_t\phi < \phi_{max}$ by considering the capacity loss. The first approach is utilized throughout the chapter except to obtain the

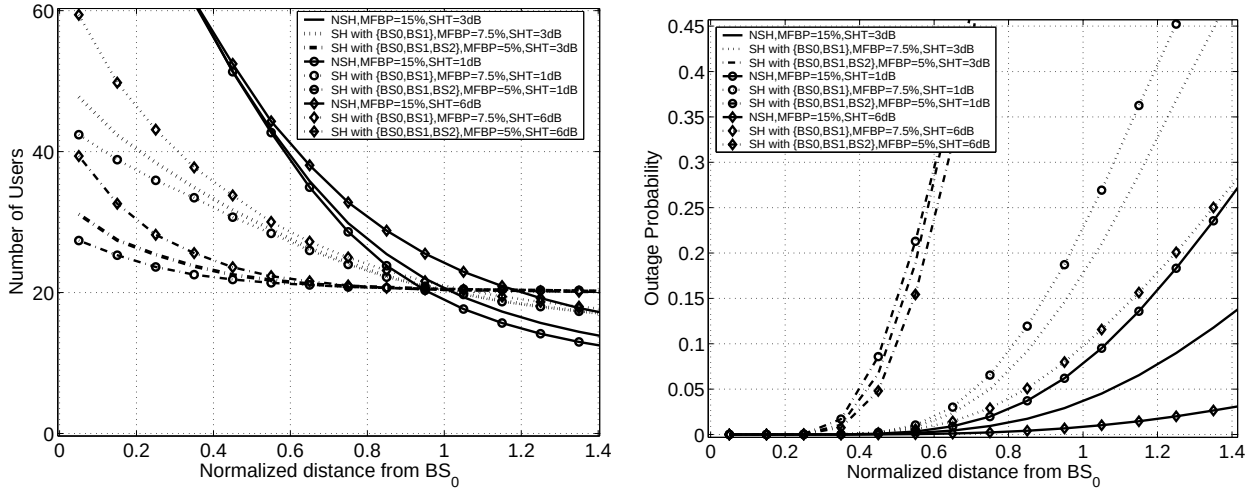

(a) (b)

Figure 4.4 Capacity (a) and outage (b) with a 15 % total MFBP.

results in Fig. 4.4 and Fig. 4.6. The second one is used only to obtain the results in Fig. 4.4, Fig. 4.6 and part of Fig. 4.7.

4.6.1 The Effects of the Finger Limitation on the Rake Receiver

The default finger allocation scheme discussed above assumes that the total number of fingers in the Rake receiver is limited to 6 and each BS in the active set is included in the soft handoff set. Usually, the number of BS's in the active set is chosen to be less than 4, since the probability that more than 4 BS's simultaneously in the active set is negligible. Therefore, the Rake receiver assigns at least one finger to each BS in the active set.

Fig. 4.3(a) and Fig. 4.3(b) show the capacity and outage by using the first approach, respectively, for a 10 % MFBP and a 3 dB SHT along the x-axis in Fig. 4.2. The capacity is obtained by using (4.29) and outage is obtained by using (4.30). We notice that the PCE decreases the capacity and increases the outage. At the cell boundary (coordinate of the MS is $[1.05, 0]$ according to our placement of the bins), the PCE

increases the outage by about 15 % and has almost no effect on the capacity for all the soft handoff combinations. For the MS in the middle of the cell (coordinate of the MS is $[0.55, 0]$), the PCE increases the outage by about 50 % and decreases the capacity by about 1 % for all soft handoff combinations. Therefore, the PCE has significant effects on the outage but insignificant effects on the capacity. In addition, the PCE has more effects on the outage when the MS moves closer to the owner BS_0.

We further notice that at the cell boundary, when more BS's included in the the soft handoff set (e.g. the soft handoff set increases from $\{BS_0\}$ to $\{BS_0, BS_1\}$), the capacity is reduced by 10 % at the cell boundary and 30 % in the middle of the cell. The outage is decreased by about 47 % for the MS at the cell boundary and 68 % for the MS in the middle of the cell when the soft handoff set increases from BS_0 to $\{BS_0, BS_1\}$. When the soft handoff set increases from $\{BS_0, BS_1\}$ to $\{BS_0, BS_1, BS_2\}$, the outage decreases by about 22 % for the MS at the cell boundary and 28 % for the MS in the middle of the cell. Therefore, we show that more BS's included in the soft handoff set has the disadvantage of decreasing the capacity while providing the advantage of less outage. The soft handoff has more effects on the MS's in the middle of the cell than those at the edge of the cell boundary. Furthermore, increasing the number of BS's in the soft handoff set decreases the outage in a gradually less effective way.

In [1], it was shown that about 7 % capacity was achieved without considering the capacity loss and insignificant capacity loss was resulted by considering the capacity loss due to one more channel used for the 2-BS soft handoff in an unsectorized cell. We show that without considering the capacity loss due to additional channels used in the soft handoff, the soft handoff can not provide any capacity gain but result in a significant capacity loss if the total number of Rake receiver fingers is limited. This is because each of the BS is assigned less fingers and captures less percentage of the energy from the multipath components when more BS's are involved in the active set, which results in

more multipath interference and reduces the diversity gain. However, more BS's involved in the soft handoff set decreases the outage, which is because that the probability that the MS requires more power than the maximum fraction from all BS's in the active set simultaneously is less.

Fig. 4.4(a) and Fig. 4.4(b) show the capacity and outage by using the second approach, respectively. Here we assume the maximum total fraction of BS is 15 %, which means that the fraction of power allocated from the BS in the NSH is 15 %, the fraction of power allocated from each BS in the 2-BS soft handoff set is 7.5 % and the fraction of power allocated from each BS in the 3-BS soft handoff set is 5 %.

We could see from Fig. 4.4(a) that increasing the SHT increases the capacity for a specific active set, this is because signals from each BS in that specific active set are tracked by the Rake receiver at the MS. Therefore, the larger the SHT, the weaker the interference from BS's not in the active set is and we can allocate less fraction of BS power to the MS to achieve a certain SIR. It is also shown that the SHT has more effects on the capacity for the MS's in the NSHM and less effects on the capacity for the MS's in the SHM when the MS is farther away from the owner BS_0. This can be explained as follows: according to the soft handoff model in section 4.3.1, increasing the SHT not only reduces the amount of interference from BS's not in the active set but also reduces the combination gain if there is soft handoff. For the MS in the NSHM and at the cell boundary, the improvement of the capacity is due to the reduction of the amount of interference. When the MS is in the NSHM and closes to the owner BS, the capacity gain is negligible since the amount of interference is already negligible. For the MS in the SHM and at the cell boundary, the amount of capacity gain achieved by the reduction of the interference due to a larger SHT is minimized by the reduction in the combination gain. When the MS is in the SHM and closes to the owner BS, the amount of interference is negligible, so the combination gain dominates and achieves the capacity gain.

In [1], the capacity loss was said to be insignificant by considering the capacity loss due to additional channels used in the soft handoff. We notice that for MS's within the owner cell, there are always capacity losses if there is limitation on the number of available Rake fingers by considering the capacity loss due to more channels used in the soft handoff.

We can also observe from Fig. 4.4(b) that increasing the SHT has the benefit of reducing the outage for a specific active set. Further comparing Fig. 4.4(a) to Fig. 4.3(a) and Fig. 4.4(b) to Fig. 4.3(b), we could see that increasing the MFBP from 10 % to 15 % results in insignificant capacity loss but significantly reduction in the outage by 70 % at the cell boundary for the MS in the NSHM. If the MFBP decreases from 10 % to 7.5 %, the capacity increases by only 6 % but the outage increases by about 170 % for the MS at the cell boundary and in soft handoff with $\{BS_0, BS_1\}$. When the soft handoff set is $\{BS_0, BS_1, BS_2\}$ and the MFBP decreases from 10 % to 5 %, the capacity increases about 24 % but the outage increases significantly and is unacceptable for the MS at the cell boundary. Therefore, since the outage is more likely to be affected by the MFBP limitation, the MFBP should be relaxed to a certain value to achieve an affordable outage. When the MFBP is at a lower value, the changes of the MFBP have more effects on the outage.

The above comparison of the SH to NSH in terms of capacity and outage is based on their absolute values. An alternative comparison needs to multiply the capacity and outage with their corresponding occurrence probability defined in (4.1). This will provide a base to compare the SH and NSH statistically (or on the average). Therefore, by using the first approach to calculate the outage and capacity, (4.31) is used to obtain the weighed (or average) capacity shown in Fig. 4.5(a) and (4.32) is used to obtain the weighed (or average) outage shown in Fig. 4.5(b). The average capacity decreases with the increase of the SHT for the MS in the NSHM, which is different from the observation

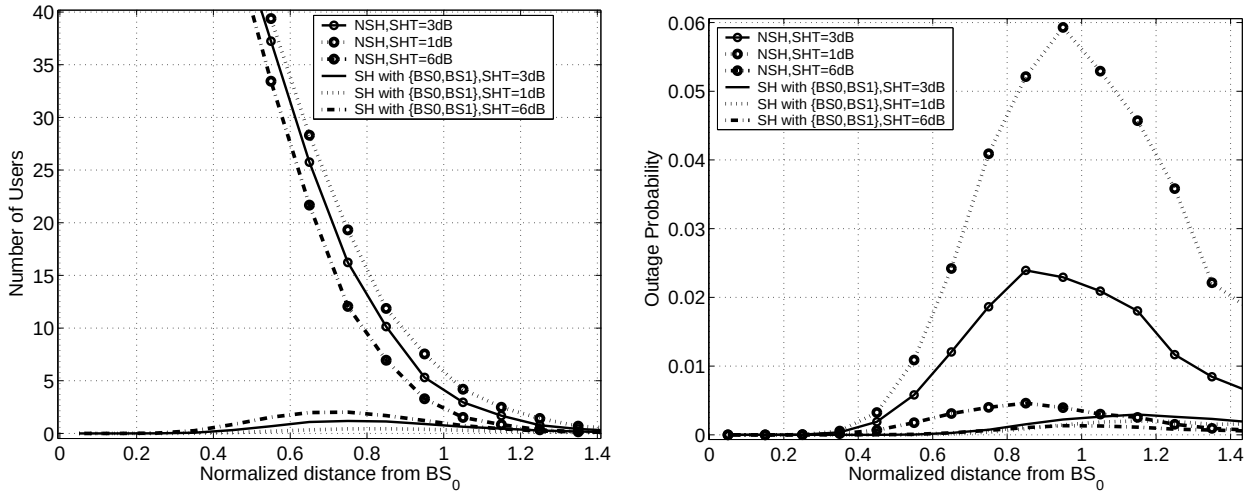

(a) (b)

Figure 4.5 Average capacity (a) and outage (b) with a 10 % MFBP.

in the Fig. 4.4(a). This is because the NSH probability decreases with the increase of the SHT, which overwhelms the capacity gain effects on the average capacity. The average capacity increases with the increase of the SHT for the MS in the SHM, which is similar to the observations in the Fig. 4.4(a). This is expected since the probability of the SH is increased with the SHT. The average outage decreases with the increase of the SHT for the MS in the NSHM, which is also due to the corresponding decrease of the NSHM probability. Because the SH probability increases with the SHT, the average outage is the largest for the SHT equals to 3 dB and is smallest for the SHT equals to 6 dB.

By using the second approach to calculate the outage and capacity, the average capacity and average outage are shown in Figs. 4.6(a) and 4.6(b) respectively. We could see that when SHT equals to 1 dB, smallest average outage but smallest average capacity is achieved for the MS in the SHM. When the SHT increases to 3 dB for the MS in the NSHM, we achieve a larger average capacity but also a larger average outage.

The results of the average capacity and outage by using the first approach or the second approach show that increasing or decreasing the SHT to achieve a high capacity

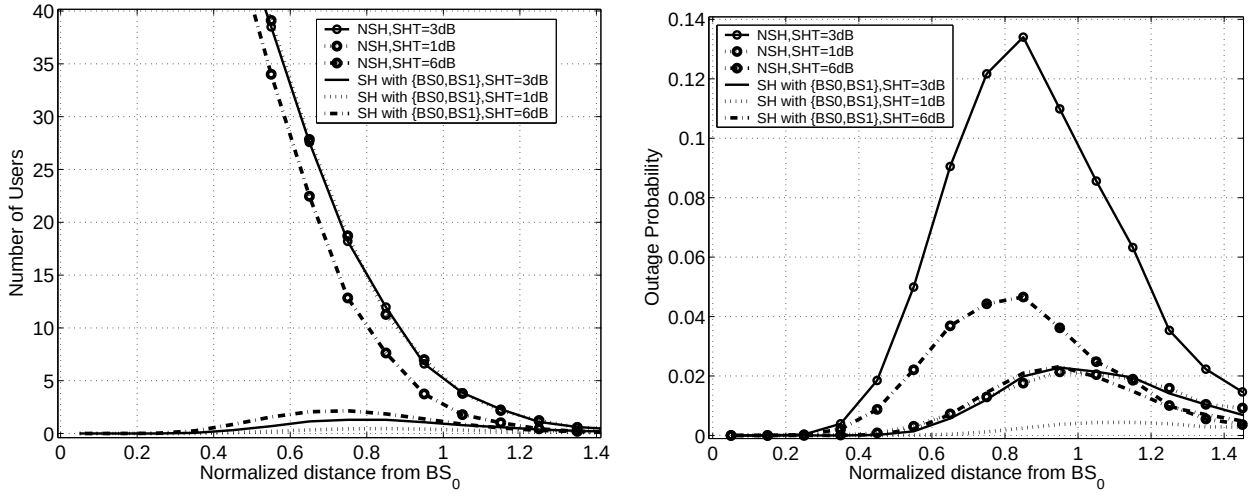

(a) (b)

Figure 4.6 Average capacity (a) and outage (b).

or less outage depends on the whether the MS is in the NSHM or SHM. But a high capacity and less outage can not be achieved for a certain SHT simultaneously. Notice that the capacity achieved by the 2-BS soft handoff as shown in Fig. 4.6(a) is very small. The total average capacity achieved by the MS at a certain location needs to consider the capacity achieved by all the soft handoff cases and when the owner BS is not BS_0, which is not the main purpose of this chapter and will be treated in a later chapter.

4.6.2 Without the Limitation on the Number of Rake Fingers

Let us consider a second finger allocation scheme, where there is no limitation on the number of fingers in the Rake receiver and for each BS in the active set, the MS allocates 4 fingers to capture most of the energy (about 80 % at the cell edge) from the multipath components. In this case, the soft handoff set is the same as the active set.

Fig. 4.7(a) and Fig. 4.7(b) show the capacity and outage with different MFBP limitations, respectively with a 3 dB SHT. A similar result can be observed as that

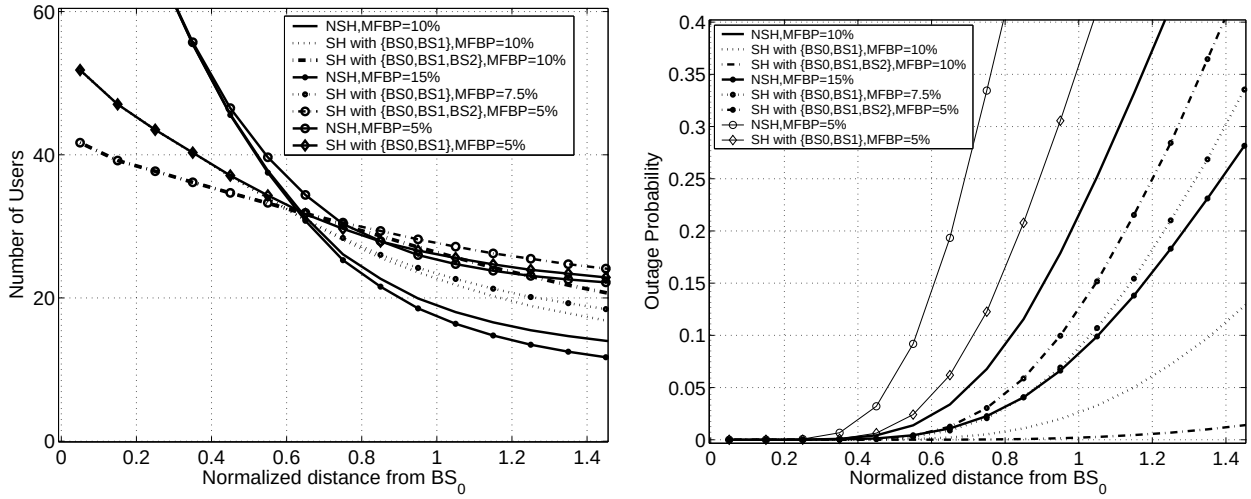

(a) (b)

Figure 4.7 Capacity (a) and outage (b) without finger limitation.

obtained from the previous case of a limited number of Rake fingers, that is, increasing the MFBP decreases the capacity but results in a significant outage reduction.

We notice from Fig. 4.7(a) that when each BS allocates maximum power of 10 % to the MS regardless its soft handoff mode, the capacity is limited by the MS's located at the normalized distance 0.65. When the second approach to calculate the capacity and outage is used and the total MFBP is 15 %, the location of the capacity limitation [1] is still around 0.65. This is because when the MFBP changes from a lower level of 10 % to 15 % for the MS's in the NSHM, there are insignificant capacity loss. Since the NSH has larger effect on the intersection of the capacities of the NSH and SH, the location of the capacity limitation does not change much.

We further notice that when the MFBP changes from 10 % to 5 %, the capacity gain of the NSH is significant, since the capacity is more likely to be affected by a lower

[1]The location of the capacity limitation is the location in the cell that beyond which the non-soft handoff has less capacity than the soft handoff does [1].

MFBP. The changes of the MFBP has less effects on the capacity when more BS's are included in the soft handoff set.

When the MFBP decreases to a lower value (5 %) and the first approach is used, the capacity is limited by the MS's located at a normalized distance about 0.78. In [1], the capacity was said to be limited by the MS located at a fixed normalized distance 0.84. In [24], it was argued that changing the SHZ boundaries affected the capacity but no convincing reason was given. We show that the boundaries of capacity limitation are different at different MFBP's. Recall that when there is no limitation on the number fingers in the Rake receiver, the boundary of capacity limitation moves closer to the cell center at a higher MFBP and the capacity limitation is less severe at the cell edge. Furthermore, in [1], it was observed that there was a sudden capacity drop at the SHZ boundary. The reason for that is that they did not consider that the MS in NSHZ could also be in the SHM and vice versa.

In [1], it was shown that the capacity gain of the 2-BS soft handoff was about 7 % and the capacity loss due to one additional channel in the 2-BS soft handoff is almost the same as that in an unsectorized cell. In [23], it was shown that the capacity loss is about $13\ \% - 15\ \%$. Our simulation results show that there is about 20 % capacity gain at the cell boundary and 90 % outage reduction when the soft handoff set increases from $\{BS_0\}$ to $\{BS_0, BS_1\}$ and the MFBP is set to 10 % for both the NSH and SH and the first approach is used to calculated the capacity. For a normalized total MFBP of 15 % and the second approach is used, the net capacity gain considering the capacity loss due to the 2-BS soft handoff is about 38 % but the outage increase about 8 % at the cell boundary. Therefore, the capacity gain and the outage reduction achieved by the SH can not be obtained simultaneously unless the MFBP limitation is relaxed.

Recall the discussions in section 4.6.1, there is no capacity gain within the cell, that is, the capacity limitation is outside the cell. This is because when there is limitation

on the number of fingers in the Rake receiver, MS's in the SHM can not catch enough energy from each BS in the soft handoff set and thereby, achieve less capacity comparing to the case of no limitation on the number of fingers in the Rake receiver. This can be shown by comparing Figs. 4.7 to Figs. 4.3.

We further notice that employing more fingers can increase the capacity and reduce the outage for both the NSH and SH. For example, the capacity decrease about 4 % and the outage increases about 72 % for the NSH when the number of fingers reduced from 6 to 4 at a 10 % MFBP. The capacity increase about 6 % and the outage reduces about 58 % for the 2-BS SH with $\{BS_0, BS_1\}$ if the number of fingers increases from 3 to 4 at a 10 % MFBP.

Based on the discussions in section 4.6.1 and this section, we could see that the location of the boundary of the limitation of the capacity depends on the limitations on the MFBP and the number of fingers in the Rake receiver.

4.6.3 The Effects of the Strong Interference

In previous discussions, we assume that each BS in the active set is assigned at least one finger by the MS and the active set is the same as the soft handoff set. The BS not in the soft handoff set always has a path loss greater than that of the owner BS_0 by the SHT. If the Rake receiver in the MS can not catch the signal from a specific BS in the active set due to the limitation on the number of available Rake fingers or temporary failures such as the loss of synchronization during the soft handoff, the signal from that BS acts as a strong interference at the MS and results in the performance degradation. In the simulation, The Rake receiver is assumed to assign total 6 fingers to only the owner BS_0. Therefore, if the active set is $\{BS_0, BS_1\}$, only BS_0 is in the soft handoff set.

Fig. 4.8(a) and Fig. 4.8(b) show the capacity and outage with a 10 % MFBP limitation and different SHT's for a 2-BS soft handoff with $\{BS_0, BS_1\}$ and a 3-BS soft

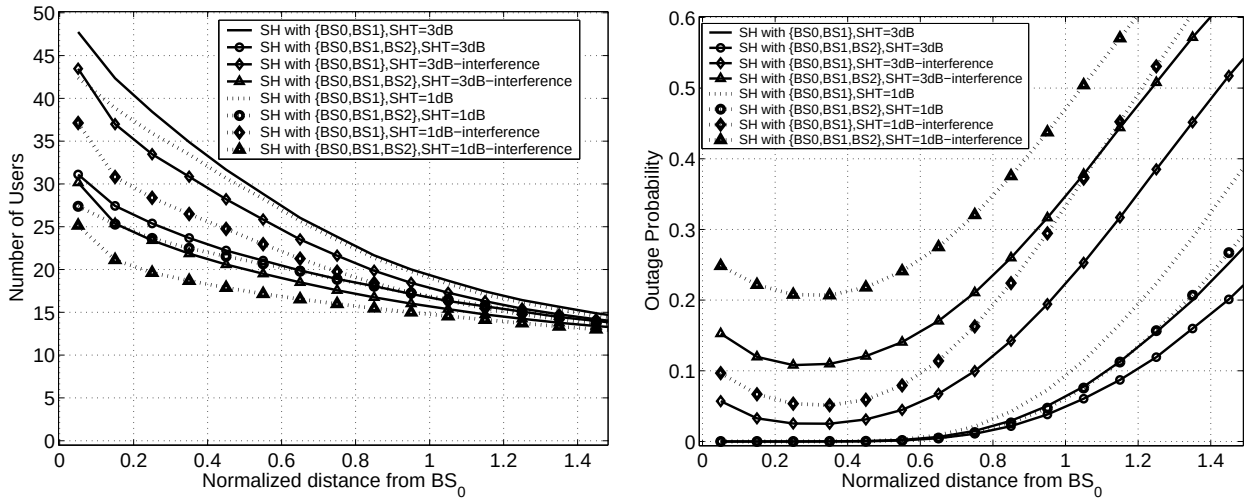

(a) (b)

Figure 4.8 Capacity (a) and outage (b) with strong interference.

handoff with $\{BS_0, BS_1, BS_2\}$ at the presence of the strong interference, respectively. The plot with the legend $interference$ is obtained by above finger allocation scheme. The plot without the legend $interference$ is obtained by the default finger allocation scheme.

We observe that when the SH set is $\{BS_0, BS_1\}$, the capacity loss is about 7 % and the outage increases about 226 % for a 3 dB SHT at the presence of the strong interference. If the SHT decreases to 1 dB, the capacity loss is about 11 % and the outage increases about 226 %. Recall that by referring to Fig. 4.4, when the SHT becomes less (e.g. changes from 3 dB to 1 dB), the capacity is decreased and the outage is increased for a certain MFBP. Here we show that when the SHT is smaller, the strong interference has more impacts on the capacity but almost the same impacts on the outage for a certain MFBP. Furthermore, we could see that at a location closer to the owner BS_0, considerable outage exists.

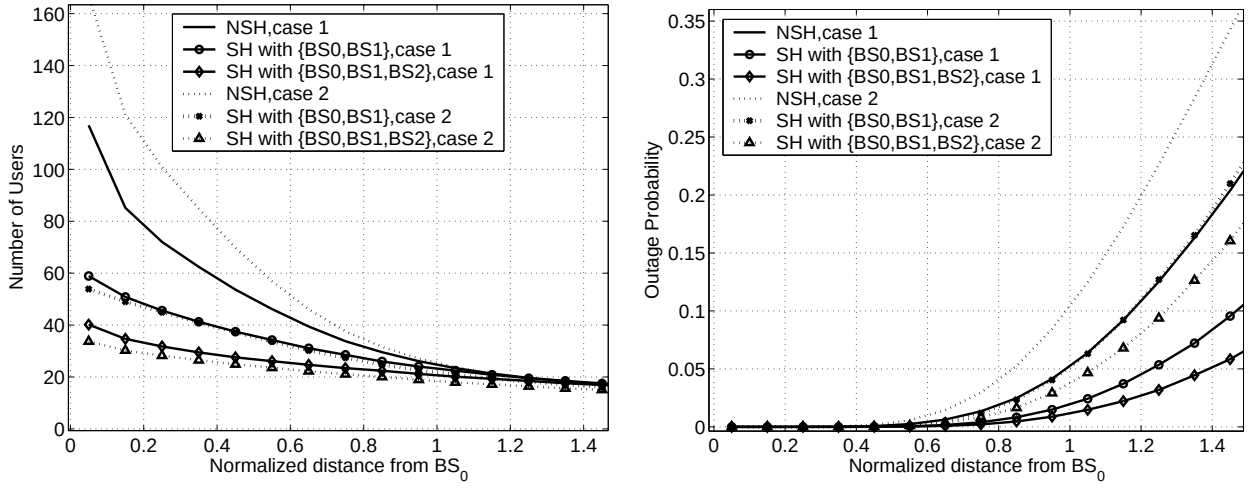

(a) (b)

Figure 4.9 Capacity (a) and outage (b) with a 10 % MFBP and a 3 dB SHT.

4.6.4 The Effects of Unequal BS Power

In above discussions, the total power from all BS is assumed to be the same. However, in the real CDMA systems, the unequal BS power always exists. Let us consider two cases, the first case assumes that BS_0 is heavily loaded with $\varphi_0 = 1.0$ and other cells serve less MS's and consume less BS power with $\varphi_1 = \varphi_2 = \cdots = 0.7$. The second case considers BS_0 is lightly loaded with $\varphi_0 = 0.7$ and other cells is heavily loaded $\varphi_1 = \varphi_2 = \cdots = 1.0$. The finger allocation scheme is chosen to be the default finger allocation scheme discussed in the beginning of section 4.6 for both cases. The first approach to calculate the capacity and outage is used in this subsection.

Fig. 4.9(a) and Fig. 4.9(b) show the capacity and outage with a 10 % MFBP limitation and a 3 dB SHT, respectively. The plot with the *highload* legend corresponds to the first case and the one with the *lowload* legend corresponds to the second case. It is obvious that the SIR of the case 1 is always larger than that of the case 2. Therefore, the outage of case 1 is less than that of case 2. When the system condition changes from case 2 to case 1 and the MS is at the cell boundary, the outage reduces about 49 % for

the NSH, 62 % for the 2-BS soft handoff with $\{BS_0, BS_1\}$, and 67 % for the 3-BS soft handoff with $\{BS_0, BS_1, BS_2\}$.

When the system condition changes from case 2 to case 1, there are capacity losses for the NSH and capacity gain for both the 2-BS soft handoff with $\{BS_0, BS_1\}$ and the 3-BS soft handoff with $\{BS_0, BS_1, BS_2\}$. This can be explained that for the NSH, the fraction of BS power has a similar distribution in the interval the minimum fraction of BS power and the MFBP for both the case 1 and case 2, which indicates a larger average value of the fraction of BS power for the case 1 since the SIR of case 1 is always larger than that of the case 2 and thereby, results in less capacity for case 1. For the SH cases, since the fraction of BS power of the case 2 is concentrated in the vicinity of the MFBP, we have a larger average value of the fraction of BS power for the case 2 and thereby, a less capacity for the case 2.

4.6.5 A Comparison of the WCDMA and MC-CDMA Systems

The performance comparison of the WCDMA system to the MC-CDMA system is an interesting topic. In [55], a rough comparison of the WCDMA and MC-CDMA in CDMA 2000 was addressed by neglecting the multipath fading. By using our model, the performance of the WCDMA system can be compared to that of the MC-CDMA by considering the multipath fading and other system parameters in details. For the WCDMA system, we choose the chip rate to be 3.84 $Mcpc$ and the data rate to be 30 $kbps$. For the MC-CDMA system, 3 multicarriers are assumed and each of the muticarrier has a chip rate of 1.2288 $Mcpc$ and a data rate of 9.6 $kbps$. First, we assume the default finger allocation scheme is used. For the MC-CDMA system, each carrier is assigned 2 fingers, which captures almost the same amount of energy from the multipath components of a certain BS as the 6 fingers in the WCDMA system do. Therefore, the BS in the NSH is allocated 2 fingers, each BS in the the 2-BS soft handoff is allocated 1 finger. When

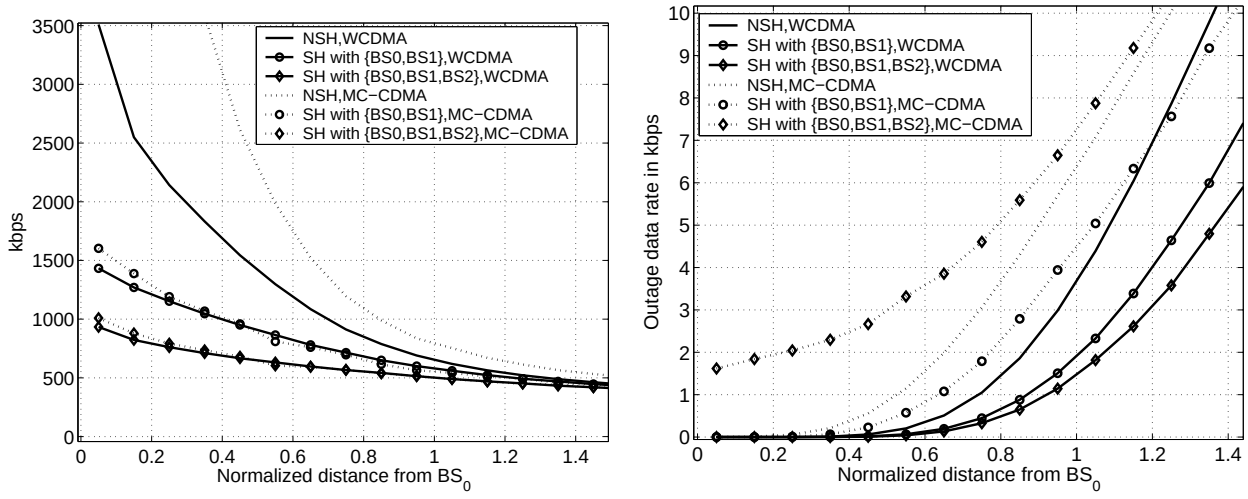

(a) (b)

Figure 4.10 User data rate (a) and outage (b) of the WCMA and MC-CDMA.

there are 3 BS's in the soft handoff with the MS, the 2 fingers are assigned to the two BS's with the smallest number as in Fig. 4.1. We assume that each of the subcarriers consumes one third of the total BS power dedicated to the data transmission and the fraction of power is defined as the ratio of the power allocate to a MS and the total power available to a subcarrier. Since the power of the interference for MS's tuning to a certain subcarrier comes only from that carrier and only 1/3 of that in the WCDMA systems, the MFBP limitation for the WCDMA and MC-CDMA is the same. The user data rate of the MC-CDMA system is calculated by multiplying the data rate of the individual MC-CDMA by 3. The outage in the unit of data rate is calculated by multiplying the outage probability with the data rate.

From Fig. 4.10(a) and Fig. 4.10(b), we could see that MC-CDMA system has more capacity than that of the WCDMA system at the cost of a surge of the outage for the MS's in the NSHM. The capacity is increased because when the MS is in the NSHM, there is SIR loss due to the usage of more fingers to capture the same amount of energy from the multipath components from a certain BS in the WCDMA system compared with each

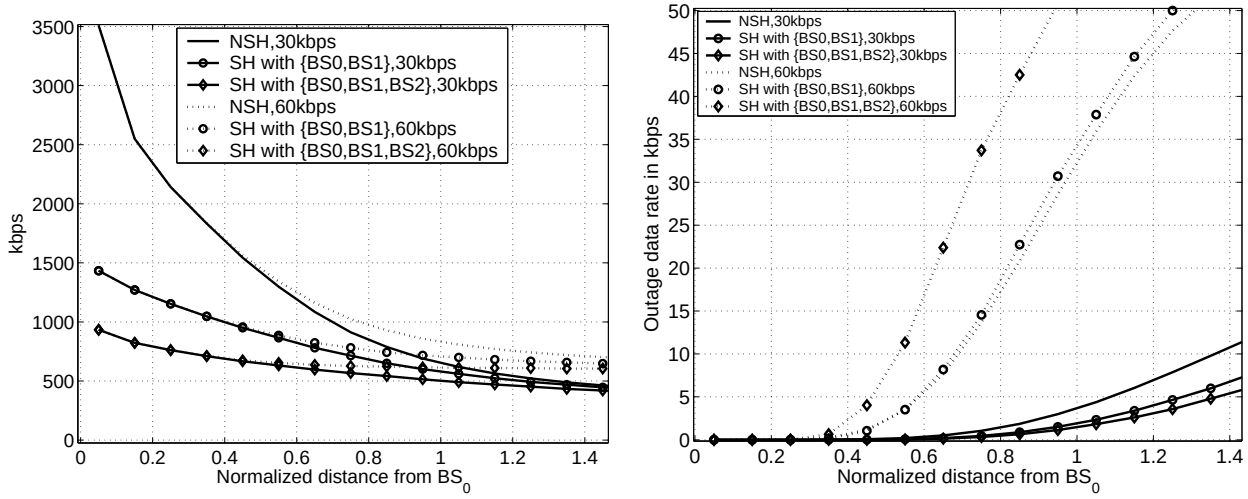

(a) (b)

Figure 4.11 User data rate (a) and outage (b) of different user data rate sets.

carrier in the MC-CDMA system. For example, the total SIR in the WCDMA systems is the summation of 6 individual SIR's according to above finger allocation scheme while in the MC-CDMA system, the the total SIR is only the summation of 3 individual SIR's from the Rake receiver. Since the signal term in one branch of the Rake receive poses as the interference term in another term, the SIR loss is resulted for the WCDMA system.

When the MS is in the SHM, almost equivalent capacity is achieved. This is because the BS diversity rather than the multipath diversity is dominant. In that case, the number of fingers used to capture the multipath fading components is not a significant factor to impact the capacity, since the total number of fingers used in these two systems is the same and the finger allocation scheme is the same. The outage of the MC-CDMA can be improved if it can share the BS power among the carriers rather than treating them as independent systems.

4.6.6 The Effects of the Data Rate

In above discussions, we assume a spread gain $G = 128$. Since multiple data rate services are deployed in the real CDMA system, it is interesting to study the data rate impacts on the system performance. The default simulation setup discussed in the beginning of section 4.6 is chosen and the chip rate is kept at 3.84 $Mcpc$. If the data rate is changed from 30 $kbps$ to 60 $kbps$, the spreading gain is changed from 128 to 64. Both the capacity and outage are calculated in term of the data rate.

The simulation results are shown in Fig. 4.11(a) and Fig. 4.11(b). We could see that increasing the data rate can increase the capacity at the cost of a surge of the outage in the transmitted data. This is because the outage can affect larger amount of data if a higher data rate is used.

It is instructive to design and compare the CDMA systems in term of equal outage, we can calculate the MFBP to achieve this outage probability by using (4.30) and then find out the capacity by using (4.29). Let us study the MS in the cell and in the NSHM. We find out that for a outage probability of 5 % and the MFBP is 0.115, the capacity is 600 $kbps$ for a data rate of 30 $kbps$. For a data rate of 60 $kbps$, the MFBP is doubled to 0.23 to achieve the same capacity and outage.

4.7 Comparison with Previous Works

4.7.1 Lee's Model

Hereafter in this chapter,we assume that the MS is in NSHM to compare Lee's model with our proposed model. For the MS in SHM, similar results can be obtained. In Lee's model [1], it is assumed that there are M channels and each channel is allocated to the same fraction of BS power and all BS's are equally loaded with the same power. Assuming voice activity factor is 1 and the total BS power is P_t, then the signal power

received from BS_0 by the MS is $S = P_t/(Ml_0)$. The intracell interference from other channels in the same cell is $P_t(M-1)/(Ml_0)$. The intercell interference from surrounding BS's is $P_t \sum_{i=1}^{N}(1/l_i)$. Then, the E_b/I_0 at the MS connected to BS_0 is written as

$$\left(\frac{E_b}{I_0}\right)_0 = \frac{G}{(M-1) + M\sum_{i=1}^{N}(l_0/l_i)} \tag{4.33}$$

Assuming M is large enough, (4.33) can be approximated by

$$\left(\frac{E_b}{I_0}\right)_0 = \frac{G/M}{1 + \sum_{i=1}^{N}(l_0/l_i)} \tag{4.34}$$

Using Jensen's inequality, the following result is derived from (4.34) as

$$E[\left(\frac{E_b}{I_0}\right)_0] \geq \frac{G/M}{1 + \sum_{i=1}^{N} E[l_0/l_i]} \tag{4.35}$$

The $E[(E_b/I_0)_0]$ is defined as the target SIR γ_{req} that the MS tries to maintain. Solving (4.35), the number of channel is obtained as

$$M \geq \frac{G/\gamma_{req}}{1 + \sum_{i=1}^{N} E[l_0/l_i]} \tag{4.36}$$

The outage is not defined in Lee's model. However, following similar arguments in [1], where the E_b/I_0 is a random variable, the outage can be defined as

$$P_{outa} = P[E[\left(\frac{E_b}{I_0}\right)_0] \leq \gamma_{req}]. \tag{4.37}$$

By using (4.35), equation (4.37) can be rewritten as

$$\begin{aligned} P_{outa} &= P[\frac{G/M}{1 + \sum_{i=1}^{N} E[l_0/l_i]} \leq \gamma_{req}] \\ &= P[\frac{1}{M} \geq \gamma_{req}(1 + \sum_{i=1}^{N} E[l_0/l_i])/G \end{aligned} \tag{4.38}$$

4.7.2 Comparison between Lee's Model and Our Proposed Model

4.7.2.1 Outage Comparison

By taking average over the fast fading and path loss terms in (4.10), neglecting the PCE, and comparing with (4.37), the following equivalent condition to equal the outage probability of our proposed model to that of Lee's model is

$$E[\frac{G\phi_{max}\sum_{i=1}^{f_k} X_{ki}/l_k}{h_k/l_k + \sum_{n=1,n\neq k}^{N} X_n/l_n}] = \gamma_{req} \tag{4.39}$$

This means that if the BS always allocates the maximum fraction of power ϕ_{max} to the MS, the average $E[E_b/I_0]$ in our proposed model is the target γ_{req} in Lee's model.

By defining the outage as $P[\phi > \phi_{max}]$, comparing to (4.38) and letting $\phi = \frac{1}{M}$, the same equivalent condition to equal the outage probability of our proposed model to that of Lee's model is

$$\phi_{max} = \gamma_{req}(1 + \sum_{i=1}^{N} E[l_0/l_i])/G \tag{4.40}$$

4.7.3 Capacity Comparison

Taking average over the fast fading and path loss terms in (4.10) and comparing to the lower bound of (4.36), the equivalent condition to equal the capacity of our proposed model and Lee's model is $\phi_{min} = 0$ and $\phi_{max} = +\infty$. Lee's model does not limit the BS power, but the maximum fraction of BS power is at most 1 in practical CDMA systems. By comparing the outage and capacity of Lee's model to those in our proposed model for the MS in the SHM, the same conclusions could be reached.

4.7.4 Summary

In summary, Lee's model and our proposed model is equivalent in the calculating of outage probability. However, the capacity calculated using our model is more practical and accurate in a power-controlled CDMA system, as we consider the limitation of the

maximum fraction of BS power. The maximum fraction of BS power allocated to a MS is a limited value less than 1 in our model. But in Lee' model, the maximum fraction of BS power allocated to a MS can go to infinity and thereby, is incorrect to model the practical power-controlled CDMA systems. This is because the E_b/I_0 in Lee's model is treated as a random variable, while the E_b/I_0 in our proposed model is a constant value under perfect power control and a range of values in presence of power-control error.

4.8 Mathematical Derivations

4.8.1 The Macrodiversity Non-orthogonality Factor

The analytical expression of the normalized macrodiversity non-orthogonality factor (MNOF) h_c is discussed in section 4.4. The default simulation setup in section 4.6 is used. Let us further fix the fraction of BS power ϕ in (4.9) and (4.10) to be 10 %. Here we choose a fixed ϕ, since we just want to study the accuracy of using (4.10) to approximate the SIR in (4.10). Notice that choosing different values of ϕ and G only shrinks or expands the CDF of E_b/I_0 but does not affect the accuracy of using the normalized MNOF in (4.10) to approximate the E_b/I_0 in (4.9).

Fig. 4.13(a) is plotted for MS's at different locations of the cell to compare the accuracy of using the MNOF to approximate the actual E_b/I_0. MS #1 is located at coordinate $[1.55, 0]$, MS #2 is located at $[1.05, 0]$, and MS #3 is located at $[0.55, 0]$. Hereafter, the *actual* SIR in the figures is obtained by using (4.9) and the approximation SIR is calculated by using (4.10) and simulating $100,000$ samples. Since the approximation SIR is so close to the *actual* SIR, the CDFs of their SIR's are superposed. Choosing other values of ϕ and G only shrinks or expands the CDF of the SIR but does not affect the relative relation between the CDF of the *actual* SIR and that of the approximation SIR. The difference between their distributions is insignificant at the 5 % level by using the

KS-test [46]. Furthermore, we could see that the farther the MS is away from the owner BS_0, the more likely the E_b/I_0 at the MS exceeds a certain value and the MS is in a worse situation.

Fig. 4.13(b) focuses on a MS located at the cell edge (MS #2 in Fig. 4.13(a)) according to the following cases: case 1 assumes that the PCE is increased to 2 dB and the SHT is set to 6 dB. Case 2 assumes that the active set is expanded to $\{BS_0, BS_1, BS_2\}$, but we assume only $\{BS_0, BS_1\}$ are included in the soft handoff set and each provides 3 multipath components, the SHT is chosen to be 6 dB, and the PCE is set to be 2 dB. Case 3 considers the unequal situation, where BS_0 is heavily loaded with $\varphi_0 = 1.0$ and other cells utilize less power, $\varphi_1 = \varphi_2 = \cdots = 0.7$. Case 4 considers the unequal situation, where BS_0 is lightly loaded with $\varphi_0 = 0.7$ and other cells is heavily loaded $\varphi_1 = \varphi_2 = \cdots = 1.0$. Case 5 assumes the chip rate is decreased to 1.2288 $Mcps$ and the data rate is 9.6 $kbps$, which is a typical setup in the IS-95 system.

For all these cases, the KS test is passed at the 5 % significant level. Although not shown here, we try more cases with different fading situations and system parameters and find out that KS test at a 5 % significant level is passed for all these cases. Actually, the largest difference between the CDFs is less than 1 %. The closeness of the approximation can also be observed that the plot of the approximation SIR is so close to the *actual* SIR in Figs. 4.13 that they overlap each other.

It is interesting to study the property of h_c and obtain a simplified calculation of the fraction of BS power ϕ in (4.14). These results are shown in Fig. 4.12. The *actual* value is calculated by using (4.13a) and the approximation value is obtained by using (4.14). The simulation setup is the same to the default simulation setup except we assign 6 Rake fingers to each BS in the soft handoff set for MS #1,#2a, and #3.

MS #2b has the same allocation as MS #2a (coordinate $[1.05, 0]$), except the number of Rake fingers tuning each BS in the soft handoff set is reduced to 3. Comparing

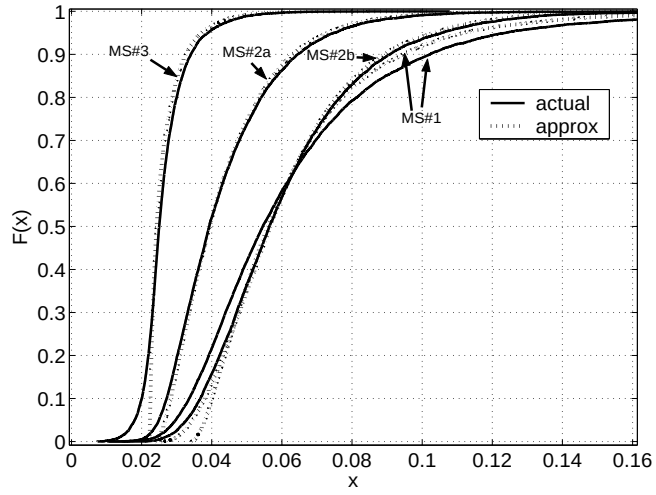

Figure 4.12 The CDFs of the fraction of BS power.

the accuracy of the approximation for MS #2a to that for MS #2b, we could also see that when the Rake receiver can catch larger amount of multipath components energy from the BS in the active set, the fraction of BS power ϕ is well approximated even by averaging the normalized macrodiversity non-orthogonality h_c. By observing the results obtained for MS#2b, the averaging effect on ϕ by using (4.14) is obvious since the slope of its CDF (the approximation CDF) is sharper. The utilization of the average value of h_c to approximate the fraction of BS power in the real CDMA systems is further explained in section 4.5.

4.8.2 Derivation of the Gamma Parameters

We defined the Gamma distribution as $Gamma(b, c)$, which has PDF $f(x) = c^b x^{b-1} e^{-cx}/\Gamma(b)$, $x \geq 0$ [45] and $\Gamma(b) = \int_0^\infty x^{b-1} e^{-x} dx$ is the complete gamma function. Assume U follows a Gamma distribution of $Gamma(b_u, c_u)$ and V follows a Gamma distribution of $Gamma(b_v, c_v)$. By equating the first and second moments of the left and

right sides of U in (4.13b) and using the fact that the average value of X_k is normalized to 1, we have

$$E[U] = \sum_{n \notin N_{set}} \varphi_n E\left[\frac{l_0}{l_n}\right] + \sum_{n \in N_{sh}^c} \varphi_n E\left[\frac{l_0}{l_n}\right] \tag{4.24}$$

and

$$\begin{aligned} E[U^2] = & \sum_{\substack{n,k \notin N_{set} \\ k \neq n}} \varphi_n \varphi_k E\left[\frac{l_0^2}{l_n l_k}\right] + \sum_{\substack{n \notin N_{set} \\ or\ n \in N_{sh}^c}} \varphi_n^2 E[X_n^2] E\left[\frac{l_0^2}{l_n^2}\right] + \\ & \sum_{\substack{n,k \in N_{sh}^c \\ k \neq n}} \varphi_n \varphi_k E\left[\frac{l_0^2}{l_n l_k}\right] + 2 \sum_{\substack{n \notin N_{set} \\ k \in N_{sh}^c}} \varphi_n \varphi_k E\left[\frac{l_0^2}{l_n l_k}\right] \end{aligned} \tag{4.25}$$

In the calculation of $E[U^2]$, we need to use

$$E[X_n^2] = \sum_{i=1}^{F_n} E[X_{ni}'^2](1-q_n)^2 q_n^{2(i-1)} + \sum_{\substack{i,j=1 \\ i \neq j}}^{F_n} E[X_{ni}' X_{nj}'](1-q_n)^2 q_n^{i-1+j-1} = \frac{1-q_n}{\rho(1+q_n)} + 1 \tag{4.26}$$

where q_k is defined in section 4.5.

By using the fact that $E[U] = \frac{b_u}{c_u}$ and $E[U^2] = \frac{b_u(b_u+1)}{c_u^2}$, we can obtain that $c_u = E[U]/(E[U^2] - E^2[U])$ and $b_u = c_u E[U]$. Similarly, by equating the first and second moments of the left and right sides of V in (4.13b), we have

$$E[V] = \sum_{k \in N_{sh}} (1 - q_k^{f_k}) E\left[\frac{l_0}{l_k}\right] \exp\left(\frac{\sigma_e^2 \delta^2}{2}\right) \tag{4.27}$$

and

$$\begin{aligned} E[V^2] = & \sum_{n \in N_{sh}} \left[\frac{1-q_n}{\rho(1+q_n)}(1 - q_n^{2f_n}) + (1 - q_n^{f_n})^2\right] E\left[\frac{l_0^2}{l_n^2}\right] \exp\left(2\sigma_e^2 \delta^2\right) \\ & + \sum\nolimits_{\substack{k,n \in N_{sh} \\ k \neq n}} (1 - q_n^{f_n})(1 - q_k^{f_k}) E\left[\frac{l_0^2}{l_n l_k}\right] \exp\left((\alpha^2 + 1)\sigma_e^2 \delta^2\right). \end{aligned} \tag{4.28}$$

We can obtain that $c_v = E[V]/(E[V^2] - E^2[V])$ and $b_v = c_v E[V]$. In equations (4.24-4.28), the following results are used:

$$E\left[\frac{l_0}{l_n}\right] = \exp\left(\frac{\sigma_b^2\delta^2}{2}\right)\frac{r_0^u}{r_n^u}E_x[\frac{Q(\frac{x-\gamma_{n1}+\sigma_b^2\delta}{\sigma_b}) - Q(\frac{x-\gamma_{n2}+\sigma_b^2\delta}{\sigma_b})}{Q(\frac{x-\gamma_{n1}}{\sigma_b}) - Q(\frac{x-\gamma_{n2}}{\sigma_b})}\exp(\delta x)] \tag{4.29a}$$

$$, n \in N_{set}, n \neq 0 \tag{4.29b}$$

$$E\left[\frac{l_0}{l_n}\right] = \exp\left(\frac{\sigma_b^2\delta^2}{2}\right)\frac{r_0^u}{r_n^u}E_x[\frac{Q(\frac{x-\gamma_{n1}}{\sigma_b} + \sigma_b\delta)}{Q(\frac{x-\gamma_{n1}}{\sigma_b})}\exp(\delta x)], n \notin N_{set} \tag{4.29c}$$

$$E\left[\frac{l_0^2}{l_n^2}\right] = \exp\left(2\sigma_b^2\delta^2\right)\frac{r_0^{2u}}{r_n^{2u}}E_x[\frac{Q(\frac{x-\gamma_{n1}+2\sigma_b^2\delta}{\sigma_b}) - Q(\frac{x-\gamma_{n2}+2\sigma_b^2\delta}{\sigma_b})}{Q(\frac{x-\gamma_{n1}}{\sigma_b}) - Q(\frac{x-\gamma_{n2}}{\sigma_b})}\exp(2\delta x)] \tag{4.29d}$$

$$, n \in N_{set}, n \neq 0 \tag{4.29e}$$

$$E\left[\frac{l_0^2}{l_n^2}\right] = \exp\left(2\sigma_b^2\delta^2\right)\frac{r_0^{2u}}{r_n^{2u}}E_x[\frac{Q(\frac{x-\gamma_{n1}+2\sigma_b^2\delta}{\sigma_b})}{Q(\frac{x-\gamma_{n1}}{\sigma_b})}\exp(2\delta x)], n \notin N_{set} \tag{4.29f}$$

$$E\left[\frac{l_0^2}{l_n l_k}\right] = \exp(\sigma_b^2\delta^2)\frac{r_0^{2u}}{r_k^u r_n^u}E_x[\frac{Q(\frac{x-\gamma_{n2}+\sigma_b^2\delta}{\sigma_b}) - Q(\frac{x-\gamma_{n1}+\sigma_b^2\delta}{\sigma_b})}{Q(\frac{x-\gamma_{n2}}{\sigma_b}) - Q(\frac{x-\gamma_{n1}}{\sigma_b})} \times \tag{4.29g}$$

$$\frac{Q(\frac{x-\gamma_{k2}+\sigma_b^2\delta}{\sigma_b}) - Q(\frac{x-\gamma_{k1}+\sigma_b^2\delta}{\sigma_b})}{Q(\frac{x-\gamma_{k2}}{\sigma_b}) - Q(\frac{x-\gamma_{k1}}{\sigma_b})}\exp(2\delta x)], n, k \in N_{set}, n, k \neq 0, n \neq k$$

$$E\left[\frac{l_0^2}{l_n l_k}\right] = \exp(\sigma_b^2\delta^2)\frac{r_0^{2u}}{r_k^u r_n^u}E_x[\frac{Q(\frac{x-\gamma_{n1}+\sigma_b^2\delta}{\sigma_b})}{Q(\frac{x-\gamma_{n1}}{\sigma_b})}\frac{Q(\frac{x-\gamma_{k1}+\sigma_b^2\delta}{\sigma_b})}{Q(\frac{x-\gamma_{k1}}{\sigma_b})}\exp(2\delta x)] \tag{4.29h}$$

$$, n, k \notin N_{set}, n \neq k \tag{4.29i}$$

$$E\left[\frac{l_0^2}{l_n l_k}\right] = \exp(\sigma_b^2\delta^2)\frac{r_0^{2u}}{r_k^u r_n^u}E_x[\frac{Q(\frac{x-\gamma_{n1}+\sigma_b^2\delta}{\sigma_b})}{Q(\frac{x-\gamma_{n1}}{\sigma_b})}\frac{Q(\frac{x-\gamma_{k2}+\sigma_b^2\delta}{\sigma_b}) - Q(\frac{x-\gamma_{k1}+\sigma_b^2\delta}{\sigma_b})}{Q(\frac{x-\gamma_{k2}}{\sigma_b}) - Q(\frac{x-\gamma_{k1}}{\sigma_b})}\exp(2\delta x)]$$

$$, n \notin N_{set}, k \in N_{sh}^c \tag{4.29j}$$

where $\sigma_b = b\sigma$, $\delta = \ln(10)/10$, $\gamma_{n1} = (10\mu\log_{10}(r_n/r_0) - Th)$, $\gamma_{n2} = 10\mu\log_{10}(r_n/r_0)$ and $E_x[.]$ means evaluating the expression by using a Gaussian random variable x with zero mean and σ_b standard deviation.

Similar to the simulation setup used in chapter 4.8.1, the *actual* value of U/V obtained by using (4.13b) and (4.13b) is compared with the approximation value of U/V characterized by using the ratio of Gamma variables. Fig. 4.14(a) shows the accuracy of the approximation value of U/V approaches the *actual* value of U/V for MS's in difference

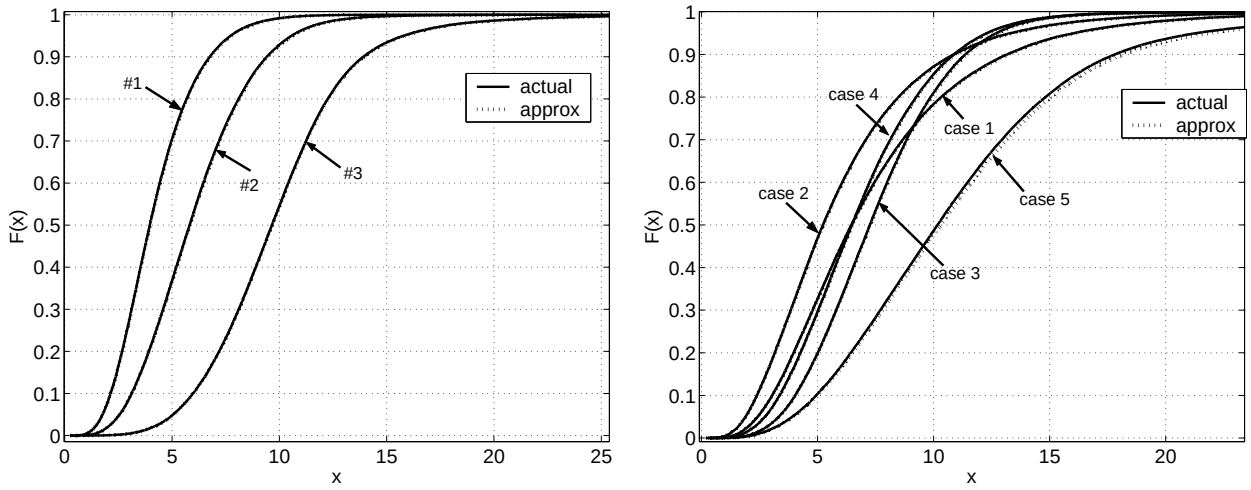

(a) (b)

Figure 4.13 CDFs of E_b/I_0. Different locations (a) and soft handoff cases (b).

locations of the cell. For MS #1, $b_u = 4.6105$, $c_u = 2.4722$, $b_v = 5.2965$, $c_v = 4.9645$, and the correlation coefficient between U and V is 0.014. For MS #2, $b_u = 2.1054$, $c_u = 2.2011$, $b_v = 5.1779$, $c_v = 4.7134$, and the correlation coefficient between U and V is 0.031. For MS #3, $b_u = 0.5853$, $c_u = 3.2013$, $b_v = 4.7211$, $c_v = 4.1127$, and the correlation coefficient between U and V is 0.029. The maximum difference between these CDFs is less than 5%.

For a given MS at the cell edge (MS #2), the accuracy of the approximation value of U/V is shown in Fig. 4.14(b), where five fading cases are taken into considerations. These cases are the same as those defined in chapter 4.8.1, except that we change the PCE to 1 dB in the case 1 and case 2. For the case 1, $b_u = 2.8448$, $c_u = 4.3743$, $b_v = 3.6743$, $c_v = 3.5854$, and the correlation coefficient between U and V is 0.054. For case 2, $b_u = 4.3183$, $c_u = 3.9770$, $b_v = 3.6743$, $c_v = 3.5854$, and the correlation coefficient between U and V is 0.068. For case 3, $b_u = 2.1054$, $c_u = 3.1444$, $b_v = 5.1780$, $c_v = 4.7134$, and the correlation coefficient between U and V is 0.031. For case 4, $b_u = 2.1054$, $c_u = 2.2011$, $b_v = 5.1780$, $c_v = 4.7134$, and the correlation coefficient between U and V is

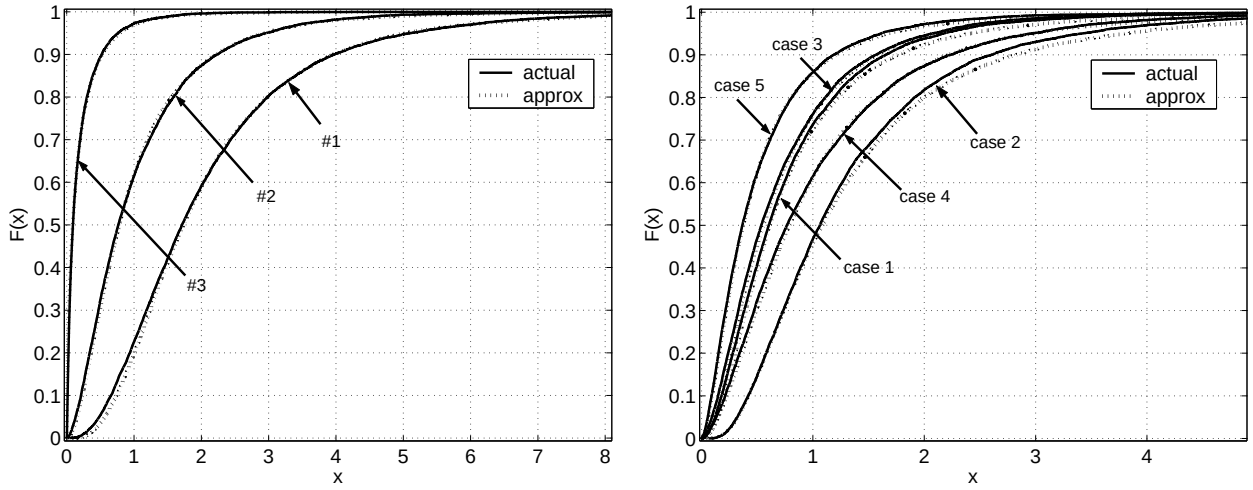

(a) (b)

Figure 4.14 CDFs of U/V. Different locations (a) and soft handoff cases (b).

0.031. For case 5, $b_u = 1.8467$, $c_u = 2.7580$, $b_v = 3.5648$, $c_v = 2.1573$, and the correlation coefficient between U and V is 0.028.

We could see that even if the SHT is increased to a larger value (e.g. 6 dB), the correlation between U and V can be neglected. Therefore, we can treat U and V as independent gamma variables to approximate the *actual* value of U/V. The maximum difference between the CDF is less than 5 % for all the cases, which is negligible. In addition, the effect of the approximation error is lessened since $(E_b/I_0)/G$ is multiplied to obtain the fraction of BS power by using (4.13a) and $(E_b/I_0)/G = 0.0247$ for $E_b/I_0 =$ 5 dB and $G = 128$. Simulation results also show that the approximation deteriorates if the PCE is increased to a very high level (e.g. 2 dB). However, if the CDMA system can control the the PCE around 1 dB, an accurate approximation can be obtained.

4.9 Conclusions

In this chapter, we propose a unified analytical approach to derive the analytical expression of the SIR in the forward link of CDMA systems for MS's in either the soft

handoff or non-soft handoff mode by considering the multipath fading. Therefore, the analytical expression of the fraction of BS power allocated to the MS in the forward link of an SIR-based power control is obtained, which can be further approximated by a function of the ratio of two Gamma variables. Therefore, the capacity and outage are calculated by a simple integral and an incomplete Beta function as a function of the maximum fraction of BS power (MFBP), respectively. Non-soft handoff is shown to be the primary cause of the outage. MS's in non-soft handoff mode always suffer from larger outage probability than those MS's in soft handoff mode. The capacity and outage are shown to be affected by the limitation on the maximum fraction of BS power, the limitation on the Rake fingers, the power control error, the unequal BS power, and the soft handoff threshold, which has not been addressed in previous literature [1] [24] [23] [56].

We show that the PCE (e.g. 1 dB) results in an insignificant capacity loss but produces a significant outage (e.g. 15 % at the cell boundary and 50 % in the middle of the cell for a 10 % MFBP). When more BS's included in the soft handoff set and there is a limitation on the number of available Rake fingers, each BS can utilize less number of Rake fingers. Therefore, the capacity is reduced (e.g. 10 % at the cell boundary). However, less outage (47 %) is achieved due to the diversity gain achieved by including more BS's into the soft handoff. At the same time, the soft handoff is shown to result in only capacity loss but provide a outage reduction regardless of the MS's location in the cell. When there are enough number of Rake fingers, the capacity of soft handoff exceeding that of the non-soft handoff is possible. The amount of the capacity gain of the soft handoff and the location of the capacity limitation is shown to be affected by the SHT and the MFBP. We show that the larger the MFBP or the SHT is, the less the capacity of the soft handoff compared to that of the non-soft handoff will be. For a larger the SHT or a smaller MFBP, the location of the limitation on the capacity moves

to the cell edge and soft handoff is less likely to provide the capacity gain. Therefore, the contradicting arguments among [1] [24] [23] and [56] can be reconciled if proper choice of the MFBP, the number of Rake fingers, and the SHT are made.

A larger MFBP or a smaller SHT, however, can provide a benefit of less outage. When there is limitation on the Rake fingers or failure in the MS causing the inability to track the signals in the active set, a significant outage is resulted even for a MS closes to the owner BS. The MC-CDMA system is shown to achieve almost the same capacity as that in the WCDMA for soft handoff but a larger capacity for non-soft handoff at the cost of an insurgent of outage.

CHAPTER 5

The Distribution of the BS Power and Call Admission Control

5.1 Overview

By extending the approach in previous chapter, we introduce an analytical model to characterize the distributions of the base station power required by a single soft handoff set, a single mobile station, and all mobile stations in the cell in the forward link of a power-controlled CDMA system, which leads to a closed-form expression of the capacity at specific outage and blocking probabilities. By considering real system parameters, such as the soft handoff threshold and the power control error, simulation results show that the statistics of the distributions of BS power experienced in the system are consistent with assuming that these probability densities can be used to characterize the BS power. The knowledge of the distributions of the BS power can be used to design the call admission control in the level of a single soft handoff set.

5.2 Introduction

In the 3G CDMA system, a carefully designed call admission control algorithm can utilize the base station (BS) power efficiently and improve the forward link capacity in terms of the maximum number of mobile stations (MS's) supported by a BS at certain outage and blocking probabilities. The knowledge of the blocking probability at a certain maximum number of MS's supported in the system and the amount of BS power needed by a MS to maintain a certain outage probability is crucial in designing an effective call admission control algorithm. However, it is commonly believed that a closed-form expression of the blocking probability, which is defined when the BS consumes all its

power and still can not accommodate more MS's into the system, is not available [16, pg. 298]. Computer simulation was the commonly used approach to obtain the BS power and estimate the blocking probability [34]. Recently, a Chernoff bound of the blocking probability was obtained in [35]. However, an exact closed-form expression of the blocking probability is still unavailable. The focus of our work is to establish an accurate analytical model to derive the distributions of the BS power allocated to a single soft handoff set, a single MS, and all MS's in the system, so that a fine call admission control can be conducted in the level of a single soft handoff set.

In the previous chapter, we proposed an analytical model introducing the concept of macrodiversity non-orthogonality factor to simplify the SIR into one term for any MS connected to different soft handoff sets. Since the fraction of the BS power required by a MS is inversely proportional to the SIR, an analytical expression of the distribution of the BS power was derived. But the analysis in above section assumes the reference BS should be the owner BS. By extending the model in the previous chapter and considering the case when the reference BS is not the owner BS, we show the fraction of BS power required by a MS communicating with any soft handoff set can be characterized by a ratio of two gamma variates. Therefore, the outage probability of a MS communicating with a specific soft handoff set, which happens when the MS asks the BS to allocate more power than the maximum fraction, is expressed as an incomplete Gamma function.

For a certain SHT, the MS connects to different soft handoff sets with different probabilities. By multiplying the fraction of BS power required by every possible soft handoff set at the MS with the corresponding probability and summing them together, we show that a Gamma variate can be used to model the power required by any single MS. The parameters of the Gamma variate can be obtained analytically from the system parameters. The outage probability of a single MS, which is defined as the probability that the MS asks the BS to allocate more power than a maximum limit by averaging over

the BS powers required by all possible soft handoff sets, can be obtained in a closed form by using an incomplete Gamma function. By summing the fractions of BS power required from all the MS's in different locations around a specific BS, we show that a Gamma variate can be used to model the distribution of the BS power. Therefore, a closed form of blocking probability is obtained by using the incomplete Gamma distribution. In addition, the flexibility of our model is embodied by considering real system parameters such as the power control error (PCE), the number of Rake fingers, and non-uniform user density.

This chapter is organized as follows: section 4.3 describes the system model. Section 5.4 shows the unified approach to characterize the distribution of the BS power when the MS connects to any soft handoff set. Based on that, the distribution of the BS power required by a single BS and all the MS's in the cell are derived. Section 5.5 gives the numerical results. Section 5.7 summarizes the results of the paper.

5.3 Soft Handoff Model

Multipath fading is not considered in the selection of the soft handoff set since the MS needs to maintain a relative stable soft handoff set in the real system. By following the analysis in [36] and referring to the soft handoff model in the real CDMA systems [16], our proposed soft handoff model is as follows: assuming the owner BS is BS_0 with a smallest path loss of L_0 (in dB), BS's in the soft handoff set should have path losses greater than the owner BS_0 by less than the soft handoff threshold Th (in dB) in order to have the requirement to be put into the soft handoff set. However, due to the limitation of the Rake fingers at the MS, only some of the qualified BS's are taken into the soft handoff set. Other qualified BS's unable to squash into the soft handoff set and together with unqualified BS's having path losses larger than $L_0 + Th$ are collected into the non-soft handoff set.

When a BS having a path loss less than that of BS_0, that BS is promoted to be the new owner BS replacing BS_0. When the BS other than BS_0 (for example $BS_i,\ i \neq 0$) is the owner BS, BS_0 can also be in soft handoff set. In that case, the path loss of BS_0 is greater than that of BS_i by less than $Th\ dB$. Other BS's not in the soft handoff set have path losses larger than that of BS_i but not necessary larger than that of BS_0.

Regardless whether BS_0 is the owner BS or not, if BS_0 is in the soft handoff set, the path losses of other BS's in the soft handoff set are within the range of $[L_0 - Th, L_0 + Th]$. The BS's not in the soft handoff set should have path losses greater than that of the owner BS. Since the owner BS has the smallest path loss, if BS_0 is in the soft handoff set, we know that path losses from BS's not in the soft handoff set are greater than $\min\{L_0, \cdots, L_i\}, i \neq 0$, where L_i is the path loss of BS_i in the soft handoff set. To simplify the analysis, we set the path losses from BS's not in the soft handoff set to be in the interval of $[L_0, +\infty]$, which causes a slight decrease in the interference strength when BS_0 is not the owner BS. The soft handoff model is shown in Fig. 5.1.

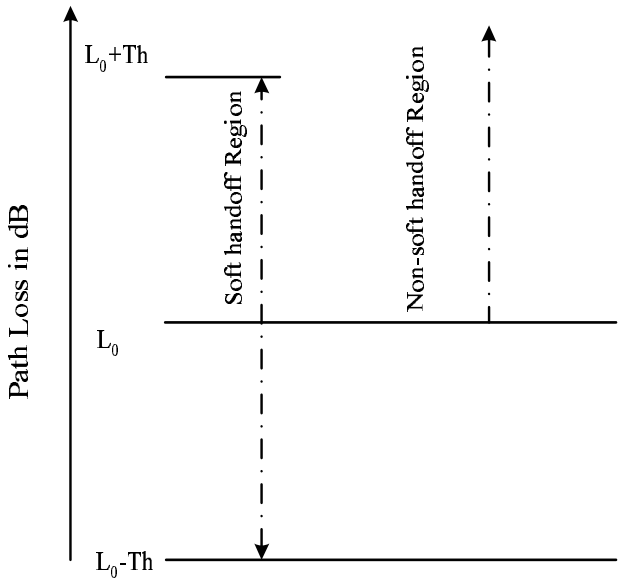

Figure 5.1 Soft handoff model.

Denote the soft handoff set as $N_{sh} = \{0, i_1, i_2, ..., i_M\}$, $i_k \in \{1, 2, \ldots, N\}$, where $M+1$ is the total number of BS's in the soft handoff set including BS_0 and N is the total number of BS's taken into consideration (referring to Fig. 4.1, N is 13). According to the soft handoff model established above, the probability of soft handoff with N_{sh} is

$$\begin{aligned} P_{N_{sh}} =& P\{L_0 - Th < L_i < L_0 + Th, L_j > L_0, i \in N_{sh}, i \neq 0, j \notin N_{sh}\} \\ =& E_z[\prod_{\substack{i \in N_{sh} \\ i \neq 0}} \{Q(z + c_{1i}) - Q(z + c_{2i})\} \prod_{j \notin N_{sh}} Q(z + c_j)] \end{aligned} \tag{5.1}$$

where $c_{li} = (M_0 - M_i - Th)/(b\sigma)$, $c_{2i} = (M_0 - M_i + Th)/(b\sigma)$, $c_j = (M_0 - M_j)/(b\sigma)$, Th is the SHT, $Q(z) = \int_z^{+\infty} \frac{1}{\sqrt{2\pi}} \exp(-x^2/2)dx$, and $E_z\{.\}$ is the mean value evaluated by assuming that z is a Gaussian random variable with zero mean and unit standard deviation.

When the MS is only connected to BS_0, BS_0 should be the owner BS and no other BS has the qualification to be in the soft handoff set, that is, all other BS's have path losses greater than that of the BS_0 by more than Th dB. The probability of non-soft handoff is

$$P\{L_0 + Th < L_i, i = 1, \cdots, N\} = E_z[\prod_{i=1}^{N} Q(z + c_{2i})]. \tag{5.2}$$

5.4 The Distributions of the BS Power and Call Admission Control

The Rake receiver at the MS usually uses the MRC to combine the multipath signals from these BS's in the soft handoff set to achieve optimal macrodiversity gain [1]. By assuming that the first f_k multipath components from BS_k in the soft handoff set are tracked by the Rake receiver at the MS, the target SIR (γ) with power control error can be expressed as

$$\gamma 10^{\xi_e/10} = \sum_{k \in N_{sh}} \sum_{i=1}^{f_k} \gamma_{ki} \tag{5.3}$$

where γ_{ki} is the SIR at the output of the Rake receiver of the MS tracking the i^{th} multipath of BS_k, ξ_e is PCE in dB following a normal distribution with zero mean and standard deviation σ_e [24].

Following the analysis in [36] [27], the SIR γ_{ki} is expressed as

$$\gamma_{ki} = \frac{G\frac{P_{ku}X_{ki}}{l_k}}{\frac{P_kX^c_{ki}}{l_k} + \sum\limits_{\substack{n=1\\n\neq k}}^{N}\frac{P_nX_n}{l_n}} = \frac{G\phi_u\frac{X_{ki}}{l_k}}{\frac{X^c_{ki}}{l_k} + \sum\limits_{\substack{n=1\\n\neq k}}^{N}\frac{X_n}{l_n}} \tag{5.4}$$

where G is the spreading gain and N is total number of BS's in a cell cluster. In addition, $X^c_{ki} = \sum_{f=1,f\neq i}^{\infty} X_{kf}$ is the power summation of all the multipath components from BS_k except the i^{th} multipath, $X_n = \sum_{f=1}^{\infty} X_{kf}$ is the power summation of all the multipath components from BS_n. The Gaussian noise is neglected. Moreover, $P = P_n$ is the actual utilized power from BS_n in the data channel and is assumed to be equal for all BS's in the soft handoff set as in [35] [1] [24]. P_{ku} is the transmitted power allocated from BS_k to MS_u dedicated to the data transmission. $\phi_u = P_{ku}/P$ is the fraction of BS power allocated by BS_k to MS_u in the data transmission and is assumed to be equal for all BS's in the soft handoff set [35] [1, eqn. 12].

By using (5.3) and (5.4), the target SIR can be written as

$$\gamma 10^{\frac{\xi_e}{10}} = \sum_{k\in N_{sh}}\sum_{i=1}^{f_k}\frac{G\phi_u\frac{X_{ki}}{l_k}}{\frac{X^c_{ki}}{l_k} + \sum\limits_{\substack{n\in N_{sh}\\n\neq k}}\frac{X_n}{l_n} + \sum\limits_{n\notin N_{sh}}\frac{X_n}{l_n}} \approx \frac{G\phi_u\sum\limits_{k\in N_{sh}}\sum\limits_{i=1}^{f_k}\frac{X_{ki}}{l_k}}{\sum\limits_{k\in N_{sh}}\frac{h_k}{l_k} + \sum\limits_{n\notin N_{sh}}\frac{X_n}{l_n}} \tag{5.5}$$

where

$$h_k = h_c\sum_{i=1}^{f_k}X_{ki} \tag{5.6}$$

$$h_c = [\sum_{k\in N_{sh}}\sum_{i=1}^{f_k}\frac{\frac{X_{ki}}{l_k}}{\frac{X^c_{ki}}{l_k} + \sum\limits_{\substack{n\in N_{sh}\\n\neq k}}\frac{X_n}{l_n}}]^{-1}. \tag{5.7}$$

h_k is obtained by equating both sides of (5.5) and setting the interference term $\sum_{n \notin N_{sh}} X_n/l_n$ from BS's that are not in the soft handoff set to be zero, which utilizes the symmetric property in the summation. h_c is independent of the BS_k and is called the normalized macrodiversity non-orthogonality factor. h_k is called the the macrodiversity non-orthogonality factor (MNOF). Letting $N_{sh} = \{k\}$ and the MS is only connected to BS_k, h_k is simplified to the non-orthogonality factor extensively discussed in the literature [51]. The validation of the approximation in (5.5) is shown in chapter 5.6.1. An upper bound on h_c is given by

$$h_c \leq [\sum_{k \in N_{sh}} \sum_{i=1}^{f_k} \frac{\frac{X_{ki}}{l_k}}{\sum\limits_{n \in N_{sh}} \frac{X_n}{l_n}}]^{-1} = 1 + \frac{\sum\limits_{k \in N_{sh}} \sum\limits_{i=f_k+1}^{\infty} \frac{X_{ki}}{l_k}}{\sum\limits_{k \in N_{sh}} \sum\limits_{i=1}^{f_k} X_{ki}/l_k} \tag{5.8}$$

By inverting (5.5) and using the upper bound of h_c, an upper bound of the fraction of power needed by MS_u to achieve a target γ is

$$\phi_u \leq \frac{\gamma 10^{\frac{\xi_e}{10}}}{G}[1 + \frac{U}{V}] = \phi_{uh} \tag{5.9}$$

and

$$\begin{aligned} U &= \sum_{n \notin N_{sh}} \frac{X_n l_0}{l_n} + \sum_{k \in N_{sh}} \sum_{i=f_k+1}^{\infty} \frac{X'_{ki}(1-q_k)q_k^{i-1} l_0}{l_k} \\ V &= \sum_{k \in N_{sh}} \sum_{i=1}^{f_k} \frac{X'_{ki}(1-q_k)q_k^{i-1} l_0}{l_k} \end{aligned} \tag{5.10}$$

where ϕ_{uh} is the upper bound of ϕ_u.

Traditional approach that treats the interference and signal in U and V as lognormal variates is not applicable [24] [1], since the SHT limits the range of the path losses according to the soft handoff model in section 5.3 and multipath fading is taken into consideration. Our simulation results show that U and V can be closely approximated by independent gamma variates for a SHT less than 3 dB as shown in chapter 5.6.2.

U is assumed to follow the distribution $Gamma(b_u, c_u)$ and V follows the distribution $Gamma(b_v, c_v)$. The calculation of the parameters b_u, c_u, b_v, and c_v is given in chapter 5.6.2. Since the PCE will result in temporal fluctuation of the target SIR γ, the MS will require a certain range of power to maintain the target SIR. Therefore, in the calculation of the outage, we had better mitigate this temporal fluctuation in the SIR. Without considering the PCE, that is, $\xi_e = 0$, the power $\gamma/G[1 + U/V]$ required by the MS from the BS should be less than a maximum fraction ϕ_{umax}. If a MS requires power more than the maximum fraction, the MS can not maintain the target SIR and will be in outage. The outage probability is

$$\begin{aligned} P_{out} &= P(\gamma/G[1 + U/V] > \phi_{umax}) = B(b_v, b_u, \chi_{umax}) \\ &= \frac{\chi_{umax}^{b_v}(1 - \chi_{umax})^{b_u}}{b_v B(b_v, b_u)}[1 + \sum_{n=0}^{\infty} \frac{B(b_v + 1, n + 1)}{B(b_v + b_u, n + 1)}\chi_{umax}^{n+1}] \end{aligned} \tag{5.11}$$

where $\chi_{u\max} = [(G\phi_{u\max}/\gamma - 1)(c_u/c_v) + 1]^{-1}$, $B(b_v, b_u, \alpha) = \frac{\int_0^{\chi_{u\max}} z^{b_v-1}(1-z)^{b_u-1}dz}{B(b_v,b_u)}$ is the incomplete beta function, and $B(b_v, b_u) = \int_0^1 x^{b_v-1}(1 - x)^{b_u-1}dx = \frac{\Gamma(b_v)\Gamma(b_u)}{\Gamma(b_v+b_u)}$ [30, page 258]. The series expansion in (5.11) is obtained by using equation (26.5.4) in [30].

For a target outage probability $\wp$, we can solve (5.11) for ϕ_{umax}. If ϕ_{umax} is greater than a certain value ϕ_{mbs}, we simply know that the MS can not communicate with the soft handoff set N_{sh} to maintain the target outage probability. We can choose ϕ_{mbs} to be any value less than 1. We will show later that the choice of ϕ_{mbs} affects the coverage of BS_0 and the maximum number of MS's that BS_0 can support.

As discussed above, regardless the soft handoff set that the MS is connecting to, the MS maintains the target outage probability. Therefore, the average outage probability is the same as the target outage probability $\wp$. By considering all the handoff combination

including the soft handoff's and non-soft handoff, the average power required by MS_u from BS_0 is

$$\phi_{ut} = \frac{\sum_{N_{sh}} \phi_{uh}|_{SH\ with\ N_{sh}\&\gamma/G[1+U/V]\leq\phi_{umax}} P_{N_{sh}}}{\sum_{N_{sh}} P_{N_{sh}}} \tag{5.12}$$

Our simulation results show that ϕ_{ut} can be closely approximated by a Gamma variate with a distribution $Gamma(b_{\phi ut}, c_{\phi ut})$. The parameters $b_{\phi ut}$ and $c_{\phi ut}$ can be obtained by equating the first and second moments of ϕ_{ut} and given by $c_{\phi ut} = E[\phi_{ut}]/(E[\phi_{ut}^2] - E^2[\phi_{ut}])$ and $b_{\phi ut} = c_{\phi ut}E[\phi_{ut}]$. The expressions of $E[\phi_{ut}]$ and $E[\phi_{ut}^2]$ and the accuracy of treating ϕ_{ut} as a Gamma variate are shown in chapter 5.6.3.

Assume the number of MS's at a certain location of the cell is $\Re_p$, the power summation of all these users is

$$\phi_p = \sum_{u=1}^{\Re_p} \phi_{ut} \tag{5.13}$$

Since ϕ_{ut} follows i.i.d Gamma distribution $Gamma(b_{\phi ut}, c_{\phi ut})$, we can easily show that the summation ϕ_p follows a Gamma distribution $Gamma(b_{\phi p}, c_{\phi p})$ with $b_{\phi p} = \Re_p b_{\phi ut}$ and $c_{\phi p} = c_{\phi ut}$. Due to the symmetry of the cell, each MS_p located at position p in one of the triangle in Fig. 4.1 has the other 11 identical MS's requiring powers from BS_0 with the same distribution. By denoting the summation of the powers from these MS's having the same distribution of power requirement at location p as ϕ_{pa}, we can easily show that ϕ_{pa} follows a Gamma distribution $Gamma(b_{\phi pa}, c_{\phi pa})$, where $b_{\phi pa} = 12\Re_p b_{\phi ut}$ and $c_{\phi pa} = c_{\phi ut}$. The summation of the powers required from all the MS's at different locations surrounding BS_0 is

$$\phi = \sum_{p} \phi_{pa} \tag{5.14}$$

where the location p of MS_p is in the triangle in Fig. 4.1. It is well known that the sum of Gamma variates can be closely approximated by another Gamma variate or series [53].

ϕ can be approximated by a Gamma variate with a distribution $Gamma(b_\phi, c_\phi)$ [53]. The parameters b_ϕ and c_ϕ can be obtained by equating the first and second moments of ϕ and given by $c_\phi = E[\phi]/(E[\phi^2] - E^2[\phi])$ and $b_\phi = c_\phi E[\phi]$, where $E[\phi] = \sum_p E[\phi_{pa}]$ and $E[\phi^2] = \sum_{p \neq q} E[\phi_{pa}]E[\phi_{qa}] + \sum_p E[\phi_{pa}^2]$.

The system blocking probability is related to the maximum number of MS's by

$$P_b(\phi > 1) = 1 - Gaminc(b_\phi, c_\phi, 1) \tag{5.15}$$

where $Gaminc(b, c, y) = \frac{c^b}{\Gamma(b)} \int_0^y x^{b-1} \exp(-cx) dx$ is the incomplete gamma function. By solving (5.15) to obtain $\Re_p$ at different locations and summing them up, we can obtain the maximum number of MS's supported by BS_0 at a certain blocking probability.

The user density at different locations in the cell can be different. For simplicity, we consider two special cases: the first case assumes a uniformly distributed user density $\Re_p = \Re$ and the second one assumes that the user density $\Re_p = \Re f(d)$ is a function of d, where d is the distance between the MS and BS_0. When $f(d) = 1$, it is reduced to the uniformly distributed user density. For example, we can choose $f(d) = \eta^d, d \leq D$, where D is the radius of the coverage area of BS_0, $\eta \leq 1$ is the decay constant. If $\eta = 1$, it becomes the uniformly distributed user density. For the above two special cases, a simpler approach exists to solve (5.15) for the number of MS's as follows: we can first assume the user density $\Re$ equals to one and sum all the power required from MS's in the triangle of Fig. 4.1 around BS_0 as

$$\phi_{tri} = \sum_{MS_u \in \ triangle} \sum_{u=1}^{f(d)} \phi_{ut} \tag{5.16}$$

By denoting $\phi_{ud} = \sum_{u=1}^{f(d)} \phi_{ut}$, we know that ϕ_{ud} follows a Gamma distribution $Gamma(b_{ud}, c_{ud})$, where $b_{ud} = f(d) b_{\phi ut}$ and $c_{ud} = c_{\phi ut}$. Since ϕ_{ud} has a Gamma distribution, ϕ_{tri} follows a Gamma distribution $Gamma(b_{tri}, c_{tri})$. The parameters $b_{\phi_{tri}}$ and $c_{\phi_{tri}}$ can be obtained from the first and second moments of ϕ_{tri} and given by $c_{\phi_{tri}} =$

$E[\phi_{tri}]/(E[\phi_{tri}^2] - E^2[\phi_{tri}])$ and $b_{\phi ut} = c_{\phi_{tri}} E[\phi_{tri}]$, where $E[\phi_{tri}] = \sum_{MS_u \in \ triangle} E[\phi_{ud}]$ and $E[\phi_{tri}^2] = \sum_{MS_p, MS_q \in \ triangle, p \neq q} E[\phi_{pd}]E[\phi_{qd}] + \sum_{MS_p \in \ triangle} E[\phi_{pd}^2]$. Then if the number of MS's at every point of the cell is scaled by $\Re$ and we assume 12 identical triangles in the cell, we need to sum these $12\Re$ identically distributed Gamma variates to obtain ϕ in (5.14). The parameters of the Gamma distributed variable ϕ is given by $b_\phi = 12\Re b_{tri}$ and $c_\phi = c_{tri}$. Therefore, we can solve (5.15) for $\Re$ and subsequently, $\Re_p$.

5.5 Numerical results and analysis

The triangle shown in Fig. 1 is divided into 30 bins in x-axis and 18 bins in y-axis to achieve a uniformly distributed user density. The default simulation configuration is used throughout our work unless otherwise explicitly stated as follows: the spreading gain G is 128 for a chip rate of 3.84 $Mchip/s$ and a data rate of 30 $kbps$, which is a typical setup in the wide-band CDMA (WCDMA). The path loss slope u is chosen to be 4. Standard deviation σ of shadowing is 8 dB. Correlation coefficient of the shadowing a^2 is chosen to be 0.5. The default soft handoff set is $\{BS_0, BS_1\}$. The target SIR γ is chosen to be 5 dB. For a specific soft handoff set, the maximum fraction ϕ_{mbs} of BS power available to an individual MS is set to 1. The Rake receiver deploys 6 fingers and equally assigns them to the BS's in the soft handoff set, which is chosen to accommodate maximum of 4 BS's including the owner BS_0. The probability that more than 4 BS's simultaneously in the soft handoff set is negligible. Throughout of the paper, without explicitly stated, a uniformly distributed user density is assumed.

5.5.1 The Limitations on the Rake Fingers

The default finger allocation scheme discussed above is used to study the effects of the limitation of the Rake fingers on the capacity. Our simulation results show that for a 3 dB SHT, no PCE, a target outage probability $\wp = 0.01$, and $\phi_{mbs} = 1$, BS_0

can support MS's in an area with radius more than 1.6 from the BS_0. If we restrict $\phi_{mbs} = 0.2$, BS_0 can only support MS's in an area within a 0.87 radius from the owner BS_0. In another word, for a MS at a distance farther than 0.87 from BS_0, every soft handoff combination at the MS requires power from BS_0 more than the maximum limit (i.e. 0.2) in order to achieve the target outage probability $\wp = 0.01$. Further restriction on ϕ_{mbs} (e.g. 0.1) results in a 0.53 radius of the coverage area by BS_0. If we relax the target outage probability $\wp$ to 0.05 but still assume no PCE, BS_0 can cover an area with a radius more than 1.6 for $\phi_{mbs} = 0.2$ or an area with a radius 0.73 for $\phi_{mbs} = 0.1$. Let us now consider a 1 dB PCE at a 3 dB SHT. The coverage area is almost the same as there is no PCE regardless the ϕ_{mbs} and $\wp$ values. This is because the ϕ_{mbs} just limits the maximum value of the fraction of BS power and the PCE mainly affects the average value of the fraction of BS power available to the MS. If we reduce the SHT to 1 dB and keep no PCE, the radius of coverage area is 0.98 for $\wp = 0.01$ and $\phi_{mbs} = 0.2$. Other choices of ϕ_{mbs} and $\wp$ also show that a smaller SHT provides a large coverage area. Therefore, a larger target outage probability causes a larger coverage area. At the same time, a larger target outage probability provides a larger number of MS's supported by a BS, which will be addressed later. Furthermore, relaxing the maximum fraction of BS power limitation ϕ_{mbs} on the soft handoff set or choosing a smaller SHT leads to a larger coverage area by a BS. However, this benefit is achieved at the cost of less number of MS's that can be supported by the BS at a certain blocking probability, which will be discussed below.

Fig. 5.2 shows the average fraction of BS power allocated to a single MS along the base line of the triangle in Fig. 4.1. Comparing the dotted line ($\phi_{mbs} = 0.2$) to the solid line ($\phi_{mbs} = 1$), we could see that the average fraction of BS power is almost the same for MS's located at a distance less than 0.9 from BS_0. When the maximum fraction of BS power ϕ_{mbs} available to a MS is reduced from 1 to 0.2, MS's at a distance larger than 0.9 from BS_0 consume less average fraction of BS power. This is because when we limit ϕ_{mbs},

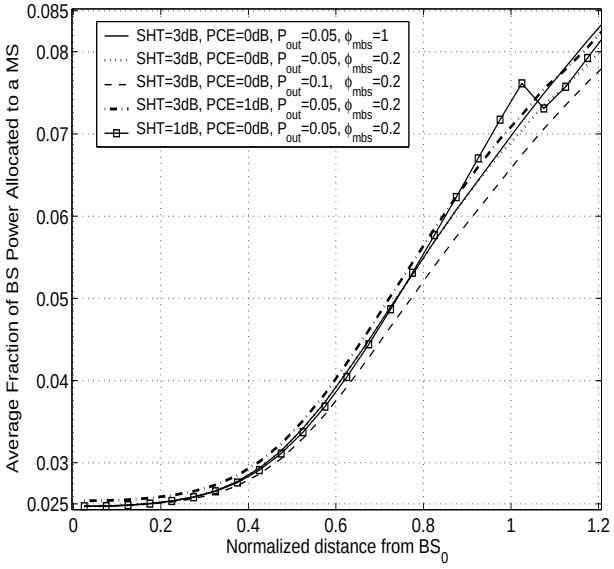

Figure 5.2 Average fraction of BS power allocated to a single MS.

the power requirements from those power-greedy soft handoff sets with maximum fraction of power consumption exceeding ϕ_{mbs} are no longer accommodated by BS_0. Comparing the dotted line ($P_{out} = 0.1$) to the dashed line ($P_{out} = 0.05$), we could see that relaxing the target outage probability makes the MS requires less average fraction of BS power regardless the MS's location. Comparing the dash-dot line ($PCE = 1\ dB$) to the dotted line (no PCE), we can easily observe that MS's suffering from a larger PCE need more average fraction of power from BS_0 regardless its location. Furthermore, the solid line with square marker ($SHT = 1\ dB$) intersects with the dotted line ($SHT = 3\ dB$) at 0.75 normalized distance from BS_0. When the MS is far from the BS_0 (> 0.75), a larger SHT will provide the benefit of requiring less average fraction of power from BS_0. However, when the MS is close to BS_0 (< 0.75), it requires more average fraction of power from the BS to maintain the same target outage. This can be explained as follows: increasing the SHT enlarges the strength of signals from BS's in the soft handoff set, while introducing more interference from BS's not in the soft handoff set. When the MS is close to the

BS, increasing the SHT will not significantly increase the signal level, but introduce a larger interference. Therefore, MS's closer to BS_0 should reduce the SHT. However, the situation is changed when the MS is far away from BS_0, where the interference level is already high. For these MS's far away from BS_0, a larger SHT increases the signal level but introducing a small amount of interference increase, which causes these MS's to use less fraction of BS power to achieve the target outage probability. Therefore, MS's far away from BS_0 should increase the SHT. In addition, a ripple is observed for the solid line with square marker ($SHT = 1\ dB$) at a distance of 1.02 from BS_0. This is because at the cell edge, the maximum fractions of BS power required by some of the power-greedy soft handoff sets at the MS exceed the threshold ϕ_{mbs}. The BS declines the power requirement from these power-greedy soft handoff sets and thereby, reduces the average fraction of power consumed by the MS.

The average fraction of BS power required by MS's shown in Fig. 5.2 directly related to the capacity, which is the maximum number of MS's supported by BS_0 as shown in Fig. 5.3. Since the MS's at the cell edge consume a larger amount of BS power, even if BS_0 can support MS's at a larger distance, it had better only support MS's within a certain distance to improve the capacity. Fig. 5.3 shows the capacity achieved if BS_0 only support MS's within a normalized distance less than 1.2. It shows that a tighter limitation on the maximum fraction of BS power that a soft handoff set can use, a larger target outage probability, or a smaller PCE leads to a larger capacity. For example, when ϕ_{mbs} is reduced from 1 to 0.2, BS_0 can support 0.2 more MS's at a 0.1 blocking probability. If P_{out} is relaxed from 0.05 to 0.1, BS_0 can support 1 more MS's at a 0.1 blocking probability. When the PCE is reduced from 1 dB to 0 dB, BS_0 can support 0.7 more MS's at a 0.1 blocking probability. Since MS's at cell edge consume a significant amount of BS power and limit the capacity, a smaller SHT (e.g. 1 dB) does not provide enough diversity gain for MS's at the cell edge and therefore, causes a decrease of the

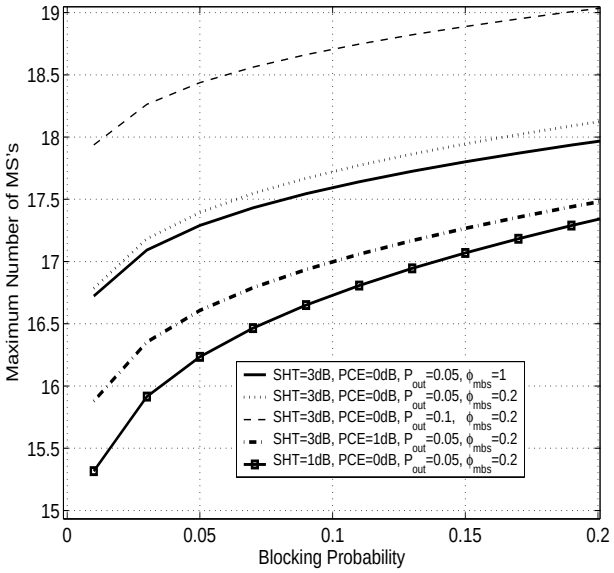

Figure 5.3 Capacity of BS_0 covering an area with a 1.2 radius.

capacity (e.g. 1 MS less) at a 0.1 blocking probability. For other blocking probabilities, similar results can be observed.

Fig. 5.4 shows the capacity achieved if BS_0 restricts the radius of the coverage area to 1. Compared to Fig. 5.3, we observe that limiting the coverage area increases the capacity (e.g. 3-4 more MS's). Notice that the capacity provided by $\phi_{mbs} = 0.2$ is almost the same as $\phi_{mbs} = 1$. This is because the maximum fraction of BS power required to maintain the target outage probability at the MS is well restricted within 0.2 for both cases. In addition, as shown in both Fig. 5.3 and Fig. 5.4, BS_0 can support more MS's with the increasing of the blocking probability.

Let us consider a decreased user density within the cell with $\Re_p = \Re\eta^d, d \leq 1$ and the decay constant $\eta = 1/2$. At the cell edge, $\Re_p = \Re/2$. The results are shown in Fig. 5.5. As expected, we could see a significant capacity increase (at least 12 more MS's) compared to the results obtained for uniformly distributed user density in Fig. 5.4.

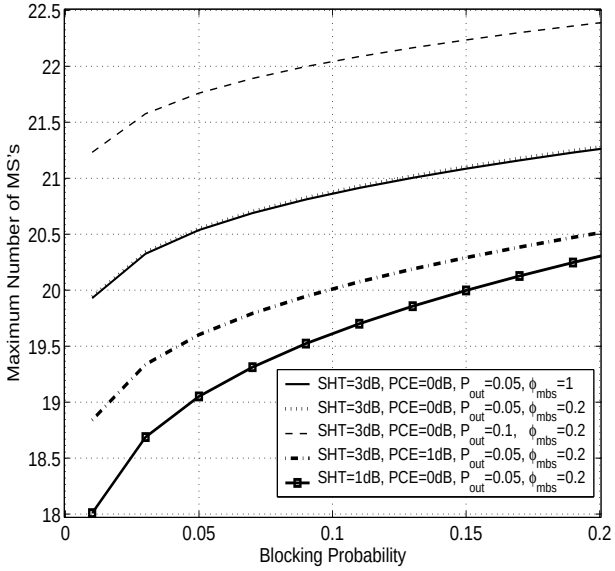

Figure 5.4 Capacity of BS_0 covering an area with a 1 radius.

5.5.2 Without Limitations on the Rake Fingers

Let us consider a second finger allocation scheme, where there is no limitation on the number of fingers in the Rake receiver. For each BS in the soft handoff set, the MS allocates 6 fingers to capture most of the energy (more than 85 % at the cell edge by using our simulation) from the multipath components.

Our simulation results show that for a 3 dB SHT, no PCE, a target outage probability $\wp = 0.01$ and $\phi_{mbs} = 1$, the BS_0 can support MS's in an area with radius more than 1.6 from the BS_0, which is the same as the result obtained with limitation on the Rake fingers. If we restrict $\phi_{mbs} = 0.2$, BS_0 can still support MS's in an area within a 1.6 radius from BS_0, which shows that employing more Rake fingers to tract multipath components can provide more coverage. Similar to the result obtained for the case of limited number of Rake fingers, the coverage area at 1 dB PCE is almost the same as there is no PCE regardless the ϕ_{mbs} and $\wp$ values. If we reduce the SHT to 1 dB and keep no PCE, the radius of coverage area can still be up to 1.6 for $\wp = 0.01$ and $\phi_{mbs} = 0.2$. Therefore,

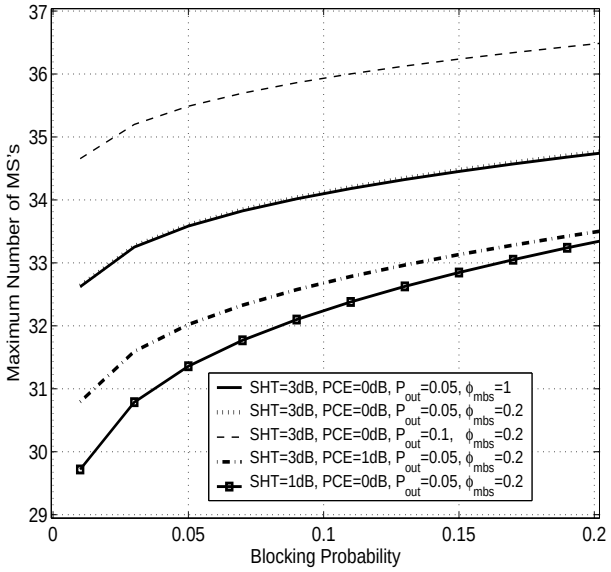

Figure 5.5 Capacity of BS_0 with deceased user density.

if we can deploy enough number of Rake fingers to tract the multipath components, the coverage area of the BS_0 can be extended much farther.

Fig. 5.6 shows the average fraction of BS power allocated to a single MS along the base line of the triangle in Fig. 4.1. Compared to the results obtained for the case with limited number of Rake fingers shown in Fig. 5.2, the same results can be observed, that is, the MS needs less average fraction of BS power for a smaller PCE, a larger target outage probability, or a tighter restriction on the maximum fraction of BS power that a soft handoff set can use. The difference is that if there is no limitation on the number of Rake fingers, the MS needs less average fraction of BS power to maintain the target outage probability for the same simulation parameters.

The solid line with square marker ($SHT = 1\ dB$) intersects with the dotted line ($SHT = 3\ dB$) at 0.35 normalized distance from BS_0. Compared to the intersection point at 0.75 for the case with limitation on the number of Rake fingers, we could see that if there is no limitation on the number of Rake fingers, the fraction of BS power

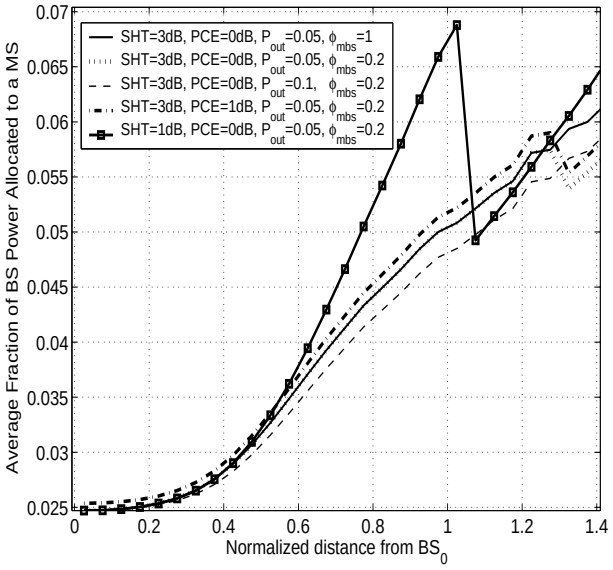

Figure 5.6 Average fraction of BS power (no limit on the Rake fingers).

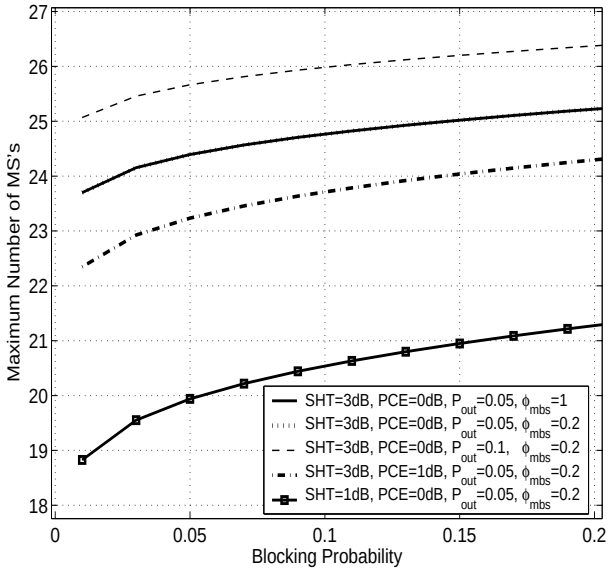

Figure 5.7 Capacity of BS_0 (no limit on the Rake fingers).

required by MS's using a larger SHT is smaller. This is because employing more Rake fingers to track the multipath components can provide a better macrodiversity gain and therefore, require a larger SHT to provide a larger range of signal strength. A ripple is also observed for $SHT = 1\ dB$ at a distance 1.02 from BS_0, which happens at the same location as the case of no limitation on the number of Rake fingers. However, this ripple is much larger than that happens for the case of no limitation on the number of Rake fingers. This is because that when there is no limitation on the number of Rake fingers, the average fraction of BS power consumed by each soft handoff set is smaller but variance of the fraction of BS power is larger. The larger variance is caused because when more Rake fingers are deployed to catch more multipath components, the number of terms in the summation of calculating the SIR by using MRC becomes larger.

Fig. 5.7 shows the capacity achieved if BS_0 restricts the radius of the coverage area to 1 with no limitation on the number of Rake fingers. Notice that since the average fraction of BS power required by the MS when $\phi_{mbs} = 0.2$ is the same as when $\phi_{mbs} = 1$, the capacity is the same for $\phi_{mbs} = 0.2$ and $\phi_{mbs} = 1$. Compared to Fig. 5.4, we could see that at a 0.1 blocking probability, the capacity gain for $SHT = 1\ dB$ is about 1 more MS. For other simulation configurations, 4 more MS's are observed. Therefore, at a larger SHT (e.g. 3 dB), a significant capacity gain can be achieved. However, we should aware that a smaller SHT can provide a large coverage area, which is much obvious for limited number of Rake fingers as addressed in section 5.5.1.

5.6 Mathematical Derivations

5.6.1 The Approximation of SIR

The analytical expression of the normalized macrodiversity non-orthogonality factor (MNOF) h_c is discussed in section 5.4. The default simulation setup in section 5.5

is used. Let us further fix the fraction of BS power ϕ_u in (5.10) to be 10%. Notice that choosing different values of ϕ_u and G only shrinks or expands the CDF of E_b/I_0 but does not affect the accuracy of using the normalized MNOF to approximate the E_b/I_0.

Fig. 5.8(a) is plotted for MS's at different locations of the cell to compare the accuracy of using the MNOF to approximate the actual E_b/I_0. MS #1 is located at coordinate $[1.55, 0]$, MS #2 is located at $[1.05, 0]$, and MS #3 is located at $[0.55, 0]$. The *actual* SIR is obtained by using left hand side of (5.5) and the approximation SIR is calculated by using the right hand side of (5.5) by simulating $100,000$ samples. Since the approximation SIR is so close to the *actual* SIR, the CDFs of their SIR's are superposed. The difference between their distributions is insignificant at the 5 % significant level by using the KS-test [46]. Fig. 5.8(b) focuses on a MS located at the cell edge (MS #2) according to the following configurations: case 1 assumes that the soft handoff set is reduced to $\{BS_0\}$. Case 2 assumes that the soft handoff set is expanded to $\{BS_0, BS_1, BS_2\}$, the SHT is chosen to be 6 dB, and $\rho = 2$. Case 3 considers more severe fading condition with ρ=2. Case 4 assumes the chip rate is decreased to 1.2288 $Mchip/s$ and the data rate is 9.6 $kbps$, which is a typical setup in the IS-95 system. For all these cases, the KS tests are passed at the 5 % significant level. Although not shown here, we try more cases with different fading situations and system parameters and find out that KS test at the 5 % significant level is passed for all these cases. Actually, the largest difference between the CDFs is found out to be less than 1 %. The closeness of the approximation can also be observed that the plot of the approximation SIR is so close to the *actual* SIR in Figs. 5.8 that they overlap each other.

5.6.2 The Parameters of U and V

Assume U follows a Gamma distribution of $Gamma(b_u, c_u)$ and V follows a Gamma distribution of $Gamma(b_v, c_v)$. By equating the first and second moments of both sides

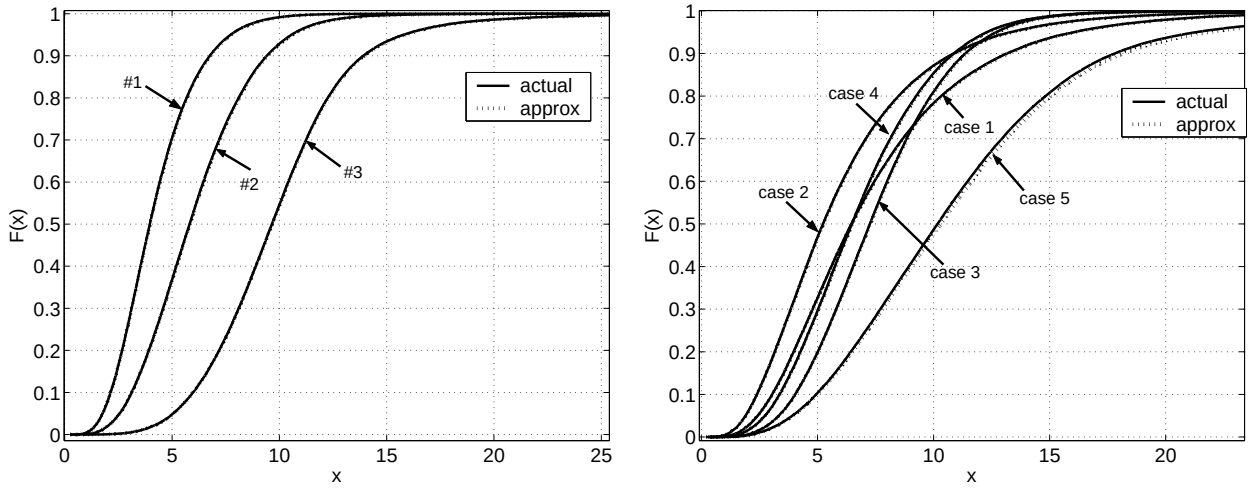

(a) (b)

Figure 5.8 CDFs of E_b/I_0. Different locations (a) and soft handoff cases (b).

of U in (5.10) and using the fact that the average power $E[X_k]$ of all the multipath components from BS_k is normalized to 1, we have

$$E[U] = \sum_{n \notin N_{sh}} E\left[\frac{l_0}{l_n}\right] + \sum_{k \in N_{sh}} q_k^{f_k} E\left[\frac{l_0}{l_k}\right] \tag{5.17}$$

$$\begin{aligned} E[U^2] = & \sum_{\substack{n,k \notin N_{sh} \\ k \neq n}} E\left[\frac{l_0^2}{l_n l_k}\right] + \sum_{n \notin N_{sh}} E[X_n^2] E\left[\frac{l_0^2}{l_n^2}\right] + 2 \sum_{\substack{n \notin N_{sh} \\ k \in N_{sh}}} q_k^{f_k} E\left[\frac{l_0^2}{l_n l_k}\right] \\ & + \sum_{\substack{k,n \in N_{sh} \\ k \neq n}} q_n^{f_n} q_k^{f_k} E\left[\frac{l_0^2}{l_n l_k}\right] + \sum_{k \in N_{sh}} \left[\frac{1-q_k}{\rho(1+q_k)} q_k^{2f_k} + q_k^{2f_k}\right] E\left[\frac{l_0^2}{l_n^2}\right] \end{aligned} \tag{5.18}$$

In the calculation of $E[U^2]$, we need to use

$$E[X_n^2] = \sum_{i=1}^{\infty} E[X_{ni}'^2](1-q_n)^2 q_n^{2(i-1)} + \sum_{\substack{i,j=1 \\ i \neq j}}^{\infty} E[X_{ni}' X_{nj}'](1-q_n)^2 q_n^{i-1+j-1} = \frac{1-q_n}{\rho(1+q_n)} + 1 \tag{5.19}$$

By using the fact that $E[U] = \frac{b_u}{c_u}$ and $E[U^2] = \frac{b_u(b_u+1)}{c_u^2}$, we can obtain that $c_u = E[U]/(E[U^2] - E^2[U])$ and $b_u = c_u E[U]$. Similarly, by equating the first and second moments of the both sides of V in (5.10), we have

$$E[V] = \sum_{k \in N_{sh}} (1 - q_k^{f_k}) E\left[\frac{l_0}{l_k}\right] \tag{5.20}$$

$$E[V^2] = \sum_{n \in N_{sh}} [\frac{1-q_n}{\rho(1+q_n)}(1 - q_n^{2f_n}) + (1 - q_n^{f_n})^2] E\left[\frac{l_0^2}{l_n^2}\right] + \sum_{\substack{k,n \in N_{sh} \\ k \neq n}} (1 - q_n^{f_n})(1 - q_k^{f_k}) E\left[\frac{l_0^2}{l_n l_k}\right] \tag{5.21}$$

We can obtain that $c_v = E[V]/(E[V^2] - E^2[V])$ and $b_v = c_v E[V]$. In equations (5.17-5.21), the following results are used:

$$E\left[\frac{l_0}{l_n}\right] = \exp\left(\frac{\sigma_b^2\delta^2}{2}\right) \frac{r_0^u}{r_n^u} E_x[\frac{Q(\frac{x-\gamma_{n1}+\sigma_b^2\delta}{\sigma_b}) - Q(\frac{x-\gamma_{n2}+\sigma_b^2\delta}{\sigma_b})}{Q(\frac{x-\gamma_{n1}}{\sigma_b}) - Q(\frac{x-\gamma_{n2}}{\sigma_b})} \exp(\delta x)], n \in N_{sh}, n \neq 0 \tag{5.22}$$

$$E\left[\frac{l_0}{l_n}\right] = \exp\left(\frac{\sigma_b^2\delta^2}{2}\right) \frac{r_0^u}{r_n^u} E_x[\frac{Q(\frac{x-\gamma_{n1}}{\sigma_b} + \sigma_b\delta)}{Q(\frac{x-\gamma_{n1}}{\sigma_b})} \exp(\delta x)], n \notin N_{sh} \tag{5.23}$$

$$E\left[\frac{l_0^2}{l_n^2}\right] = \exp\left(2\sigma_b^2\delta^2\right) \frac{r_0^{2u}}{r_n^{2u}} E_x[\frac{Q(\frac{x-\gamma_{n1}+2\sigma_b^2\delta}{\sigma_b}) - Q(\frac{x-\gamma_{n2}+2\sigma_b^2\delta}{\sigma_b})}{Q(\frac{x-\gamma_{n1}}{\sigma_b}) - Q(\frac{x-\gamma_{n2}}{\sigma_b})} \exp(2\delta x)], n \in N_{sh}, n \neq 0 \tag{5.24}$$

$$E\left[\frac{l_0^2}{l_n^2}\right] = \exp\left(2\sigma_b^2\delta^2\right) \frac{r_0^{2u}}{r_n^{2u}} E_x[\frac{Q(\frac{x-\gamma_{n1}+2\sigma_b^2\delta}{\sigma_b})}{Q(\frac{x-\gamma_{n1}}{\sigma_b})} \exp(2\delta x)], n \notin N_{sh} \tag{5.25}$$

$$\begin{aligned} E\left[\frac{l_0^2}{l_n l_k}\right] =& E_x[\frac{Q(\frac{x-\gamma_{n2}+\sigma_b^2\delta}{\sigma_b}) - Q(\frac{x-\gamma_{n1}+\sigma_b^2\delta}{\sigma_b})}{Q(\frac{x-\gamma_{n2}}{\sigma_b}) - Q(\frac{x-\gamma_{n1}}{\sigma_b})} \frac{Q(\frac{x-\gamma_{k2}+\sigma_b^2\delta}{\sigma_b}) - Q(\frac{x-\gamma_{k1}+\sigma_b^2\delta}{\sigma_b})}{Q(\frac{x-\gamma_{k2}}{\sigma_b}) - Q(\frac{x-\gamma_{k1}}{\sigma_b})} \exp(2\delta x)] \\ & \times \exp(\sigma_b^2\delta^2) \frac{r_0^{2u}}{r_k^u r_n^u}, n, k \in N_{sh}, n, k \neq 0, n \neq k \end{aligned} \tag{5.26}$$

$$E\left[\frac{l_0^2}{l_n l_k}\right] = \exp(\sigma_b^2\delta^2) \frac{r_0^{2u}}{r_k^u r_n^u} E_x[\frac{Q(\frac{x-\gamma_{n1}+\sigma_b^2\delta}{\sigma_b})}{Q(\frac{x-\gamma_{n1}}{\sigma_b})} \frac{Q(\frac{x-\gamma_{k1}+\sigma_b^2\delta}{\sigma_b})}{Q(\frac{x-\gamma_{k1}}{\sigma_b})} \exp(2\delta x)], n, k \notin N_{sh}, n \neq k \tag{5.27}$$

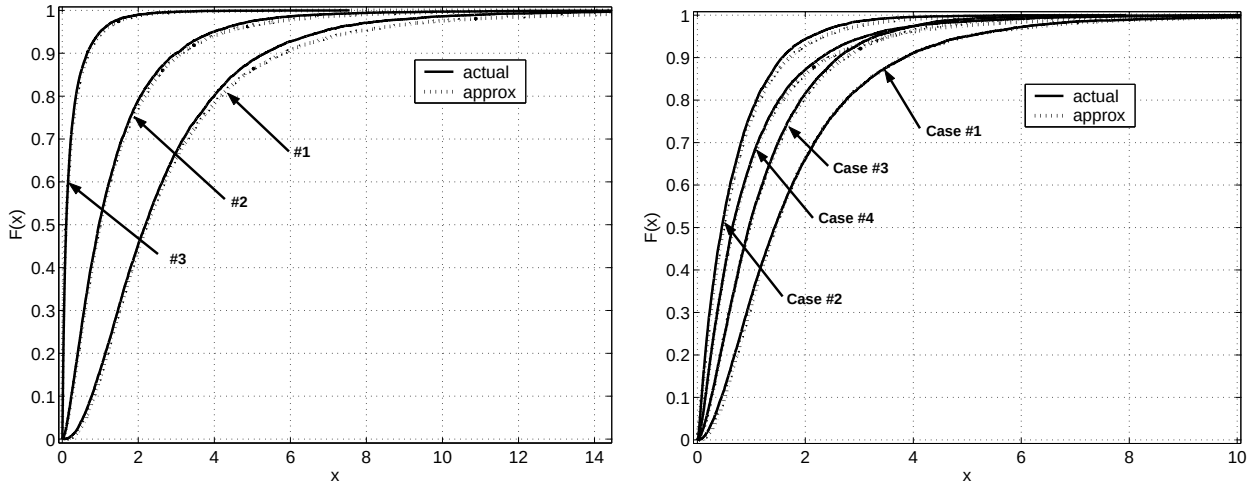

(a) (b)

Figure 5.9 CDFs of U/V. Different locations (a) and soft handoff cases (b).

$$E\left[\frac{l_0^2}{l_n l_k}\right] = \exp(\sigma_b^2\delta^2)\frac{r_0^{2u}}{r_k^u r_n^u} E_x\left[\frac{Q(\frac{x-\gamma_{n1}+\sigma_b^2\delta}{\sigma_b})}{Q(\frac{x-\gamma_{n1}}{\sigma_b})} \frac{Q(\frac{x-\gamma_{k2}+\sigma_b^2\delta}{\sigma_b}) - Q(\frac{x-\gamma_{k1}+\sigma_b^2\delta}{\sigma_b})}{Q(\frac{x-\gamma_{k2}}{\sigma_b}) - Q(\frac{x-\gamma_{k1}}{\sigma_b})} \exp(2\delta x)\right]$$
$$, n \notin N_{sh}, k \in N_{sh} \tag{5.28}$$

where $\sigma_b = b\sigma$ and $\delta = \ln(10)/10$. When $n \in N_{sh}$ and more than one BS in N_{sh}, $\gamma_{n1} = (10\mu \log_{10}(r_n/r_0) - Th)$ and $\gamma_{n2} = (10\mu \log_{10}(r_n/r_0) + Th)$. When $n \notin N_{sh}$ and more than one BS in N_{sh}, $\gamma_{n1} = 10\mu \log_{10}(r_n/r_0)$. When $n \notin N_{sh}$ and only BS_0 in N_{sh}, $\gamma_{n1} = 10\mu \log_{10}(r_n/r_0) - Th$. $E_x[.]$ means evaluating the expression by using a Gaussian random variable x with zero mean and standard deviation σ_b.

Similar to the simulation setup used in chapter 5.6.1, the *actual* value of U/V obtained by using (5.10) is compared with the approximation value of U/V characterized by the ratio of Gamma variables. Fig. 5.9(a) shows the accuracy of the approximation value of U/V approaches the *actual* value of U/V for MS's in difference locations of the cell. For MS #1, $b_u = 3.7111$, $c_u = 1.1805$, $b_v = 4.1543$, $c_v = 2.9814$, and the correlation coefficient between U and V is 0.1. For MS #2, $b_u = 1.7420$, $c_u = 1.1588$,

$b_v = 4.2431$, $c_v = 3.2015$, and the correlation coefficient between U and V is 0.1. For MS #3, $b_u = 0.4705$, $c_u = 1.8822$, $b_v = 4.4223$, $c_v = 3.6111$, and the correlation coefficient between U and V is 0.05. The maximum difference between these CDFs is less than 5%.

For a given MS at the cell edge (MS #2), the accuracy of the approximation value of U/V is shown in Fig. 5.9(b), where four cases are taken into consideration. These cases are the same as those defined in chapter 5.6.1 except the SHT is set to be 3 dB in case 2. We find out the approximation is not good enough for a larger SHT (e.g. 6 dB). For case 1, $b_u = 2.9797$, $c_u = 2.2802$, $b_v = 4.6174$, $c_v = 5.3448$, and the correlation coefficient between U and V is -0.016. For case 2, $b_u = 1.0762$, $c_u = 1.0575$, $b_v = 7.4894$, $c_v = 4.71037$, and the correlation coefficient between U and V is 0.18. For case 3, $b_u = 1.8100$, $c_u = 1.2041$, $b_v = 7.2133$, $c_v = 5.4427$, and the correlation coefficient between U and V is 0.13. For case 4, $b_u = 1.5208$, $c_u = 1.0117$, $b_v = 3.0721$, $c_v = 1.5359$, and the correlation coefficient between U and V is 0.01. Even though not given here, simulation results show that when the SHT is less than 3 dB, we obtain a smaller correlation between U and V and much better approximation. Simulation results also show that when the SHT is less than 3 dB, we obtain a smaller correlation between U and V and much better approximation.

Therefore, we can treat U and V as independent Gamma variables to approximate the *actual* value of U/V for a SHT less than 3 dB and the maximum difference between the CDFs is less than 5 % for all the cases. In addition, the effect of the approximation error is lessened since γ/G is multiplied to obtain the fraction of BS power by using (5.9) and $\gamma/G = 0.0247$ for $\gamma = 5$ dB and $G = 128$. Simulation results also show that the approximation deteriorates if the SHT is increased to a high level (e.g. 6 dB).

5.6.3 Approximation of the Fraction of Power Required by a MS

By assuming that ϕ_{ut} is independent for different soft handoff sets, the mean and second moments of ϕ_{ut} in (5.12) are given as follows:

$$E[\phi_{ut}] = \frac{\sum_{N_{sh}} E[\phi_{uh}|SH\ with\ N_{sh}|\gamma/G[1+U/V] \le \phi_{u\max}]P_{N_{sh}}}{\sum_{N_{sh}} P_{N_{sh}}} \tag{5.29}$$

$$E[\phi_{ut}^2] = \frac{\sum_{N_{sh}} E[\phi_{uh}^2|SH\ with\ N_{sh}|\gamma/G[1+U/V] \le \phi_{u\max}]P_{N_{sh}}^2}{(\sum_{N_{sh}} P_{N_{sh}})^2} \tag{5.30}$$

The mean of ϕ_{uh} is

$$\begin{aligned} & E[\phi_{uh}|SH\ with\ N_{sh}|\gamma/G[1+U/V] \le \phi_{u\max}] \\ =& \frac{\exp(\frac{\sigma_e^2\delta^2}{2})E[\frac{\gamma}{G}[1+\frac{U}{V}], \frac{\gamma}{G}[1+\frac{U}{V}] \le \phi_{u\max}|SH\ with\ N_{sh}]}{P[\frac{\gamma}{G}[1+\frac{U}{V}] \le \phi_{u\max}]} \\ =& [1 - \frac{c_v}{c_u} + \frac{c_v}{c_u}\frac{B(b_v-1,b_u)}{B(b_v,b_u)}\frac{1-B(b_v-1,b_u,\chi_{umax})}{1-\wp}]\exp(\frac{\sigma_e^2\delta^2}{2})\frac{\gamma}{G} \end{aligned} \tag{5.31}$$

where $B(b_v-1,b_u,\chi_{umax}) = \wp + \frac{\Gamma(b_v-1+b_u)}{\Gamma(b_v)\Gamma(b_u)}\chi_{umax}^{b_v-1}(1-\chi_{umax})^{b_u}$ [30, eqn. 26.5.16] is a function of the target outage probability $\wp$ and $B(b_v-1,b_u)/B(b_v,b_u) = 1 + b_u/(b_v-1)$ is obtained by using equation (6.2.2) in [30].

The second moment of ϕ_{uh} is

$$\begin{aligned} & E[\phi_{uh}^2|SH\ with\ N_{sh}|\gamma/G[1+U/V] \le \phi_{u\max}] \\ =& [-(1-\frac{c_v}{c_u})^2 + \frac{c_v^2}{c_u^2}\frac{B(b_v-2,b_u)}{B(b_v,b_u)}\frac{1-B(b_v-2,b_u,\chi_{umax})}{1-\wp}]\exp(2\sigma_e^2\delta^2)\frac{\gamma^2}{G^2} \\ & + 2(1-\frac{c_v}{c_u})\exp(1.5\sigma_e^2\delta^2)\frac{\gamma}{G}E[\phi_{uh}] \end{aligned} \tag{5.32}$$

where $B(b_v-2,b_u,\chi_{umax}) = B(b_v-1,b_u,\chi_{umax}) + \frac{\Gamma(b_v-2+b_u)}{\Gamma(b_v-1)\Gamma(b_u)}\chi_{umax}^{b_v-2}(1-\chi_{umax})^{b_u}$ is also a function of the target outage probability $\wp$ and $B(b_v-2,b_u)/B(b_v,b_u) = [1+b_u/(b_v-1)][1+b_u/(b_v-2)]$.

Fig. 5.10 shows the fraction of BS power by considering all the handoff combinations including soft handoff and non-soft handoff, which is obtained by using (5.12)

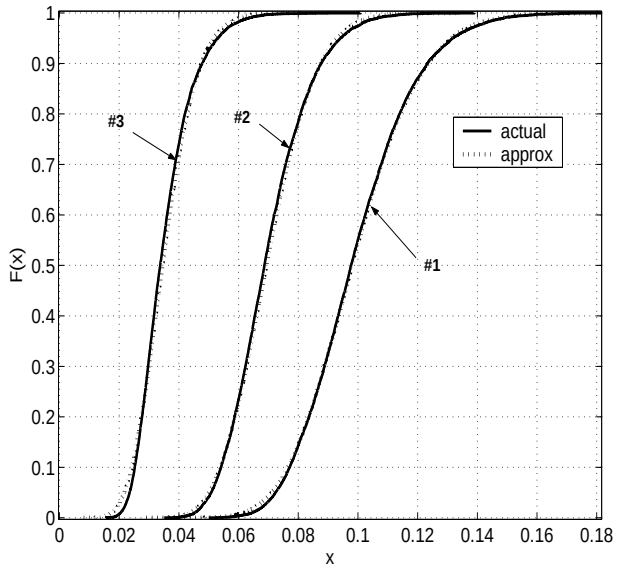

Figure 5.10 Fraction of BS power required by a MS .

with a 3 dB soft handoff threshold, a 1 dB PCE, and a 0.1 outage probability. The *actual* value is obtained by generating $10,000$ samples of ϕ_{uh} for each handoff combination, multiplying with the corresponding probability, and summing them together. The approximation value is obtained by generating a gamma distributed samples using the statistical values by using (5.29) and (5.30). We can observe that the approximation value can well approximate the *actual* value of the fraction of BS power required by a MS.

5.7 Conclusions

In this chapter, we derive the BS power distributions required by a specific soft handoff set, a single MS, and all MS's in the cell. Closed-form expression of capacity in terms of maximum number of MS's supported by a BS at certain outage and blocking probabilities is obtained. Our analytical model provides the way to fine control the behavior of an individual MS at the level of soft handoff set and study its effects on the

total capacity of the BS. We show that at a larger outage probability or a larger power control error, the MS needs more power from the BS and degrades the capacity. A larger soft handoff threshold is shown to provide a larger coverage area but results in capacity loss for MS's far away from the BS. When we can use enough number of Rake fingers, the coverage area is significantly extended and the fraction of BS power required by the MS is reduced. We further show that by limiting the maximum fraction of BS power available to a MS and rejecting the power requirements from power-greedy soft handoff sets, a significant capacity gain can be achieved. In addition, we show that the BS can support more MS's if it covers less area.

CHAPTER 6

The Dynamic Capacity with Correlated BS Powers

6.1 Overview

The capacity of a power-controlled CDMA system is commonly obtained by assuming equal BS power throughout the system and neglecting the correlation and interaction among BS powers, which is rarely true in real CDMA systems. We propose an analytical process to determine the dynamic capacity in CDMA systems with unequal BS power by considering the correlation and interaction among BS powers. Simulation results show that the Erlang capacity is significantly different by assuming that the BS power is a random variate instead of a constant value. We also show that correlation among BS powers can be up to 0.13 and the reduction in Erlang capacity can be up to 30 %. To efficiently evaluate the dynamic Erlang capacity and correlation among BS powers, a closed-form expression of the capacity in terms of certain outage and blocking probabilities is obtained by using the distribution of the base station power. By considering the ON/OFF mixed traffic in the real network and other system parameters, such as the soft handoff threshold and the power control error, simulation results show that the statistics of the distributions of BS power experienced in the system is consistent with the assumption that such a probability density can be used to characterize the BS power. The knowledge of the dynamic capacity can be used to design an accurate and effective call control algorithm.

6.2 Introduction

The third generation (3G) code division multiple access (CDMA) system is designed to support both high-speed data and low-speed voice traffic. The forward link of the 3G CDMA systems is considered to be the capacity bottleneck due to the heavy-volume and high-speed data traffic. There are many recent papers addressing the forward link capacity. In [1], an analytical model has been proposed to show the effects of soft handoff on the forward link capacity, where the tradeoff between capacity loss due to additional channels used by soft handoff and capacity gain from macro-diversity is analyzed. In [27], a closed-form expression of capacity was derived by assuming Gamma distributions for the interference and signals. However, the effects of soft handoff were not adequately addressed and the power-control was assumed to be able to completely mitigate the effects of shadowing, which hinders its application to the real system. In [24], the system capacity of soft handoff was obtained by mostly computer simulation and rough estimations, where there are discrepancies between the simulation results and theoretical analysis. In [35], an ON/OFF mixed traffic model was used to study the forward link capacity by obtaining a Chernoff bound of the outage probability. The characteristics of the BS power in the forward link has not been adequately addressed and the limit of the BS power on the capacity was not fully investigated. Furthermore, the majority of the previous work studying the forward link performance assumes equal BS power throughout the system and obtains a static capacity without considering the correlation and interaction among BS powers [1] [27] [24] [35]. In fact, the BS power is a random variate and unequal BS power is expected in the system due to the following observations. Firstly, the fraction of BS power required to support a single MS at a target SIR is a random variate due to the continuously changing wireless channel. Secondly, random BS power is also the natural result of random call arrivals and departures. In addition, due to the universal frequency reuse in every cell of CDMA system and the use of soft handoff, the BS powers

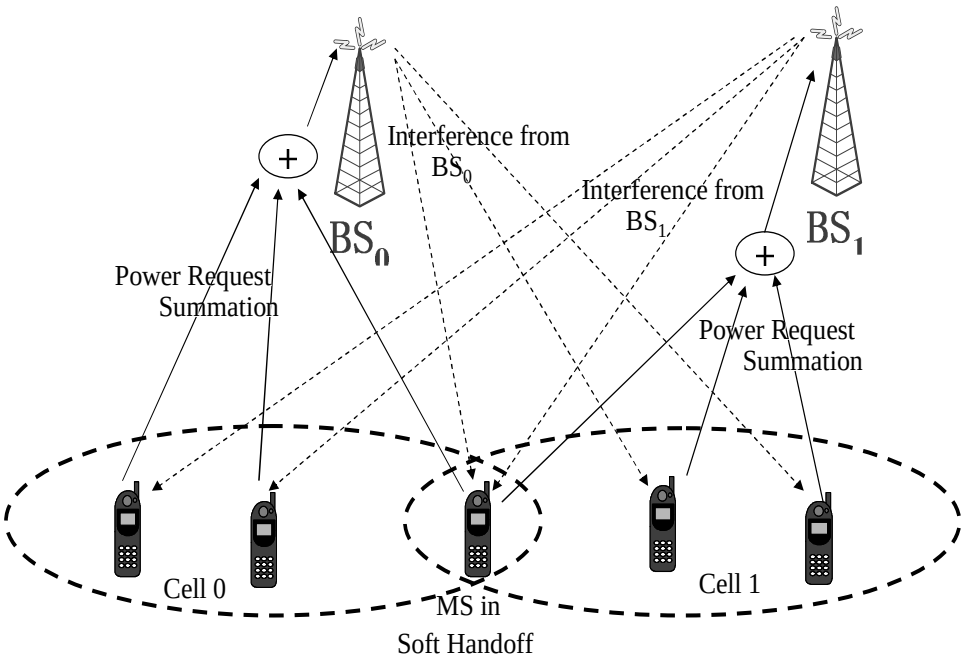

Figure 6.1 Dynamic capacity and power correlation among BS's.

are correlated and the correlation significantly affects the capacity as shown later in this chapter. Due to the interaction and correlation among BS powers, the determination of the BS power distribution and the forward link capacity is actually a dynamic process.

The dynamic process is illustrated in Fig. 6.1 to show the interaction and correlation among BS power and explained as follows. MS's in cell 0 require power from BS_0 to maintain a target SIR in an SIR-based power-controlled CDMA system. The power of BS_0 is, therefore, a function of the SIR level perceived at every MS in cell 0. Because universal frequency is reused in every cell of CDMA systems, the power of BS_0 acts as interference to MS's in cell 1. So the power of BS_0 affects the SIR levels perceived by MS's in cell 1. Since MS's in cell 1 monitor their SIR levels and send power requirements to BS_1, the power of BS_1 is a function of the SIR level perceived at MS's in cell 1 and therefore, a function of power of BS_0. In turn, the power of BS_1 acts as interference to MS's in cell 0 and subsequently, affects the power of BS_0. Therefore, after a feedback

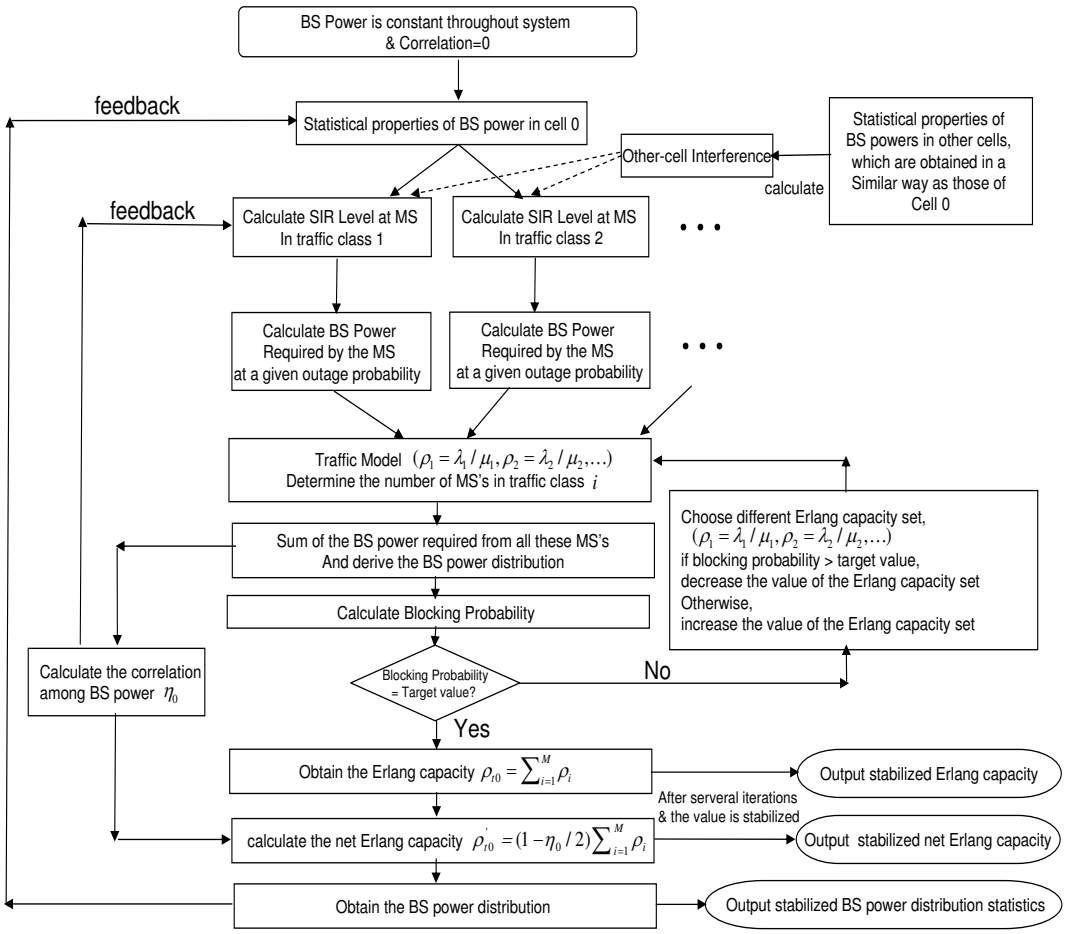

Figure 6.2 Block diagram to obtain the dynamic Erlang capacity.

loop, the power of BS_0 needed to support a certain number of MS's is actually affected by the power of BS_0 itself. This interactive relationship of the BS powers in the CDMA system is further complicated by the use of soft handoff. MS's in soft handoff mode communicate with multiple BS's in the soft handoff set and combines signals from these BS's to achieve a better SIR. If the MS senses a degraded SIR, it sends power-up command to inform the BS's in the soft handoff set to allocate more power to it, and vice versa. As illustrated in Fig. 6.1, MS's in the overlapping serving area of BS_0 and BS_1 need power from both BS's, which results into correlation among BS powers.

By considering the correlation and interaction of BS powers, in this chapter, we propose an analytically iterative process to determine the dynamic capacity in the CDMA systems, which has not been addressed in the open literature. A block diagram of the proposed approach to derive the BS_0 power distribution is shown in Fig. 6.2 and briefly introduced as follows:

1. The BS powers are initially assumed to be equal and constant throughout the system and the correlation among BS power is assumed to be equal to 0.
2. The statistical properties of the interference suffered by a MS are obtained as a function of the statistics of the power distributions of the surrounding BS's and the correlation among them derived in step 1 (or step 6 after a feedback loop). By using the statistics of the interference and the power of BS_0, the statistics of the SIR perceived at the MS is calculated and subsequently, the distribution of the fraction of BS_0 power required by the MS is derived at a given target SIR.
3. By using the distribution of BS_0 power needed by a MS derived in step 2, we can solve for the maximum fraction of BS power needed by the MS at a target outage probability.
4. By assuming a certain ON/OFF mixed traffic pattern, which decides the number and types of MS's in the cell, and summing the fractions of BS power of all MS's requiring power from BS_0, the distribution of BS_0 power is derived. Then we use the close-form expression of the capacity to calculate the Erlang traffic that BS_0 can support at a given blocking probability.
5. Following the same procedure, we find out the power distributions and the Erlang capacity of every BS in the system at a given blocking probability. Then, we use the analytical approach introduced in the chapter to calculate the correlations among BS powers from the statistics of BS power distributions.

6. Feed the power distributions of all BS's and the correlation among them back to step 2.

The Erlang capacity obtained in step 4 is the dynamic capacity supported by a BS. After several iterations, the value of the capacity becomes stable and is called the stabilized Erlang capacity. By considering the capacity loss caused by the correlation among BS powers, the stabilized Erlang capacity is scaled down to a smaller value and we can obtain the stabilized net Erlang capacity. This iterative process is simplified by finding the distribution of the BS power and by obtaining the closed-form expression of forward link Erlang capacity.

By simulating a real CDMA network taking into account the power control algorithm, soft handoff strategies, ON/OFF mixed traffic patterns, call queuing approaches, multipath fading environment, the correlation among BS powers, and the feedback of surrounding BS power as interference, we find out that the distribution of the fraction of BS power required by a single MS communicating with a specific soft handoff set, a single MS, and all MS's in the network can be well approximated by lognormal distributions. Rather than using traditional approach of pure computer simulation, the statistic of the lognormal variates can be obtained directly from the system parameters, such as the power control error (PCE), soft handoff threshold, ON/OFF session periods, call arrival/departure rates, and so on. Furthermore, we show that the correlation among BS powers can also be obtained analytically from these parameters and surrounding BS power levels. Therefore, we provide an efficient approach to obtain the dynamic capacity analytically.

This chapter is organized as follows: section 6.3 describes the soft handoff model. Section 6.4 shows the derivation of the dynamic capacity by finding out the distributions of BS power for a single soft handoff, a single MS, and all MS's in the cell. Section 6.5 gives the numerical results. Section 6.7 summarizes the results of the chapter.

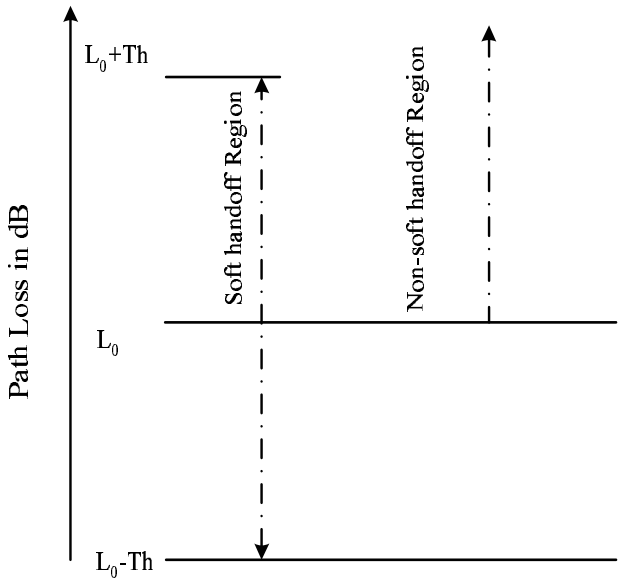

Figure 6.3 Soft handoff model.

6.3 Soft Handoff Model

In an SIR-based power-controlled CDMA system, the MS always monitors the signal strengths of surrounding BS's to select the soft handoff set. Then it uses Rake receiver to capture multipath signals from BS's in the soft handoff set to achieve macro-diversity gain. By referring to the soft handoff strategies in the real systems [16] [22] and the soft handoff model established in [36] [57] [58], the soft handoff model used in this chapter is shown in Fig. 6.3 and introduced as explained hereafterwards. We choose a 19-cell cluster as shown in Fig. 6.4 to study the system capacity. Assume BS_0 is the reference BS, which means that BS_0 is always in the soft handoff set. Further assume the path loss between BS_i and the MS is L_i dB. Then, if both BS_i and BS_0 are in the soft handoff set of a MS, the path loss L_i is Th db around the path loss L_0, where Th is the soft handoff threshold. If BS_0 is in the soft handoff set but not BS_i, the path loss L_i is Th db greater than L_0.

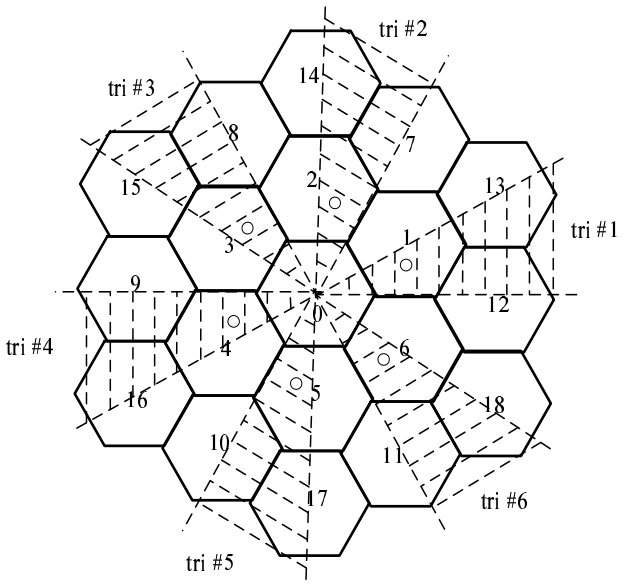

Figure 6.4 19-cell cluster.

The path loss l_i from BS_i can be expressed as $l_i = r_i^u 10^{(a\xi + b\xi_i)/10}$ [19], where r_i is the normalized distance from BS_i to the MS (normalized to the cell radius), u is the path loss slope. Both ξ and ξ_i are independent Gaussian random variables with identical zero mean and σ standard deviation to account for correlation effects and $a^2 + b^2 = 1$. The path loss can be expressed in dB as $L_i = 10 \log_{10} l_i = M_i + a\xi + b\xi_i$, where $M_i = 10u \log_{10}(r_i)$. Signals from different BS's have the same correlation coefficient of $E[x_i x_j]/\sigma^2 = a^2$, $i \neq j$.

The soft handoff set is denoted as $N_{sh} = \{0, i_1, i_2, ..., i_k, ...\}$, $i_k \in \{1, 2, \ldots, N\}$, where N is the total number of BS's taken into consideration (referring to Fig. 6.4, N is 19). According to the soft handoff model established above, the probability of a MS in the soft handoff with N_{sh} is

$$\begin{aligned} P_{N_{sh}} =& P\{L_0 - Th < L_i < L_0 + Th, L_j > L_0, i \in N_{sh}, i \neq 0, j \notin N_{sh}\} \\ =& E_z[\prod_{\substack{i \in N_{sh} \\ i \neq 0}} \{Q(z + c_{1i}) - Q(z + c_{2i})\} \prod_{j \notin N_{sh}} Q(z + c_j)] \end{aligned} \tag{6.1}$$

where $c_{1i} = (M_0 - M_i - Th)/(b\sigma)$, $c_{2i} = (M_0 - M_i + Th)/(b\sigma)$, $c_j = (M_0 - M_j)/(b\sigma)$, $Q(z) = \int_z^{+\infty} \frac{1}{\sqrt{2\pi}} \exp(-x^2/2)dx$, and $E_z[.]$ is the mean value evaluated by assuming that z is normal distributed with zero mean and unit standard deviation, that is, $z \sim N(0,1)$.

As a special case, when the MS is only connected to BS_0 and in the non-soft handoff mode, all other BS's having path loss greater than that of the BS_0 by more than Th dB. The probability of non-soft handoff is

$$P\{L_0 + Th < L_i, i = 1, \cdots, N\} = E_z[\prod_{i=1}^{N} Q(z + c_{2i})]. \tag{6.2}$$

The interested reader can find a 3-dimension view of the soft handoff and non-soft handoff probabilities in [57].

6.4 The Dynamic Capacity

6.4.1 The Distribution of the BS Power Allocated to a MS

After the MS selects its soft handoff set, it uses Rake receiver to track the multipath signals from BS's in the soft handoff set and uses the maximum ratio combining to combine these signals to achieve the optimal macrodiversity gain [1]. By assuming that the first f_k multipath components from BS_k in the soft handoff set N_{sh} are tracked by the Rake receiver at the MS and following the analysis in [27] [36], the SIR (γ) with power control error can be expressed as

$$\gamma 10^{\frac{\xi_e}{10}} = \sum_{k \in N_{sh}} \sum_{i=1}^{f_k} \frac{G\phi_u \frac{X_{ki}}{l_k}}{\frac{\varphi_k X_{ki}^c}{l_k} + \sum\limits_{\substack{n \in N_{sh} \\ n \neq k}} \frac{\varphi_n X_n}{l_n} + \sum\limits_{n \notin N_{sh}} \frac{\varphi_n X_n}{l_n}} \approx \frac{G\phi_u \sum\limits_{k \in N_{sh}} \sum\limits_{i=1}^{f_k} \frac{X_{ki}}{l_k}}{\sum\limits_{k \in N_{sh}} \frac{h_k}{l_k} + \sum\limits_{n \notin N_{sh}} \frac{\varphi_n X_n}{l_n}} \tag{6.3}$$

where G is the spreading gain. The Gaussian noise is neglected. P_n is the actual utilized BS power allocated to all MS's and P is the maximum BS power, which is a constant value. $\varphi_n = P_n/P$ is the fraction of actual utilized power of BS_n, which is normalized by P and takes value in the interval $[0, 1]$. $\phi_u = P_{ku}/P$ is the fraction of BS power allocated

by BS_k to MS_u and is also normalized by P. ϕ_u is assumed to be equal for all BS's in the soft handoff set [59] [1] [35]. P_{ku} is the power allocated from BS_k to MS_u. ξ_e is the PCE in dB following a normal distribution with zero mean and standard deviation σ_e [24].

The i^{th} multipath component from BS_k to the MS is denoted as α_{ki}, where $X_{ki} = |\alpha_{ki}|^2$ is the power. $X_{ki}^c = \sum_{f=1,f\neq i}^{\infty} X_{kf}$ is the power summation of all the multipath components from BS_k except the i^{th} multipath due to the use of the orthogonal Walsh code. $X_n = \sum_{f=1}^{\infty} X_{kf}$ is the power summation of all the multipath components from BS_n. Without loss of generality, we assume the average powers of the multipath components are sorted in descending order and the Rake receiver always tracks the multipath component having a larger average power. The average power $E[X_{ki}]$ of the i^{th} multipath component from BS_k is exponentially distributed as $E[X_{ki}] = E[X_{k1}]\exp(-(i-1)T_c/\tau_{avg})$ [16, page 244], where T_c is the chip duration and τ_{avg} is the average value of the root mean square (RMS) of the delay spread (DS) τ_{rms}. By using the Greenstein's model [41], we have $\tau_{avg} = E[\tau_{rms}] = T_1 r_k^{\epsilon} E[y] = \exp\left(\frac{(\sigma_y \ln 10/10)^2}{2}\right) T_1 r_k^{\epsilon}$ at a distance r_k from BS_0 [58] [41] [40], where T_1 is the median DS at distance 1 km, ϵ is an exponent of the distance, and $10\log_{10}(y) \sim N(0, \sigma_y^2)$. In this chapter, T_1 is chosen to be 0.5 μs, ϵ is chosen to be 0.5, and σ_y is set to be 4 dB [41] [40], which are typical values for the urban area. The BS-to-BS distance is chosen to be 1.5 km.

For a normalized total average power of the multipath components, we have the following $\sum_{i=1}^{\infty} E[X_{ki}] = 1$. Therefore, $E[X_{ki}] = (1-q_k)q_k^{i-1}$, where $q_k = \exp(-T_c/\tau_{avg})$. We can further express X_{ki} as $X_{ki} = X_{ki}^{'}(1-q_k)q_k^{i-1}$, where $X_{ki}^{'}$'s are Gamma variates with i.i.d distribution of $Gamma(\rho, \rho)$. The gamma distribution $Gamma(b, c)$ has the probability density function $f(x) = c^b x^{b-1} e^{-cx}/\Gamma(b)$, $x \geq 0$, where $\Gamma(b) = \int_0^{\infty} x^{b-1}e^{-x}dx$ is the complete gamma function. As a special case, by assuming that the non-line of sight

(NLOS) path exists between the BS and MS in this chapter, $\rho = 1$ and α_k^i is Rayleigh distributed.

The approximation in equation (6.3) is obtained by using the macrodiversity orthogonal factor. In [58] [29], the SIR expression is simplified into one term by using the macrodiversity orthogonal factor, where the BS power is assumed to be constant. In this chapter, we extend the use of the macrodiversity orthogonal factor and show that even though the BS power is a random variate, macrodiversity orthogonal factor is still applicable. By using the symmetric form in the left hand side of (6.3), we set the term $\sum_{n \notin N_{sh}} \varphi_n X_n / l_n$ to be zero at both sides of (6.3) and have

$$h_k = h_c \sum_{i=1}^{f_k} X_{ki} \tag{6.4}$$

$$h_c = [\sum_{k \in N_{sh}} \sum_{i=1}^{f_k} \frac{\frac{X_{ki}}{l_k}}{\frac{\varphi_k X_{ki}^c}{l_k} + \sum\limits_{\substack{n \in N_{sh} \\ n \neq k}} \frac{\varphi_n X_n}{l_n}}]^{-1}. \tag{6.5}$$

h_k is called the macrodiversity non-orthogonality factor. h_c is called the normalized macrodiversity non-orthogonality factor. If we set $N_{sh} = \{k\}$, which means the MS is in the non-soft handoff mode and only connected to BS_k, h_k is simplified to the non-orthogonality factor extensively addressed in the literature [51]. The validation of the approximation in (6.3) is shown in chapter 6.6.1. An upper bound of h_c is given by

$$h_c \leq [\sum_{k \in N_{sh}} \sum_{i=1}^{f_k} \frac{\frac{X_{ki}}{l_k}}{\sum\limits_{n \in N_{sh}} \frac{\varphi_n X_n}{l_n}}]^{-1} \leq 1 + \frac{\sum\limits_{k \in N_{sh}} \sum\limits_{i=f_k+1}^{\infty} \frac{\varphi_k X_{ki}}{l_k}}{\sum\limits_{k \in N_{sh}} \sum\limits_{i=1}^{f_k} X_{ki}/l_k} \tag{6.6}$$

where the second inequality uses the fact that $\varphi_n \leq 1$.

By inverting (6.3) and using the upper bound of h_c in (6.6), an upper bound of the fraction of power needed by MS_u to achieve a target SIR γ is

$$\phi_u \leq \frac{\gamma 10^{\frac{\xi_e}{10}}}{G}[1 + \frac{I}{S}] = \phi_{uh} \tag{6.7}$$

where

$$
\begin{aligned}
S &= \sum_{k \in N_{sh}} \sum_{i=1}^{f_k} \frac{X'_{ki}(1-q_k)q_k^{i-1}l_0}{l_k} \\
I &= \sum_{n \notin N_{sh}} \frac{\varphi_n X_n l_0}{l_n} + \sum_{k \in N_{sh}} \sum_{i=f_k+1}^{\infty} \frac{\varphi_k X'_{ki}(1-q_k)q_k^{i-1}l_0}{l_k}
\end{aligned}
\tag{6.8}
$$

and q_k and X'_{ki}'s are defined at the beginning of this section. ϕ_{uh} is the upper bound of ϕ_u.

Simulation results show that both the signal S and interference I can be approximated by independent lognormal variates and I/S can be well-approximated by a lognormal variate. The accuracy of these approximations is shown in chapter 6.6.2.

If a MS requires power more than the maximum fraction ϕ_{umax}, the MS can not maintain the target SIR and will be in outage. Assume $X = 10\log_{10}(I)$ is normal distributed with mean μ_x and standard deviation σ_x, that is, $X \sim N(\mu_x, \sigma_x^2)$. Further assume $Y = 10\log_{10}(S) \sim N(\mu_y, \sigma_y^2)$. By using the upper bound of the fraction of BS power required by a MS, that is, ϕ_{uh} derived in (6.6), an upper bound of the outage probability is

$$
\begin{aligned}
P_{out} &= P(\phi_{uh} = \gamma 10^{\frac{\xi_e}{10}}/G[1 + I/S] > \phi_{umax}) \\
&= \begin{cases}
Q\left(\frac{10\log_{10}(G\phi_{umax}/\gamma - 1) - \mu_{xy}}{\sigma_{xy}}\right) & \sigma_e = 0 \\
\int_{-\infty}^{+\infty} Q\left(\frac{10}{\sigma_e}\log_{10}\left(\frac{G\phi_{umax}}{\gamma(1+10^{w/10})}\right)\right)\frac{1}{\sqrt{2\pi}\sigma_{xy}}\exp\left(-\frac{(w-\mu_{xy})^2}{2\sigma_{xy}^2}\right)dw & \sigma_e \neq 0 \\
= E_z[Q\left(\frac{10}{\sigma_e}\log_{10}\left(\frac{G\phi_{umax}}{\gamma(1+10^{(\sigma_{xy}z+\mu_{xy})/10})}\right)\right)] &
\end{cases}
\end{aligned}
\tag{6.9}
$$

where $\mu_{xy} = \mu_x - \mu_y$ and $\sigma_{xy}^2 = \sigma_x^2 + \sigma_y^2$. As denoted before, $E_z[.]$ is the mean value evaluated by assuming that $z \sim N(0,1)$.

For a target outage probability $\wp$, we can solve (6.9) for ϕ_{umax}. If ϕ_{umax} is greater than a certain threshold value ϕ_{uth}, the BS knows that the soft handoff set N_{sh} used by

MS_u is a power-greedy soft handoff combination and rejects the power requirement from that MS. ϕ_{uth} should be less than or equal to 1.

As discussed above, regardless of the soft handoff set that the MS is connecting to, the MS maintains the target outage probability. Therefore, the average outage probability is the same as the target outage probability $\wp$.

By averaging the power requirements of soft handoff's and non-soft handoff, the average power required by MS_u in location p from BS_0 is

$$\phi_{up} = \sum_{\substack{P_{N_{sh}} \\ over\ all\ N_{sh}}} \phi_{uh}|_{SH\ with\ N_{sh}\&\phi_{uh}\leq\phi_{umax}} \tag{6.10}$$

where instead of multiplying ϕ_{uh} with the probability $P_{N_{sh}}$, we use the summation form of $P_{N_{sh}}$ to weight ϕ_{uh}, since every occurrence of ϕ_{uh} is essentially an independent varaible. By equating the first and second moments of ϕ_{up} in both sides of equation (6.10), we have the mean $E[\phi_{up}] = \sum_{N_{sh}} E[\phi_{uh}|_{SH\ with\ N_{sh}\&\phi_{uh}\leq\phi_{umax}}]P_{N_{sh}}$ and the second moment $E[\phi_{up}^2] = \sum_{N_{sh}} E[\phi_{uh}^2|_{SH\ with\ N_{sh}\&\phi_{uh}\leq\phi_{umax}}]P_{N_{sh}}$. In above calculations, the first and second moments of ϕ_{uh} are obtained as follows

$$\begin{aligned} E[\phi_{uh}] =& E\left[\frac{\gamma}{G}10^{\frac{\xi_e}{10}}[1+I/S]|\frac{\gamma}{G}10^{\frac{\xi_e}{10}}[1+I/S] < \phi_{umax}\right] \\ =& \begin{cases} \frac{\gamma}{G}Q\left(\frac{\mu_{xy}-10\log_{10}(G\phi_{umax}/\gamma-1)}{\sigma_{xy}}\right) + & \\ \frac{\gamma}{G}\exp\left(\mu_{xy}\delta+\frac{\sigma_{xy}^2\delta^2}{2}\right)Q\left(\frac{(\mu_{xy}+\sigma_{xy}^2\delta)-10\log_{10}(G\phi_{umax}/\gamma-1)}{\sigma_{xy}}\right) & \sigma_e = 0 \\ E_z[\frac{r}{G}(1+10^{\frac{(\sigma_{xy}z+\mu_{xy})}{10}})\exp(\frac{\sigma_e^2\delta^2}{2}) & \\ Q\left(\sigma_e\delta-\frac{10}{\sigma_e}\log_{10}\left(\frac{G\phi_{umax}}{\gamma(1+10^{(\sigma_{xy}z+\mu_{xy})/10})}\right)\right)] & \sigma_e \neq 0 \end{cases} \end{aligned} \tag{6.11}$$

and

$$E[\phi_{uh}^2] = E\left[\frac{\gamma^2}{G^2}10^{\frac{2\xi_e}{10}}[1+I/S]^2 | \frac{\gamma}{G}10^{\frac{\xi_e}{10}}[1+I/S] < \phi_{umax}\right]$$

$$= \begin{cases} \frac{\gamma^2}{G^2}Q\left(\frac{\mu_{xy} - 10\log_{10}(G\phi_{umax}/\gamma - 1)}{\sigma_{xy}}\right) + 2\frac{\gamma^2}{G^2}\exp\left(\mu_{xy}\delta + \frac{\sigma_{xy}^2\delta^2}{2}\right) & \\ \times Q\left(\frac{(\mu_{xy} + \sigma_{xy}^2\delta) - 10\log_{10}(\frac{G\phi_{umax}}{\gamma} - 1)}{\sigma_{xy}}\right) + & \sigma_e = 0 \\ \frac{\gamma^2}{G^2}\exp\left(2\mu_{xy}\delta + 2\sigma_{xy}^2\delta^2\right)Q\left(\frac{(\mu_{xy} + 2\sigma_{xy}^2\delta) - 10\log_{10}(\frac{G\phi_{umax}}{\gamma} - 1)}{\sigma_{xy}}\right) & \\ E_z[\frac{r^2}{G^2}(1+10^{\frac{(\sigma_{xy}z+\mu_{xy})}{10}})^2\exp(2\sigma_e^2\delta^2) & \\ \times Q\left(2\sigma_e\delta - \frac{10}{\sigma_e}\log_{10}\left(\frac{G\phi_{umax}}{\gamma(1+10^{(\sigma_{xy}z+\mu_{xy})/10})}\right)\right)] & \sigma_e \neq 0 \end{cases} \tag{6.12}$$

where $E_z[.]$ means evaluating the expression by assuming $z \sim N(0,1)$.

6.4.2 Traffic Model

After deriving the power used by a MS, we can derive the BS power distribution by assuming a certain traffic pattern. The number of MS's surrounding BS_0 can be determined by using the ON/OFF source traffic model, where burst data is transmitted in the ON period and no data is transmitted in the OFF period. The durations t of both the ON and OFF periods can be modeled by the heavy-tailed distribution such as the Pareto distribution as follows [60] [61] [62]:

$$f(t) = \frac{\alpha\beta^\alpha}{(1+\beta)^{\alpha+1}} \tag{6.13}$$

where $\alpha > 1$ is used to characterize the heaviness (or burstness) of the traffic. If α is close to 1, the data traffic becomes more burst. The mean value of the duration is $E[t] = \frac{\beta}{(\alpha-1)}$. If $\alpha > 2$, the variance of t is infinity. If $1 < \alpha < 2$, we have finite variance of $E[t^2] - E^2[t] = \frac{2\beta^2}{(\alpha-2)(\alpha-1)} - \frac{\beta^2}{(\alpha-1)^2} = \frac{\beta^2\alpha}{(\alpha-2)(\alpha-1)^2}$.

For both the data and voice user, the active factor of the i^{th} traffic class can be expressed as $\nu_i = \frac{E[t^i_{on}]}{E[t^i_{on}]+E[t^i_{off}]}$, where $E[t^i_{on}]$ is the average duration of the ON-period of the i^{th} traffic class and $E[t^i_{off}]$ is the average duration of the OFF-period of the i^{th} traffic class. Both t^i_{on} and t^i_{off} follow the Pareto distributions in (6.13).

Several of these ON/OFF periods consist of a session. The difference between data and voice traffic is that the holding time of the data session follows the Pareto distribution instead of the exponential distribution. However, Since the arrival rates of both the data and voice users are Poison distributed [35] [60], we can apply the M/G/c/c queueing model, where M indicates the Poission arrivals (i.e. exponential call inter-arrival time), G means a general distribution of the call holding time, the first c is the number of parallel servers, and the second c is the maximum number of users in the system. Theoretically, c can be infinity. The probability that n users of the i^{th} traffic class in the system p_{ni} is given by [63, pg. 103]

$$p_{ni} = \exp(-\rho_i)\rho_i^n/n!, n \geq 0 \tag{6.14}$$

where $\rho_i = \lambda_i/\mu_i$, λ_i is the call arrival rate of the i^{th} traffic class, and $1/\mu_i$ is the average call holding time of the i^{th} traffic class .

6.4.3 The Distribution of BS Power

Let us assume that the total number of traffic classes is M. By considering all the traffic classes and referring to the process outlined in Fig. 6.2, the average power consumption of all MS's at location p is

$$\phi_p = \sum_{i=1}^{M} \sum_{\substack{p_{ni} \\ over\ n}} \sum_{u=1}^{n} \sum_{\nu_i} \phi^{(i)}_{up} = \sum_{i=1}^{M} \sum_{\substack{p_{ni} \\ over\ n}} \sum_{u=1}^{n} \phi^{(i)}_{u\nu} = \sum_{i=1}^{M} \sum_{\substack{p_{ni} \\ over\ n}} \phi^{(i)}_{pn} = \sum_{i=1}^{M} \phi^{(i)}_{p} \tag{6.15}$$

where $\phi^{(i)}_{up}$ is the average power used by MS_u at location p in the i^{th} traffic class and given in equation (6.10) by replacing G with the spreading gain of the i^{th} traffic class G_i.

Notice that as a simplified denotation, $\phi_{up}^{(i)}$ in the summation of equation (6.10) should be treated as identical but independent variants. For the same reason as in equation (6.10), each occurrence of $\phi_{up}^{(i)}$ is treated as independent varaible and weighted by p_{ni} and ν_i. In above model, we assume that different traffic classes use separate queues, which is actually adopted in the design of practical wireless systems [64].

In addition, we denote $\phi_p = \sum_{i=1}^{M} \phi_p^{(i)}$, $\phi_p^{(i)} = \sum_{over\ n}^{p_{ni}} \phi_{pn}^{(i)}$, $\phi_{pn}^{(i)} = \sum_{u=1}^{n} \phi_{u\nu}^{(i)}$, and $\phi_{u\nu}^{(i)} = \sum_{\nu_i} \phi_{up}^{(i)}$. By equating the mean and variance of ϕ_p in both sides of equation (6.15), we have $E[\phi_p] = \sum_{i=1}^{M} E[\phi_p^{(i)}]$ and $VAR[\phi_p] = \sum_{i=1}^{M} VAR[\phi_p^{(i)}]$, where $VAR[.] = E[(.)^2] - E^2[.]$. According to the denotation of $\phi_p^{(i)}$, we have $E[\phi_p^{(i)}] = \sum_{n=1}^{\infty} p_{ni} E[\phi_{pn}^{(i)}]$ and $E[(\phi_p^{(i)})^2] = \sum_{n=1}^{\infty} p_{ni} E[(\phi_{pn}^{(i)})^2]$. Then by using the denotation of $\phi_{pn}^{(i)}$, we have $E[\phi_{pn}^{(i)}] = nE[\phi_{u\nu}^{(i)}]$ and $VAR[\phi_{pn}^{(i)}] = nVAR[\phi_{u\nu}^{(i)}]$. Further using the denotation of $\phi_{u\nu}^{(i)}$, we have $E[\phi_{u\nu}^{(i)}] = \nu_i \phi_{up}^{(i)}$ and $E[(\phi_{u\nu}^{(i)})^2] = \nu_i E[(\phi_{up}^{(i)})^2]$. After some mathematical manipulations, we have $E[\phi_p] = \sum_{i=1}^{M} \rho_i \nu_i E[\phi_{up}^{(i)}]$ and $VAR[\phi_p] = \sum_{i=1}^{M} \rho_i \nu_i E[(\phi_{up}^{(i)})^2]$, where $E[\phi_{up}^{(i)}]$ and $E[(\phi_{up}^{(i)})^2]$ are obtained by replacing G in $E[\phi_{up}]$ and $E[(\phi_{up})^2]$ with the spreading gain of the i^{th} traffic class G_i, respectively. ϕ_p can be approximated as a lognormal distributed variate as shown in the chapter 6.6.3. It is interesting to notice that in [35], the authors also mention that a lognormal variate can be used to approximate the BS power distribution if there are no multipath components.

By applying the traffic model to the system level, we can obtain the BS power distribution as follows. To reduce the simulation and computation complexity, we restrict MS's in one of the 30 degree triangles in the 19-cell cluster (e.g. *tri* #1 in Fig. 6.4). For simplicity, we assume the user density distribution is the same in every triangle. Therefore, by using the symmetry assumption of the cell cluster, each MS located in one 30 degree triangle has the other 11 identical MS's requiring powers from BS_0 with the

same distribution, which are represented by circles in Fig. 6.4. Therefore, the summation of the powers required by all the MS's from BS_0 is

$$\varphi_0 = \sum_{i=1}^{M} \sum_{\substack{p_{ni} \\ over\ n}} \sum_{u=1}^{n} \sum_{\nu_i} \sum_{triangles=1}^{12} \sum_{p} \sum_{u_p} \phi_{up}^{(i)} = \sum_{i=1}^{M} \sum_{\substack{p_{ni} \\ over\ n}} \sum_{u=1}^{n} \sum_{\nu_i} \phi_{ucell}^{(i)} \tag{6.16}$$

where the user density at location p is u_p and $\sum_{triangle=1}^{12} \sum_p u_p = 1$. The average power usage in the system level is denoted by $\phi_{ucell}^{(i)} = \sum_{triangle=1}^{12} \sum_p \sum_{u_p} \phi_{up}^{(i)}$. Following the similar procedure of deriving the mean and variance of ϕ_p in the earlier part of this section, we have $E[\varphi_0] = \sum_{i=1}^{M} \rho_i \nu_i E[\phi_{ucell}^{(i)}]$ and $VAR[\varphi_0] = \sum_{i=1}^{M} \rho_i \nu_i E[(\phi_{ucell}^{(i)})^2]$. By using the denotation of $\phi_{ucell}^{(i)}$, we have $E[\phi_{ucell}^{(i)}] = 12 \sum_p u_p E[\phi_{up}^{(i)}]$ and $VAR[\phi_{ucell}^{(i)}] = 12 \sum_p VAR[\sum_{u_p} \phi_{up}^{(i)}] = 12 \sum_p u_p E[(\phi_{up}^{(i)})^2] - 12 \sum_p u_p^2 E^2[\phi_{up}^{(i)}]$. It is well-know that the sum of lognormal variables can be approximated by another lognormal variate [65] [66] and was used in many literature to study the system performance [24] [35]. Since φ_0 can be expressed as a summation of ϕ_p as defined in equation (6.15) and ϕ_p is lognormal distributed as shown in chapter 6.6.3, φ_0 can be approximated by a lognormal variate. By denoting $10 \log_{10}(\varphi_0) = W_0 \sim N(\mu_{w0}, \sigma_{w0}^2)$, we have $E[\varphi_0] = \exp(\mu_{w0}\delta + \delta^2\sigma_{w0}^2/2)$ and $E[\varphi_0^2] = \exp(2\mu_{w0}\delta + 2\delta^2\sigma_{w0}^2)$. Then we have $\mu_{w0} = \{2 \ln(E[\varphi_0]) - \ln(E[\varphi_0^2])/2\}/\delta$ and $\sigma_{w0}^2 = \{\ln(E[\varphi_0^2]) - 2 \ln(E[\varphi_0])\}/\delta^2$, where $\delta = \ln(10)/10$.

Since the total fraction of BS power consumed by all MS's should be less than 1, the system blocking probability is

$$P_o = P(\varphi_0 > 1) = Q(-\mu_{w0}/\sigma_{w0}). \tag{6.17}$$

Notice that μ_{w0} and σ_{w0} are the mean and standard deviation of $10 \log_{10}(\varphi_0)$, respectively. We can solve (6.17) to get the total Erlang capacity ρ_{t0} at a given blocking probability as

$$\rho_{t0} = \sum_{i=1}^{M} \rho_i. \tag{6.18}$$

The detailed process to obtain ρ_{t0} is shown in Fig. 6.2. We initially choose a tentative value of ρ_{t0} and assume a certain traffic composition, that is, a certain ratio between $\rho_1 : \rho_2 : \cdots$. Then we use equation (6.18) to obtain the actual value of ρ_i's. Next, we use equation (6.17) to calculate the blocking probability, since both μ_{w0} and σ_{w0} are functions of ρ_i. If the blocking probability is larger than a predefined target value, e.g. 1 %, we decrease the value of ρ_{t0}. Otherwise, we increase the value of ρ_{t0} until the difference between the blocking probability and the target blocking probability is less than a very small value, e.g. 10^{-7}. By replacing φ_0 with φ_i in equation (6.16) to obtain the power of BS_i and using the Erlang capacity in equation (6.17), we can obtain the power distributions of every BS_i and then feed them back to equation (6.7). After several iterations, there is very small change of the value of ρ_{t0} and the stabilized value of ρ_{t0} is called the stabilized Erlang capacity.

Since MS's in soft handoff mode require powers from BS's in the soft handoff set as discussed in chapter 6.6.4, the Erlang capacity derived above should be scaled down to the net Erlang capacity from a system viewpoint. The scale factor is decided by the percentage of shared BS_0 power with nearby BS's given in equation (6.36) in chapter 6.6.4. Let us take BS_0 and BS_1 as an example. If all of the BS_0 power is shared by BS_0 and BS_1 due to soft handoff, the net capacity of BS_0 should be equal to half of the capacity obtained in equation (6.18) from a system viewpoint. On the other hand, if the BS_0 power is unshared, there is no capacity reduction from a system viewpoint and the net capacity of BS_0 should be equal to the capacity obtained in equation (6.18). Therefore, the percentage of reduction in the capacity from a system viewpoint is equal to half of the percentage of shared BS_0 power and we can express the scale factor as

$1-\eta_0/2$. By using the scale factor, we can express the net Erlang capacity supported by BS_0 as

$$\rho_{t0}^{'} = (1-\eta_0/2)\sum_{i=1}^{M}\rho_i. \tag{6.19}$$

6.5 Numerical results and analysis

Without loss of generality, three traffic classes are considered in the simulation as shown in table 6.1. The first one is a 9.6 *kbps* voice traffic and we choose a 1 s ON-Period and 1.35 s OFF-period [60], which gives a $\nu_1 = 0.426$ voice active factor. The second one is a 60 *kbps* web data traffic. The ON-period is related to the file size for the data traffic. For a typical web file with a 6.4 kbytes average size, the ON-period has a mean of 7.2 s and is a Pareto distributed with $\alpha = 1.35$. The OFF-period of data is less sensitive to the file size and has a mean idle time of 10.5 s and a typical Pareto distribution with $\alpha = 1.2$. This gives a $\nu_2 = 0.4$ data active factor. The third one is a 120 *kbps* continuously data traffic (e.g. the video traffic) with an active factor $\nu_3 = 1$. To study the effects of ON/OFF mixed traffic, three sets of traffic composition scenarios are chosen as shown in Table 6.2 to simulate the voice traffic dominated, voice/data shared, and data dominated scenarios, respectively. The soft handoff threshold Th is set to be 3 dB. The maximum fraction of BS power ϕ_{uth} that a soft handoff set can utilize is set to 1, that is, a soft handoff set can use the whole BS power if necessary. The target SIR in equation (6.7) is set to 5 dB. The target outage probability given in equation (6.9) is set to 0.1 and the system blocking probability given by equation (6.17) is set to 0.01.

The Rake receiver is assumed to deploy total of 6 fingers, that is, $\sum_{k\in N_{sh}} f_k = 6$ according to equation (6.3), and equally assign them to BS's in the soft handoff set. Maximum 4 BS's is considered in the soft handoff set, since the probability that more than 4 BS's in soft handoff set is too small to be taken into consideration [57]. The path

Table 6.1 Traffic Parameters

Traffic Type	Active Factor ν_i	Rate (kpbs)	Spreading Gain G_i in WCDMA	Spreading Gain G_i in CDMA 2000
Voice	0.426	9.6	400	128
Data	0.4	60	64	20
Video	1	120	32	10

Table 6.2 Traffic Composition Config

Traffic Composition	Erlang Ratio $\rho_1(voice) : \rho_2(data) : \rho_3(video)$
#1 (Voice Dominated)	0.8 : 0.15 : 0.05
#2 (Voice/Data Shared)	0.5 : 0.3 : 0.2
#3 (Data Dominated)	0.2 : 0.5 : 0.3

loss slop u is set to 4 dB, and correlation coefficient among the path losses a is chosen to be 0.5, and the standard deviation of the shadowing is set to 8 dB. These are typical values in unburn area.

BS_0 is the BS that we choose to study its power and capacity. Three sets of BS loading scenarios are used to study the effects of the loadings of other BS's on BS_0. Loading scenario #1 assumes that all BS are equally loaded, that is, the traffic loadings are the same throughout the system. Loading scenario #2 assumes that BS_0 is heavily loaded and as an example, traffic loadings of BS's other than BS_0 are 80 % of the traffic load of BS_0. Loading scenario #3 assumes that BS_0 is lightly loaded and as an example, traffic loading of BS_0 is 80 % of the traffic load of other BS's. Without explicit stated, equally loaded scenario #1 is assumed. For simplicity, the user density is assumed to be uniformly distributed in the simulation, even though we can change the user density according the approach outlined in section 6.4.3.

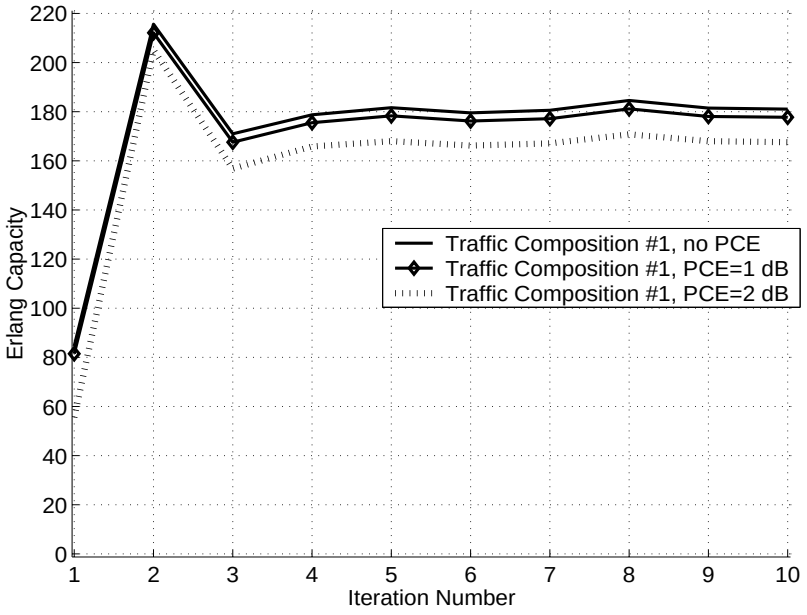

Figure 6.5 Dynamic Erlang capacity of traffic composition #1.

6.5.1 Erlang Capacity of WCDMA System

Firstly, we take a wide-band CDMA (WCDMA) system with a chip rate of $3.84Mcps$ as an example. The simulation results are shown in Fig. 6.5, 6.6, and 6.7, where the Erlang capacity is obtained by using (6.18). We could see that there are significantly changes of the Erlang capacity when the BS power changes from constant to a stabilized distribution. After several iterations, the Erlang capacity becomes stable. Since the initial states of all BS powers are the same throughout the system and equal to $\varphi_1 = \varphi_2 = \cdots = 1$. Therefore, we are expecting to see an initial lower Erlang capacity as shown in these figures. Then, since the Erlang capacity is lower throughout the system, the powers of surrounding BS's become lower and the interferences to MS's served by BS_0 also become lower, which leads to a surge of Erlang capacity in the subsequent iteration. After that, since the Erlang capacity is higher now throughout the system, the powers of surrounding BS's become higher and the interferences to MS's served by BS_0 also become higher, which results into a lower Erlang capacity in the subsequent

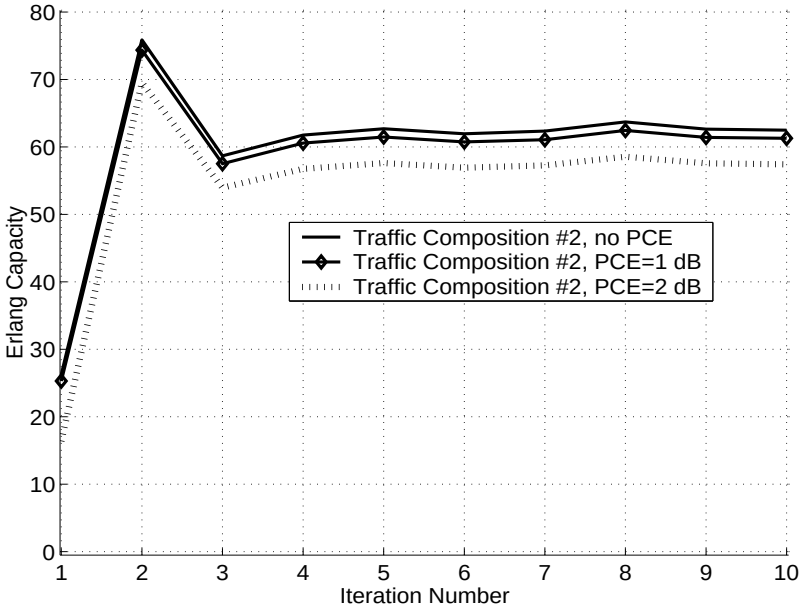

Figure 6.6 Dynamic Erlang capacity of traffic composition #2.

iteration. Comparing Fig. 6.5, 6.6, and 6.7, it is obvious that traffic compositions significantly affect the Erlang capacity as expected. The correlation coefficient between BS_0 and BS_1 with traffic composition #1 are shown in Fig. 6.8, which illustrates that the determination of the correlation is also a dynamic process.

To evaluate the effects of PCE and traffic compositions on the capacity, it is more meaningful to use the net Erlang capacity given in equation (6.19). The BS power distribution, stabilized Erlang capacity, and stabilized net Erlang capacity with different traffic compositions and PCE's in a WCDMA system are given in Table 6.3. Hereafter, *stabilized* means the value obtained at the 10^{th} iteration, where there is insignificant change of the value afterward. From Table 6.3, we notice that there is only $1-2\%$ of capacity loss when the PCE increases from 0 dB to 1 dB, but there is $5-6\%$ of capacity loss when the PCE increases from 1 dB to 2 dB. We also observe that at a higher PCE, the spread of the BS power, which is quantified by the standard deviation of the BS power, becomes larger. We further notice that a larger PCE tends to reduce the amount

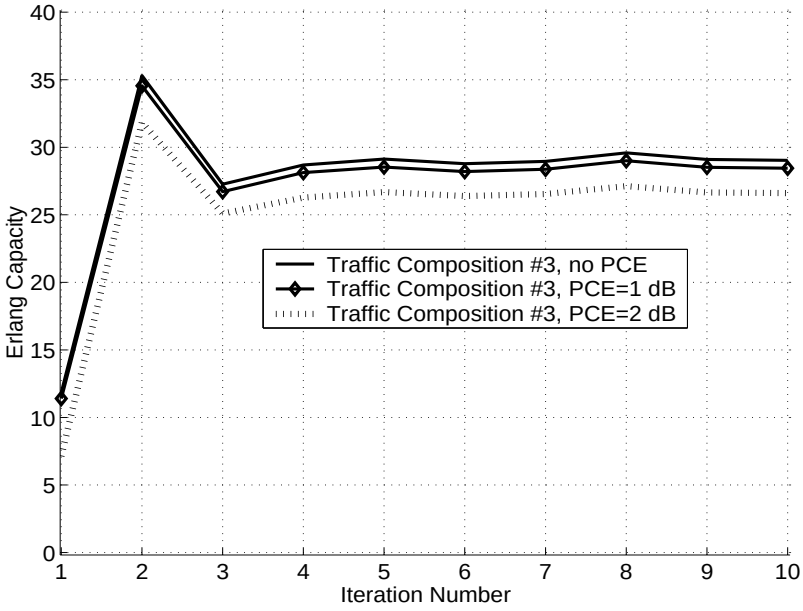

Figure 6.7 Dynamic Erlang capacity of traffic composition #3.

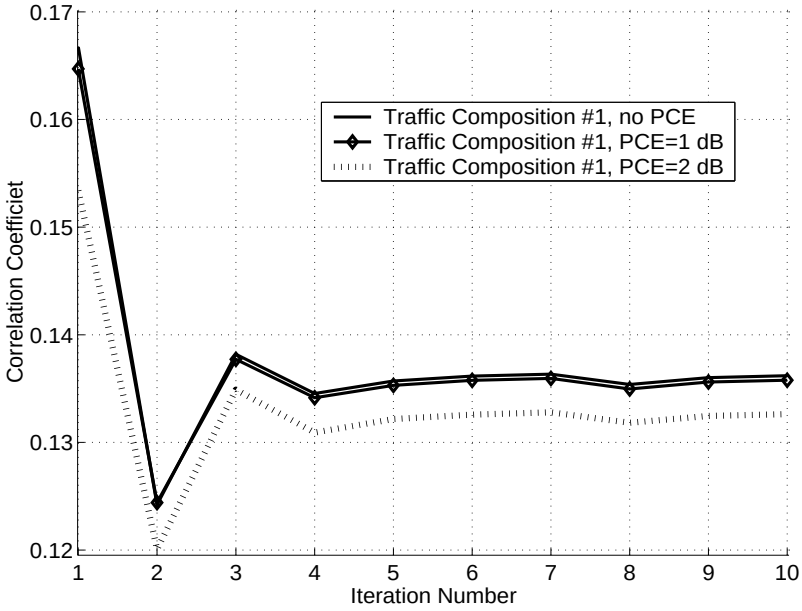

Figure 6.8 Correlation in WCDMA system with traffic composition #1.

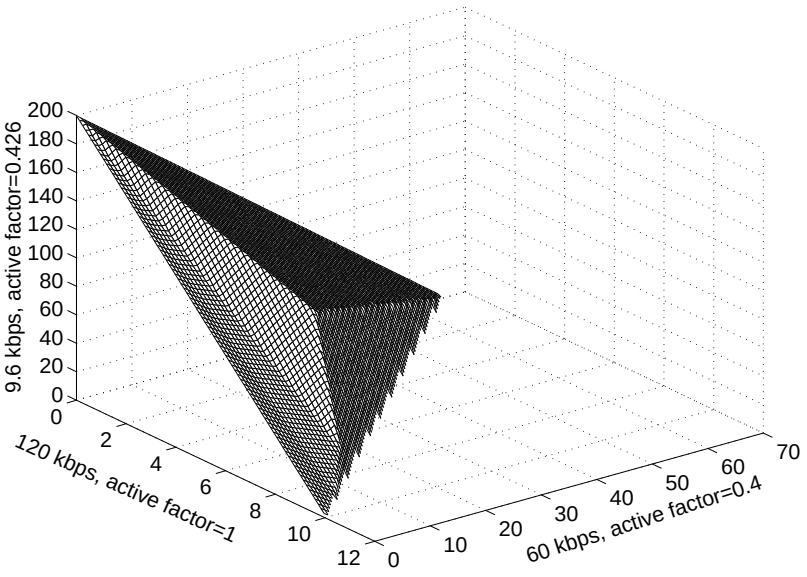

Figure 6.9 Stabilized Net Erlang capacity in a WCDMA system.

of correlation among BS powers and result into a larger scale factor. The scale factor is about 0.7 for all simulation setups, that is, about 30 % reduction in the capacity. In previous studies [1] [23], similar values of capacity reduction are also observed by using a simplified channel concept and calculating the percentage of additional channels used due to soft handoff. A surface plot of the net Erlang capacity with a 2 dB PCE is shown in Fig. 6.9, where similar shapes are obtained in [35]. As expected, we obtain much larger net Erlang values than previous works, since the Erlang values calculated in previous work are based on the assumption of equal BS power throughout the system and equivalent to the Erlang value obtained at the 1^{st} iteration in our approach.

In Fig. 6.10, we choose different BS loading scenarios as described at the beginning of this section to show the effects of traffic loading on the capacity and correlation. The BS power distribution, stabilized Erlang capacity, and stabilized net Erlang capacity is given in Table 6.4. Since the loading scenario #2 assumes that the traffic load BS_0 is larger than the rest BS's at a ratio of 1:0.8, the amount of other-cell interference perceived by

Table 6.3 BS power distribution and Erlang Capacity in WCDMA systems

(Traffic Composition, PCE)	BS Power $E[\varphi_0]$, $\sqrt{VAR[\varphi_0]}$	Stabilized Erlang Capacity	Correlation Coefficient	Scale Factor	Stabilized Net Erlang Capacity
#1, 0 dB	0.3763, 0.1857	181.1	0.136	0.680	123.2
#1, 1 dB	0.3684, 0.1868	177.7	0.136	0.681	121.0
#1, 2 dB	0.3483, 0.1894	167.6	0.133	0.685	114.7
#2, 0 dB	0.3222, 0.1925	62.5	0.131	0.686	42.9
#2, 1 dB	0.3147, 0.1933	61.3	0.131	0.687	42.1
#2, 2 dB	0.2953, 0.1952	57.4	0.128	0.690	39.6
#3, 0 dB	0.3013, 0.1946	29.0	0.129	0.689	20.0
#3, 1 dB	0.2941, 0.1954	28.5	0.129	0.689	19.6
#3, 2 dB	0.2753, 0.1971	26.6	0.126	0.693	18.4

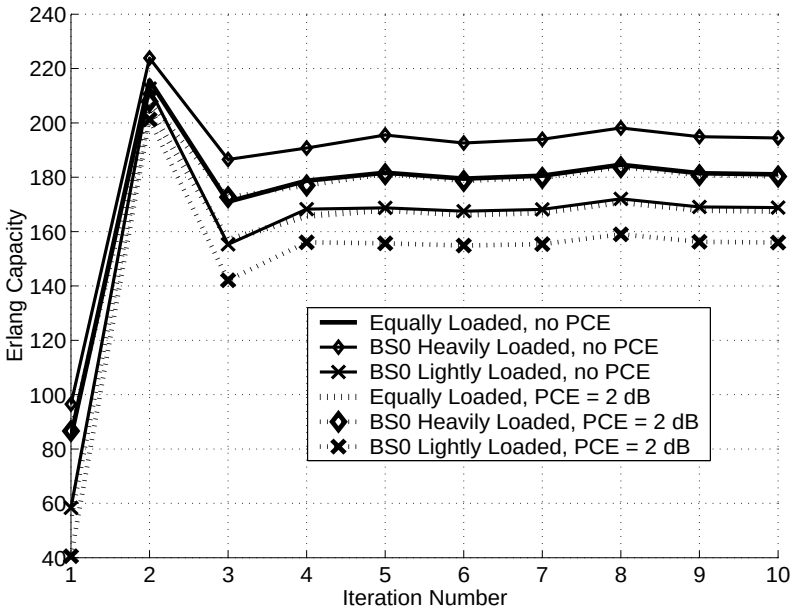

Figure 6.10 Dynamic capacity with different loading scenarios.

MS power-controlled by BS_0 is less than that in the case of equally loading scenario #1. Therefore, MS's in loading scenario #2 requires less power from BS_0 and subsequently, BS_0 can accommodate more MS's than in equally loaded scenario #1. Similarly, since the loading scenario #3 assumes that the traffic load BS_0 is less than the rest of the BS at a ratio of 0.8:1, MS's served by BS_0 experience less other-cell interference and therefore, BS_0 accommodates less MS's than in equally loaded scenario #1.

Table 6.4 BS power distribution and Capacity with different loadings

(Loading Scenario, PCE)	BS Power $E[\varphi_0]$, $\sqrt{VAR[\varphi_0]}$	Stabilized Erlang Capacity	Correlation Coefficient	Scale Factor	Stabilized Net Erlang Capacity
#1, 0 dB	0.3763, 0.1857	181.1	0.136	0.680	123.2
#2, 0 dB	0.3901, 0.1838	194.4	0.132	0.685	133.2
#3, 0 dB	0.3627, 0.1876	168.8	0.140	0.676	114.2
#1, 2 dB	0.3483, 0.1894	167.6	0.133	0.685	114.7
#2, 2 dB	0.3615, 0.1878	180.3	0.129	0.689	124.2
#3, 2 dB	0.3351, 0.1910	156.0	0.136	0.681	106.2

6.5.2 Erlang Capacity of CDMA2000 System

In this section, we taken a CDMA2000 system with a 1.2288 $Mchip/s$ chip rate as an example. The BS power distribution, stabilized Erlang capacity, and stabilized net Erlang capacity with different traffic compositions and PCE's in a CDMA2000 system are given in Table 6.3, where similar but smaller values are obtained comparing to the results obtained in WCDMA systems.

Comparing Table 6.5 to Table 6.3, we notice that correlation among BS powers in WCDMA systems is less than that in CDMA 2000 systems, e.g., reducing from 0.13 to 0.1. Furthermore, the spread of the BS power in CDMA 2000 system, which is characterized

Table 6.5 BS power distribution and Erlang Capacity in CDMA2000 systems

(Traffic Composition, PCE)	BS Power $E[\varphi_0]$, $\sqrt{VAR[\varphi_0]}$	Stabilized Erlang Capacity	Correlation Coefficient	Scale Factor	Stabilized Net Erlang Capacity
#1, 0 dB	0.1965, 0.2047	37.2	0.098	0.728	27.1
#1, 1 dB	0.1917, 0.2054	36.5	0.098	0.729	26.6
#1, 2 dB	0.1784, 0.2074	33.8	0.096	0.731	24.7
#2, 0 dB	0.1605, 0.2112	12.0	0.097	0.730	8.7
#2, 1 dB	0.1572, 0.2121	11.8	0.097	0.730	8.6
#2, 2 dB	0.1473, 0.2152	11.0	0.095	0.733	8.1
#3, 0 dB	0.1489, 0.2145	5.5	0.097	0.730	4.0
#3, 1 dB	0.1461, 0.2156	5.4	0.097	0.731	4.0
#3, 2 dB	0.1374, 0.2193	5.1	0.095	0.733	3.7

by the standard deviation of the power, is larger than that in WCDMA systems. While the mean value of the BS power in CDMA 2000 systems is less than that in WCDMA systems. This is because the spreading gain in CDMA 2000 systems with a chip rate of 1.2288 $Mchip/s$ is less than that in WCDMA systems with a chip rate of 3.84 $Mchip/s$. A surface plot of the stabilized net Erlang capacity with a 2 dB PCE in CDMA 2000 system is shown in Fig. 6.11, where similar shapes but smaller values are obtained in [35] as expected.

6.6 Mathematic Derivations

6.6.1 The Approximation of SIR

In this section, simulations are conducted to validate the approximation in equation (6.3) in section 6.4. The fraction of BS power ϕ_u is assumed to be constant and equal to 1%. The spreading gain is set to $G = 64$. Notice that choosing different values of ϕ_u and G only shrinks or expands the CDF of SIR but does not affect the accuracy of the approximation. As an example, we assume that the BS powers φ_n are lognormal

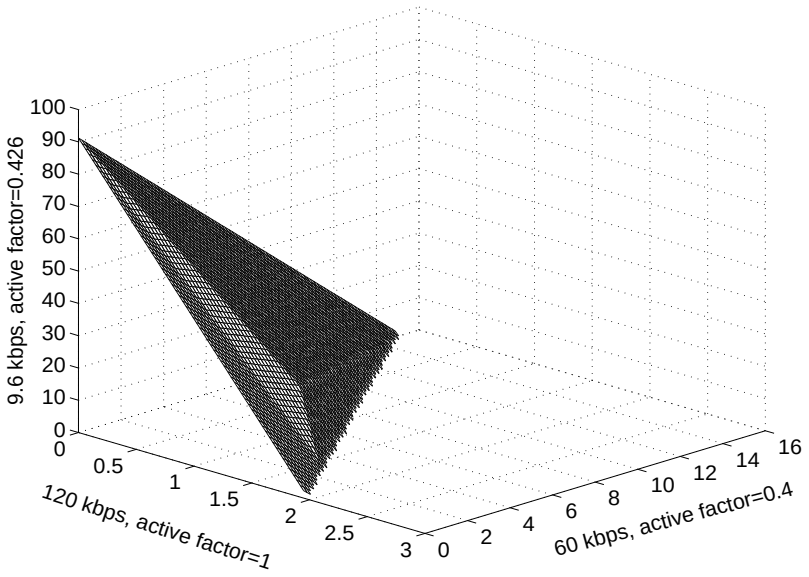

Figure 6.11 Stabilized Net Erlang capacity in a CDMA 2000 system .

distributed and $10\log_{10}(\varphi_n) \sim N(0.3483, 0.1894^2)$ as shown in Table 6.3. We denote that the MS near BS_0, MS at cell boundary, and MS far from BS_0 is located at normalized distance 0.5, 1.0, and 1.5 to the horizon of BS_0, respectively. The rest simulation parameters are the same as those in section 6.5. The simulation results are shown in Fig. 6.12. The *actual* SIRs in the figure are obtained by using left side of (6.3) and the *approx* SIRs are calculated by using the right side of (6.3) by simulating $100,000$ samples.

The difference between the *actual* and *approx* SIR distributions is insignificant at the 5 % level by using the Kolmogorov-Smirnov (KS) [46], which also can be seen from Fig. 6.12 that the CDFs of *actual* and *approx* SIRs overlap each other. Although not shown here, we try more simulation scenarios with different soft handoff combinations and system parameters and KS test at 5 % significant level is passed for all these scenarios.

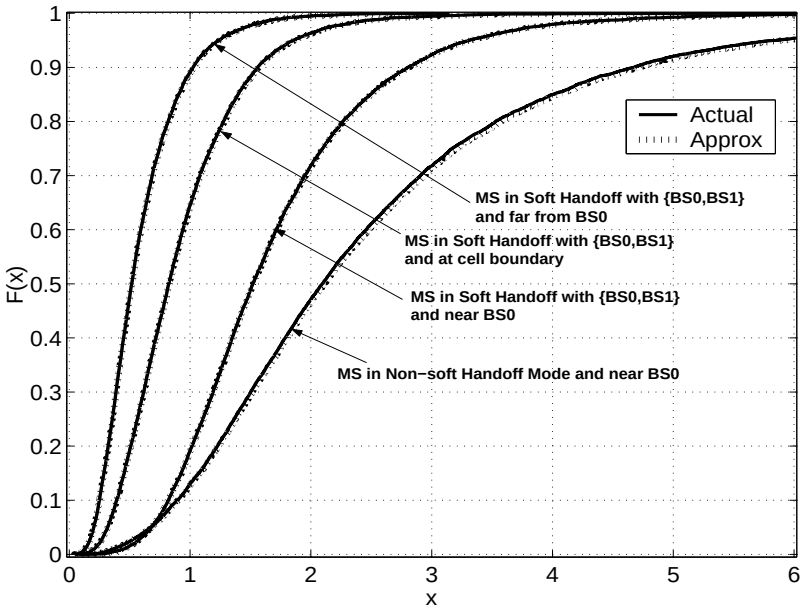

Figure 6.12 SIR approximation.

6.6.2 The Parameters of S and I

Assume $X = 10\log_{10}(I) \sim N(\mu_x, \sigma_x^2)$ and $Y = 10\log_{10}(S) \sim N(\mu_y, \sigma_y^2)$. By equating the first and second moments of the left and right sides of I in (6.8) and using the fact that the average power $E[X_k]$ of all the multipath components from BS_k is normalized to 1 as discussed in section 6.4.1, we have

$$E[I] = \sum_{n \notin N_{sh}} E\left[\varphi_n\right] E\left[\frac{l_0}{l_n}\right] + \sum_{k \in N_{sh}} q_k^{f_k} E\left[\varphi_k\right] E\left[\frac{l_0}{l_k}\right] \tag{6.20}$$

$$\begin{aligned} E[I^2] = & \sum_{\substack{n,k \notin N_{sh} \\ k \neq n}} E\left[\varphi_n \varphi_k\right] E\left[\frac{l_0^2}{l_n l_k}\right] + \sum_{n \notin N_{sh}} E\left[\varphi_n^2\right] \left(\frac{1-q_n}{\rho(1+q_n)} + 1\right) E\left[\frac{l_0^2}{l_n^2}\right] \\ & + \sum_{\substack{k,n \in N_{sh} \\ k \neq n}} E\left[\varphi_n \varphi_k\right] q_n^{f_n} q_k^{f_k} E\left[\frac{l_0^2}{l_n l_k}\right] + \sum_{k \in N_{sh}} \left[\frac{1-q_k}{\rho(1+q_k)} q_k^{2f_k} + q_k^{2f_k}\right] E\left[\varphi_k^2\right] E\left[\frac{l_0^2}{l_k^2}\right] \\ & + 2 \sum_{\substack{n \notin N_{sh} \\ k \in N_{sh}}} q_k^{f_k} E\left[\varphi_n \varphi_k\right] E\left[\frac{l_0^2}{l_n l_k}\right] \end{aligned} \tag{6.21}$$

where q_k is defined in section 6.4.1. The correlation among BS powers $E[\varphi_n \varphi_k]$ is derived in chapter 6.6.4.

Since the fraction of power of BS_n φ_n is lognormal distributed and less than or equal to 1, we can derive the first and second moments of φ_n as

$$E[\varphi_n] = \exp(\sigma_{wn}^2 \delta^2/2 + \mu_{wn}\delta) Q\left(\frac{\mu_{wn} + \sigma_{wn}^2 \delta}{\sigma_{wn}}\right) \tag{6.22}$$

$$E[\varphi_n^2] = \exp(2\sigma_{wn}^2 \delta^2 + 2\mu_{wn}\delta) Q\left(\frac{\mu_{wn} + 2\sigma_{wn}^2 \delta}{\sigma_{wn}}\right) \tag{6.23}$$

where $10\log_{10}(\varphi_n) = W_n \sim N(\mu_{wn}, \sigma_{wn}^2)$ and μ_{wn} and σ_{wn}^2 are obtained by using the same approach to derive μ_{w0} and σ_{w0}^2 in section 6.4.3. $\delta = \ln(10)/10$.

Since $X = 10\log_{10}(I) \sim N(\mu_x, \sigma_x^2)$, we have $E[I] = \exp(\mu_x \delta + \delta^2 \sigma_x^2/2)$ and $E[I^2] = \exp(2\mu_x \delta + 2\delta^2 \sigma_x^2)$. Therefore, by using equations (6.20) and (6.21), we have $\mu_x = \{2\ln(E[I]) - \ln(E[I^2])/2\}/\delta$ and $\sigma_x^2 = \{\ln(E[I^2]) - 2\ln(E[I])\}/\delta^2$.

Similarly, by equating the first and second moments of the left and right sides of S in (6.8), we have

$$E[S] = \sum_{k \in N_{sh}} (1 - q_k^{f_k}) E\left[\frac{l_0}{l_k}\right] \tag{6.24}$$

$$E[S^2] = \sum_{n \in N_{sh}} \left[\frac{1 - q_n}{\rho(1 + q_n)}(1 - q_n^{2f_n}) + (1 - q_n^{f_n})^2\right] E\left[\frac{l_0^2}{l_n^2}\right] + \sum_{\substack{k, n \in N_{sh} \\ k \neq n}} (1 - q_n^{f_n})(1 - q_k^{f_k}) E\left[\frac{l_0^2}{l_n l_k}\right] \tag{6.25}$$

Then, we have $\mu_y = \{2\ln(E[S]) - \ln(E[S^2])/2\}/\delta$ and $\sigma_y^2 = \{\ln(E[S^2]) - 2\ln(E[S])\}/\delta^2$.

Equations (6.20-6.23) use the following results:

$$E\left[\frac{l_0}{l_n}\right] = \exp\left(\frac{\sigma_b^2\delta^2}{2}\right)\frac{r_0^u}{r_n^u}E_x[\frac{Q(\frac{x-\gamma_{n1}+\sigma_b^2\delta}{\sigma_b}) - Q(\frac{x-\gamma_{n2}+\sigma_b^2\delta}{\sigma_b})}{Q(\frac{x-\gamma_{n1}}{\sigma_b}) - Q(\frac{x-\gamma_{n2}}{\sigma_b})}\exp(\delta x)], n \in N_{sh}, n \neq 0 \tag{6.26}$$

$$E\left[\frac{l_0}{l_n}\right] = \exp\left(\frac{\sigma_b^2\delta^2}{2}\right)\frac{r_0^u}{r_n^u}E_x[\frac{Q(\frac{x-\gamma_{n1}}{\sigma_b}+\sigma_b\delta)}{Q(\frac{x-\gamma_{n1}}{\sigma_b})}\exp(\delta x)], n \notin N_{sh} \tag{6.27}$$

$$E\left[\frac{l_0^2}{l_n^2}\right] = \exp\left(2\sigma_b^2\delta^2\right)\frac{r_0^{2u}}{r_n^{2u}}E_x[\frac{Q(\frac{x-\gamma_{n1}+2\sigma_b^2\delta}{\sigma_b}) - Q(\frac{x-\gamma_{n2}+2\sigma_b^2\delta}{\sigma_b})}{Q(\frac{x-\gamma_{n1}}{\sigma_b}) - Q(\frac{x-\gamma_{n2}}{\sigma_b})}\exp(2\delta x)], n \in N_{sh}, n \neq 0 \tag{6.28}$$

$$E\left[\frac{l_0^2}{l_n^2}\right] = \exp\left(2\sigma_b^2\delta^2\right)\frac{r_0^{2u}}{r_n^{2u}}E_x[\frac{Q(\frac{x-\gamma_{n1}+2\sigma_b^2\delta}{\sigma_b})}{Q(\frac{x-\gamma_{n1}}{\sigma_b})}\exp(2\delta x)], n \notin N_{sh} \tag{6.29}$$

$$\begin{aligned}E\left[\frac{l_0^2}{l_n l_k}\right] =& E_x[\frac{Q(\frac{x-\gamma_{n2}+\sigma_b^2\delta}{\sigma_b}) - Q(\frac{x-\gamma_{n1}+\sigma_b^2\delta}{\sigma_b})}{Q(\frac{x-\gamma_{n2}}{\sigma_b}) - Q(\frac{x-\gamma_{n1}}{\sigma_b})}\frac{Q(\frac{x-\gamma_{k2}+\sigma_b^2\delta}{\sigma_b}) - Q(\frac{x-\gamma_{k1}+\sigma_b^2\delta}{\sigma_b})}{Q(\frac{x-\gamma_{k2}}{\sigma_b}) - Q(\frac{x-\gamma_{k1}}{\sigma_b})}\exp(2\delta x)] \\ &\times \exp(\sigma_b^2\delta^2)\frac{r_0^{2u}}{r_k^u r_n^u}, n, k \in N_{sh}, n, k \neq 0, n \neq k\end{aligned} \tag{6.30}$$

$$E\left[\frac{l_0^2}{l_n l_k}\right] = \exp(\sigma_b^2\delta^2)\frac{r_0^{2u}}{r_k^u r_n^u}E_x[\frac{Q(\frac{x-\gamma_{n1}+\sigma_b^2\delta}{\sigma_b})}{Q(\frac{x-\gamma_{n1}}{\sigma_b})}\frac{Q(\frac{x-\gamma_{k1}+\sigma_b^2\delta}{\sigma_b})}{Q(\frac{x-\gamma_{k1}}{\sigma_b})}\exp(2\delta x)], n, k \notin N_{sh}, n \neq k \tag{6.31}$$

$$\begin{aligned}E\left[\frac{l_0^2}{l_n l_k}\right] =& \exp(\sigma_b^2\delta^2)\frac{r_0^{2u}}{r_k^u r_n^u}E_x[\frac{Q(\frac{x-\gamma_{n1}+\sigma_b^2\delta}{\sigma_b})}{Q(\frac{x-\gamma_{n1}}{\sigma_b})}\frac{Q(\frac{x-\gamma_{k2}+\sigma_b^2\delta}{\sigma_b}) - Q(\frac{x-\gamma_{k1}+\sigma_b^2\delta}{\sigma_b})}{Q(\frac{x-\gamma_{k2}}{\sigma_b}) - Q(\frac{x-\gamma_{k1}}{\sigma_b})}\exp(2\delta x)] \\ &, n \notin N_{set}, k \in N_{sh}\end{aligned} \tag{6.32}$$

where $\sigma_b = b\sigma$ and $\delta = \ln(10)/10$. When $n \in N_{sh}$ and more than one BS in N_{sh}, $\gamma_{n1} = (10\mu\log_{10}(r_n/r_0) - Th)$ and $\gamma_{n2} = (10\mu\log_{10}(r_n/r_0) + Th)$. When $n \notin N_{sh}$ and more than one BS in N_{sh}, $\gamma_{n1} = 10\mu\log_{10}(r_n/r_0)$. When $n \notin N_{sh}$ and only BS_0 in N_{sh}, $\gamma_{n1} = 10\mu\log_{10}(r_n/r_0) - Th$. $E_x[.]$ means evaluating the expression by using a Gaussian random variable x with zero mean and standard deviation σ_b.

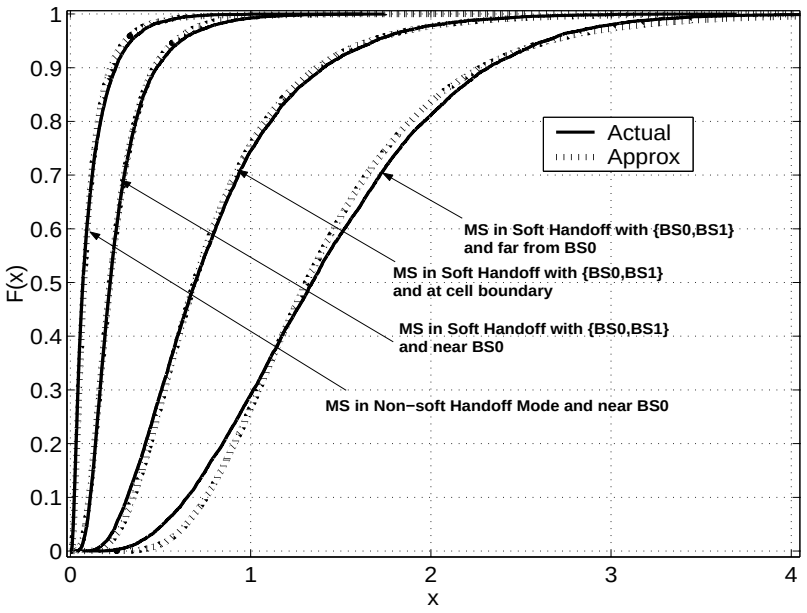

Figure 6.13 CDFs of I.

The same simulation setup as in chapter 6.6.1 is used in this section to validate the use of lognormal distributions to approximate I, S, and I/S in equation (6.8). The simulation results are shown in Fig. 6.13, 6.14, and 6.15. The *actual* values of I, S, I/S are obtained by using (6.8) is compared with the *approx* values of I, S, I/S given by assuming they are lognormal distributed. These figures show that we can achieve a well-approximation of I/S by assuming it is lognormal distributed. The maximum difference between the *approx* and *actual* values is less than 5 % for MS's in soft handoff mode.

6.6.3 The BS Power Distribution Used by a MS

In this section, we show that the BS power used by a MS ϕ_p in equation (6.15) can be approximated as a lognormal variate. The simulation results are shown in Fig. 6.16. The *actual* value of ϕ_p is obtained by simulating 100,000 samples according to equation (6.15), where the procedures of simulation are shown in Fig. 6.17. As an example, we assume that the BS powers φ_n are lognormal distributed and $10\log_{10}(\varphi_n) \sim N(0.2953, 0.1952^2)$,

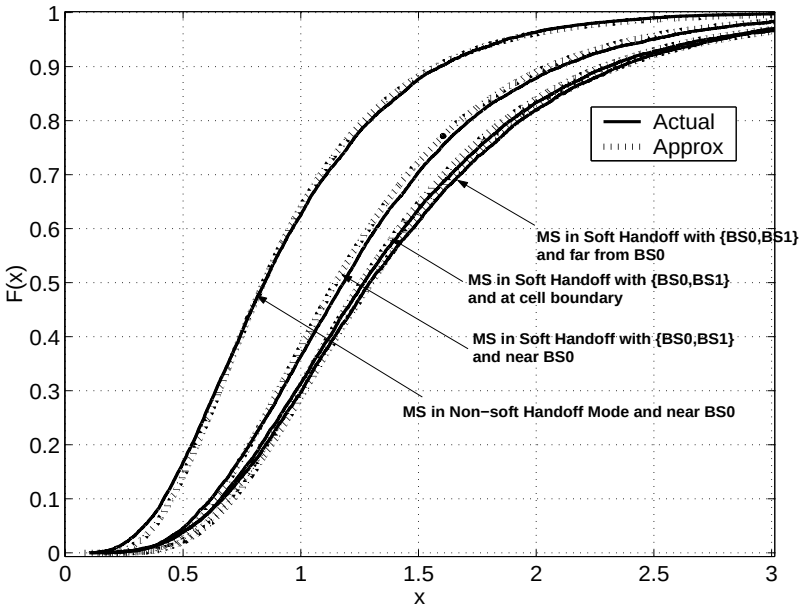

Figure 6.14 CDFs of S.

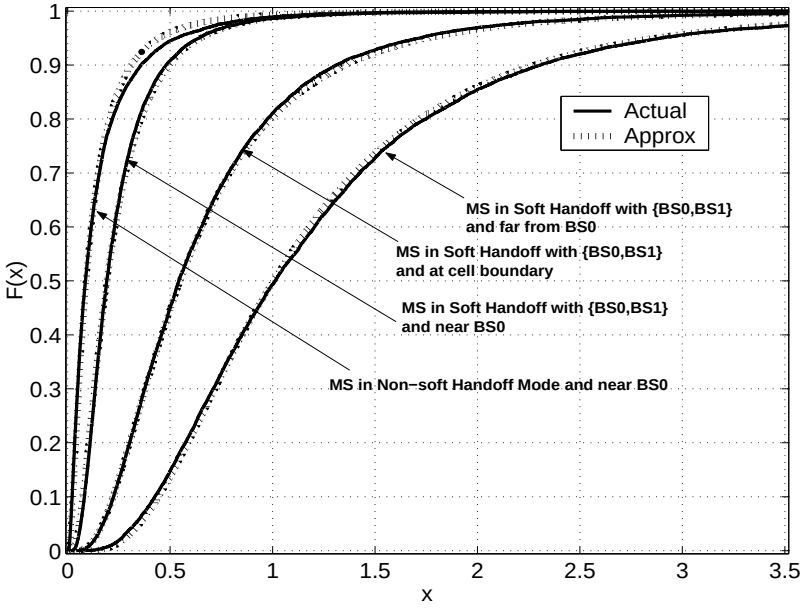

Figure 6.15 CDFs of I/S.

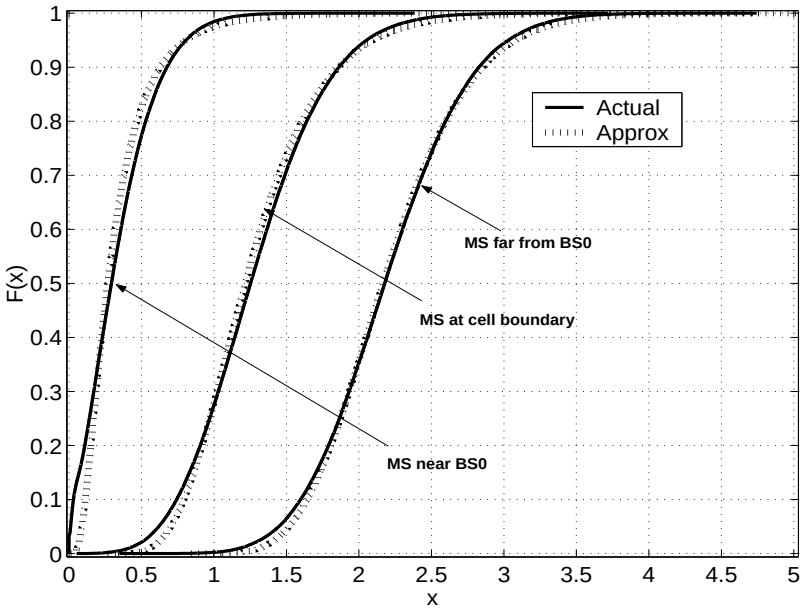

Figure 6.16 BS power distributions of MS's at different locations.

that is, the traffic composition #1 and $PCE = 2\ dB$ are chosen, as shown in Table 6.3. The total Erlang in the simulation is set to 80, that is, $\sum_{i=1}^{3} \rho_i = 80$ and $\rho_1 : \rho_2 : \rho_3 = 0.5 : 0.3 : 0.2$. The *approx* value of ϕ_p is obtained by assuming $\log_{10}(\phi_p) \sim N(\mu_p, \sigma_p^2)$, where $\mu_{\phi_p} = \{2\ln(E[\phi_p]) - \ln(E[\phi_p^2])/2\}/\delta$ and $\sigma_{\phi_p}^2 = \{\ln(E[\phi_p^2]) - 2\ln(E[\phi_p])\}/\delta^2$. $E[\phi_p]$ and $E[\phi_p^2]$ are defined in section 6.4.3. We could see that a better approximation is achieved when MS closes to the serving BS and the maximum difference between *approx* and *actual* values is less than 3% at the tail of the BS power distribution.

6.6.4 The Correlation among BS Powers

In this section, we show how to derive the correlation among BS powers and the percentage of shared BS power used for soft handoff. Let us divide BS's in Fig. 6.4 around BS_0 into 3 tiers: the first tier consists of BS $1-6$, the second tier consists of BS $7-12$, and the third tier consists of BS $13-18$. Due to the symmetry of the cell cluster, we observe that the correlations between BS_0 and BS's in the first tier are the

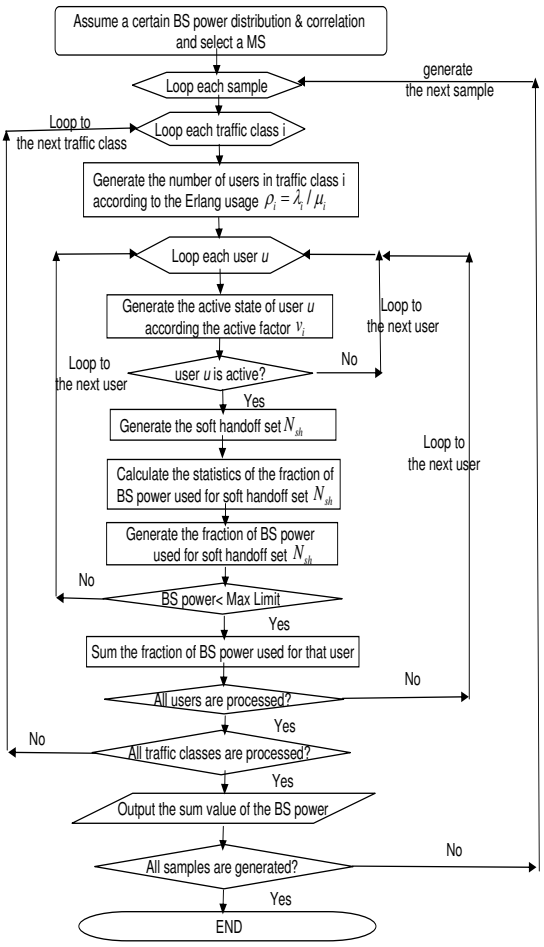

Figure 6.17 Simulation diagram.

same. Let us take BS_0 and BS_1 in Fig. 6.4 as an example and find out their correlation. In order to find out the correlation, the general approach is to count all the soft handoff sets including BS_0 and BS_1 at every location around BS_0. However, a simpler approach exists to determine the correlation. The idea is trying to find out the equivalent soft handoff combinations in tri #1 for all soft handoff combinations including BS_0 and BS_1 in terms of equal BS power consumptions as follows.

Due to symmetry, tri #1 − #6 is enough to be taken into consideration in the calculation of the correlation. Let us focus on the first tier. Assume the soft handoff set

is $\{0, 1\}$, which means both BS_0 and BS_1 are in the soft handoff set. MS's are indicated by a circle in Fig. 6.4. These MS's are identical in terms of the amount of BS power required. If a MS is in soft handoff with $\{0, 1\}$ in *tri* #6, the required BS power for that MS is equivalent for a MS in *tri* #1 connecting to soft handoff set $\{0, 2\}$. Similarly, soft handoff set $\{0, 1\}$ in *tri* #5 is equivalent to soft handoff set $\{0, 3\}$ in *tri* #1; soft handoff set $\{0, 1\}$ in *tri* #4 is equivalent to soft handoff set $\{0, 4\}$ in *tri* #1; soft handoff set $\{0, 1\}$ in *tri* #3 is equivalent to soft handoff set $\{0, 5\}$ in *tri* #1; soft handoff set $\{0, 1\}$ in *tri* #2 is equivalent to soft handoff set $\{0, 5\}$ in *tri* #6. Therefore, we say *tri* #2 and *tri* #6 is a relocation pair, that is, if a MS uses soft handoff set $\{0, 1\}$ in *tri* #6, we can change BS_1 in the soft handoff set to BS_2 and the MS will be relocated to *tri* #1. Similarly, *tri* #3 and *tri* #5 is a relocation pair and *tri* #4 is pair with itself as shown in Table 6.6. By using these relocation pairs, the soft handoff set $\{0, 1\}$ in *tri* $\#1 - \#6$ is equivalent to an unique soft handoff pair in *tri* #1. All these relocated soft handoff set combinations are equivalent to all possible 2-BS soft handoff sets and each of these possible 2-BS soft handoff sets is counted once as shown in Table 6.7, where BS_0 is in the soft handoff set and the other BS is from BS set $1 - 6$.

Table 6.6 Relocation Pairs Respecting to Tri #1

Original Triangle	Relocation Pair
#1	#1
#2	#6
#3	#5
#4	#4
#5	#3
#6	#2

Table 6.7 Equivalent 2-BS Soft Handoff Set in Tri #1

Soft Handoff Set	$Tri\#1$	$Tri\#2$	$Tri\#3$	$Tri\#4$	$Tri\#5$	$Tri\#6$
$\{0,1\}$	$\{0,1\}$	$\{0,6\}$	$\{0,5\}$	$\{0,4\}$	$\{0,3\}$	$\{0,2\}$

Table 6.8 Equivalent 3-BS Soft Handoff Set in Tri #1

Soft Handoff Set	$Tri\#1$	$Tri\#2$	$Tri\#3$	$Tri\#4$	$Tri\#5$	$Tri\#6$
$\{0,1,2\}$	$\{0,1,2\}$	$\{0,6,1\}$	$\{0,5,6\}$	$\{0,4,5\}$	$\{0,3,4\}$	$\{0,2,3\}$
$\{0,1,3\}$	$\{0,1,3\}$	$\{0,6,2\}$	$\{0,5,1\}$	$\{0,4,6\}$	$\{0,3,5\}$	$\{0,2,4\}$
$\{0,1,4\}$	$\{0,1,4\}$	$\{0,6,3\}$	$\{0,5,2\}$	$\{0,4,1\}$	$\{0,3,6\}$	$\{0,2,5\}$
$\{0,1,5\}$	$\{0,1,5\}$	$\{0,6,4\}$	$\{0,5,3\}$	$\{0,4,2\}$	$\{0,3,1\}$	$\{0,2,6\}$
$\{0,1,6\}$	$\{0,1,6\}$	$\{0,6,5\}$	$\{0,5,4\}$	$\{0,4,3\}$	$\{0,3,2\}$	$\{0,2,1\}$
$\{0,1,7\}$	$\{0,1,7\}$	$\{0,6,12\}$	$\{0,5,11\}$	$\{0,4,10\}$	$\{0,3,9\}$	$\{0,2,8\}$
$\{0,1,8\}$	$\{0,1,8\}$	$\{0,6,7\}$	$\{0,5,12\}$	$\{0,4,11\}$	$\{0,3,10\}$	$\{0,2,9\}$
$\{0,1,9\}$	$\{0,1,9\}$	$\{0,6,8\}$	$\{0,5,7\}$	$\{0,4,12\}$	$\{0,3,11\}$	$\{0,2,10\}$
$\{0,1,10\}$	$\{0,1,10\}$	$\{0,6,9\}$	$\{0,5,8\}$	$\{0,4,7\}$	$\{0,3,12\}$	$\{0,2,11\}$
$\{0,1,11\}$	$\{0,1,11\}$	$\{0,6,10\}$	$\{0,5,9\}$	$\{0,4,8\}$	$\{0,3,7\}$	$\{0,2,12\}$
$\{0,1,12\}$	$\{0,1,12\}$	$\{0,6,11\}$	$\{0,5,10\}$	$\{0,4,9\}$	$\{0,3,8\}$	$\{0,2,7\}$
$\{0,1,13\}$	$\{0,1,13\}$	$\{0,6,18\}$	$\{0,5,17\}$	$\{0,4,16\}$	$\{0,3,15\}$	$\{0,2,14\}$
$\{0,1,14\}$	$\{0,1,14\}$	$\{0,6,13\}$	$\{0,5,18\}$	$\{0,4,17\}$	$\{0,3,16\}$	$\{0,2,15\}$
$\{0,1,15\}$	$\{0,1,15\}$	$\{0,6,14\}$	$\{0,5,13\}$	$\{0,4,18\}$	$\{0,3,17\}$	$\{0,2,16\}$
$\{0,1,16\}$	$\{0,1,16\}$	$\{0,6,15\}$	$\{0,5,14\}$	$\{0,4,13\}$	$\{0,3,18\}$	$\{0,2,17\}$
$\{0,1,17\}$	$\{0,1,17\}$	$\{0,6,16\}$	$\{0,5,15\}$	$\{0,4,14\}$	$\{0,3,13\}$	$\{0,2,18\}$
$\{0,1,18\}$	$\{0,1,18\}$	$\{0,6,17\}$	$\{0,5,16\}$	$\{0,4,15\}$	$\{0,3,14\}$	$\{0,2,13\}$

Now let us consider a 3-BS soft handoff set $\{0,1,2\}$. We know from the relocation pair *tri* #2 and *tri* #6 that soft handoff set $\{0,1,2\}$ in *tri* #6 is equivalent to $\{0,2,3\}$ in *tri* #1 by replacing BS_1 with BS_2 and rotating BS_2 anti-clockwise to BS_3. By using a similar approach, we can find equivalent soft handoff sets in *tri* #1 for soft handoff set $\{0,1,2\}$, $\{0,1,3\}$, $\{0,1,4\}$, $\{0,1,5\}$, $\{0,1,6\}$ in other triangles as shown in Table 6.8 and each of these combinations is counted twice, where BS_0 is in the soft handoff set, one BS is from BS set $1-6$, and the other BS is also from BS set $1-6$. The soft handoff

sets $\{0,1,7\}$, $\{0,1,8\}$, $\cdots$, $\{0,1,18\}$ in $tri\ \#1-\#6$ is equivalent to all 3-BS soft handoff combinations in $tri\ \#1$ and each of the soft handoff is counted once, where BS_0 is in the soft handoff set, one BS is from BS set $1-6$, and the other BS is from BS set $7-18$.

The probability that 4-BS soft handoff set is too small to be taken into the consideration in the calculation of the correlation. By using above approaches, the calculation of the correlation between BS_0 and BS_1 can be conducted by focusing on $tri\ \#1$ as follows. Let us focus on deriving the total fraction of BS power required from $tri\ \#1-\#6$. Without loss of generality, let us denote denote the number of occurrence of soft handoff set N_{sh} after the relocation to $tri\ \#1$ as $R_{N_{sh}}$. Similar to equation (6.10), the average power in the calculation of the correlation among BS_0 and BS_1 for MS_u in position p is $\overline{\phi_{up}} = \sum_{P_{N_{sh}} over\ all\ N_{sh}} \sum_{i=1}^{R_{N_{sh}}} \phi_{uh}|_{SH\ with\ N_{sh} \& \phi_{uh} \le \phi_{umax}}$, which is the weighted summation of $P_{N_{sh}}$. Then we have $E[(\overline{\phi_{up}^{(i)}})] = \sum_{N_{sh}} E[\phi_{uh}] R_{N_{sh}} P_{N_{sh}}$ and $E[(\overline{\phi_{up}^{(i)}})^2] = \sum_{N_{sh}} VAR[\phi_{uh}] R_{N_{sh}} P_{N_{sh}} + \sum_{N_{sh}} R_{N_{sh}}^2 E^2[\phi_{uh}] P_{N_{sh}}$. Similar to equation (6.16), we can express the fraction of power allocated by BS_0 and BS_1 to MS's in triangles $\#1-\#6$ as

$$\begin{aligned}
\phi_{<0,1>} &= \sum_{i=1}^{M} \sum_{\substack{p_{ni} \\ over\ n}} \sum_{u=1}^{n} \sum_{\nu_i} \sum_{\substack{p\ in\ tri\ \#1-\#6\& \\ BS0\&BS1\ in\ N_{sh}}} \sum_{u_p} \phi_{up}^{(i)} \\
&= \sum_{i=1}^{M} \sum_{\substack{p_{ni} \\ over\ n}} \sum_{u=1}^{n} \sum_{\nu_i} \sum_{\substack{p\ in\ tri\ \#1\& \\ SHM}} \sum_{u_p} \overline{\phi_{up}^{(i)}} \\
&= \sum_{i=1}^{M} \sum_{\substack{p_{ni} \\ over\ n}} \sum_{u=1}^{n} \sum_{\nu_i} \overline{\phi_{ucell}^{(i)}}
\end{aligned} \tag{6.33}$$

where $\overline{\phi_{ucell}^{(i)}} = \sum_{p\ in\ tri\ \#1\&SHM} \sum_{u_p} \overline{\phi_{up}^{(i)}}$ and SHM means MS is in the soft handoff mode and BS_0 is in the soft handoff set.

Following the similar procedure in section 6.4.3, we have the mean $E[\phi_{<0,1>}] = \sum_{i=1}^{M} \rho_i \nu_i E[\overline{\phi_{ucell}^{(i)}}]$ and the variance $VAR[\phi_{<0,1>}] = \sum_{i=1}^{M} \rho_i \nu_i E[(\overline{\phi_{ucell}^{(i)}})^2]$. We also have

$E[\overline{\phi^{(i)}_{ucell}}] = \sum_{p\ in\ tri\ \#1\&SHM} u_p E[\overline{\phi^{(i)}_{up}}]$ and $VAR[\overline{\phi^{(i)}_{ucell}}] = \sum_{p\ in\ tri\ \#1\&SHM} u_p E[(\overline{\phi^{(i)}_{up}})^2] - \sum_{p\ in\ tri\ \#1\&SHM} u_p^2 E^2[\overline{\phi^{(i)}_{up}}]$.

Due to symmetry, the fraction of power allocated from BS_0 and BS_1 to MS's in triangles $\#7 - \#12$ $\phi^c_{<0,1>}$ follows the same distribution as $\phi_{<0,1>}$ but independent of $\phi_{<0,1>}$. Then we can write the power required from both BS_0 and BS_1 as $\phi^t_{<0,1>} = \phi_{<0,1>} + \phi^c_{<0,1>}$. According to the soft handoff model in section 6.3, the MS asks all BS's in the soft handoff set to allocate the same amount of power. Then we can write $\varphi_0 = \phi^t_{<0,1>} + \phi_{pt0}$ and $\varphi_1 = \phi^t_{<0,1>} + \phi_{pt1}$, where ϕ_{pt0}, $\phi^t_{<0,1>}$, ϕ_{pt0}, and ϕ_{pt1} are independent of each other. Therefore, we can write the cross correlation between φ_0 and φ_1 as

$$\begin{aligned} E[\varphi_0\varphi_1] =& E[{\phi^t_{<0,1>}}^2] + E[\phi^t_{<0,1>}]E[\phi_{pt0}] + E[\phi^t_{<0,1>}]E[\phi_{pt1}] + E[\phi_{pt0}]E[\phi_{pt1}] \\ =& VAR[\phi^t_{<0,1>}] + E[\varphi_0]E[\varphi_1] \\ =& 2VAR[\phi_{<0,1>}] + E[\varphi_0]E[\varphi_1] \end{aligned} \tag{6.34}$$

The correlation between BS's in the first tier and the second tier is negligible, since the probability that one BS in the soft handoff set is from the first tier and the other from the second tier is very small.

Therefore, the correlation coefficient between φ_0 and φ_1 is given by

$$\varrho_{0,1} = \frac{E[\varphi_0\varphi_1] - E[\varphi_0][\varphi_1]}{\sqrt{VAR[\varphi_0]VAR[\varphi_1]}}, \tag{6.35}$$

which can be easily calculated by using equations (6.22), (6.23), (6.33), and (6.34).

Next, let us find out the percentage of shared BS_0 power used by BS_0 and any of nearby BS_0 due to the use of soft handoff. This percentage can be quantified by using the amount of correlation between the BS_0 power and the amount of shared BS_0 power. Due to symmetry, the amount of shared BS_0 power used by BS_0 and any of the nearest 6 surrounding BS's is $\phi^t_{<0,.>} = \sum_{i=1}^{6} \phi^t_{<0,i>}$. Then we can express the power used by BS_0

as $\varphi_0 = \phi^t_{<0,.>} + \phi'_{t0}$, where $\phi^t_{<0,.>}$ is independent of ϕ'_{t0}. So the correlation coefficient between φ_0 and $\phi^t_{<0,.>}$ is

$$\eta_0 = \frac{E[\varphi_0 \phi^t_{<0,.>}] - E[\varphi_0]E[\phi^t_{<0,.>}]}{\sqrt{VAR[\varphi_0]VAR[\phi^t_{<0,.>}]}} = \sqrt{\frac{VAR[\phi^t_{<0,.>}]}{VAR[\varphi_0]}} = \sqrt{\frac{6VAR[\phi^t_{<0,1>}]}{VAR[\varphi_0]}}. \quad (6.36)$$

6.7 Conclusions

In this chapter, we introduce an analytical approach to derive the dynamic Erlang capacity in the forward link of CDMA system by considering the interaction and correlation among BS powers. The closed-form expression of the dynamic Erlang capacity is obtained by analytically deriving the BS power distribution and correlation among BS powers for a given pattern of ON/OFF mixed traffic, power control error, and limitation of BS power available to a MS. Simulation results show that the determination of the Erlang capacity is a dynamic process and the Erlang capacity is significantly different by modeling the BS power as a random variate instead of a constant value. We also show that the interaction and correlation among BS powers can significantly affect the Erlang capacity. The correlation among BS power can be up to 0.13 and the reduction in Erlang capacity can be up to 30 %. With the increasing of the PCE, the reduction of the Erlang capacity becomes more significant. We also show that the PCE tends to reduce the correlation among BS powers.

CHAPTER 7

Conclusions and Future Research

7.1 Summary of Results

In this thesis, a general analytical framework to derive the forward link capacity is proposed. This framework is built on characterizing the BS power distributions and correlation among BS powers. By considering the correlation and interaction among BS powers, an iterative process to determine the BS power distributions is suggested. Based on the knowledge of the BS power distributions, we obtain the *static* forward link capacity by neglecting the interaction among BS powers. Then we introduce an iterative process to derive the *dynamic* capacity by considering the interaction among BS power.

In both cases, the determination of the fractional power that is allocated to any MS by the BS in continuously changing wireless environment is the basis of this approach. This fraction is different when the MS combines different number of multipath components from a single BS in the non-soft handoff mode (NSHM) or we add multipath components from multiple BS's in the soft handoff mode (SHM). By simulating the number of users in a real CDMA network and taking into consideration the fading environment, handoff strategies and power-control algorithms, we find out that a ratio of two Gamma variates can be used to characterize the distribution of power allocated to any MS by the BS in the study of the *static* capacity. While studying the *dynamic* capacity and further considering the interaction among BS power, we suggest that a lognormal variate can be used to characterize that distribution. The valid of these results is verified by using the Kolmogorov-Smirnov test.

By using that distribution, we analytically obtain the distribution of the BS power needed by a single MS by summing the BS powers required by every soft handoff set. Subsequently, the powers needed by all MS's around a specific BS can be obtained. By limiting the maximum fraction of BS power available to a MS, the outage and capacity can be obtained. Consequently, a fine power control can be conducted on the level of soft handoff set and its effects on the system performance can be determined analytically. Since the BS power distribution characteristics are analytically obtained as a function of system parameters, our model develops an easy and effective way to investigate the effects of system parameters, such as the available Rake fingers, the soft handoff threshold, the power control error, and the ON/OFF data traffic, on the system performance from viewpoint of the limitation of the fraction of BS power allocated to a MS.

In the determination of the *dynamic* capacity, the above obtained distributions of BS powers are further used and we study how the BS power changes when summing the fractions of BS powers needed by all MS's in a cell. Therefore, the distribution of the BS power changes after a feedback loop and the determination of the BS power distribution is a dynamic process. After several iterations, we can obtain a stabilized BS power distribution and therefore, a stabilized forward link capacity. Since statistical characteristics of the distribution of BS power are obtained during each iteration, an efficient and accurate evaluation of the *dynamic* capacity is made possible.

Several results are obtained as follows: our approach provides a theoretical basis to study if capacity gain is achievable in the case of soft handoff. In the literature, some studies show insignificant capacity loss or even capacity gain of soft handoff, while other studies show significant capacity loss due to the usage of soft handoff. Our analysis shows that the inconsistency is caused by the omission of some important system parameters such as the multipath fading, number of available Rake fingers, and the soft handoff threshold. By using our proposed model, we show that the possible capacity gain depends

on the choice of the maximum fraction of base station power allocated to the MS, the available Rake fingers, and the soft handoff threshold. In Chapter 5, we introduce an analytical model to characterize the BS power distribution and obtain the static capacity. We show that at a larger outage probability or a larger power control error, the MS needs more power from the BS and degrades the capacity. A larger soft handoff threshold is shown to provide a larger coverage area but result in capacity loss for MS's far away from the BS. When we can use enough number of Rake fingers, the coverage area is significantly extended and the fraction of BS power required by the MS is reduced. We further show that by limiting the maximum fraction of BS power available to a MS and rejecting the power requirements from power-greedy soft handoff sets, a significant capacity gain can be achieved. Most important of all, in Chapter 6, we show that the determination of the BS power distribution and the forward-link capacity is essentially an iterative process by considering the correlation and interaction among BS powers.

7.2 Future Research

Since we have established an analytical and dynamic process to characterize the BS power distribution and forward link capacity, we can easily extend our work by incorporating different techniques in the analysis. Finally, we can extend our analysis but changing the interference model. For example, in a suburban area, there is line-of-sight path between BS and MS. So we need to change the channel modeling in our SIR expressions. Secondly, we can incorporate new technique into the analysis. For example, in a multi-user detection system, part of the interference is mitigated and the SIR expression need to be modified to reflect the difference. One of the restriction of our analysis is that we did not consider the cell sectorization in CDMA systems. Further work can be done by taking the sectorization into considerations.

APPENDIX A

Programs To Calculate the Forward Link Capacity

The following program is used to calculate the dynamic forward link capacity.

```
//include header files
#include "stdio.h"
#include "math.h"
#include "stdlib.h"
#include "string.h"
#include "time.h"
#define ITMAX 200
#define EPS 1.0e-10
#define FPMIN 1.0e-30 //Number near the smallest representable
const double epsilonlittle=1e-8;
static double pi=3.14159265358979;
double uniform(void);
double gaussian (double,double);
double erfc(double x);
double qfunc(double x);
double lognormaldis(double std);
double evaluate_phi_avg(double mean,double std,double x,int traffic_class_num);
double evaluate_phi_avgsquare(double mean,double std,
  double x,int traffic_class_num);
void initbspos(double d);
double rhon_over_n(double x,double n);
static double bs_power[19];
static double bs_phi_mean[19];
static double bs_phi_mean2[19];
static double bs_phi_variance[19];
static double bs_phi_std[19];
```

```
static double bs_power_mean[19];
static double bs_power_mean2[19];
static double bs_power_variance[19];
static double bs_power_std[19];
static double bs_pos[19][2];
static double ms_pos[1000][2];
static double ds[19];
static double pathloss[19];
static double fastfading[19];
static double fastfadingki[19];
static double fastfadingkn[19];
static double sir[19];
static double interference[19];
static double gaussvariable[100001];
static double gaussmatrix[100001];
//set simulation parameters
double extra_power;
double old_extra_power;
static double spreadgain[10];
static int config=3; //traffic composition
double phith=1; //maximum fraction of BS power that a MS can use
static double pcerrordb=2; //power control error
static double targetsir=pow(10.0,5.0/10.0); // target SIR
double targetoutage=0.1; //outage probability
static double targetblocking=0.01; // blocking probability
double constantlamda=log(10.0)/10.0;
double correlation_power_scale;
```

```
double sumtotalavgphi[10][1000],sumtotalavgsquarephi[10][1000];
double sumtotalavgphi_corr[10][1000],sumtotalavgsquarephi_corr[10][1000];
// main function
int main(int argc, char* argv[])
{
char outfilename[80];
char outfilename1[80];
char outfilename2[80];
char outfilename3[80];
char outfilename4[80];
char outfilename5[80];
char outfilename6[80];
char outfilename7[80];
char outfilename8[80];
FILE *outfile1;
FILE *outfile2;
FILE *outfile3;
FILE *outfile4;
FILE *outfile5;
FILE *outfile6;
FILE *outfile7;
FILE *outfile8;
int totalN,totalMSN;
int tempbs;
double c[19][2],cnodiv[19];
double th;
double msxlow,msxhigh,msylow,msyhigh;
```

```
double radius,tempgaus;
double nsh,sh,nshinrage,shinrage;
double shadow,shadowdb,pathlossfactor;
double correlationa,correlationb;
double gausimnum;
double probdiv,bsprobdiv[18];
int bsdivset[1000][19],bsnodivset[1000][19],bsdiv,bsnodiv;
int nearpos[19];
int bsdivnum[1000],bsnodivnum[1000],i,j;
double nshdivprobtot[1000];
double *shdivprobtot[1000];
double sumprob;
int count;
int bs;
int exitcount,exitfix,p,q;
clock_t start, finish;
double  duration;
radius=1.5/sqrt(3.0);
initbspos(radius); //init BS pos
double active_factor[11],erlang[11],traffic_fraction[11];
int traffic_class_total=3;
//set active_factor
active_factor[0]=0.426;
active_factor[1]=0.4;
active_factor[2]=1.0;
//set Erlang ratio
erlang[0]=0.2;
```

```
erlang[1]=0.4;
erlang[2]=0.4;
if(config==1)
{
traffic_fraction[0]=0.8;
traffic_fraction[1]=0.15;
traffic_fraction[2]=0.05;
}
if(config==2)
{
traffic_fraction[0]=0.5;
traffic_fraction[1]=0.3;
traffic_fraction[2]=0.2;
}
if(config==3)
{
traffic_fraction[0]=0.2;
traffic_fraction[1]=0.3;
traffic_fraction[2]=0.5;
}
if(config==4)
{
traffic_fraction[0]=1;
traffic_fraction[1]=0;
traffic_fraction[2]=0;
}
if(config==5)
```

```
{
traffic_fraction[0]=0;
traffic_fraction[1]=1;
traffic_fraction[2]=0;
}

if(config==6)
{
traffic_fraction[0]=0;
traffic_fraction[1]=0;
traffic_fraction[2]=1;
}
double rate=1.2288*1e6;
spreadgain[0]=rate/(9.6*1e3);
spreadgain[1]=rate/(60*1e3);
spreadgain[2]=rate/(120*1e3);
int traffic_index;
for(i=0;i<=13;i++)
{
bs_power[i] = 1.0;
bs_power_mean[i]    = 1.0;
bs_power_mean2[i]   = 1.0;
bs_power_variance[i]    = 1.0;
bs_power_std[i] = 1.0;
bs_phi_mean[i]  = 1.0;
bs_phi_mean2[i] = 1.0;
bs_phi_variance[i]  = 1.0;
```

```
bs_phi_std[i]   = 1.0;
}
bs_power[0]=1.0;
exitcount=0;
exitfix=1; //modify this to get diff position
th=3; //in db;
shadow=8;
pathlossfactor=4;
double pcecorrelationa, pcecorrelationb;
double begindivcount=0;
double enddivcount=87;
int begin=1;
double mssimnum=160;//
gausimnum=1e3;
correlationa=sqrt(0.5);
correlationb=sqrt(1.0-correlationa*correlationa);
pcecorrelationa=sqrt(0.5);
pcecorrelationb=sqrt(1.0-pcecorrelationa*pcecorrelationa);
int thtt=th;
int shadowdbtt=shadow;
int pathlossfactortt=pathlossfactor*10;
int totalxbs,totalybs,mm;
double xlength,ylength;
totalxbs = 15;
totalybs = 9;
xlength = radius*3.0/totalxbs;
ylength = xlength;
```

```
mm=0;
for(p=0;p<totalybs;p++)
{
for(q=floor(1.0*p/(sqrt(3.0)/3.0));q<totalxbs;q++)
{
mm += 1;
ms_pos[mm][0] = (xlength*q + xlength*(q + 1))/2.0;
ms_pos[mm][1] = (ylength*p + ylength*(p + 1))/2.0;
}
}
double little=pow(10,-10);
//mssimnum=max mm=321; max divcount=92
//generate active set
for(i=0;i<1000;i++)
{
shdivprobtot[i]=(double *)malloc(sizeof(double)*1000);
if(shdivprobtot[i]==NULL)
{
printf("\n malloc overflow \n");
return 1;
}
}
for(mm=begin;mm<=mssimnum;mm++)//for a specific ms
{
nshdivprobtot[mm]=0.0;
}
for(i=0;i<1000;i++)//for a specific ms
```

```
{
for(j=0;j<1000;j++)
{
shdivprobtot[i][j]=0.0;
}
}
int divcount;
divcount=0;
int ia,ib,ic;
bsdivnum[0]=0;
bsdivset[0][0]=0;
for(ia=1;ia<=13;ia++)
{
divcount++;
bsdivset[divcount][0]=0;
bsdivset[divcount][1]=ia;
bsdivnum[divcount]=1;
}
for(ia=1;ia<=3;ia++)
{
for(ib=ia+1;ib<=13;ib++)
{
divcount++;
bsdivset[divcount][0]=0;
bsdivset[divcount][1]=ia;
bsdivset[divcount][2]=ib;
bsdivnum[divcount]=2;
```

```
}
}
for(ia=1;ia<=3;ia++)
{
for(ib=ia+1;ib<=3;ib++)
{
for(ic=ib+1;ic<=13;ic++)
{
divcount++;
bsdivset[divcount][0]=0;
bsdivset[divcount][1]=ia;
bsdivset[divcount][2]=ib;
bsdivset[divcount][3]=ic;
bsdivnum[divcount]=3;
}
}
}
int id;
for(ia=1;ia<=3;ia++)
{
for(ib=ia+1;ib<=3;ib++)
{
for(ic=ib+1;ic<=3;ic++)
{
for(id=ic+1;id<=13;id++)
{
divcount++;
```

```
bsdivset[divcount][0]=0;
bsdivset[divcount][1]=ia;
bsdivset[divcount][2]=ib;
bsdivset[divcount][3]=ic;
bsdivset[divcount][4]=id;
bsdivnum[divcount]=4;
}
}
}
}
/*divcount++;
bsdivset[divcount][0]=0; // no active set
bsdivset[divcount][1]=1; // {BS0 and BS1}
bsdivset[divcount][2]=14; // {BS0 , BS1, and BS2}
bsdivset[divcount][3]=47; // {BS0 , BS1, BS2, and BS3}
bsdivnum[divcount]=3;*/
int tempcount,k,flag;
flag=0;
//generate the active set and non-active set
//and the corresponding number of BSs in the set.
for(i=0;i<=divcount;i++)
{
tempcount=0;
for(j=1;j<=13;j++)
{
flag=0;
for(k=1;k<=bsdivnum[i];k++)
```

```
{
if(bsdivset[i][k]==j)
{
flag=1;
}
}
if(flag==0)
{
tempcount++;
bsnodivset[i][tempcount]=j;
bsnodivnum[i]=tempcount;
}
}
}
double decreaseprob;
double decreaseproblu;
double decreaseprobll;
double decreaseprobsu;
double decreaseprobsl;
double temprthlu;
double temprthll;
double temprthsu;
double temprthsl;
double nn;
start = clock(); //start to count the time that the program runs
sprintf(outfilename1,"divprob");
sprintf(outfilename2,"maxphi");
```

```
sprintf(outfilename3,"sumdivprob");
sprintf(outfilename4,"outage_over_phi");
sprintf(outfilename5,"avgphivalue");
sprintf(outfilename6,"final_results");
sprintf(outfilename7,"dynamic_capacity");
sprintf(outfilename8,"corr_coeff");
if( !(outfile1=fopen(outfilename1,"w+")) ){
printf("Can't open file %s \n",outfilename1);
return 1;
}
if( !(outfile2=fopen(outfilename2,"w+")) ){
printf("Can't open file %s \n",outfilename2);
return 1;
}
if( !(outfile3=fopen(outfilename3,"w+")) ){
printf("Can't open file %s \n",outfilename3);
return 1;
}
if( !(outfile4=fopen(outfilename4,"w+")) ){
printf("Can't open file %s \n",outfilename4);
return 1;
}
if( !(outfile5=fopen(outfilename5,"w+")) ){
printf("Can't open file %s \n",outfilename5);
return 1;
}
if( !(outfile6=fopen(outfilename6,"w+")) ){
```

```
printf("Can't open file %s \n",outfilename6);
return 1;
}
if( !(outfile7=fopen(outfilename7,"w+")) ){
printf("Can't open file %s \n",outfilename7);
return 1;
}
if( !(outfile8=fopen(outfilename8,"w+")) ){
printf("Can't open file %s \n",outfilename8);
return 1;
}
int simnum;
int catchfinger[20];
double valuecatchfinger[20][40];
double totalvaluecatchfinger[20];
double partvaluecatchfinger[20];
double avgsir=0.0;
double avgnum;
double totalavgnum=1e0;
double totalsir=0.0;
int orderpathloss[20];
int divset[20];
double tmppathlosslow;
double tmppathlosshigh;
int bsnum,bsnum1,bsnum2;
double sumofpath;
double sumofpathapprox;
```

```
double tempgamma,templow,temphigh,temp,cigma,qfunclow,qfunchigh;
double tt1,tt2,tt3,tt4,tte,avgratio;
double pvaluediv,pvaluenodiv;
double qvaluediv,qvaluenodiv;
double bvaluediv,bvaluenodiv;
double cvaluediv,cvaluenodiv;
double catchedfinger[20];
double sumavglog,sumavglogsquare;
double aconstant;
double numtosimulate=1e3;
double actualnumtosimulate1=1e3;
double actualnumtosimulate2=1e3;
double sumavg,sumavgsquare,temphigh1,temphigh2,templow1,templow2;
double meangauss_s,mean2gauss_s,variancegauss_s,stdgauss_s;
double meangauss_i,mean2gauss_i,variancegauss_i,stdgauss_i;
double meangauss_si,mean2gauss_si,variancegauss_si,stdgauss_si;
int totaldivbsnum=3; //2 means bs0 and another bs in diversity
for(i=0;i<=13;i++)
{
catchfinger[i]=0;
}
double gaussianrnd;
int countdivnum,countdivnumsec;
//parameters for Greenstein's multipath fading
double t1=0.5*1e-6; //1 us
double epsilon=0.5;
double cigmay=4; //4 dB
```

```
double tc=1.0/(rate);
// gammab=gammac=1 means it is rayleigh fading
double gammab=1.0;
double gammac=1.0;
double tauavg, qqq[20], pce[20],anothertmp;
double ofvalue,sirapprox,sirtrue, nsr=0.01, phi=0.01;
double actualu,actualv,approxu,approxv;
double gaussnum=1e3;
double tmpuvalue;
// begin: begin MS location; mssimnum: total number of MS location
// begindivcount: first diversity combination;
//enddivcount: last diversity combination
begin=1;  //6-0.52543799069381,11-1.0031088913246,16-1.4807797919553
mssimnum=77;
begindivcount=0;
enddivcount=87;
numtosimulate=1e4;
double cigmab=correlationb*shadow;
double tmpcigmab=correlationb*shadow;
int bsnumtmpk,bsnumtmpn,n;
int fingersofeachbs=15;
double fractionofbspower[20];
double meanbspower[20];
double stdbspower[20];
for(simnum=0;simnum<=1e5;simnum++)  //generate Gaussian R.V.s
{
gaussmatrix[simnum]=gaussian(0,cigmab);
```

```
gaussvariable[simnum]=gaussian(0,1);
}
double maxphi,xmaxphi,avgphi,avgsquarephi;
double totalavgphi[5][1000],totalavgsquarephi[5][1000];
double totalavgphi_corr[5][1000],totalavgsquarephi_corr[5][1000];
double totalprob[10];
double outageprob_over_phith[10];
int total_iteration_num=10;
int iteration;
double lognormal_phi_mean=0.0;
double lognormal_phi_std=0.0;
double final_phi_mean;
double final_phi_mean2;
bool corr_flag=true;
for(iteration=1;iteration<=total_iteration_num;iteration++)
{
printf("\n\nIteration Number=%d\n",iteration);
old_extra_power=extra_power;
extra_power=0;
for(i=0;i<=13;i++)
{
if(iteration==1) //initial power is assumed to be equal to 1
{
bs_power_mean[i]=1;
bs_power_mean2[i]=1;

}else
```

```
{
bs_power_mean[i]=exp(lognormal_phi_std*lognormal_phi_std*
constantlamda*constantlamda/2.0+lognormal_phi_mean*
constantlamda)*qfunc(lognormal_phi_mean/lognormal_phi_std
+lognormal_phi_std*constantlamda);
bs_power_mean2[i]=exp(2.0*lognormal_phi_std*lognormal_phi_std
*constantlamda*constantlamda+2.0*lognormal_phi_mean*
constantlamda)*qfunc(lognormal_phi_mean/lognormal_phi_std
+2.0*lognormal_phi_std*constantlamda);
}
}
for(mm=begin;mm<=mssimnum;mm++)
{
for(int outage_i=0;outage_i<traffic_class_total;outage_i++)
{
outageprob_over_phith[outage_i]=0.0;
totalprob[outage_i]=0.0;
sumtotalavgphi[outage_i][mm]=0.0;
sumtotalavgsquarephi[outage_i][mm]=0.0;
sumtotalavgphi_corr[outage_i][mm]=0.0;
sumtotalavgsquarephi_corr[outage_i][mm]=0.0;
}
//for a specific divesity set
for(countdivnum=begindivcount;countdivnum<=enddivcount;countdivnum++)
{ //allocate Rake fingers
int tmpbsnum=bsdivnum[countdivnum];
switch(tmpbsnum)
```

```
{
case 0:
for(n=0;n<=bsdivnum[countdivnum];n++)
{
bsnumtmpn=bsdivset[countdivnum][n];
catchfinger[bsnumtmpn]=6;
};
break;
case 1:
for(n=0;n<=bsdivnum[countdivnum];n++)
{
bsnumtmpn=bsdivset[countdivnum][n];
catchfinger[bsnumtmpn]=3;
};
//  bsnumtmpn=bsdivset[countdivnum][1];
//  catchfinger[bsnumtmpn]=0;
break;
case 2:
for(n=0;n<=bsdivnum[countdivnum];n++)
{
bsnumtmpn=bsdivset[countdivnum][n];
catchfinger[bsnumtmpn]=2;
};
break;
case 3:
for(n=0;n<=bsdivnum[countdivnum];n++)
{
```

```
bsnumtmpn=bsdivset[countdivnum][n];
catchfinger[bsnumtmpn]=1;
};
bsnumtmpn=bsdivset[countdivnum][0];
catchfinger[bsnumtmpn]=2;
bsnumtmpn=bsdivset[countdivnum][1];
catchfinger[bsnumtmpn]=2;
break;
}
for(i=0;i<=13;i++)
{
ds[i]=sqrt(pow(bs_pos[i][0]-ms_pos[mm][0],2)
+pow(bs_pos[i][1]-ms_pos[mm][1],2));
tauavg=exp(pow(cigmay*log(10.0)/10.0,2.0)/2.0)
*t1*pow(ds[i],epsilon);
qqq[i]=exp(-tc/tauavg);
}
for(j=1;j<=13;j++)
{
cnodiv[j]=(10*pathlossfactor*log10(ds[0]/ds[j]))
/(correlationb*shadow);
c[j][0]=(10*pathlossfactor*log10(ds[0]/ds[j])-th)
/(correlationb*shadow);
c[j][1]=(10*pathlossfactor*log10(ds[0]/ds[j])+th)
/(correlationb*shadow);
}
gausimnum=1e3;
```

```
for(totalN=0;totalN<gausimnum;totalN=totalN+1)
{
tempgaus=gaussian(0,1);
probdiv=1.0;//calculate div prob
for(j=1;j<=bsdivnum[countdivnum];j++)
{
bsdiv=bsdivset[countdivnum][j];
probdiv*=qfunc(tempgaus+c[bsdiv][0])
-qfunc(tempgaus+c[bsdiv][1]);
if(probdiv<little)
{
goto importantcal;
}
}
for(j=1;j<=bsnodivnum[countdivnum];j++)
{
bsdiv=bsnodivset[countdivnum][j];
if(countdivnum==0)
{
probdiv*=qfunc(tempgaus+c[bsdiv][1]);
}else{
probdiv*=qfunc(tempgaus+cnodiv[bsdiv]);
}

if(probdiv<little)
{
goto importantcal;
```

```
};
}
importantcal:
shdivprobtot[mm][countdivnum]+=probdiv;
}
shdivprobtot[mm][countdivnum]=shdivprobtot[mm][countdivnum]
/gausimnum;
if(iteration==1)
{
fprintf(outfile1,"%f\n",shdivprobtot[mm][countdivnum]);
}
if(shdivprobtot[mm][countdivnum]>1e-4)
{
avgratio=0.0;
double tmpsir=0.0,tmpinterference=0.0,
ofnumerator=0.0,ofdenominator=0.0,
ofvalue=0.0,phivalue=0.0;
double avgof=0.0,avgofsquare=0.0,actualofvalue=0.0,
tmpofvalue=0.0,tmpofvaluetwo=0.0;
// get gamma parameters for U and V
// get gamma parameters for U, U is I
double eu,eu2,ev,ev2;
double tmpu,tmpu2,tmpv, tmpv2;
double tmpmidn1, tmpmidn2, tmpmidk1, tmpmidk2,
paracu,parabu,paracv,parabv;
int actualsimnum;
double tmpvalue, ttt1,ttt2,ttt3,ttt4;
```

```
eu=0.0;
eu2=0.0;
for(n=1;n<=bsnodivnum[countdivnum];n++)
{
bsnumtmpn=bsnodivset[countdivnum][n];
if(countdivnum==0)
{
tmpmidn1=(10*pathlossfactor*
log10(ds[bsnumtmpn]/ds[0])-th)/cigmab;
}else{
tmpmidn1=(10*pathlossfactor*
log10(ds[bsnumtmpn]/ds[0]))/cigmab;
}
tmpu2=0.0;
actualsimnum=gaussnum;
for(i=1;i<=gaussnum;i++)
{
ttt1=qfunc(gaussmatrix[i]
/cigmab-tmpmidn1+cigmab*constantlamda);
ttt2=qfunc(gaussmatrix[i]/cigmab-tmpmidn1);
if(ttt2!=0)
{
tmpu2+=ttt1/ttt2*exp(constantlamda*gaussmatrix[i]);
}else{actualsimnum--;}
}
if(actualsimnum!=0){
tmpu2=tmpu2*exp(cigmab*cigmab*constantlamda*constantlamda/2.0)
```

```
*pow(ds[0]/ds[bsnumtmpn],pathlossfactor)/actualsimnum;
}
eu+=bs_power_mean[bsnumtmpn]*tmpu2;
tmpu2=0.0;
actualsimnum=gaussnum;
for(i=1;i<=gaussnum;i++)
{
ttt1=qfunc(gaussmatrix[i]/cigmab-tmpmidn1+2.0*cigmab*constantlamda);
ttt2=qfunc(gaussmatrix[i]/cigmab-tmpmidn1);
if(ttt2!=0)
{
tmpu2+=ttt1/ttt2*exp(2.0*constantlamda*gaussmatrix[i]);
}else{actualsimnum--;}
}
if(actualsimnum!=0){
tmpu2=tmpu2*exp(2.0*cigmab*cigmab*constantlamda*constantlamda)*
pow(ds[0]/ds[bsnumtmpn],2.0*pathlossfactor)/actualsimnum;
}
eu2+=bs_power_mean2[bsnumtmpn]*tmpu2*((1.0-qqq[bsnumtmpn])
/(gammab*(1.0+qqq[bsnumtmpn]))+1.0);
for(k=1;k<=bsnodivnum[countdivnum];k++)
{
bsnumtmpk=bsnodivset[countdivnum][k];
if(bsnumtmpk!=bsnumtmpn)
{
if(countdivnum==0)
{
```

```
tmpmidk1=(10*pathlossfactor*log10(ds[bsnumtmpk]/ds[0])-th)/cigmab;
}else{
tmpmidk1=(10*pathlossfactor*log10(ds[bsnumtmpk]/ds[0]))/cigmab;
}
tmpu2=0.0;
actualsimnum=gaussnum;
for(i=1;i<=gaussnum;i++)
{
ttt1=qfunc(gaussmatrix[i]/cigmab-tmpmidn1+cigmab*constantlamda);
ttt2=qfunc(gaussmatrix[i]/cigmab-tmpmidn1);
ttt3=qfunc(gaussmatrix[i]/cigmab-tmpmidk1+cigmab*constantlamda);
ttt4=qfunc(gaussmatrix[i]/cigmab-tmpmidk1);
if(ttt2!=0 & ttt4!=0)
{
tmpu2+=ttt1/ttt2*ttt3/ttt4*exp(2*constantlamda*gaussmatrix[i]);
}else{actualsimnum--;}
}
if(actualsimnum!=0){
tmpu2=tmpu2*exp(cigmab*cigmab*constantlamda*constantlamda)*
pow(ds[0]*ds[0]/(ds[bsnumtmpn]*ds[bsnumtmpk]),pathlossfactor)/actualsimnum;
}
correlation_power_scale=bs_power_mean[bsnumtmpn]*bs_power_mean[bsnumtmpk];
if(corr_flag)
{
correlation_power_scale+=old_extra_power;
}
eu2+=correlation_power_scale*tmpu2;
```

```
}
}
}
// some of the interference from BSs in the active set
//due to the finger limitation of the rake receiver
for(n=0;n<=bsdivnum[countdivnum];n++)
{
bsnumtmpn=bsdivset[countdivnum][n];
tmpmidn1=(10*pathlossfactor*log10(ds[bsnumtmpn]/ds[0])-th)/cigmab;
tmpmidn2=(10*pathlossfactor*log10(ds[bsnumtmpn]/ds[0])+th)/cigmab;
if(bsnumtmpn!=0)
{
tmpu2=0.0;
actualsimnum=gaussnum;
for(i=1;i<=gaussnum;i++)
{
ttt1=qfunc(gaussmatrix[i]/cigmab-tmpmidn1+cigmab*constantlamda)
-qfunc(gaussmatrix[i]/cigmab-tmpmidn2+cigmab*constantlamda);
ttt2=qfunc(gaussmatrix[i]/cigmab-tmpmidn1)-qfunc(gaussmatrix[i]
/cigmab-tmpmidn2);
if(ttt2!=0)
{
tmpu2+=ttt1/ttt2*exp(constantlamda*gaussmatrix[i]);
}else{actualsimnum--;}
}
if(actualsimnum!=0){
tmpu2=tmpu2*exp(cigmab*cigmab*constantlamda*constantlamda/2.0)
```

```
*pow(ds[0]/ds[bsnumtmpn],pathlossfactor)/actualsimnum;
}
}else{
tmpu2=1.0;
}
eu+=bs_power_mean[bsnumtmpn]*pow(qqq[bsnumtmpn],catchfinger[bsnumtmpn])*tmpu2;
if(bsnumtmpn!=0)
{
tmpu2=0.0;
actualsimnum=gaussnum;
for(i=1;i<=gaussnum;i++)
{
ttt1=qfunc(gaussmatrix[i]/cigmab-tmpmidn1+2.0*cigmab*constantlamda)
-qfunc(gaussmatrix[i]/cigmab-tmpmidn2+2.0*cigmab*constantlamda);
ttt2=qfunc(gaussmatrix[i]/cigmab-tmpmidn1)-qfunc(gaussmatrix[i]/
 cigmab-tmpmidn2);
if(ttt2!=0)
{
tmpu2+=ttt1/ttt2*exp(2.0*constantlamda*gaussmatrix[i]);
}else{actualsimnum--;}
}
if(actualsimnum!=0){
tmpu2=tmpu2*exp(2.0*cigmab*cigmab*constantlamda*constantlamda)
*pow(ds[0]/ds[bsnumtmpn],2.0*pathlossfactor)/actualsimnum;
}
}else{
tmpu2=1.0;
```

```
}
double tmptt;
tmptt=((1.0-qqq[bsnumtmpn])*pow(qqq[bsnumtmpn],2.0*catchfinger[bsnumtmpn])
   /(gammab*(1.0+qqq[bsnumtmpn]))+pow(qqq[bsnumtmpn],2.0*
   catchfinger[bsnumtmpn]));
eu2+=bs_power_mean2[bsnumtmpn]*tmptt*tmpu2;
for(k=0;k<=bsdivnum[countdivnum];k++)
{
bsnumtmpk=bsdivset[countdivnum][k];
if(bsnumtmpk!=bsnumtmpn)
{
tmpmidk1=(10*pathlossfactor*log10(ds[bsnumtmpk]/ds[0])-th)/cigmab;
tmpmidk2=(10*pathlossfactor*log10(ds[bsnumtmpk]/ds[0])+th)/cigmab;
if(bsnumtmpn==0)
{
tmpu2=0.0;
actualsimnum=gaussnum;
for(i=1;i<=gaussnum;i++)
{
ttt1=qfunc(gaussmatrix[i]/cigmab-tmpmidk1+cigmab*constantlamda)
-qfunc(gaussmatrix[i]/cigmab-tmpmidk2+cigmab*constantlamda);
ttt2=qfunc(gaussmatrix[i]/cigmab-tmpmidk1)-qfunc(gaussmatrix[i]/cigmab
 -tmpmidk2);
if(ttt2!=0)
{
tmpu2+=ttt1/ttt2*exp(constantlamda*gaussmatrix[i]);
}else{actualsimnum--;}
```

```
}
if(actualsimnum!=0)
{
tmpu2=tmpu2*exp(cigmab*cigmab*constantlamda*constantlamda/2.0)
*pow(ds[0]/ds[bsnumtmpk],pathlossfactor)/actualsimnum;
}
}else if(bsnumtmpk==0)
{
tmpu2=0.0;
actualsimnum=gaussnum;
for(i=1;i<=gaussnum;i++)
{
ttt1=qfunc(gaussmatrix[i]/cigmab-tmpmidn1+cigmab*constantlamda)
-qfunc(gaussmatrix[i]/cigmab-tmpmidn2+cigmab*constantlamda);
ttt2=qfunc(gaussmatrix[i]/cigmab-tmpmidn1)-
qfunc(gaussmatrix[i]/cigmab-tmpmidn2);
if(ttt2!=0)
{
tmpu2+=ttt1/ttt2*exp(constantlamda*gaussmatrix[i]);
}else{actualsimnum--;}
}
if(actualsimnum!=0){
tmpu2=tmpu2*exp(cigmab*cigmab*constantlamda*constantlamda/2.0)
*pow(ds[0]/ds[bsnumtmpn],pathlossfactor)/actualsimnum;
}
}else{
tmpu2=0.0;
```

```
actualsimnum=gaussnum;
for(i=1;i<=gaussnum;i++)
{
ttt1=qfunc(gaussmatrix[i]/cigmab-tmpmidn1+cigmab*constantlamda)
-qfunc(gaussmatrix[i]/cigmab-tmpmidn2+cigmab*constantlamda);
ttt2=qfunc(gaussmatrix[i]/cigmab-tmpmidn1)-qfunc(gaussmatrix[i]
/cigmab-tmpmidn2);
ttt3=qfunc(gaussmatrix[i]/cigmab-tmpmidk1+cigmab*constantlamda)
-qfunc(gaussmatrix[i]/cigmab-tmpmidk2+cigmab*constantlamda);
ttt4=qfunc(gaussmatrix[i]/cigmab-tmpmidk1)-qfunc(gaussmatrix[i]
/cigmab-tmpmidk2);
if(ttt2!=0 & ttt4!=0)
{
tmpu2+=ttt1/ttt2*ttt3/ttt4*exp(2*constantlamda*gaussmatrix[i]);
}else{actualsimnum--;}
}
if(actualsimnum!=0){
tmpu2=tmpu2*exp(cigmab*cigmab*constantlamda*constantlamda)*pow(ds[0]
*ds[0]/(ds[bsnumtmpn]*ds[bsnumtmpk]),pathlossfactor)/actualsimnum;
}
}
//tmpu2 is E[l0^2/ln lk], n,k in Nsh, and n<>k
correlation_power_scale=bs_power_mean[bsnumtmpn]*
bs_power_mean[bsnumtmpk];
if(corr_flag)
{
correlation_power_scale+=old_extra_power;
```

```
}
eu2+=correlation_power_scale*pow(qqq[bsnumtmpn],
 catchfinger[bsnumtmpn])
*pow(qqq[bsnumtmpk],catchfinger[bsnumtmpk])*tmpu2;
}
}
//nsh
for(k=1;k<=bsnodivnum[countdivnum];k++)
{
bsnumtmpk=bsnodivset[countdivnum][k];
if(bsnumtmpn!=0)
{
if(countdivnum==0)
{
tmpmidk1=(10*pathlossfactor*log10(ds[bsnumtmpk]/ds[0])-th)/cigmab;
}else{
tmpmidk1=10*pathlossfactor*log10(ds[bsnumtmpk]/ds[0])/cigmab;
}
tmpu2=0.0;
actualsimnum=gaussnum;
for(i=1;i<=gaussnum;i++)
{
ttt1=qfunc(gaussmatrix[i]/cigmab-tmpmidn1+cigmab*constantlamda)
-qfunc(gaussmatrix[i]/cigmab-tmpmidn2+cigmab*constantlamda);
ttt2=qfunc(gaussmatrix[i]/cigmab-tmpmidn1)-qfunc(gaussmatrix[i]
/cigmab-tmpmidn2);
ttt3=qfunc(gaussmatrix[i]/cigmab-tmpmidk1+cigmab*constantlamda);
```

```
ttt4=qfunc(gaussmatrix[i]/cigmab-tmpmidk1);
if(ttt2!=0 & ttt4!=0)
{
tmpu2+=ttt1/ttt2*ttt3/ttt4*exp(2*constantlamda*gaussmatrix[i]);
}else{actualsimnum--;}
}
if(actualsimnum!=0){
tmpu2=tmpu2*exp(cigmab*cigmab*constantlamda*constantlamda)
*pow(ds[0]*ds[0]/(ds[bsnumtmpn]*ds[bsnumtmpk]),pathlossfactor)/actualsimnum;
}
}else{ //sh includes the zeroth BS
if(countdivnum==0)
{
tmpmidk1=(10*pathlossfactor*log10(ds[bsnumtmpk]/ds[0])-th)/cigmab;
}else{
tmpmidk1=10*pathlossfactor*log10(ds[bsnumtmpk]/ds[0])/cigmab;
}
tmpu2=0.0;
actualsimnum=gaussnum;
for(i=1;i<=gaussnum;i++)
{
ttt1=qfunc(gaussmatrix[i]/cigmab-tmpmidk1+cigmab*constantlamda);
ttt2=qfunc(gaussmatrix[i]/cigmab-tmpmidk1);
if(ttt2!=0)
{
tmpu2+=ttt1/ttt2*exp(constantlamda*gaussmatrix[i]);
}else{actualsimnum--;}
```

```
}
if(actualsimnum!=0){
tmpu2=tmpu2*exp(cigmab*cigmab*constantlamda*constantlamda/2.0)
*pow(ds[0]/ds[bsnumtmpk],pathlossfactor)/actualsimnum;
}
}
//tmpu2 is E[l0^2/ln lk], n,k in Nsh, and n<>k
correlation_power_scale=bs_power_mean[bsnumtmpk]*bs_power_mean[bsnumtmpn];
if(corr_flag)
{
correlation_power_scale+=old_extra_power;
}

eu2+=2.0*correlation_power_scale*pow(qqq[bsnumtmpn],
 catchfinger[bsnumtmpn])*tmpu2;
}
}
meangauss_i=(2.0*log(eu)-log(eu2)/2.0)/constantlamda;
stdgauss_i=sqrt((log(eu2)-2.0*log(eu))/(constantlamda*constantlamda));
// get gamma parameters for V, V is S
ev=0.0; //
ev2=0.0; //
for(n=0;n<=bsdivnum[countdivnum];n++)
{
bsnumtmpn=bsdivset[countdivnum][n];
if(catchfinger[bsnumtmpn]!=0)
{
```

```
tmpmidn1=(10*pathlossfactor*log10(ds[bsnumtmpn]/ds[0])-th)/cigmab;
tmpmidn2=(10*pathlossfactor*log10(ds[bsnumtmpn]/ds[0])+th)/cigmab;
if(bsnumtmpn!=0)
{
tmpu=0.0;
actualsimnum=gaussnum;
for(i=1;i<=gaussnum;i++)
{
ttt1=qfunc(gaussmatrix[i]/cigmab-tmpmidn1+cigmab*constantlamda)
-qfunc(gaussmatrix[i]/cigmab-tmpmidn2+cigmab*constantlamda);
ttt2=qfunc(gaussmatrix[i]/cigmab-tmpmidn1)-qfunc(gaussmatrix[i]
/cigmab-tmpmidn2);
if(ttt2!=0)
{
tmpu+=ttt1/ttt2*exp(constantlamda*gaussmatrix[i]);
}else{actualsimnum--;}
}
if(actualsimnum!=0){
tmpu=tmpu*exp(cigmab*cigmab*constantlamda*constantlamda/2.0)
*pow(ds[0]/ds[bsnumtmpn],pathlossfactor)/actualsimnum;
}
tmpu2=0.0;
actualsimnum=gaussnum;
for(i=1;i<=gaussnum;i++)
{
ttt1=qfunc(gaussmatrix[i]/cigmab-tmpmidn1+2.0*cigmab*constantlamda)
-qfunc(gaussmatrix[i]/cigmab-tmpmidn2+2.0*cigmab*constantlamda);
```

```
ttt2=qfunc(gaussmatrix[i]/cigmab-tmpmidn1)-qfunc(gaussmatrix[i]
/cigmab-tmpmidn2);
if(ttt2!=0)
{
tmpu2+=ttt1/ttt2*exp(2.0*constantlamda*gaussmatrix[i]);
}else{actualsimnum--;}
}
if(actualsimnum!=0){
tmpu2=tmpu2*exp(2.0*cigmab*cigmab*constantlamda*constantlamda)
*pow(ds[0]/ds[bsnumtmpn],2.0*pathlossfactor)/actualsimnum;
}
}else
{
tmpu=1.0;
tmpu2=1.0;
}
//tmpu is E[l0/ln], n in Nsh
ev+=(1-pow(qqq[bsnumtmpn],catchfinger[bsnumtmpn]))*tmpu;
double tmptt;
tmptt=((1.0-qqq[bsnumtmpn])*(1.0-pow(qqq[bsnumtmpn],2.0*
   catchfinger[bsnumtmpn]))/(gammab*(1.0+qqq[bsnumtmpn]))
   +(1.0-pow(qqq[bsnumtmpn],catchfinger[bsnumtmpn]))*
   (1.0-pow(qqq[bsnumtmpn],catchfinger[bsnumtmpn])));
ev2+=tmptt*tmpu2;
for(k=0;k<=bsdivnum[countdivnum];k++)
{
bsnumtmpk=bsdivset[countdivnum][k];
```

```
if(catchfinger[bsnumtmpk]!=0)
{
if(bsnumtmpk!=bsnumtmpn)
{
tmpmidk1=(10*pathlossfactor*log10(ds[bsnumtmpk]/ds[0])-th)/cigmab;
tmpmidk2=(10*pathlossfactor*log10(ds[bsnumtmpk]/ds[0])+th)/cigmab;
if(bsnumtmpk==0)
{
tmpu2=0.0;
actualsimnum=gaussnum;
for(i=1;i<=gaussnum;i++)
{
ttt1=qfunc(gaussmatrix[i]/cigmab-tmpmidn1+cigmab*constantlamda)
-qfunc(gaussmatrix[i]/cigmab-tmpmidn2+cigmab*constantlamda);
ttt2=qfunc(gaussmatrix[i]/cigmab-tmpmidn1)-qfunc(gaussmatrix[i]
/cigmab-tmpmidn2);
if(ttt2!=0)
{
tmpu2+=ttt1/ttt2*exp(constantlamda*gaussmatrix[i]);
}else{actualsimnum--;}
}
if(actualsimnum!=0){
tmpu2=tmpu2*exp(cigmab*cigmab*constantlamda*constantlamda/2.0)
*pow(ds[0]/ds[bsnumtmpn],pathlossfactor)/actualsimnum;
}
}else if(bsnumtmpn==0)
{
```

```
tmpu2=0.0;
actualsimnum=gaussnum;
for(i=1;i<=gaussnum;i++)
{
ttt1=qfunc(gaussmatrix[i]/cigmab-tmpmidk1+cigmab*constantlamda)
-qfunc(gaussmatrix[i]/cigmab-tmpmidk2+cigmab*constantlamda);
ttt2=qfunc(gaussmatrix[i]/cigmab-tmpmidk1)-qfunc(gaussmatrix[i]
/cigmab-tmpmidk2);
if(ttt2!=0)
{
tmpu2+=ttt1/ttt2*exp(constantlamda*gaussmatrix[i]);
}else{actualsimnum--;}
}
if(actualsimnum!=0){
tmpu2=tmpu2*exp(cigmab*cigmab*constantlamda*constantlamda/2.0)
*pow(ds[0]/ds[bsnumtmpk],pathlossfactor)/actualsimnum;
}
}else{
tmpu2=0.0;
actualsimnum=gaussnum;
for(i=1;i<=gaussnum;i++)
{
ttt1=qfunc(gaussmatrix[i]/cigmab-tmpmidn1+cigmab*constantlamda)
-qfunc(gaussmatrix[i]/cigmab-tmpmidn2+cigmab*constantlamda);
ttt2=qfunc(gaussmatrix[i]/cigmab-tmpmidn1)-qfunc(gaussmatrix[i]
/cigmab-tmpmidn2);
ttt3=qfunc(gaussmatrix[i]/cigmab-tmpmidk1+cigmab*constantlamda)
```

```
-qfunc(gaussmatrix[i]/cigmab-tmpmidk2+cigmab*constantlamda);
ttt4=qfunc(gaussmatrix[i]/cigmab-tmpmidk1)-qfunc(gaussmatrix[i]
/cigmab-tmpmidk2);
if(ttt2!=0 & ttt4!=0)
{
tmpu2+=ttt1/ttt2*ttt3/ttt4*exp(2*constantlamda*gaussmatrix[i]);
}else{actualsimnum--;}
}
if(actualsimnum!=0){
tmpu2=tmpu2*exp(cigmab*cigmab*constantlamda*constantlamda)
*pow(ds[0]*ds[0]/(ds[bsnumtmpn]*ds[bsnumtmpk]),pathlossfactor)
/actualsimnum;
}
}
ev2+=tmpu2*(1-pow(qqq[bsnumtmpn],catchfinger[bsnumtmpn]))
*(1-pow(qqq[bsnumtmpk],catchfinger[bsnumtmpk]));
}
}
}
}
}
//U is I, V is S
meangauss_s=(2.0*log(ev)-log(ev2)/2.0)/constantlamda;
stdgauss_s=sqrt((log(ev2)-2.0*log(ev))/(constantlamda*constantlamda));
//
meangauss_si=meangauss_i-meangauss_s;
stdgauss_si=sqrt(stdgauss_s*stdgauss_s+stdgauss_i*stdgauss_i);
```

```
//

for(traffic_index=0;traffic_index<traffic_class_total;traffic_index++)
{
maxphi=outageinv(meangauss_si,stdgauss_si,targetoutage,traffic_index);
//paracv=ev/(ev2-ev*ev);
//parabv=ev*paracv;

double avgphi,avgphisquare;
avgphi=0.0;
avgphisquare=0.0;
if(maxphi>phith)
{
outageprob_over_phith[traffic_index]+=shdivprobtot[mm][countdivnum];
totalavgphi[traffic_index][countdivnum]=0.0;
totalavgsquarephi[traffic_index][countdivnum]=0.0;
totalavgphi_corr[traffic_index][countdivnum]=0.0;
totalavgsquarephi_corr[traffic_index][countdivnum]=0.0;
printf("\n ms=%d, div=%d,traffic_class=%d, maxphi=%f,avgphi=%e,
   avgphisquare=%e\n",
mm,countdivnum,traffic_index,maxphi,totalavgphi[traffic_index][countdivnum],
totalavgsquarephi[traffic_index][countdivnum]);
}else{
fprintf(outfile2,"%e\n",maxphi);
tmpvalue=evaluate_phi_avg(meangauss_si,stdgauss_si,maxphi,traffic_index);
avgphi+=tmpvalue;
tmpvalue=evaluate_phi_avgsquare(meangauss_si,stdgauss_si,maxphi,traffic_index);
```

```
avgphisquare+=tmpvalue;
totalavgphi[traffic_index][countdivnum]=avgphi*shdivprobtot[mm][countdivnum];
totalavgsquarephi[traffic_index][countdivnum]=(avgphisquare)
*shdivprobtot[mm][countdivnum];
totalprob[traffic_index]+=shdivprobtot[mm][countdivnum];
if(countdivnum>=1 && countdivnum<14) //2 BS diversity
{
totalavgphi_corr[traffic_index][countdivnum]=
totalavgphi[traffic_index][countdivnum];
totalavgsquarephi_corr[traffic_index][countdivnum]=
(avgphisquare-avgphi*avgphi)
*shdivprobtot[mm][countdivnum]+(avgphi*avgphi)*
shdivprobtot[mm][countdivnum];
}
else if(countdivnum>=14 && countdivnum<20) //more than 2 BS diversity
{
totalavgphi_corr[traffic_index][countdivnum]=totalavgphi
[traffic_index][countdivnum]*2.0;
totalavgsquarephi_corr[traffic_index][countdivnum]=
(avgphisquare-avgphi*avgphi)
*shdivprobtot[mm][countdivnum]*2.0+(avgphi*avgphi)*
shdivprobtot[mm][countdivnum]*4.0;
}else if(countdivnum>=20 && countdivnum<47) //more than 2 BS diversity
{
totalavgphi_corr[traffic_index][countdivnum]=
totalavgphi[traffic_index][countdivnum];
totalavgsquarephi_corr[traffic_index][countdivnum]=
```

```
(avgphisquare-avgphi*avgphi)
*shdivprobtot[mm][countdivnum]+(avgphi*avgphi)*
shdivprobtot[mm][countdivnum];
}else if(countdivnum>=47)
{
totalavgphi_corr[traffic_index][countdivnum]=
totalavgphi[traffic_index][countdivnum];
totalavgsquarephi_corr[traffic_index][countdivnum]=
(avgphisquare-avgphi*avgphi)
*shdivprobtot[mm][countdivnum]+(avgphi*avgphi)*
shdivprobtot[mm][countdivnum];
}else
{
totalavgphi_corr[traffic_index][countdivnum]=0.0;
totalavgsquarephi_corr[traffic_index][countdivnum]=0.0;
}
fprintf(outfile3,"%e\n",totalprob[traffic_index]);
printf("\n ms=%d, div=%d,traffic_class=%d, maxphi=%f,
   avgphi=%e, std=%e\n",mm,countdivnum,
   traffic_index,maxphi,totalavgphi[traffic_index][countdivnum],
   sqrt(totalavgsquarephi[traffic_index][countdivnum]));
}
}
}else{
for(int traffic_index=0;traffic_index<traffic_class_total;traffic_index++)
{
maxphi=0.0;
```

```
totalavgphi[traffic_index][countdivnum]=0.0;
totalavgsquarephi[traffic_index][countdivnum]=0.0;
totalavgphi_corr[traffic_index][countdivnum]=0.0;
totalavgsquarephi_corr[traffic_index][countdivnum]=0.0;
fprintf(outfile3,"%e\n",totalprob[traffic_index]);
printf("\n ms=%d, div=%d,traffic_class=%d, maxphi=%f, avgphi=%e,
avgphisquare=%e\n",mm,countdivnum,traffic_index,maxphi,
totalavgphi[traffic_index][countdivnum],totalavgsquarephi
[traffic_index][countdivnum]);
}
}
}
//for a cell
for(traffic_index=0;traffic_index<traffic_class_total;traffic_index++)
{
printf("\n mm=%d,traffic_class=%d,outage_over_phi_th=%f\n",
   mm,traffic_index,outageprob_over_phith[traffic_index]);

fprintf(outfile4,"\n mm=%d,traffic_class=%d,
outage_over_phi_th=%f\n",traffic_index,
outageprob_over_phith[traffic_index]);
for(countdivnum=begindivcount;countdivnum<=enddivcount;countdivnum++)/
{
sumtotalavgphi[traffic_index][mm]+=totalavgphi[traffic_index][countdivnum];
sumtotalavgsquarephi[traffic_index][mm]+=
totalavgsquarephi[traffic_index][countdivnum];
sumtotalavgphi_corr[traffic_index][mm]+=
```

```
totalavgphi_corr[traffic_index][countdivnum];
sumtotalavgsquarephi_corr[traffic_index][mm]+=
totalavgsquarephi_corr[traffic_index][countdivnum];

}
fprintf(outfile5,"traffic class=%d,avg=%f,avgsquare=%f,
avg_corr=%f,avgsquare_corr=%f\n",
traffic_index,sumtotalavgphi[traffic_index][mm],
sumtotalavgsquarephi[traffic_index][mm],sumtotalavgphi_corr
[traffic_index][mm],sumtotalavgsquarephi_corr[traffic_index][mm]);
printf("\n traffic class=%d,avg=%f,avgsquare=%f,
   avg_corr=%f,avgsquare_corr=%f\n",
   traffic_index,sumtotalavgphi[traffic_index][mm],
   sumtotalavgsquarephi[traffic_index][mm],
   sumtotalavgphi_corr[traffic_index][mm],
   sumtotalavgsquarephi_corr[traffic_index][mm]);
}
}
double tmp_sum_1[10];
double tmp_sum_2[10];
double tmp_sum_3[10];
double tmp_sum_4[10];
double tmp_sum_5[10];
double tmp_sum_6[10];
for(traffic_index=0;traffic_index<traffic_class_total;traffic_index++)
{
tmp_sum_1[traffic_index]=0.0;
```

```
tmp_sum_2[traffic_index]=0.0;
tmp_sum_3[traffic_index]=0.0;
tmp_sum_4[traffic_index]=0.0;
tmp_sum_5[traffic_index]=0.0;
tmp_sum_6[traffic_index]=0.0;
}
int total_pos_num[10];
for(traffic_index=0;traffic_index<traffic_class_total;traffic_index++)
{
total_pos_num[traffic_index]=0;
for(mm=begin;mm<=mssimnum;mm++)
{
if(sumtotalavgphi[traffic_index][mm]!=0&&
   sumtotalavgsquarephi[traffic_index][mm]!=0)
{
tmp_sum_1[traffic_index]+=sumtotalavgphi[traffic_index][mm];
tmp_sum_2[traffic_index]+=(sumtotalavgsquarephi[traffic_index][mm]);
tmp_sum_5[traffic_index]+=sumtotalavgphi[traffic_index][mm]
*sumtotalavgphi[traffic_index][mm]; //E[x^2] value
tmp_sum_3[traffic_index]+=(sumtotalavgphi_corr[traffic_index][mm]);
tmp_sum_4[traffic_index]+=(sumtotalavgsquarephi_corr[traffic_index][mm]);
tmp_sum_6[traffic_index]+=sumtotalavgphi_corr[traffic_index][mm]
*sumtotalavgphi_corr[traffic_index][mm]; //E[x^2] value
total_pos_num[traffic_index]++;
}
}
}
```

```
for(traffic_index=0;traffic_index<traffic_class_total;traffic_index++)
{
printf("\n total_mm_number = %d \n",total_pos_num[traffic_index]);
if(total_pos_num[traffic_index]!=0)
{
tmp_sum_1[traffic_index]=tmp_sum_1[traffic_index]
/(total_pos_num[traffic_index]);
tmp_sum_2[traffic_index]=(tmp_sum_2[traffic_index])
/(total_pos_num[traffic_index])
-tmp_sum_5[traffic_index]/(12.0*
total_pos_num[traffic_index]*total_pos_num[traffic_index]);
//var value
tmp_sum_3[traffic_index]=tmp_sum_3[traffic_index]
/(total_pos_num[traffic_index]*12.0);
tmp_sum_4[traffic_index]=(tmp_sum_4[traffic_index])
/(total_pos_num[traffic_index]*12.0)-tmp_sum_6[traffic_index]
/(12.0*12.0*total_pos_num[traffic_index]*total_pos_num[traffic_index]);
}else
{
tmp_sum_1[traffic_index]=0.0;
tmp_sum_2[traffic_index]=0.0;
tmp_sum_3[traffic_index]=0.0;
tmp_sum_4[traffic_index]=0.0;
}
}
//estimate the capacity
double rho_value[10];
```

```
double tmp_value_0;
double tmp_value_1;
double tmp_value_2;
double tmp_value_3;
double tmp_value_4;
double tmp_value_5;
double final_outage=0.0;
double old_outage=0.0;
double old_mean=0.0;
double old_std=0.0;
double beginvalue=0.0, endvalue=800.0,tmpvalue,tol,
new_differvalue,old_differvalue;
tmpvalue=endvalue/2.0;
old_differvalue=100.0;
new_differvalue=0.0;
old_outage=-1000;
final_outage=1000;
double common_value;
while(fabs(targetblocking-final_outage)>0.000001)
{
old_outage=final_outage;
final_phi_mean=0.0;
final_phi_mean2=0.0;
tmp_value_0=0.0;
tmp_value_1=0.0;
tmp_value_2=0.0;
tmp_value_3=0.0;
```

```
tmp_value_4=0.0;
tmp_value_5=0.0;
for(traffic_index=0;traffic_index<traffic_class_total;traffic_index++)
{
rho_value[traffic_index]=traffic_fraction[traffic_index]*tmpvalue;
common_value=rho_value[traffic_index];
tmp_value_1+=active_factor[traffic_index]*
common_value*tmp_sum_1[traffic_index];
tmp_value_2+=active_factor[traffic_index]*
common_value*tmp_sum_2[traffic_index];
tmp_value_3+=active_factor[traffic_index]*
common_value*tmp_sum_3[traffic_index];
tmp_value_4+=active_factor[traffic_index]*
common_value*tmp_sum_4[traffic_index];
}
final_phi_mean=tmp_value_1;
final_phi_mean2=tmp_value_2+tmp_value_1*tmp_value_1;
lognormal_phi_mean=(2.0*log(final_phi_mean)-
log(final_phi_mean2)/2.0)/constantlamda;
lognormal_phi_std=sqrt((log(final_phi_mean2)
-2.0*log(final_phi_mean)))/constantlamda;
final_outage=qfunc(-1.0*lognormal_phi_mean
   /lognormal_phi_std);
if(fabs(targetblocking-final_outage)<0.00001)
{
break;
}
```

```
if(final_outage>targetblocking)
{
endvalue=tmpvalue;
tmpvalue=(beginvalue+endvalue)/2.0;
}else
{
beginvalue=tmpvalue;
tmpvalue=(beginvalue+endvalue)/2.0;
}
}
extra_power=2.0*tmp_value_4;
double final_phi_mean_corr=tmp_value_3;
double final_phi_mean2_corr=tmp_value_4+tmp_value_3*tmp_value_3;
double lognormal_phi_mean_corr=(2.0*log(final_phi_mean_corr)
-log(final_phi_mean2_corr)/2.0)/constantlamda;
double lognormal_phi_std_corr=sqrt((log(final_phi_mean2_corr)
-2.0*log(final_phi_mean_corr)))/constantlamda;
printf("\n rho=%f- outage=%f--log_mean=%f--log_std=%f,
final_mean=%f, final_var=%f,std=%f, correlation coeff=%f,
final_mean_corr=%f , final_var_corr=%f, log_final_mean_corr=%f ,
log_final_std_corr=%f\n",tmpvalue,final_outage,lognormal_phi_mean,
lognormal_phi_std,final_phi_mean,tmp_value_2,sqrt(final_phi_mean2-
final_phi_mean*final_phi_mean),extra_power/(final_phi_mean2-
final_phi_mean*final_phi_mean),tmp_value_3,tmp_value_4,
lognormal_phi_mean_corr,lognormal_phi_std_corr);
fprintf(outfile6,"rho=%f- outage=%f--log_mean=%f--log_std=%f,
final_mean=%f, final_var=%f,std=%f, correlation coeff=%f,
```

```
final_mean_corr=%f , final_var_corr=%f, log_final_mean_corr=%f ,
log_final_std_corr=%f\n",tmpvalue,final_outage,lognormal_phi_mean,
lognormal_phi_std,final_phi_mean,tmp_value_2,sqrt(final_phi_mean2-
final_phi_mean*final_phi_mean),extra_power/(final_phi_mean2-
final_phi_mean*final_phi_mean),tmp_value_3,tmp_value_4,
lognormal_phi_mean_corr,lognormal_phi_std_corr);
fprintf(outfile7,"%e\n",tmpvalue);
fprintf(outfile8,"%e\n",extra_power/(final_phi_mean2-
final_phi_mean*final_phi_mean));
}
finish = clock();


fclose(outfile1);
fclose(outfile2);
fclose(outfile3);
fclose(outfile4);
fclose(outfile5);
fclose(outfile6);
fclose(outfile7);
fclose(outfile8);
duration = (double)(finish - start) / CLOCKS_PER_SEC;
printf( "\n %f seconds\n", duration );
return 0;
}/* end of main */
double outageinv(double a,double b,double prob,int traffic_class_num)
{
if(prob>1.0 || prob<0.0)
```

```
{
return 0.0;
}
double beginvalue=targetsir/spreadgain[traffic_class_num]+0.00000001,
endvalue=10.0,tmpvalue,tol,new_differvalue,old_differvalue;
tmpvalue=endvalue/2.0;
tol=0.5;
old_differvalue=100.0;
new_differvalue=0.0;
int iteration_num=0;

while(tol>epsilonlittle)
{
iteration_num++;
if(iteration_num>200)
{
return 1.01;
break;
}
old_differvalue=new_differvalue;

new_differvalue=outageinc(a,b,tmpvalue,traffic_class_num)-prob;

if(new_differvalue>0.0)
{
beginvalue=tmpvalue;
tmpvalue=(beginvalue+endvalue)/2.0;
```

```
}else{
endvalue=tmpvalue;
tmpvalue=(beginvalue+endvalue)/2.0;
}
tol=fabs(beginvalue-endvalue);
}
return tmpvalue;
}
double evaluate_phi_avg(double mean,double std,double x,int traffic_class_num)
{
double tmp,sum=0.0;
int numtosim=1e4;
if(pcerrordb==0)
{
if(spreadgain[traffic_class_num]*x/targetsir-1.0<0)
{
int yy=11;
yy=22;
}
tmp=10.0*log10(spreadgain[traffic_class_num]*x/targetsir-1.0);

return targetsir/spreadgain[traffic_class_num]*(qfunc((mean-tmp)/std)+
exp(mean*constantlamda+std*std*constantlamda*constantlamda/2.0)
*qfunc((mean+std*std*constantlamda-tmp)/std));
}

for(int i=0;i<numtosim;i++)
```

```
{
tmp=1.0+pow(10.0,(gaussvariable[i]*std+mean)/10.0);
sum+=targetsir/spreadgain[traffic_class_num]*tmp*exp(pcerrordb
*pcerrordb*constantlamda*constantlamda/2.0)*
qfunc(constantlamda*pcerrordb-10.0/pcerrordb*
  log10(spreadgain[traffic_class_num]*x/(targetsir*tmp)));
}
sum=sum/numtosim;
return sum;
}
double evaluate_phi_avgsquare(double mean,double std,
  double x,int traffic_class_num)
{
double tmp,sum=0.0;
int numtosim=1e4;
if(pcerrordb==0)
{
tmp=10.0*log10(spreadgain[traffic_class_num]
*x/targetsir-1.0);
return targetsir/spreadgain[traffic_class_num]
*targetsir/spreadgain[traffic_class_num]*
(qfunc((mean-tmp)/std)+2.0*exp(mean*constantlamda+
 std*std*constantlamda*constantlamda/2.0)*
 qfunc((mean+std*std*constantlamda-tmp)/std)+
 exp(2.0*mean*constantlamda+2.0*std*std*constantlamda*
 constantlamda)*qfunc((mean+2.0*std*std*constantlamda-tmp)/std));
}
```

```
for(int i=0;i<numtosim;i++)
{
tmp=1.0+pow(10.0,(gaussvariable[i]*std+mean)/10.0);
sum+=targetsir/spreadgain[traffic_class_num]*targetsir
/spreadgain[traffic_class_num]*tmp*tmp*exp(2.0*pcerrordb
*pcerrordb*constantlamda*constantlamda)*
qfunc(2.0*constantlamda*pcerrordb-10.0/pcerrordb*
  log10(spreadgain[traffic_class_num]*x/(targetsir*tmp)));
}
sum=sum/numtosim;
return sum;
}
double outageinc(double mean,double std,double x,
 int traffic_class_num)
{
double tmp,sum=0.0;
int numtosim=1e4;
if(pcerrordb==0)
{
tmp=10.0*log10(spreadgain[traffic_class_num]*x/targetsir-1.0);
return qfunc((tmp-mean)/std);
}

for(int i=0;i<numtosim;i++)
{
tmp=1.0+pow(10.0,(gaussvariable[i]*std+mean)/10.0);
sum+=qfunc(10.0/pcerrordb*log10(spreadgain
```

```
   [traffic_class_num]*x/(targetsir*tmp)));
}
sum=sum/numtosim;
return sum;
}
double uniform(void)
{
static int IX=3,IY=35, IZ=127;

IX=(171*IX)%30269;
IY=(172*IY)%30307;
IZ=(170*IZ)%30323;
return(fmod((double)(IX)/30269.0 +
   (double)(IY)/30307.0 +(double)(IZ)/30323.0,1.0));
}
//d is std.
double gaussian (double mean,double d)
{
static double gausstore=0.0;
static int ready=0;

double v1,v2,r;

if (ready==0){
do{
v1=2.0 * uniform()-1.0;
v2=2.0 * uniform()-1.0;
```

```
r=v1*v1 + v2*v2;
}while ((r>=1.0) || (r==0.0) );
r=sqrt((-2.0 *log(r))/r);
gausstore=v2*r;
ready=1;
return (mean+v1 * r * d);
}else{
ready=0;
return (mean+gausstore*d);
}
}
/*calculate erfc*/
double erfc(double x)
{
double t;
static double p=0.3275911;
static double a[]={0.254829592,-0.284496736,1.421413741,
-1.453152027,1.061405429};
static double b[]={5671932,145955712,498753024,
479236096,169263104,23330816,1048576};
static double c[]={135135,26486460,282522240,678053376,553512960,
180404224,23855104,1048576};
static double d[]={-1,3,-15,105,-945,10395};
int i;
double result;
double result1,result2;
result=0.0;
```

```
result1=0.0;
result2=0.0;
if(x<0)
return(2-erfc(-x));
if(x>=0 && x<=1)
{
t=1.0/(1.0+p*x);
for(i=1;i<=5;i++)
{
result=result+a[i-1]*pow(t,i);
}
result=result*exp(-pow(x,2));
}else if(x>1 && x<=9)
{
for(i=0;i<=12;i=i+2)
{
result1=result1+b[i/2]*pow(x,i);
}
for(i=0;i<=14;i=i+2)
{
result2=result2+c[i/2]*pow(x,i);
}
result=result1/result2*(x*exp(-pow(x,2))/sqrt(pi));
}else if(x>9)
{
result=1.0;
for(i=1;i<=6;i++)
```

```
{
result=result+d[i-1]/pow(2*pow(x,2),i);
}
result=result*exp(-pow(x,2))/(x*sqrt(pi));
}
return result;
}
// qfunc(x) is defined as integrating from x to infinite here.
double qfunc(double x)
{
return(0.5*erfc(x/sqrt((float)2)));
}
double lognormaldis(double std)
{
return pow(10.0,gaussian(0,std)/10.0);
}
void initbspos(double d)
{
int i;
bs_pos[0][0]=0.0;
bs_pos[0][1]=0.0;
double angel,temp;
temp=sqrt((float)3)*d;
angel=-pi/6;
for(i=1;i<=6;i++)
{
bs_pos[i][0]=temp*cos(angel);
```

```
bs_pos[i][1]=temp*sin(angel);
angel+=pi/3;
}
bs_pos[7][0]=3.0;
bs_pos[7][1]=0.0;
angel=-pi/2.0;
for(i=8;i<=11;i++)
{
bs_pos[i][0]=3.0+temp*cos(angel);
bs_pos[i][1]=temp*sin(angel);
angel+=pi/3;
}
bs_pos[12][0]=1.5;
bs_pos[12][1]=3.0*sqrt((float)3)*d/2.0;
bs_pos[13][0]=1.5;
bs_pos[13][1]=-3.0*sqrt((float)3)*d/2.0;
}
```

REFERENCES

[1] C.-C. Lee and R. Steele, "Effect of soft and softer handoffs on cdma system capacity," *IEEE Trans. Commun.*, vol. 47, pp. 830–841, Aug. 1998.

[2] T. S. Rappaport, *Wireless Communications-principles and practice*, 1st ed. Prentice Hall, 1996.

[3] J. Scourias. (1997) Overview of the global system for mobile communications. [Online]. Available: http://www.shoshin.uwaterloo.ca/ jscouria/GSM/gsmreport.html

[4] About global system for mobile communications (gsm). Conexant Systems, Inc. [Online]. Available: http://www.conexant.com/news_events/gsm_faq.html

[5] Pdc (personal digital cellular) telephone technology. [Online]. Available: http://www.mobilecomms-technology.com/projects/pdc/

[6] The pcs technology. [Online]. Available: http://www.karnataka.dotindia.com/knowpcstech.htm

[7] Cdma - the history and geography. [Online]. Available: http://www.eprodz.com/ep/articles.cgi?id=43&city=BLR

[8] 3g and umts frequently asked questions. [Online]. Available: http://www.umtsworld.com/umts/faq.htm

[9] 3gsm - frequently asked questions. [Online]. Available: http://www.gsmworld.com/technology/3g/faq.shtml

[10] Umts: Universal mobile telecommunications system. [Online]. Available: http://www.3gamericas.org/English/Technology_Center/umts.cfm

[11] Edge - enhanced data rates for gsm evolution. [Online]. Available: http://www.umtsworld.com/technology/Edge.htm

[12] S. Buckingham. What is general packet radio service? [Online]. Available: http://www.gsmworld.com/technology/gprs/intro.shtml

[13] what_is_imt2000. [Online]. Available: http://www.umtsworld.com/umts/faq.htm

[14] Umts/3g history and future milestones. [Online]. Available: http://www.umtsworld.com/umts/history.htm

[15] Emc world cellular database, june 2003. [Online]. Available: http://www.3gamericas.org/pdfs/media_kit/stats_charts_1q2003.pdf

[16] V. K. Garg, *IS-95 CDMA and CDMA 2000: Cellular/PCS Systems Implementation*. Prentice Hall, 1999.

[17] W. C. Y. Lee, *Lee's Essentials of Wireless Communications*. McGraw-Hill, 2000.

[18] G. Maral and M. Bousque, *Satellite Communications Systems: systems,techniques and technology*, 3rd ed. John Wiley & Sons, 1998.

[19] A. J. Viterbi, A. M. Viterbi, K. S. Gilhousen, and E. Zehavi, "Soft handoff extends cdma cell coverage and increases reverse link capacity," *IEEE J. Select. Areas Commun.*, vol. 20, pp. 1281–8, Oct. 1994.

[20] W. A. Egner, "Dynamic re-configuration algorithms for wireless communication networks," Ph.D. dissertation, Univ. of Texas at Arlington, Arlington, TX, Aug. 1998.

[21] M. Vasudevan, "Interference immunity and optimum spectral reuse in pcs systems," Ph.D. dissertation, Univ. of Texas at Arlington, Arlington, TX, Aug. 1998.

[22] H. Holma and A. Toskala, Eds., *WCDMA for UMTS*, 2nd ed. John Wiley & Sons, 2002.

[23] C. Uc-Rios and D. Lara-Rodriguez, "Forward link capacity losses for soft and softer handoff in cellular systems," in *IEEE PIMRC*, vol. 1, 2001, pp. D–48–D–53.

[24] J. Y. Kim and G. L. Stüber, "Cdma soft handoff analysis in the presence of power control error and shadowing correlation," *IEEE Trans. Wireless Commun.*, vol. 1, pp. 245–255, Apr. 2002.

[25] Y.-P. E. Wang and G. E. Bottomley, "Generalized rake reception for cancelling interference from multiple base stations," in *IEEE VTC*, vol. 5, Sept. 2000, pp. 2333–2339.

[26] ——, "Cdma downlink system capacity enhancement through generalized rake reception," in *IEEE VTC*, vol. 2, Oct. 2001, pp. 1177–1181.

[27] J. Zhang and V. Aalo, "Performance analysis of a multicell ds-cdma system with base station diversity," *IEE Proceedings-Comm.*, vol. 148, pp. 112–118, Apr. 2001.

[28] K. Sipila *et al.*, "Estimation of capacity and required transmission power of wcdma downlink based on a downlink pole equation," in *IEEE VTC*, vol. 2, May 2000, pp. 1002–1005.

[29] D. Li, J. A. Khoja, and V. K. Prabhu, "Channel-gain matched macrodiversity in the forward link of cdma systems," in *IEEE PIMRC*, Sept. 2003, pp. 1370–1374.

[30] M. Abramowitz and I. A. Stegun, Eds., *Handbook of Mathematical Functions with Formulas, Graphs, and Mathematical Tables.* New York: Dover, 1972.

[31] D. K. Kim and F. Adachi, "Theoretical analysis of reverse link capacity for an sir-based power-controlled cellular cdma system in a multipath fading environment," *IEEE Trans. Veh. Technol.*, vol. 50, no. 2, pp. 452–464, Mar. 2001.

[32] C. Cordier and S. Ortega, "On wcdma downlink multiservice coverage and capacity," in *IEEE VTC*, vol. 4, 2001, pp. 2754–2758.

[33] P. Cardieri and T. S. Rappaport, "Statistics of the sum of lognormal variables in wireless communications," in *IEEE VTC*, vol. 3, May 2000, pp. 1823–1827.

[34] L. Jalloul and K. Rohani, "Cdma forward link capacity and coverage in a multipath fading channel," in *IEEE VTC*, vol. 3, May 1997, pp. 1440–1444.

[35] W. Choi and J. Y. Kim, "Forward-link capacity of a ds/cdma system with mixed multirate sources," *IEEE Trans. Veh. Technol.*, vol. 50, no. 3, pp. 737–749, May 2001.

[36] D. Li, J. A. Khoja, and V. K. Prabhu, "System capacity in the forward link of cdma systems," in *IEEE RAWCON*, Aug. 2003, pp. 27–30.

[37] J. D. Parsons, *The Mobile Radio Propagation Channel*, 2nd ed. John Wiley, 2000.

[38] W. C. Jakes, Ed., *Microwave Mobile Communications*. New Jersey: IEEE Press, 1974.

[39] H. Suzuki, "A statistical model for urban radio propagation," *IEEE Trans. Commun.*, vol. 25, pp. 673–680, July 1977.

[40] K. Pedersen and P. Mogensen, "The downlink orthogonality factors influence on wcdma system performance," in *IEEE VTC*, vol. 4, 2002, pp. 2061–2065.

[41] L. J. Greenstein, V. Erceg, Y. S. Yeh, and M. V. Clark, "A new path-gain/delay-spread propagation model for digital cellular channels," *IEEE Trans. Veh. Technol.*, vol. 46, no. 2, pp. 477–485, May 1997.

[42] S. J. Hong and I.-T. Lu, "Soft handoff algorithm parameter optimization in various propagation environments," in *IEEE VTC*, vol. 4, May 2001, pp. 2549–2553.

[43] A. A. Glazunov and J.-E. Berg, "On the distribution of relevant radio channel figures in different propagation environments for performance evaluation of wcdma systems," in *IEEE VTC*, vol. 1, 2001, pp. 269–273.

[44] H. Asplund, A. A. Glazunov, and J.-E. Berg, "An investigation of measured and simulated wideband channels with applications to 1.25 mhz and 5 mhz cdma systems," in *IEEE VTC*, vol. 1, 1998, pp. 562–566.

[45] A. Papoulis, *Probability, Random Variables and Stochastic Processes*, 3rd ed. McGraw Hill, 1991.

[46] R. B. D'Agostino and M. A. Stephens, Eds., *Goodness-of-fit Techniques*. New York: Marcel Dekker, 1986.

[47] R. Narrainen and F. Takawira, "Performance analysis of soft handoff in cdma cellular networks," *IEEE Trans. Veh. Technol.*, vol. 50, pp. 1507–1517, Nov. 2001.

[48] D. K. Kim and D. K. Sung, "Capacity estimation for an sir-based power-controlled cdma system supporting on-off traffic," *IEEE Trans. Veh. Technol.*, vol. 49, no. 4, pp. 1094–1101, July 2000.

[49] C. Passerini and G. Falciasecca, "Correlation between delay-spread and orthogonality factor in urban environments," *IEEE Electron. Lett.*, vol. 37, pp. 384–386, Mar. 2001.

[50] H. Wang and N. Wiberg, "Analysis of a cdma downlink in multipath fading channels," in *IEEE WCNC*, vol. 2, 2002, pp. 517 –521.

[51] N. Mehta, L. Greenstein, T. Willis, and Z. Kostic, "Analysis and results for the orthogonality factor in wcdma downlinks," in *IEEE VTC*, vol. 1, 2002, pp. 100–104.

[52] S. Shin, K. Lee, and K. Kim, "Performance of the packet data transmission using the other-cell-interference factor in ds/cdma downlink," in *IEEE WCNC*, vol. 1, 2002, pp. 400–404.

[53] P. G. Moschopoulos, "The distribution of the sum of independent gamma random variables," *Annals Instit. Statist. Math.*, vol. 37, no. 3, pp. 541–544, 1985.

[54] M.-S. Alouini, A. Abdi, and M. Kaveh, "Sum of gamma variates and performance of wireless communication systems over nakagami-fading channels," *IEEE Trans. Veh. Technol.*, vol. 50, pp. 1471–1480, Nov. 2001.

[55] A. Jalali and A. Gutierrez, "Performance comparison of direct spread and multicarrier cdma systems," in *IEEE VTC*, vol. 3, 1998, pp. 2042–2046.

[56] L. Dai, S. Zhou, and Y. Yao, "Effect of macrodiversity on cdma forward-link capacity," in *IEEE VTC*, vol. 4, 2001, pp. 2452–2456.

[57] D. Li, J. A. Khoja, and V. K. Prabhu, "Forward link handoff distribution with correlated lognormal fading," in *IEEE PIMRC*, Sept. 2004, pp. 2659–2663.

[58] D. Li and V. K. Prabhu, "On the distribution of the BS power in the forward link of a power-controlled cdma system," in *IEEE Globecom*, Nov. 2004, pp. 3892–3896.

[59] L. Zhuge and V. O. K. Li, "Forward link capacity in multi-service ds-cdma systems," in *IEEE Globecom*, vol. 1, 2001, pp. 609–613.

[60] M. Cheng and L. F. Chang, "Uplink system performance of high-speed is-95 cdma with mixed voice and bursty data traffic," in *IEEE PIMRC*, vol. 3, Sept. 1998, pp. 1018–1022.

[61] W. Willinger, M. S. Taqqu, R. Sherman, and D. V. Wilson, "Self-similarity through high-variability: statistical analysis of ethernet lan traffic at the source level," *IEEE/ACM Trans. Networking*, vol. 5, pp. 71–86, Feb. 1997.

[62] P. Pruthi and A. Erramilli, "Heavy-tailed on/off source behavior and self-similar traffic," *IEEE ICC*, vol. 1, pp. 445–450, June 1995.

[63] D. Gross and C. Harris, *Fundamentals of Queueing Theory*, 2nd ed. John Wiley and Sons, 1985.

[64] T. Halonen, J. Romero, and J. Melero, Eds., *GSM, GPRS and EDGE Performance: Evolution Towards 3G/UMTS*, 2nd ed. John Wiley and Sons, 2003.

[65] L. Fenton, "The sum of log-normal probability distributions in scatter transmission systems," *IEEE Trans. Commun.*, vol. 8, pp. 57–67, Mar. 1960.

[66] S. C. Schwartz and Y. S. Yeh, "On the distribution function and moments of power sums with log-normal components," *The Bell System Tech. J.*, vol. 61, no. 7, pp. 1441–1462, Mar. 1982.

BIOGRAPHICAL STATEMENT

The author was born in Linyi, Shandong Province, China, in 1976. He received his B.S. from Beijing University of Posts and Telecommunications, Beijing, China, in 1997 and M.S. degree from the same school in Telecommunication and Information System, in 2000. He got his Ph.D. degree from The University of Texas at Arlington in 2005 in Electrical Engineering. From 2004, he has been working in Cerion Inc. as a system engineer to optimize the GSM/GPRS/EDGE networks for AT&T/Cingular wireless. His current research interest is in the area of wireless communications, including system performance analysis and optimal power control of CDMA systems, fading channels modeling, diversity receptions, adaptive video transmission over wireless channels.